University of Strathclyde

PhD Thesis

A study of small signal stability in power systems with converters

Alexander Duncan Giles

supervised by

Dr. Andrew Roscoe & Prof. Olimpo Anaya-Lara

Contents

1 Introduction **12**

1.1 Project objectives and outline of the thesis 14

1.2 Scientific contributions of this thesis 15

2 Background and review **17**

2.1 Converter topology 18

2.2 DQ-axis vector current control 20

2.2.1 Basic structure 20

2.2.2 Studies on stability of dq-axis vector current control 24

2.3 Alternatives to dq-axis vector current control 26

2.4 Remarks about the literature 31

3 Single-converter system configuration **33**

3.1 Broad definitions & scope 34

3.1.1 Power system definitions 34

3.1.2 Variations in the converter control and filter equipment 35

3.1.3 Grid dq frame 36

3.2 Linear model of electrical system 37

3.2.1 LC filter 37

3.2.2 L filter 41

3.2.3 Frequency response 43

4 Analysis of dq-axis vector current control **45**

4.1 Overview of dq-axis vector current control . . . 46
4.1.1 Reference current values . . . 47
4.2 Relationship between PLL dq frames and grid dq frame . . . 47
4.3 Linear analysis of the controller . . . 50
4.3.1 Phase-tracking errors in the PLL . . . 50
4.3.2 First-order PLL . . . 50
4.3.3 Second-order PLL . . . 53
4.3.4 Frame transformations (abc→dq) . . . 54
4.3.5 The current controller . . . 56
4.3.6 Voltage signals for PWM . . . 58
4.4 Combined system of plant and controller . . . 61
4.4.1 Linear models including outer controllers . . . 65
4.4.2 Condensed models for upgrading to multi-converter system analyses . . . 70
4.5 Linear & non-linear simulations involving dq-axis vector current control . . . 72
4.5.1 Using a first-order PLL . . . 72
4.5.2 Using a second-order PLL . . . 80
4.5.3 Adding outer loop and/or droop controllers . . . 85
4.5.4 An investigation on the specific influence of the PLL . . . 86
4.6 Summary . . . 89

5 Analysis of proportional resonant control 90
5.1 Development of the linear model of proportional resonant control including PLL dynamics . . . 91
5.1.1 Block diagrams and transfer function matrix extraction . . . 94
5.2 Linear & non-linear simulations involving proportional resonant control . . . 95
5.2.1 Using a first-order PLL . . . 97
5.2.2 Using a second-order PLL . . . 108
5.3 Summary . . . 110

6 Analysis of power synchronization control 112
6.1 Overview of power synchronization control . . . 113

6.2 Linear analysis of the controller . . . 114
6.2.1 The PI controllers . . . 114
6.2.2 Voltage reference signals in the converter dq frame . . . 116
6.2.3 Voltage signals for the PWM . . . 118
6.3 Block diagrams and transfer function matrix extraction . . . 120
6.3.1 Condensed models for multi-converter system analyses . . . 123
6.4 Linear & non-linear simulations involving power synchronization control . . . 124
6.4.1 Baseline case studies (LC filter) . . . 125
6.4.2 Using an L filter . . . 131
6.5 Summary . . . 133

7 Small-signal stability in multiple-converter systems 134
7.1 Power system modelling . . . 135
7.1.1 No local loads . . . 137
7.1.2 Including local loads . . . 146
7.2 The unified linear state-space model . . . 153
7.3 Simulations ignoring local loads . . . 156
7.3.1 DQ-axis vector current control only . . . 157
7.3.2 Power synchronization control only . . . 168
7.3.3 Mixture of controllers . . . 176
7.4 Including local loads . . . 186
7.4.1 DQ-axis vector current control only . . . 186
7.4.2 Power synchronization control only . . . 190
7.4.3 Mixture of controllers . . . 194
7.5 Summary . . . 197

8 Conclusions & Future work 200
8.1 Conclusions . . . 200
8.2 Future work . . . 201

A Cross coupling terms in a dq frame 207

B Sample code for linearised models **209**

B.1 Common codes . . . 209

B.1.1 Steady state solver . . . 209

B.1.2 linearised models of plant . . . 212

B.1.3 Bode plots . . . 215

B.2 Vector current control . . . 223

B.2.1 main function . . . 223

B.2.2 Combined linear model of controller and plant . . . 233

B.3 Power synchronization control . . . 241

B.3.1 main function . . . 241

B.3.2 Combined linear model of controller and plant . . . 245

B.4 Proportional resonant control . . . 249

B.4.1 main function . . . 249

B.4.2 Combined linear model of controller and plant . . . 254

Abstract

Future power systems will source much of their electrical power from converter-based generation, be it a large scale HVDC link or a smaller system such as the back-to-back converter systems found in modern, variable-speed wind turbines. This is in stark contrast to the original AC power systems which used directly-coupled synchronous generation. The transition from the past power system to the future power system will produce power systems that have both low inertia, which compromises angular and frequency stability, and low short-circuit ratios, which compromises voltage stability.

In this thesis, the modelling and control of converter-based generation in low short-circuit ratio systems are investigated. For the modelling of AC power systems and the controllers being applied to the converter(s), the unified linear state-space approach is proposed. In this approach, linear state-space models of the electrical system are combined with linear state-space models in a manner which is highly scalable and sufficiently flexible to allow multiple control algorithms acting in a system instantaneously to be considered with relative ease.

Three control algorithms are considered in single converter systems: dq-axis vector current control, proportional resonant control, and power synchronization control. By adopting dq-axis vector current control, the system becomes ill-conditioned at the current level, primarily due to the dynamics of the phase-locked loop, which then causes stability issues for outer feedback loops (for example DC voltage and AC voltage controllers) which accompany the current controller. Proportional resonant control, also employing a phase-locked loop, exhibits poor dynamics in the low short-circuit ratio power system. By mimicking the basic synchronization process of a synchronous generator, power synchronization control is able to perform satisfactorily in a low short-circuit ratio system, much as a synchronous generator can.

Two algorithms are considered in the multi-converter, low short-circuit ratio systems: dq-axis vector current control and power synchronization control. Performance issues observed in single converter systems when dq-axis vector current control is applied are observed in the multi-converter systems. Additional sources of undesirable coupling between control loops at the current control level are observed, potentially placing more demands on the design of the outer control loops. Power synchronization control performs satisfactorily in the multi-converter systems; however, oscillatory behaviour does arise, which requires careful tuning of the controllers. In addition, it is shown that the introduction of converters using power synchronization control enables other converters (in the same system) using dq-axis vector current control to exhibit improved performance. This is due to power synchronization control causing a converter to act as an effective voltage source/regulator, and dq-axis vector current control relying on electrical proximity to a strong voltage source. This produces systems with improved conditioning, which will reduce the complexity of the design of outer controllers for dq-axis vector current controlled converters.

Keywords: control, modelling, HVDC, power systems, stability, voltage-source converter, weak AC systems, multiple-converter systems, power system planning

Acknowledgements

As a role model of mine would say, 'Alright, alright, alright'...

I would like to take this opportunity to express my humble gratitude to God, from whom all things come, for shining a light years after I had foresaken thee. Without you, I would not have been able to complete this work. I would also like to express my profound gratitude to my family, whose love and support have never gone missing when needed. Thanks to Andrew Smith and Professor William Leithead for providing me with the opportunity to work in wind engineering. I would like to extend my gratitude to Professors Mike Graham and Carlos Simao Ferreira and Dr Luis Recalde-Camacho. I would also like to thank Dr Khaled Ahmed, Dr Agusti Egea-Alvarez and Dr Rafael Pena-Alzola for their extremely useful feedback. Thanks also to my friends, particularly Eddie Corr, James Carroll, Wang Yue, Jiang Xu, Yu Mengran, Tim Rubert, Cagatay Cebeci, Efren Guillo Sansano, Euan MacMahon and Anthony Florida-James, who have been there during hard times.

Nomenclature

Controller terminology

con	converter
vcc	dq-axis vector current control
prc	proportional resonant control
psc	power synchronization control
pll	phase-locked loop
ζ	converter number

Control variables with superscript 'con' refer specifically to the outputs of the controllers, which form inputs to the electrical models. The superscript 'con' may be vcc, psc, or prc, depending on the control algorithm being applied to the converter under consideration. The exact converter to which a specific set/pair of control variables is referring is denoted by subscript 'ζ'.

Components

R_{c_ζ}	Resistive component of the phase reactor of converter ζ
L_{c_ζ}	Inductive component of the phase reactor of converter ζ
C_{f_ζ}	Capacitance of the filter of converter ζ
R_{t_ζ}	Resistance of the transmission line for converter ζ
L_{t_ζ}	Inductance of the transmission line for converter ζ

Phases, currents and voltages

$\theta_{\mathrm{v}_\zeta}^{\mathrm{abc}}$ Phase of the bridge voltage of converter ζ as expressed in the abc frame

$\theta_{\mathrm{v}_\zeta}^{\mathrm{g}}$ Phase of the bridge voltage for converter ζ as expressed in the grid dq frame

$\theta_{\mathrm{v}_\zeta}^{\mathrm{c}}$ Phase of the bridge voltage for converter ζ as expressed in the dq frame established by the PLL/PSC embedded in converter ζ

$\theta_{\zeta}^{\mathrm{abc}}$ Phase of the filter-bus voltage for converter ζ as expressed in the abc frame

$\theta_{\zeta}^{\mathrm{g}}$ Phase of the filter-bus voltage for converter ζ as expressed in the grid dq frame

$\theta_{\zeta}^{\mathrm{c}}$ Phase of the filter-bus voltage for converter ζ as expressed in the dq frame established by the PLL/PSC embedded in converter ζ

$\boldsymbol{i}_{\mathrm{c}_\zeta}^{\mathrm{abc}}$ Current flowing through the phase reactor of converter ζ as expressed in the abc frame

$\boldsymbol{i}_{\mathrm{c}_\zeta}^{\mathrm{g}}$ Current flowing through the phase reactor of converter ζ as expressed in the grid dq frame

$\boldsymbol{i}_{\mathrm{c}_\zeta}^{\mathrm{c}}$ Current flowing through the phase reactor of converter ζ as expressed in the dq frame established by the PLL embedded in converter ζ

$\boldsymbol{i}_{\mathrm{t}_\zeta}^{\mathrm{abc}}$ Current flowing through the transmission line of converter ζ as expressed in the abc frame

$\boldsymbol{i}_{\mathrm{t}_\zeta}^{\mathrm{g}}$ Current flowing through the transmission line of converter ζ as expressed in the grid dq frame

$\boldsymbol{i}_{\mathrm{t}_\zeta}^{\mathrm{c}}$ Current flowing through the transmission line of converter ζ as expressed in the dq frame established by the PLL embedded in converter ζ

$\boldsymbol{v}_{\zeta}^{\mathrm{abc}}$ Bridge voltage for converter ζ as expressed in the abc frame

$\boldsymbol{v}_{\zeta}^{\mathrm{g}}$ Bridge voltage for converter ζ as expressed in the grid dq frame

$\boldsymbol{v}_{\zeta}^{\mathrm{c}}$ Bridge voltage for converter ζ as expressed in the dq frame established by the PLL/PSC embedded in converter ζ

$\boldsymbol{e}_{\zeta}^{\mathrm{abc}}$ Filter-bus voltage for converter ζ as expressed in the abc frame

$\boldsymbol{e}_{\zeta}^{\mathrm{g}}$ Filter-bus voltage for converter ζ as expressed in the grid dq frame

$\boldsymbol{e}_{\zeta}^{\mathrm{c}}$ Filter-bus voltage for converter ζ as expressed in the dq frame established by the PLL/PSC embedded in converter ζ

$\boldsymbol{u}_{\zeta}^{\mathrm{abc}}$ Voltage at the network end of transmission line ζ as expressed in the abc frame

$\boldsymbol{u}_{\zeta}^{\mathrm{g}}$ Voltage at the network end of transmission line ζ as expressed in the grid dq frame

$\boldsymbol{u}_{\zeta}^{\mathrm{c}}$ Voltage at the network end of transmission line ζ as expressed in the dq frame established by the PLL/PSC embedded in converter ζ

Other

SCR	short-circuit ratio
PCC	point of common coupling

Chapter 1

Introduction

The continued displacement of conventional synchronous generators, predominantly driven by non-renewable energy sources, in favour of converter-interfaced generation, typically driven by renewable energy sources, is producing power systems with low short-circuit ratios (SCRs).

Vector current (dq-axis) control is a popular control approach for converters [1]. Control is implemented in a dq frame established by a phase-locked loop (PLL). The PLL employs a Park transformation to convert the voltage at the point of common coupling (PCC) into a dq frame. Assuming the PLL seeks to estimate the phase of the aforementioned voltage, the control objective of the PLL is to minimise the q-component of the transformed signal. To achieve this, the q component of the transformed voltage is fed into a loop filter, whose output passes through a voltage-controlled oscillator. The output of the voltage-controlled oscillator is an estimation of the phase of the voltage at the PCC; this output signal is then fed back into the aforementioned Park transformation.

As a result of the reduced SCR values expected in the future, it has been predicted that VCC will experience undesirable coupling. Indeed, in the single-converter case, it has been reported that a converter may become unstable when the active power output exceeds 0.4 p.u. in systems with a short-circuit ratio of one when the converter adopts VCC [2]; with significant tuning effort, this result was boosted to 0.6 p.u [3][4]. However, this is still far short of the ratings for which the converter will have been designed.

In [3], it was shown that in a low SCR system the two inner current control loops were strongly coupled, particularly in the low frequency region (sub 100 rad/s), which lies inside the region where outer controllers will be most active. In short, an ill-conditioned system is produced which, from the perspective of outer active-power and AC-voltage magnitude controllers, will be difficult to control [4]. Indeed, instabilities in VCC in the low SCR systems have been demonstrated multiple times with the relevant literature pointing to PLL dynamics having a negative impact [2], [3], [5], [6], [7], [7]. A solution involving non-linear decoupling outer controllers, enabling a converter using VCC to operate at 0.8 p.u. when the SCR is one is presented in [5]; studies were constrained to single-converter systems and those where the SCR is fixed [5].

Given the performance issues associated with the PLL, alternative control schemes have been proposed which bypass the need for a PLL [4], [6], [8]. In this family of controllers, synchronization is achieved by mimicking the way in which a synchronous generator maintains synchronism in a power system; that is, perturbations in the power output of a converter translate to perturbations in the bridge voltage phase angle. By synchronizing by power flow considerations, the converter is able to behave as a voltage source, much in the same way a synchronous generator does. The degree to which a controller forces the converter to behave as a synchronous machine varies: at one extreme, there are synchronverters which have all generator dynamics embedded into the controller [8]; on the other, only the basic synchronization mechanism is adopted, an example of which is the Power-Synchronization Controller (PSC) [4]. In [9], a small power system comprising a synchronous generator, an induction machine, a single converter controlled using the PSC algorithm, and a simple RLC load was analysed. However, this study was constrained to systems in which there was only one converter presented.

Generally speaking, multi-converter studies are fairly limited in their scope. For example, in both [10] and [11], all converters in the power system used the same controller topology. In [12], the stability of a simple power system comprising two converters and a synchronous generator was assessed. One converter was controlled using VCC, while the second employed a virtual synchronous machine (VSM) control algorithm. It was shown that the presence of a converter using VSM allowed the converter using VCC to operate in conditions it would otherwise not have been able to do so. However, this analysis involved fixing the power set-points of the converters at 30% of their

rated powers (in line with the capacity factor of a wind turbine), which, to a significant extent, eliminates issues associated with the performance of the PLL (this statement may be corroborated by considering [3]).

With the controller varying from one converter to another in any single power system, such would be the case where multiple manufacturers are involved and installation dates vary, there is a need to investigate interactions between converters on all levels, theoretical and practical.

1.1 Project objectives and outline of the thesis

The objectives of this project are as follows:

1. Investigate the performance of control algorithms in single-converter systems, identifying key factors adversely affecting system performance.
2. Develop a unified approach for modelling multi-converter systems where mixtures of control algorithms may, simultaneously, be active.
3. Investigate the performance of multi-converter systems covering a range of system configurations.

This project involves both theoretical analysis and time domain simulations. The outline of this thesis is as follows:

1. In chapter two, a review of converter control algorithms is presented, including, but not limited to, dq-axis vector current control, proportional resonant control and power synchronization control. Where applicable, literature illustrating their performance in multi-converter systems is detailed.
2. In chapter three, the linear state-space model of the electrical part of a single converter system is outlined, with the resulting model being applied in the following four chapters.
3. In chapter four, a linear state-space model of the dq-axis vector current control scheme is presented, covering both the employment of first and second order phase-locked loops (PLLs). The linear state-space model is also developed to allow the effects of outer controllers to be

studied. This linear model is linked with the electrical model outlined in chapter three, with the resulting unified linear models being validated through frequency scanning of a non-linear model. The linear model is also used to assess system performance across a range of operating points, covering variations in both power set point and short-circuit ratio.

4. In chapter five, a linear model of the proportional resonant control scheme is presented, covering both the employment of first and second order PLLs. The linear model is linked with the electrical model outlined in chapter three, with the resulting unified models being validated through frequency scanning of a non-linear model. The linear model is also used to assess system performance across a range of operating points, covering variations in both power set point and short-circuit ratio.

5. In chapter six, a linear state-space model of the power synchronization control scheme is presented. This linear model is linked with the electrical model outlined in chapter three, with the resulting unified linear models being validated through frequency scanning of a non-linear model. The linear model is also used to assess system performance across a range of operating points, covering variations in both power set point and short-circuit ratio.

6. In chapter seven, the linear model presented in chapter three is extended to cover systems comprising multiple converters. This is then combined with the linear state-space models of the controllers developed in chapters four and six to give a unified linear state-space model which is then used to assess system performance across a range of operating points, covering variations in controllers, power set points and short-circuit ratios.

7. In chapter eight, the findings of this thesis are summarised in the conclusions, and suggestions are made for future work.

1.2 Scientific contributions of this thesis

The main contributions of this thesis are as follows:

1. A novel toolbox is developed, through application of the unified linear state-space model, that can be used to study the small-signal stability of multi-converter systems where a system

comprises mixtures of control algorithms acting simultaneously.

2. The sources of coupling between control loops in multi-converter systems where only dq-axis vector current control is applied is demonstrated, which impacts on the design of outer loop controllers. Specifically, it is shown that voltage stiffness is so compromised in low short-circuit ratio systems that attempting to control power output on a converter results in larger changes in the power output of another converter than it does on the first converter (when all converters use dq-axis vector current control).

3. The interactions between two converters controlled using power synchronization control is studied, with oscillatory behaviour similar to that seen in multi-synchronous generator systems being observed.

4. The ability of power synchronization control to boost system conditioning from the perspective of the current controllers in dq-axis vector current control is demonstrated.

Chapter 2

Background and review

In this chapter, a review of existing work is presented. This includes studies of dq-axis vector current control along with a review of possible alternative control algorithms, highlighting their relative benefits and weaknesses. The assessment of said controllers in multi-converter systems is also covered.

2.1 Converter topology

Power electronic converters in power systems are found in a wide range of applications, ranging from HVDC systems to wind turbines and electric vehicles. Their role is to enable the connection of a DC power supply to an AC power system, or vice versa. An AC waveform is synthesised from a DC signal (and vice versa) by an appropriate switching sequence. In the simplest configuration for a three-phase system, a set of six thyristors are present as shown in figure 2.1.

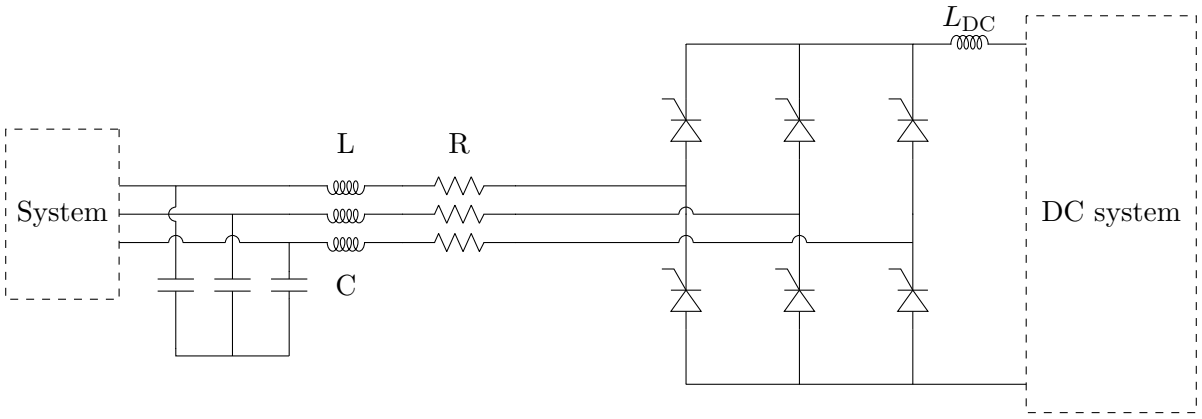

Figure 2.1: Thyristor-based converter using an LC filter [13].

The thyristor acts as a switch, conducting when the gate receives a current trigger, and continuing to do so until the voltage across the device is reversed [14]. Thus, thyristors can only be controlled one-way. As the switching off process is dictated by the voltage of the AC system, thyristor-based converters are referred to as line-commutated converters (LCC). By their very nature, the performance of LCC systems is dictated by the dynamics of the AC system to which they connect. Specifically, LCC systems experience commutation issues when the short-circuit ratio is below 1.5 [14].

The general lack of controllability of the LCC system led to the development of power electronic systems which employed more flexible devices than the thyristor such as insulated gate bipolar transistors (IGBTs). In this case, the modulation process can, in principle, be set without any need for an external voltage signal. IGBT-based converters are loosely referred to as voltage source converters; however, this naming convention should not always be applied since whether or not the

converter behaves as a voltage source is subject to the control algorithm applied.

One implementation of the IGBT is simple six-pulse IGBT-based converter, shown in figure 2.2:

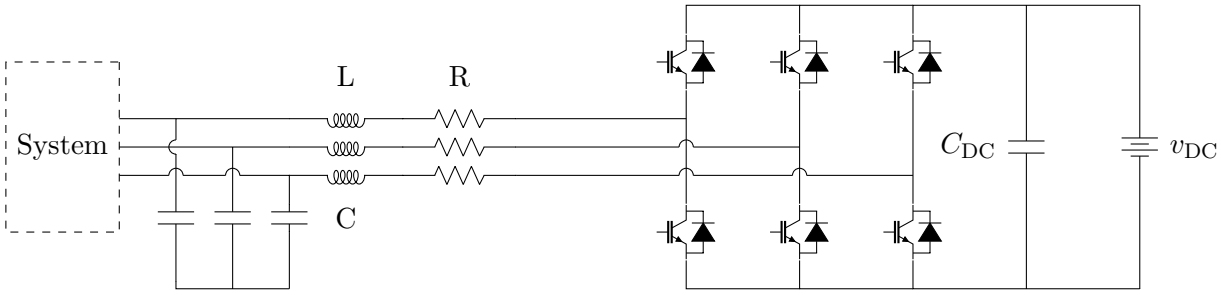

Figure 2.2: Two-level LC-filtered IGBT-based converter

To assist with grid code compliance, this content needs to be removed. The simplest form of filter is the inductor. However, this is often insufficient and so a capacitor bank is introduced as shown in figure 2.2.

It is commonplace to adopt single-line representations for convenience as shown in figure 2.3. Moreover, studies investigating the voltage stability of converters represent the power system by a simple RL circuit combined with a slack bus as shown.

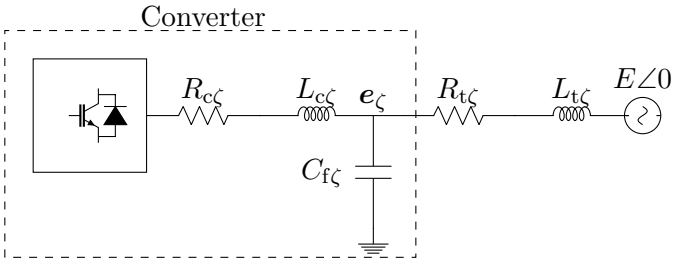

Figure 2.3: Single line illustration of a converter with an LC filter feeding a transmission line.

The subscript ζ is to identify which converter is being referred to; for example, $\zeta = 1$ means that converter one is being studied. This additional information is included in the labelling and subsequent model to enable efficient extension of the model to multi-converter systems, which are covered in chapter 7.

The resistance and inductance of the coupling inductance are given by R_{c_ζ} and L_{c_ζ} respectively; C_{f_ζ} is the capacitance in the LC filter; R_{t_ζ} and L_{t_ζ} are the resistance and inductance of a Thevenin

equivalent model of the grid (which includes the slack bus whose voltage is E). In the multi-converter studies, R_{t_ζ} and L_{t_ζ} will represent the resistance and inductance of a local line connecting converter ζ to a wider network.

Careful tuning of the controller in conjunction with appropriate values for L_{c_ζ} and C_{f_ζ} are required as it is particularly important to avoid exciting a resonant frequency.

While an LC or LCL filter does successfully remove the bulk of high frequency content from the output signal of a converter, thereby making it grid compliant, filtering equipment can be expensive; furthermore, filtering equipment can consume a lot of space. For offshore installations, this is particularly undesirable as the required structures to house such equipment push the cost of the project up considerably. To facilitate the removal of filtering equipment, there has been an uptake of interest in the Modular Multilevel Converter concept (MMC) in the last decade [15][16].

2.2 DQ-axis vector current control

2.2.1 Basic structure

The conventional converter control algorithm is dq-axis vector current control, which is illustrated in figure 2.4:

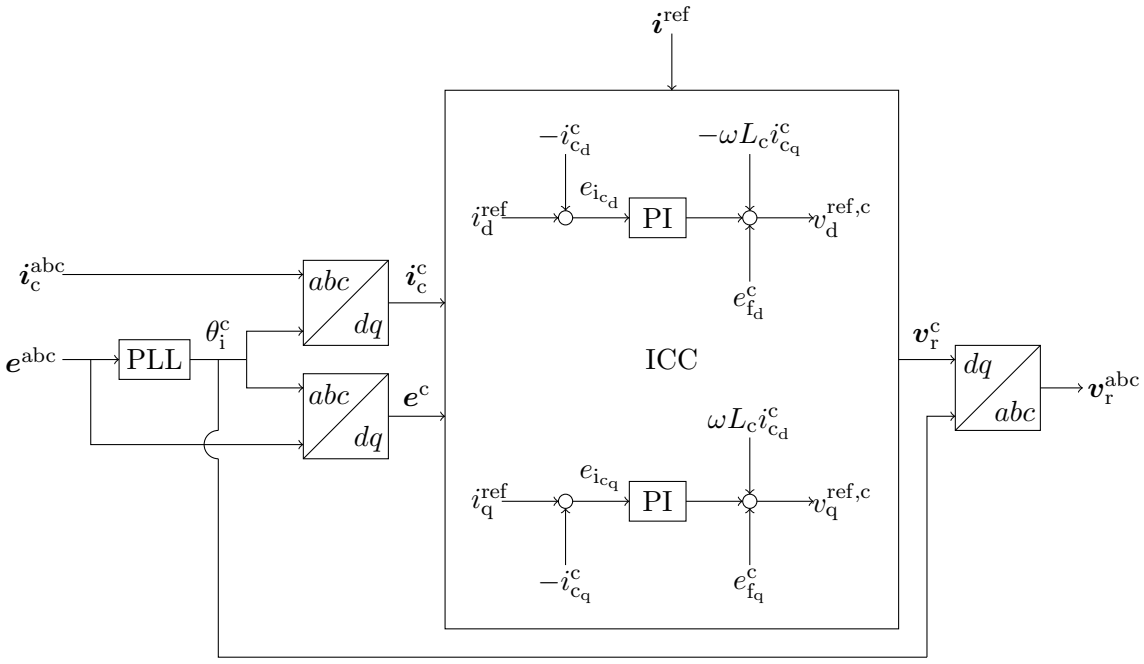

Figure 2.4: Overview of the dq-axis vector current control scheme including the frame transformations and PLL. The inner current controller block, ICC, contains two control loops, each with their own PI controller. The outer loop controllers are omitted in this block diagram.

Control is carried out in a dq frame established by a phase-locked loop, PLL. The role of the PLL is to achieve synchronization with some reference signal from the power system, typically the voltage at the point of common coupling, PCC. PLLs typically comprise a Park transformation and a PI controller [17]. The PLL takes as its input whatever signal it is trying to synchronise with, and applies to it the Park transformation. The Park transformation converts any three-phase signal expressed in a stationary reference frame into a two-phase signal expressed in a rotating reference frame, with the phase of the rotating reference frame being determined from a PI controller. These two components are referred to as the direct, d, and quadrature, q, components. Since the q component of the transformed reference signal is zero when synchronisation with the reference signal is achieved, the PI controller thus acts to minimise the q component of the transformed reference signal. For a second-order PLL, the output of the PI controller is an estimation of the perturbation in the angular grid frequency, $\Delta\omega$, which is combined with the nominal angular grid frequency, ω_0, with the result being integrated to give the estimation of the phase. Such a PLL is shown in figure 2.5:

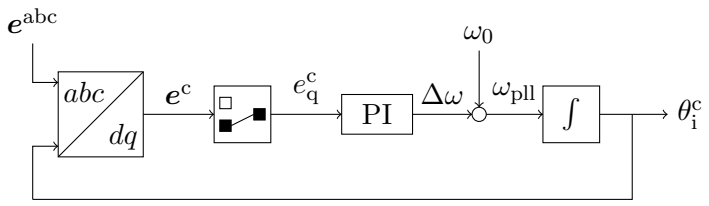

Figure 2.5: Basic second-order PLL structure. ω_{pll} is the PLL estimation of the grid angular frequency.

If the grid frequency is assumed to be constant, the PLL can be simplified such that the estimation of the phase is the sum of the output of the PI controller and an additive term, $\omega_0 t$, where t is the time. Such a PLL is referred to as a first-order PLL and is shown in figure 2.6:

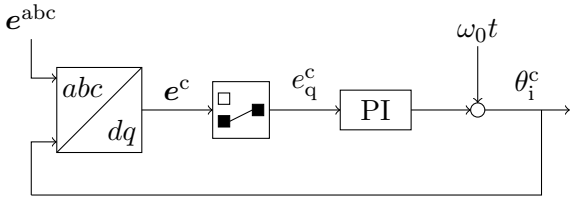

Figure 2.6: Basic first-order PLL structure.

Let us now note that power and reactive power, as expressed in a dq frame, are given by equations 2.1 and 2.2 respectively:

$$P = e_{\mathrm{d}} i_{\mathrm{d}} + e_{\mathrm{q}} i_{\mathrm{q}} \tag{2.1}$$

$$Q = e_{\mathrm{q}} i_{\mathrm{d}} - e_{\mathrm{d}} i_{\mathrm{q}} \tag{2.2}$$

where P and Q are the active and reactive power respectively, and $\boldsymbol{e}_{\mathrm{dq}}$ and $\boldsymbol{i}_{\mathrm{dq}}$ are the voltage and current components at the point of interest respectively.

If the reference signal used by the PLL is the voltage at the PCC and voltage fluctuations are negligible, it follows that changes in active power flowing through the PCC are directly proportional to changes in the d component of the current and independent of the q component of the aforementioned current, while the reverse is the case for the reactive power. Thus, in this scenario, control over active power may be achieved by controlling the d component of the current, while control

over reactive power/AC voltage is achieved through controlling the q component of the current. Thus, two PI-based inner control loops are present in dq-axis vector current control: one which acts on the d component, and one which acts on the q component. Assuming the PLL is operating satisfactorily, only weak coupling between the two loops is present due to the fundamental nature of the Park transformation; this may easily be accommodated for with simple feed-forward terms.

Reference current d and q values are set by outer controllers. Assuming the PLL synchronises with the voltage at the PCC, the d-component reference value may be set by either an active power controller or a DC bus voltage controller, while the q-component reference value may be set by either a reactive power controller or an AC voltage controller.

Between the inner and outer control loops are limiters; that is, the inner loops will only act on bounded values of i_{d} and i_{q}. This is to limit the current flowing through the converter, thus providing fault tolerance. When applying limiters, the control scheme requires anti-wind up loops also.

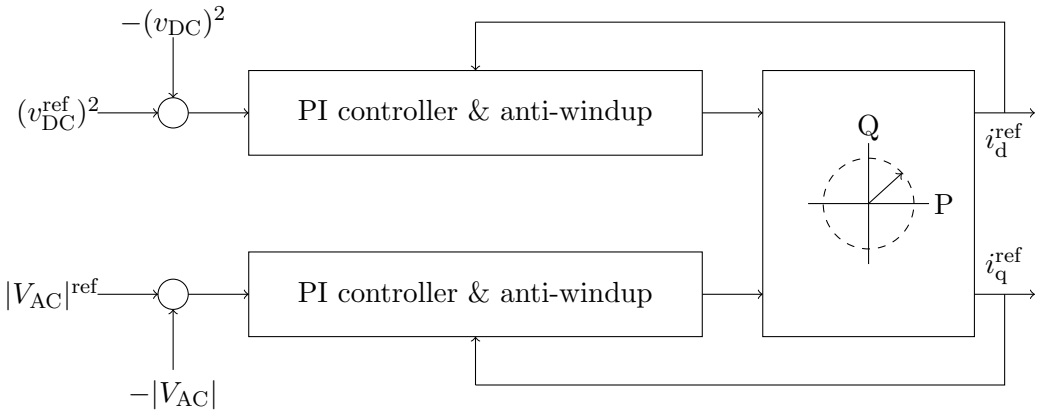

Figure 2.7: Possible outer controllers in the dq-axis vector current control scheme. The square of the DC bus voltage is used such that the dynamics are independent of operating point.

Droop controllers, both for frequency and voltage, may be introduced to, in some specific circumstances, boost system stability, examples of which may be found in [18].

For completeness, if the reference signal used by the PLL is not the voltage at the PCC, active and reactive power of both functions of both the d and q components of the current. However, control

over active and reactive power may be achieved through a reformulation of equations 2.1 and 2.2:

$$\begin{bmatrix} P \\ Q \end{bmatrix} = \begin{bmatrix} e_{\mathrm{d}} & e_{\mathrm{q}} \\ e_{\mathrm{q}} & -e_{\mathrm{d}} \end{bmatrix} \begin{bmatrix} i_{\mathrm{d}} \\ i_{\mathrm{q}} \end{bmatrix} \tag{2.3}$$

Thus,

$$\begin{bmatrix} i_{\mathrm{d}}^{\mathrm{ref}} \\ i_{\mathrm{q}}^{\mathrm{ref}} \end{bmatrix} = \frac{1}{e_{\mathrm{d}}^2 + e_{\mathrm{q}}^2} \begin{bmatrix} e_{\mathrm{d}} & e_{\mathrm{q}} \\ e_{\mathrm{q}} & -e_{\mathrm{d}} \end{bmatrix} \begin{bmatrix} P^{\mathrm{ref}} \\ Q^{\mathrm{ref}} \end{bmatrix} \tag{2.4}$$

Historically, tuning of the inner current controller involves ignoring the dynamics of the PLL [18][19][20][21]. The only part of the electrical system to be modelled in the bulk of analyses of the inner current controller is the phase reactor which links the converter terminal to the PCC. This does have the advantage of yielding simple transfer functions which can be used to guide the design of the current controllers [19][22].

2.2.2 Studies on stability of dq-axis vector current control

In [5], it was demonstrated that dq-axis vector current control experienced performance difficulties in systems with low short-circuit ratios. A non-linear (gain-scheduled) decoupling controller of the form shown in figure 2.8 was appended to the basic dq-axis vector current control. The gains of the controllers were set according to the power set point. Such an approach significantly increases the complexity of the controller. Results were only presented for a single converter operating in a system with a short-circuit ratio of one. In other words, it was not shown how the control solution performs when the short-circuit ratio varies, or when there are multiple converters present in the system. This brings up the question of how is the controller scheduled? If the short-circuit ratio is fixed, the gain-scheduling could be set according to the power set point. However, as the short-circuit ratio changes, the gain scheduling will not perform as expected. The degree to which it does not would depend on how finely tuned the original controller was. Alternatively, the gain-scheduling could be set according to the load angle at the PCC. However, this is also problematic since it would require knowledge of the phase *relative* to a reference point where the voltage is stiff. The latter method, if possible, would at least allow for more effective gain-scheduling.

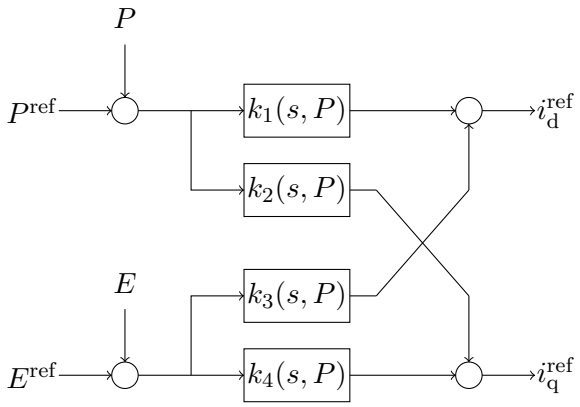

Figure 2.8: Illustration of a decoupling controller. For proportional resonant control, k_3 may not be necessary, which reduces both the complexity of the design task, while reducing the chance of developing a solution which is overly sensitive to uncertainties in the grid impedance.

Durant showed that the PLL dynamics may become significant when the reference signal is not stiff [2]. Under these circumstances, the low-bandwidth nature of the PLL means that the q component of the transformed signal is not zero. Thus, the 'd' and 'q' components as created by the PLL phase angle are functions of the real 'd' and 'q' components which would arise if the real phase were used. That is, control over active and reactive power becomes coupled in a manner that cannot be easily compensated.

A study by Givaki permitted investigation of the stability margins of dq-axis vector current control[7]. The study was restricted to a specific form of PLL, which involved inverse tangent operations seldom seen in standard PLLs.

Zhang specifically focused on the standard implemention of dq-axis vector current control; that is, one where the PLL reference signal is the voltage at the point of common coupling. In his work, it was shown that dq-axis vector current control would encounter performance issues when the system to which it was supplying power was of high impedance[3]. Only a 1st order PLL was studied with an LC filter being employed.

2.3 Alternatives to dq-axis vector current control

Zmood et al proposed the proportional resonant controller [23][24], sometimes referred to as the $\alpha\beta$ vector current controller, whose structure is illustrated in figure 2.9.

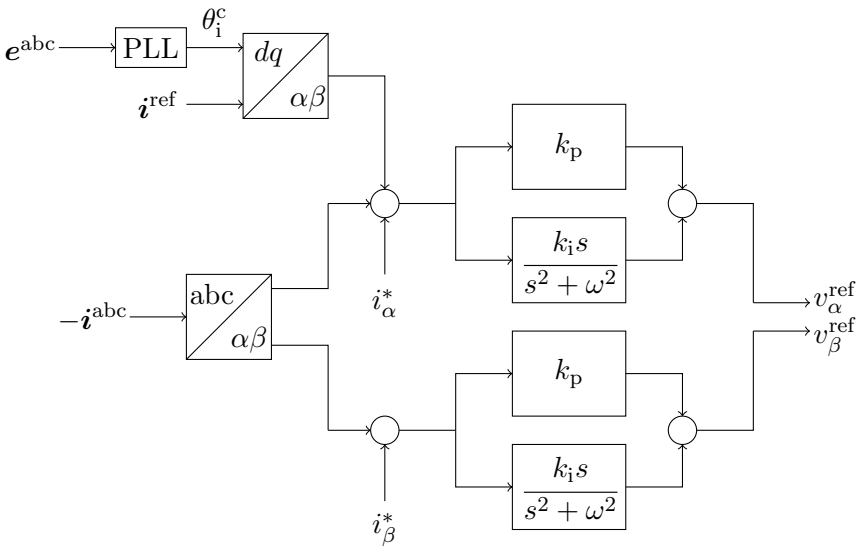

Figure 2.9: Block diagram illustrating the proportional resonant controller. The α-β output signals are converted to abc signals by a simple inverse Clarke transform.

The proportional resonant controllers mean that there is no need for the PLL phase angle to be applied *after* the resonant controllers. This means that the degree of parallel control loops present is reduced. Papers have shown variants of proportional resonant control being applied to converters on doubly-fed induction generator wind turbines [25][26] and MMC-HVDC [27]. However, to the author's best knowledge, no studies have been presented investigating the performance of proportional resonant controllers in weak AC systems.

After demonstrating performance issues with dq-axis vector current control, Zhang proposed the power synchronization control algorithm [3]. In this algorithm, synchronization is achieved by power flow considerations; specifically, the phase angle is modified according to discrepancies between the power reference of the converter and the actual power being exported to the AC network (as measured at the point of common coupling). Thus, the basic power synchronization controller structure is as shown in figure 2.10:

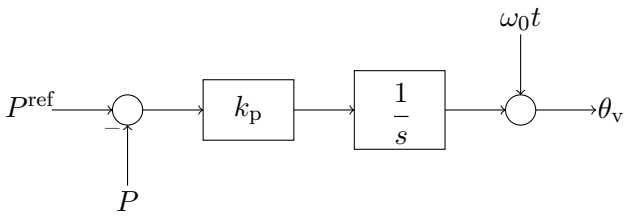

Figure 2.10: Basic power synchronization controller (suitable only for fixed-frequency systems).

The output of the power synchronization controller may then be used to transform to and from a rotating reference frame.

Operating in conjunction with the power synchronization controller was an AC voltage controller which attempts to control the voltage magnitude at the point of common coupling, E:

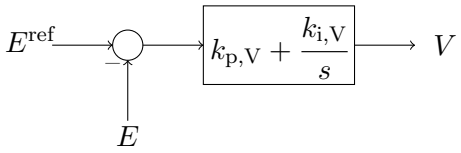

Figure 2.11: AC voltage controller that operates in parallel with the power synchronization controller

The AC voltage controller sets the magnitude of the voltage to be produced at the bridge terminal. This is coupled with θ from the power synchronization controller to set $\boldsymbol{v}_{\text{abc}}^{\text{ref}}$.

Given that power synchronization control attempts to create a dq frame aligned with the bridge voltage, the 'unfiltered' (for reasons about to be discussed) voltage reference as expressed in the controller dq frame may be expressed as $\boldsymbol{v}_{\text{un}}^{\text{ref,c}} = \begin{bmatrix} V & 0 \end{bmatrix}^{\text{T}}$.

Owing to the low resistance of converter filtering equipment, the above control system would excite a poorly damped resonance. In order to avoid this, the reference voltage for the converter bridge, as expressed in the converter dq frame, is set according to equation 2.5:

$$\boldsymbol{v}^{\text{ref,c}} = \boldsymbol{v}_{\text{un}}^{\text{ref,c}} - H_{\text{HP}}(s)\boldsymbol{i}_{\text{c}}^{\text{c}} \tag{2.5}$$

where $H_{\mathrm{HP}}(s)$ is a high pass filter of the form

$$H_{\mathrm{HP}}(s) = \frac{k_{\mathrm{v}} s}{\alpha_{\mathrm{v}} + s} \tag{2.6}$$

where k_{v} and α_{v} are respectively the gain and crossover frequency associated with the high pass filter. $\boldsymbol{i}_{\mathrm{c}}^{\mathrm{c}}$ is the current flowing through the phase reactor as expressed in the converter dq frame.

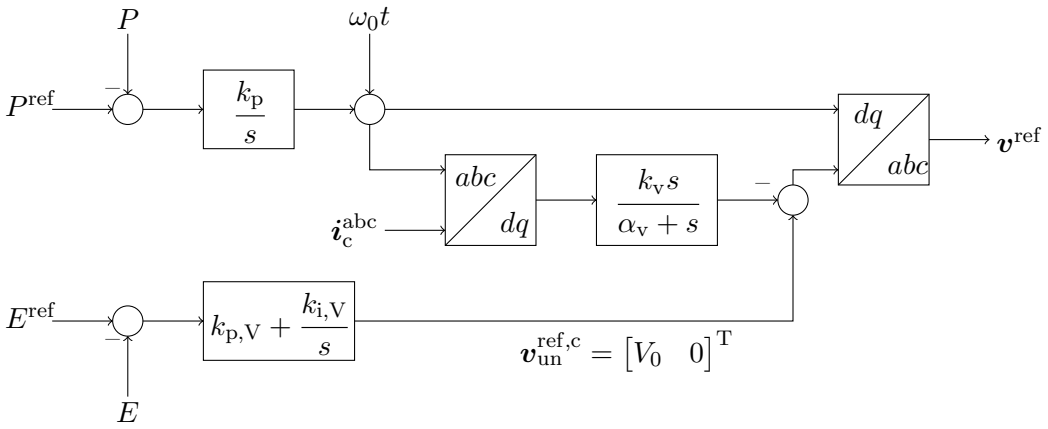

Figure 2.12: Combined power synchronization control system with damping

When the system to which the converter was providing power did not have a stiff frequency, a droop controller was appended to the power synchronization controller as shown:

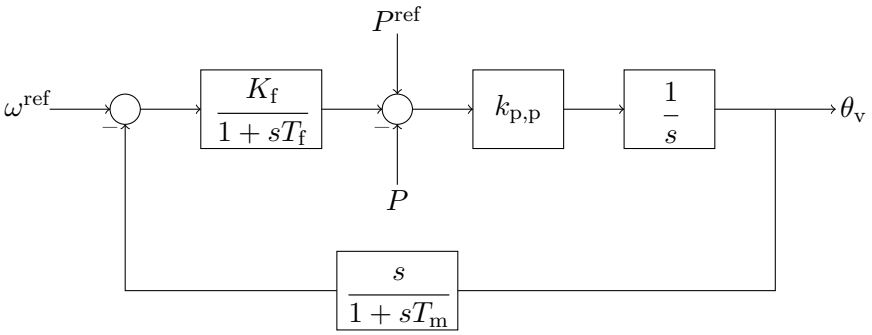

Figure 2.13: Modified power synchronization controller to provide frequency droop support

It was demonstrated that power synchronization control facilitated the stable operation of a converter in a low-inertia system, specifically a micro-grid [9]. Originally, the converter would employ dq-axis vector current control to ensure fault ride-through capabilities. More recently, Mitra applied

the power synchronization controller to a model of an offshore wind farm connected by a HVDC link [28].

Ashabani and Mohamed proposed a control system which emulates a synchronous machine in [29][6]. Variations of the virtual synchronous machine concept were proposed. Specifically, one control algorithm was proposed for frequency and DC-link regulation which was based on virtual torque control, while the second was based on direct DC-link voltage control, respectively shown in figures 2.14 and 2.15:

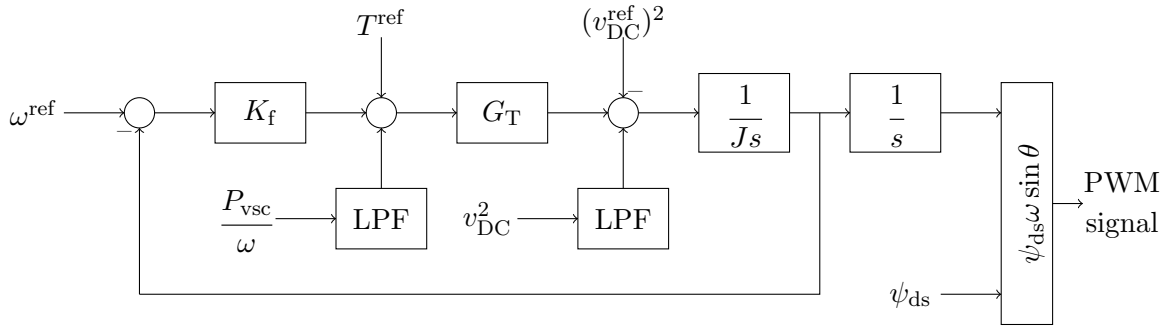

Figure 2.14: Virtual torque control strategy for frequency and DC-link voltage regulation

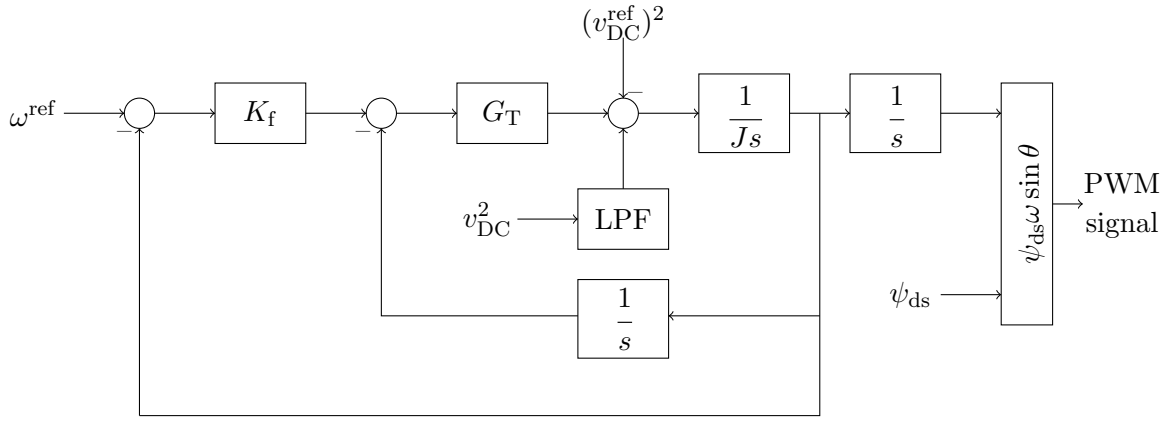

Figure 2.15: Direct DC-link voltage control strategy for frequency and DC-link voltage regulation

The virtual flux term, ψ_{ds} was set either by a reactive power controller, or an AC voltage controller, respectively shown in figures 2.16 and 2.17:

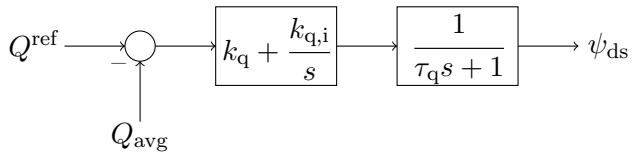

Figure 2.16: Control topology for virtual flux regulation that achieves constant reactive power operation.

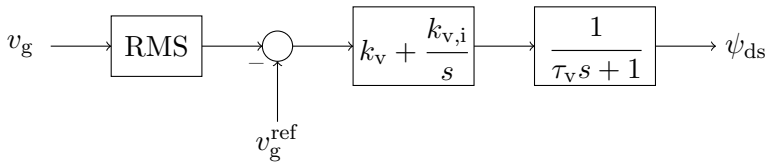

Figure 2.17: Control topology for virtual flux regulation that achieves constant voltage operation.

A rigorous small-signal stability analysis is presented for the proposed control algorithm, suggesting the stability margins and providing guidelines for tuning the controllers.

Subsequently, the proposed algorithms were compared with dq-axis vector current control. In both pieces of work, a single converter was present, feeding power into a simple network comprising a resistive load only i.e. there were no inductive/capacitive loads.

Zhong and Weiss developed a control algorithm that caused an inverter to have almost identical dynamics to a synchronous generator, leading to the system (inverter plus control algorithm) being termed a synchronverter [8][30]. The control system is shown in figure 2.18:

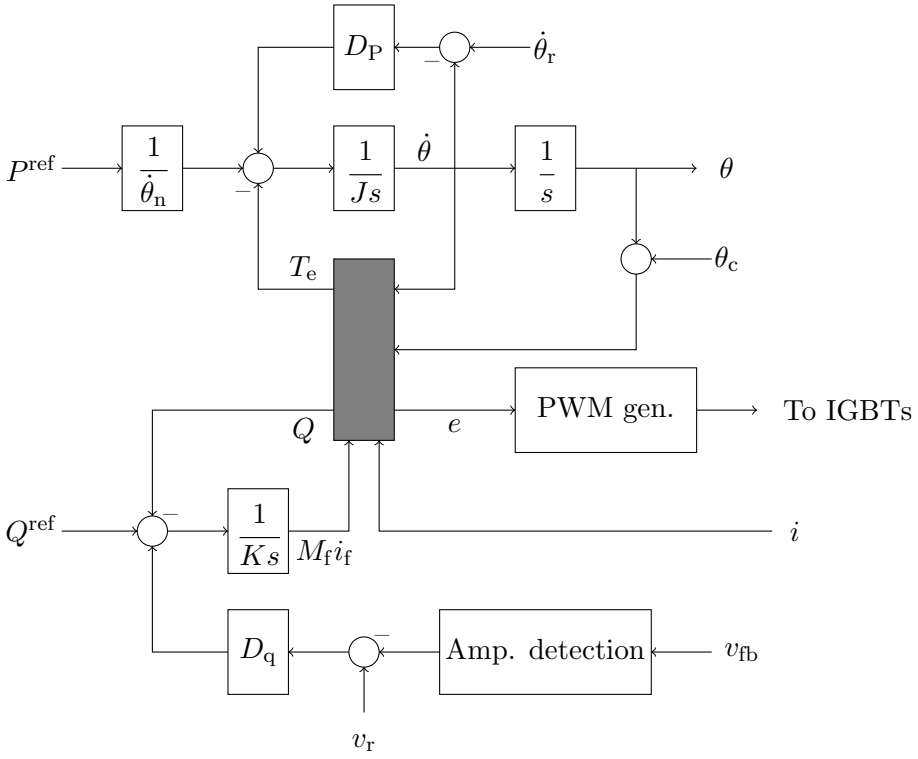

Figure 2.18: Synchronverter controller. The grey box contains equations which link flux to electrical torque.

Both simulation and experimental results were presented. However, in neither case were results presented which evaluate the performance of the inverter during a fault. Moreover, the topology of the network to which the inverter was connected was not specified.

2.4 Remarks about the literature

There is nothing in the GB grid codes requiring the developer of a renewable energy device to control the converter as though it were a synchronous machine (in any sense). Accordingly, at present, developers of renewable energy devices continue to opt for the tried and tested dq-axis vector current control or, as seems to be the case for some manufacturers of PV panels, proportional resonant control.

In all of the aforementioned cases, studies were not conducted showing the dynamics of a power system that comprised multiple converters, with some being controlled using conventional control

(dq-axis vector current) and some using some algorithm which mimics, to one degree or another, a synchronous machine. Since almost all installed converters will employ the dq-axis vector current control algorithm, this is an important study to conduct.

Pogaku and Banadaki presented multi-converter analyses, but did not consider systems in which different controllers were active at any instant in time [10][11]. All converters used dq-axis vector current control. Moreover, the impact of weak systems was not studied.

Chapter 3

Single-converter system configuration

In this chapter, an introduction to single converter systems is provided, with the definitions being given in this chapter being recycled in the subsequent three chapters.

The single converter system models serve as a stepping stone to the development of linear models in which multiple converters are present, with a given multiple-converter system potentially featuring a mixture of controllers.

3.1 Broad definitions & scope

3.1.1 Power system definitions

In the analysis of single converters, the following power system is adopted:

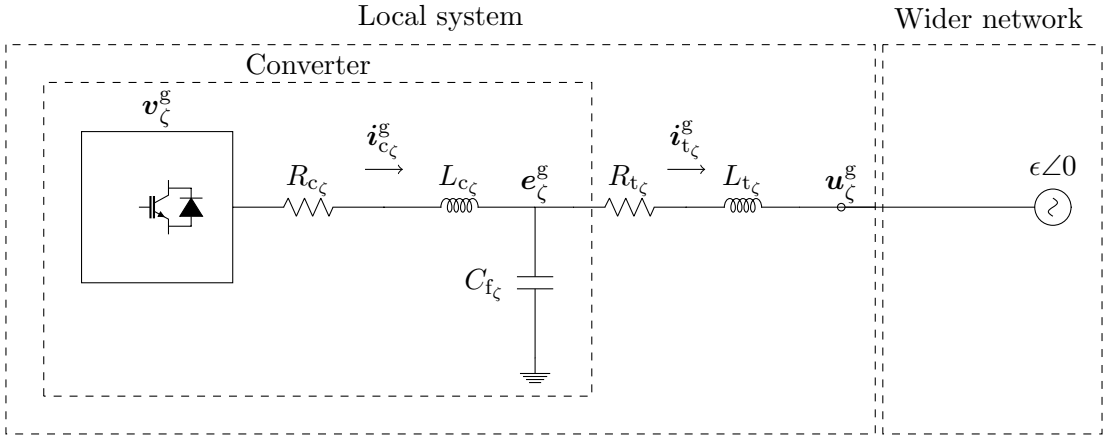

Figure 3.1: Baseline power system used for stability studies.

Here, R_{c_ζ} and L_{c_ζ} define the characteristics of the phase reactor in the AC filter of converter ζ. A capacitor bank may or may not be present.

To allow the models to be easily integrated into the multi-converter model described in chapter 7, the generalised local state-space models developed will include the option of applying perturbations to the voltage, $\boldsymbol{u}_\zeta^{\mathrm{g}}$. As a result, the generalised local state space models of the electrical part of the system will take on the following form:

$$\frac{\mathrm{d}\boldsymbol{x}_{\mathrm{E}_\zeta}^{\mathrm{loc}}}{\mathrm{d}t} = \boldsymbol{A}_{\mathrm{E}_\zeta}^{\mathrm{loc}}\boldsymbol{x}_{\mathrm{E}_\zeta}^{\mathrm{loc}} + \boldsymbol{B}_{\mathrm{E}_\zeta}^{\mathrm{loc}}\boldsymbol{z}_{\mathrm{E}_\zeta}^{\mathrm{loc}} + \boldsymbol{B}_{\mathrm{E}_\zeta}^{\mathrm{lin}_1}\boldsymbol{z}_{\mathrm{E}_\zeta}^{\mathrm{lin}} \tag{3.1}$$

where the subscript E is included simply to make it clear that the model is referring to the electrical part only i.e. the control system dynamics are not covered in this part of the overall models. The superscript 'loc' refers to the local system part of the model.

Regardless of which controller is chosen, the controller will always set the voltage reference at the bridge, $\boldsymbol{v}_\zeta^{\mathrm{ref}}$. Delays in the PWM process may be represented as $\boldsymbol{v}_\zeta^{\mathrm{g}} = e^{-st_{\mathrm{d}}}\boldsymbol{v}_\zeta^{\mathrm{ref}}$ where t_{d} is the delay,

which may in turn be approximated using a Padé approximant. Thus, the control vector of the state-space model of the electrical part of the system, $\boldsymbol{z}_{\mathrm{E}}^{\mathrm{loc}}$, is easily linked with the output vector of the controller. The 'pseudo' control vector, $\boldsymbol{z}_{\mathrm{E}}^{\mathrm{lin}}$, is the voltage at the end of the local system, $\Delta\boldsymbol{u}_{\zeta}^{\mathrm{g}}$.

When considering the single converter cases, the wider network is just a slack bus and so the voltage $\boldsymbol{u}_{\zeta}^{\mathrm{g}}$ becomes stiff. Accordingly, for the single-converter systems *only*, the $\boldsymbol{B}_{\mathrm{E}}^{\mathrm{lin}_1}\boldsymbol{z}_{\mathrm{E}}^{\mathrm{lin}} = 0$ for the linear models. In this case, the standard state-space model form is produced:

$$\frac{\mathrm{d}\boldsymbol{x}_{\mathrm{E}_1}^{\mathrm{loc}}}{\mathrm{d}t} = \boldsymbol{A}_{\mathrm{E}_1}^{\mathrm{loc}}\boldsymbol{x}_{\mathrm{E}_1}^{\mathrm{loc}} + \boldsymbol{B}_{\mathrm{E}_1}^{\mathrm{loc}}\boldsymbol{z}_{\mathrm{E}_1}^{\mathrm{loc}} \tag{3.2}$$

$$\boldsymbol{y}_{\mathrm{E}_1}^{\mathrm{loc}} = \boldsymbol{C}_{\mathrm{E}_1}^{\mathrm{loc}}\boldsymbol{x}_{\mathrm{E}_1}^{\mathrm{loc}} + \boldsymbol{D}_{\mathrm{E}_1}^{\mathrm{loc}}\boldsymbol{z}_{\mathrm{E}_1}^{\mathrm{loc}} \tag{3.3}$$

The output vector can be directly linked to the input vector by a transfer function matrix using the previously stated state matrices in equation 3.4:

$$\boldsymbol{y}_{\mathrm{E}_1}^{\mathrm{loc}} = \underbrace{[\boldsymbol{C}_{\mathrm{E}_1}^{\mathrm{loc}}(s\boldsymbol{I} - \boldsymbol{A}_{\mathrm{E}_1}^{\mathrm{loc}})^{-1}\boldsymbol{B}_{\mathrm{E}_1}^{\mathrm{loc}} + \boldsymbol{D}_{\mathrm{E}_1}^{\mathrm{loc}}]}_{\boldsymbol{G}_1(s)}\boldsymbol{z}_{\mathrm{E}_1}^{\mathrm{loc}} \tag{3.4}$$

3.1.2 Variations in the converter control and filter equipment

Voltage source converters are connected to the grid either by an L-filter, LC-filter or LCL-filter [31][32]. The exact topology depends on the type of voltage source converter being employed.

A considerable amount of variation can be found in the dq-axis vector current control algorithm. First- and second-order PLLs will be considered in this work. The latter has the ability to track frequency deviations, while the former can only track phase (and operates on the assumption that frequency deviations are negligible).

Based on this, for single converter system analysis, small-signal stability analysis of the following control systems will be presented:

- DQ-axis vector current control:
  - LC filter using a first-order PLL
  - L filter using a first-order PLL

  - LC filter using a second-order PLL
  - L filter using a second-order PLL

- Proportional resonant control:
  - LC filter using a first-order PLL
  - L filter using a first-order PLL
  - L filter using a second-order PLL

- Power synchronization control:
  - LC filter
  - L filter

As can be seen, only a handful of topologies are considered. This is for brevity reasons; the author feels the range covered herein is sufficient to highlight key dynamics and trends. However, it should be noted that the modelling techniques outlined in this chapter may easily be applied to the variations not covered.

3.1.3 Grid dq frame

For this chapter, let us define the grid dq frame to be one rotating at a fixed frequency ω_0, where the d axis is aligned with the unperturbed voltage at the end of the transmission line, $\boldsymbol{u}$. Therefore, any balanced three-phase quantity with magnitude A_0 and instantaneous phase θ_{POI}, maps to $\boldsymbol{a}^{\text{g}}$ by equation 3.5:

$$\begin{aligned}\boldsymbol{a}^{\text{g}} &= A_0 \begin{bmatrix} \cos(\omega_0 t) & \cos(\omega_0 t - 2\pi/3) & \cos(\omega_0 t + 2\pi/3) \\ -\sin(\omega_0 t) & -\sin(\omega_0 t - 2\pi/3) & -\sin(\omega_0 t + 2\pi/3) \end{bmatrix} \begin{bmatrix} \cos(\theta_{\text{POI}}) \\ \cos(\theta_{\text{POI}} - 2\pi/3) \\ \cos(\theta_{\text{POI}} + 2\pi/3) \end{bmatrix} \\ &= \frac{3A_0}{2} \begin{bmatrix} \cos(\omega_0 t)\cos\theta_{\text{POI}} + \sin(\omega_0 t)\sin\theta_{\text{POI}} \\ \cos(\omega_0 t)\sin\theta_{\text{POI}} - \sin(\omega_0 t)\cos\theta_{\text{POI}} \end{bmatrix} \end{aligned} \tag{3.5}$$

For future reference, the superscript g denotes that the quantity is being expressed in the grid dq frame.

3.2 Linear model of electrical system

3.2.1 LC filter

Figure 3.1 represents a converter, ζ, with an LC filtered connected to a slack bus via a simple transmission line. In the grid dq frame, the dynamics of the system are as follows:

$$\begin{aligned}
L_{\mathrm{c}_\zeta}\frac{\mathrm{d}\boldsymbol{i}^{\mathrm{g}}_{\mathrm{c}_\zeta}}{\mathrm{d}t} &= \boldsymbol{v}^{\mathrm{g}}_{\zeta} - \boldsymbol{e}^{\mathrm{g}}_{\zeta} - R_{\mathrm{c}_\zeta}\boldsymbol{i}^{\mathrm{g}}_{\mathrm{c}_\zeta} + \omega_0 L_{\mathrm{c}_\zeta}\begin{bmatrix} 0 & 1 \\ -1 & 0 \end{bmatrix}\boldsymbol{i}^{\mathrm{g}}_{\mathrm{c}_\zeta} \\
C_{\mathrm{f}_\zeta}\frac{\mathrm{d}\boldsymbol{e}^{\mathrm{g}}_{\zeta}}{\mathrm{d}t} &= \boldsymbol{i}^{\mathrm{g}}_{\mathrm{c}_\zeta} - \boldsymbol{i}^{\mathrm{g}}_{\mathrm{t}_\zeta} + \omega_0 C_{\mathrm{f}_\zeta}\begin{bmatrix} 0 & 1 \\ -1 & 0 \end{bmatrix}\boldsymbol{e}^{\mathrm{g}}_{\zeta} \\
L_{\mathrm{t}_\zeta}\frac{\mathrm{d}\boldsymbol{i}^{\mathrm{g}}_{\mathrm{t}_\zeta}}{\mathrm{d}t} &= \boldsymbol{e}^{\mathrm{g}}_{\zeta} - \boldsymbol{u}^{\mathrm{g}}_{\zeta} - R_{\mathrm{t}_\zeta}\boldsymbol{i}^{\mathrm{g}}_{\mathrm{t}_\zeta} + \omega_0 L_{\mathrm{t}_\zeta}\begin{bmatrix} 0 & 1 \\ -1 & 0 \end{bmatrix}\boldsymbol{i}^{\mathrm{g}}_{\mathrm{t}_\zeta}
\end{aligned} \tag{3.6}$$

where $\boldsymbol{i}^{\mathrm{g}}_{\mathrm{c}_\zeta}$ is the converter current flowing through R_{c_ζ} and L_{c_ζ}, $\boldsymbol{v}^{\mathrm{g}}_{\zeta}$ is the bridge voltage, $\boldsymbol{e}^{\mathrm{g}}_{\zeta}$ is the filter bus voltage, ω_0 is the grid frequency, $\boldsymbol{i}^{\mathrm{g}}_{\mathrm{t}_\zeta}$ is the network current flowing through R_{t_ζ} and L_{t_ζ}, and $\boldsymbol{u}^{\mathrm{g}}_{\zeta}$ is the grid terminal voltage.

The power output from the converter is given by equation 3.7:

$$P_\zeta = e^{\mathrm{g}}_{\zeta\mathrm{d}} i^{\mathrm{g}}_{\mathrm{t}_\zeta\mathrm{d}} + e^{\mathrm{g}}_{\zeta\mathrm{q}} i^{\mathrm{g}}_{\mathrm{t}_\zeta\mathrm{q}} \tag{3.7}$$

The converter bridge voltage magnitude is given by equation 3.8:

$$V_\zeta = \sqrt{(v^{\mathrm{g}}_{\zeta\mathrm{d}})^2 + (v^{\mathrm{g}}_{\zeta\mathrm{q}})^2} \tag{3.8}$$

In steady-state, equations 3.7 and 3.8 are as follows:

$$\begin{aligned} P_{\zeta,0} &= e^{\mathrm{g}}_{\zeta\mathrm{d},0} i^{\mathrm{g}}_{\mathrm{t}\zeta\mathrm{d},0} + e^{\mathrm{g}}_{\zeta\mathrm{q},0} i^{\mathrm{g}}_{\mathrm{t}\zeta\mathrm{q},0} \\ V_{\zeta,0} &= \sqrt{(v^{\mathrm{g}}_{\zeta\mathrm{d},0})^2 + (v^{\mathrm{g}}_{\zeta\mathrm{q},0})^2} \end{aligned} \tag{3.9}$$

For each single-converter case study, the steady-state power output, the voltage at the end of the transmission line and the bridge voltage are specified.

The steady-state dynamics are simply those given above but with all derivative terms set to zero. In other words,

$$\begin{aligned} 0 &= \boldsymbol{v}^{\mathrm{g}}_{\zeta,0} - \boldsymbol{e}^{\mathrm{g}}_{\zeta,0} - R_{\mathrm{c}_\zeta} \boldsymbol{i}^{\mathrm{g}}_{\mathrm{c}_\zeta,0} + \omega_0 L_{\mathrm{c}_\zeta} \begin{bmatrix} 0 & 1 \\ -1 & 0 \end{bmatrix} \boldsymbol{i}^{\mathrm{g}}_{\mathrm{c}_\zeta,0} \\ 0 &= \boldsymbol{i}^{\mathrm{g}}_{\mathrm{c}_\zeta,0} - \boldsymbol{i}^{\mathrm{g}}_{\mathrm{t}\zeta,0} + \omega_0 C_{\mathrm{f}_\zeta} \begin{bmatrix} 0 & 1 \\ -1 & 0 \end{bmatrix} \boldsymbol{e}^{\mathrm{g}}_{\zeta,0} \\ 0 &= \boldsymbol{e}^{\mathrm{g}}_{\zeta,0} - \boldsymbol{u}^{\mathrm{g}}_{\zeta,0} - R_{\mathrm{t}_\zeta} \boldsymbol{i}^{\mathrm{g}}_{\mathrm{t}_\zeta,0} + \omega_0 L_{\mathrm{t}_\zeta} \begin{bmatrix} 0 & 1 \\ -1 & 0 \end{bmatrix} \boldsymbol{i}^{\mathrm{g}}_{\mathrm{t}_\zeta,0} \end{aligned} \tag{3.10}$$

The values $\boldsymbol{i}^{\mathrm{g}}_{\mathrm{c}_\zeta,0}$, $\boldsymbol{e}^{\mathrm{g}}_{\zeta,0}$ and $\boldsymbol{i}^{\mathrm{g}}_{\mathrm{t}_\zeta,0}$ are all unknowns.

Considering the expressions for steady-state power output and steady-state bridge voltage, there are eight equations. Note that the expression for the voltage magnitude is a non-linear equation. Hence, an iterative solver can be applied to determine all the remaining steady-state values. A MATLAB implementation of this solver can be found in the Appendix.

Perturbing the system and linearising results in the following:

$$\frac{\mathrm{d}\Delta \boldsymbol{i}^{\mathrm{g}}_{\mathrm{c}_\zeta}}{\mathrm{d}t} = \frac{\Delta \boldsymbol{v}^{\mathrm{g}}_{\zeta}}{L_{\mathrm{c}_\zeta}} - \frac{\Delta \boldsymbol{e}^{\mathrm{g}}_{\zeta}}{L_{\mathrm{c}_\zeta}} + \begin{bmatrix} -R_{\mathrm{c}_\zeta}/L_{\mathrm{c}_\zeta} & \omega_0 \\ -\omega_0 & -R_{\mathrm{c}_\zeta}/L_{\mathrm{c}_\zeta} \end{bmatrix} \Delta \boldsymbol{i}^{\mathrm{g}}_{\mathrm{c}_\zeta} \tag{3.11}$$

$$\frac{\mathrm{d}\Delta \boldsymbol{e}^{\mathrm{g}}_{\zeta}}{\mathrm{d}t} = \frac{\Delta \boldsymbol{i}^{\mathrm{g}}_{\mathrm{c}_\zeta}}{C_{\mathrm{f}_\zeta}} - \frac{\Delta \boldsymbol{i}^{\mathrm{g}}_{\mathrm{t}_\zeta}}{C_{\mathrm{f}_\zeta}} + \omega_0 \begin{bmatrix} 0 & 1 \\ -1 & 0 \end{bmatrix} \Delta \boldsymbol{e}^{\mathrm{g}}_{\zeta} \tag{3.12}$$

$$\frac{\mathrm{d}\Delta \boldsymbol{i}^{\mathrm{g}}_{\mathrm{t}_\zeta}}{\mathrm{d}t} = \frac{\Delta \boldsymbol{e}^{\mathrm{g}}_{\zeta}}{L_{\mathrm{t}_\zeta}} - \frac{\Delta \boldsymbol{u}^{\mathrm{g}}_{\zeta}}{L_{\mathrm{t}_\zeta}} + \begin{bmatrix} -R_{\mathrm{t}_\zeta}/L_{\mathrm{t}_\zeta} & \omega_0 \\ -\omega_0 & -R_{\mathrm{t}_\zeta}/L_{\mathrm{t}_\zeta} \end{bmatrix} \Delta \boldsymbol{i}^{\mathrm{g}}_{\mathrm{t}_\zeta} \tag{3.13}$$

The state vector, $\boldsymbol{x}^{\mathrm{loc}}_{\mathrm{E}_\zeta}$, can then be deduced:

$$\boldsymbol{x}^{\mathrm{loc}}_{\mathrm{E}_\zeta} = \begin{bmatrix} \Delta i^{\mathrm{g}}_{\mathrm{c}_\zeta \mathrm{d}} & \Delta i^{\mathrm{g}}_{\mathrm{c}_\zeta \mathrm{q}} & \Delta e^{\mathrm{g}}_{\zeta \mathrm{d}} & \Delta e^{\mathrm{g}}_{\zeta \mathrm{q}} & \Delta i^{\mathrm{g}}_{\mathrm{t}_\zeta \mathrm{d}} & \Delta i^{\mathrm{g}}_{\mathrm{t}_\zeta \mathrm{q}} \end{bmatrix}^{\mathrm{T}} \tag{3.14}$$

The output vector, $\boldsymbol{y}_{\mathrm{E}_\zeta}$, must contain all elements that are utilised by a controller in addition to any quantities for which the response is to be studied. Since power and voltage levels are of interest, these are included. In strong systems, it may be desirable to assess the response of reactive power output of a converter to changes in its reference set points instead of voltage levels. Converter current components in the grid dq frame and the filter bus voltage components in the grid dq frame are also outputs since they are used in dq-axis vector current control and proportional resonant control. For power synchronization control, the voltage components are not necessary. However, to avoid having customised local models for the controller, they will be in the output vector even when power synchronization control is studied.

Mathematically, the outputs of the electrical part of the state-space model are as follows:

$$\boldsymbol{y}^{\mathrm{loc}}_{\mathrm{E}_\zeta} = \begin{cases} \begin{bmatrix} \Delta P_\zeta & \Delta Q_\zeta & \Delta i^{\mathrm{g}}_{\mathrm{c}_\zeta \mathrm{d}} & \Delta i^{\mathrm{g}}_{\mathrm{c}_\zeta \mathrm{q}} & \Delta e^{\mathrm{g}}_{\zeta \mathrm{d}} & \Delta e^{\mathrm{g}}_{\zeta \mathrm{q}} \end{bmatrix}^{\mathrm{T}} & \text{for strong systems} \\ \begin{bmatrix} \Delta P_\zeta & \Delta E_\zeta & \Delta i^{\mathrm{g}}_{\mathrm{c}_\zeta \mathrm{d}} & \Delta i^{\mathrm{g}}_{\mathrm{c}_\zeta \mathrm{q}} & \Delta e^{\mathrm{g}}_{\zeta \mathrm{d}} & \Delta e^{\mathrm{g}}_{\zeta \mathrm{q}} \end{bmatrix}^{\mathrm{T}} & \text{for weak systems} \end{cases} \tag{3.15}$$

Using the per unit system approach outlined in [3], the changes in the power dispatched onto the

network can be evaluated by perturbing equation 3.7:

$$\Delta P_\zeta = i^{\mathrm{g}}_{\mathrm{t}_\zeta \mathrm{d},0}\Delta e^{\mathrm{g}}_{\zeta \mathrm{d}} + i^{\mathrm{g}}_{\mathrm{t}_\zeta \mathrm{q},0}\Delta e^{\mathrm{g}}_{\zeta \mathrm{q}} + e^{\mathrm{g}}_{\zeta \mathrm{d},0}\Delta i^{\mathrm{g}}_{\mathrm{t}_\zeta \mathrm{d}} + e^{\mathrm{g}}_{\zeta \mathrm{q},0}\Delta i^{\mathrm{g}}_{\mathrm{t}_\zeta \mathrm{q}} \tag{3.16}$$

Similarly for reactive power,

$$\Delta Q_\zeta = i^{\mathrm{g}}_{\mathrm{t}_\zeta \mathrm{d},0}\Delta e^{\mathrm{g}}_{\zeta \mathrm{q}} + e^{\mathrm{g}}_{\zeta \mathrm{q},0}\Delta i^{\mathrm{g}}_{\mathrm{t}_\zeta \mathrm{d}} - e^{\mathrm{g}}_{\zeta \mathrm{d},0}\Delta i^{\mathrm{g}}_{\mathrm{t}_\zeta \mathrm{q}} - i^{\mathrm{g}}_{\mathrm{t}_\zeta \mathrm{q},0}\Delta e^{\mathrm{g}}_{\zeta \mathrm{d}} \tag{3.17}$$

Again using the per unit system approach outlined in [3], the changes in the filter bus voltage can be evaluated by perturbing equation 3.8:

$$\Delta E_\zeta = \frac{1}{E_{\zeta,0}}\left[e^{\mathrm{g}}_{\zeta \mathrm{d},0}\Delta e^{\mathrm{g}}_{\zeta \mathrm{d}} + e^{\mathrm{g}}_{\zeta \mathrm{q},0}\Delta e^{\mathrm{g}}_{\zeta \mathrm{q}}\right] \tag{3.18}$$

Thus, ΔP_ζ and ΔQ_ζ or ΔE_ζ can be linked to $\boldsymbol{x}^{\mathrm{loc}}_{\mathrm{E}_\zeta}$ meaning all the elements of the output vector can be linked to the state vector, $\boldsymbol{x}^{\mathrm{loc}}_{\mathrm{E}_\zeta}$. Thus, the state-space model can now be constructed.

$$\boldsymbol{A}^{\mathrm{loc}}_{\mathrm{E}_\zeta} = \begin{bmatrix} -\frac{R_{\mathrm{c}_\zeta}}{L_{\mathrm{c}_\zeta}} & \omega_0 & -\frac{1}{L_{\mathrm{c}_\zeta}} & 0 & 0 & 0 \\ -\omega_0 & -\frac{R_{\mathrm{c}_\zeta}}{L_{\mathrm{c}_\zeta}} & 0 & -\frac{1}{L_{\mathrm{c}_\zeta}} & 0 & 0 \\ \frac{1}{C_{\mathrm{f}_\zeta}} & 0 & 0 & \omega_0 & -\frac{1}{C_{\mathrm{f}_\zeta}} & 0 \\ 0 & \frac{1}{C_{\mathrm{f}_\zeta}} & -\omega_0 & 0 & 0 & -\frac{1}{C_{\mathrm{f}_\zeta}} \\ 0 & 0 & \frac{1}{L_{\mathrm{t}_\zeta}} & 0 & -\frac{R_{\mathrm{t}_\zeta}}{L_{\mathrm{t}_\zeta}} & \omega_0 \\ 0 & 0 & 0 & \frac{1}{L_{\mathrm{t}_\zeta}} & -\omega_0 & -\frac{R_{\mathrm{t}_\zeta}}{L_{\mathrm{t}_\zeta}} \end{bmatrix};\ \boldsymbol{B}^{\mathrm{loc}}_{\mathrm{E}_\zeta} = \begin{bmatrix} 1/L_{\mathrm{c}_\zeta} & 0 \\ 0 & 1/L_{\mathrm{c}_\zeta} \\ 0 & 0 \\ 0 & 0 \\ 0 & 0 \\ 0 & 0 \end{bmatrix} \tag{3.19}$$

For some scenarios considered in chapter seven, specifically those where there are local loads, the $\boldsymbol{A}^{\mathrm{loc}}_{\mathrm{E}_\zeta}$ matrix will change. This is addressed at the relevant time.

The $\boldsymbol{C}^{\text{loc}}_{\text{E}_\zeta}$ matrix is given by equation 3.20.

$$\boldsymbol{C}^{\text{loc}}_{\text{E}_\zeta} = \begin{bmatrix} 0 & 0 & i^{\text{g}}_{\text{t}_\zeta\text{d},0} & i^{\text{g}}_{\text{t}_\zeta\text{q},0} & e^{\text{g}}_{\zeta\text{d},0} & e^{\text{g}}_{\zeta\text{q},0} \\ 0 & 0 & \dfrac{e^{\text{g}}_{\zeta\text{d},0}}{E_{\zeta,0}} & \dfrac{e^{\text{g}}_{\zeta\text{q},0}}{E_{\zeta,0}} & 0 & 0 \\ 1 & 0 & 0 & 0 & 0 & 0 \\ 0 & 1 & 0 & 0 & 0 & 0 \\ 0 & 0 & 1 & 0 & 0 & 0 \\ 0 & 0 & 0 & 1 & 0 & 0 \end{bmatrix} \text{ or } \begin{bmatrix} 0 & 0 & i^{\text{g}}_{\text{t}_\zeta\text{d},0} & i^{\text{g}}_{\text{t}_\zeta\text{q},0} & e^{\text{g}}_{\zeta\text{d},0} & e^{\text{g}}_{\zeta\text{q},0} \\ 0 & 0 & i^{\text{g}}_{\text{t}_\zeta\text{q},0} & -i^{\text{g}}_{\text{t}_\zeta\text{d},0} & e^{\text{g}}_{\zeta\text{q},0} & -e^{\text{g}}_{\zeta\text{d},0} \\ 1 & 0 & 0 & 0 & 0 & 0 \\ 0 & 1 & 0 & 0 & 0 & 0 \\ 0 & 0 & 1 & 0 & 0 & 0 \\ 0 & 0 & 0 & 1 & 0 & 0 \end{bmatrix} \tag{3.20}$$

The first expression for $\boldsymbol{C}^{\text{loc}}_{\text{E}_\zeta}$ is used when the short-circuit ratio is one; for all other values of short-circuit ratio considered in this work, the second expression is used.

Finally, the output matrix for a single-converter model, $\boldsymbol{D}^{\text{loc}}_{\text{E}_\zeta}$, is a six-by-two zero matrix.

3.2.2 L filter

MMC-HVDC systems produce very little harmonic content; thus, such systems will not require extensive filtering equipment. That is, an L filter is sufficient for MMC-HVDC. Given that MMC-HVDC systems are increasing in popularity, it seems appropriate to include the L filter in the analysis.

In the case of a converter having an L filter, the filter may be lumped in with the local transmission line. However, it needs to be noted that the state-space model should still output the current and voltage at the local PCC. While the current will always form part of the state-vector, the voltage at the local PCC will not in the L filter case; nor will it belong to the control vector. However, by writing the dynamics of the local part of the system as two sections, the filter and the local transmission line, an expression for the voltage at the local PCC in terms of the state and control vectors can be derived. Accordingly, let us express the dynamics of the converter part of the system

as follows:

$$\frac{\mathrm{d}\Delta \boldsymbol{i}^{\mathrm{g}}_{\mathrm{t}_\zeta}}{\mathrm{d}t} = \frac{\Delta \boldsymbol{v}^{\mathrm{g}}_{\zeta}}{L_{\mathrm{c}_\zeta}} - \frac{\Delta \boldsymbol{e}^{\mathrm{g}}_{\zeta}}{L_{\mathrm{c}_\zeta}} + \begin{bmatrix} -R_{\mathrm{c}_\zeta}/L_{\mathrm{c}_\zeta} & \omega_0 \\ -\omega_0 & -R_{\mathrm{c}_\zeta}/L_{\mathrm{c}_\zeta} \end{bmatrix} \Delta \boldsymbol{i}^{\mathrm{g}}_{\mathrm{t}_\zeta} \tag{3.21}$$

$$\frac{\mathrm{d}\Delta \boldsymbol{i}^{\mathrm{g}}_{\mathrm{t}_\zeta}}{\mathrm{d}t} = \frac{\Delta \boldsymbol{e}^{\mathrm{g}}_{\zeta}}{L_{\mathrm{t}_\zeta}} - \frac{\Delta \boldsymbol{u}^{\mathrm{g}}_{\zeta}}{L_{\mathrm{t}_\zeta}} + \begin{bmatrix} -R_{\mathrm{t}_\zeta}/L_{\mathrm{t}_\zeta} & \omega_0 \\ -\omega_0 & -R_{\mathrm{t}_\zeta}/L_{\mathrm{t}_\zeta} \end{bmatrix} \Delta \boldsymbol{i}^{\mathrm{g}}_{\mathrm{t}_\zeta} \tag{3.22}$$

Thus,

$$\Delta \boldsymbol{e}^{\mathrm{g}}_{\zeta} = \frac{L_{\mathrm{t}_\zeta} L_{\mathrm{c}_\zeta}}{L_{\mathrm{c}_\zeta} + L_{\mathrm{t}_\zeta}} \left[\frac{\Delta \boldsymbol{u}^{\mathrm{g}}_{\zeta}}{L_{\mathrm{t}_\zeta}} + \frac{\Delta \boldsymbol{v}^{\mathrm{g}}_{\zeta}}{L_{\mathrm{c}_\zeta}} + \left(R_{\mathrm{t}_\zeta}/L_{\mathrm{t}_\zeta} - R_{\mathrm{c}_\zeta}/L_{\mathrm{c}_\zeta} \right) \Delta \boldsymbol{i}^{\mathrm{g}}_{\mathrm{t}_\zeta} \right] \tag{3.23}$$

That is, $\Delta \boldsymbol{e}^{\mathrm{g}}_{\zeta}$ may be expressed in terms of the state vector and control vector.

Equations 3.22 reduce to a single expression:

$$\frac{\mathrm{d}\Delta \boldsymbol{i}^{\mathrm{g}}_{\mathrm{t}_\zeta}}{\mathrm{d}t} = \frac{\Delta \boldsymbol{v}^{\mathrm{g}}_{\zeta}}{L_{\mathrm{com}_\zeta}} - \frac{\Delta \boldsymbol{u}^{\mathrm{g}}_{\zeta}}{L_{\mathrm{com}_\zeta}} + \begin{bmatrix} -R_{\mathrm{com}_\zeta}/L_{\mathrm{com}_\zeta} & \omega_0 \\ -\omega_0 & -R_{\mathrm{com}_\zeta}/L_{\mathrm{com}_\zeta} \end{bmatrix} \Delta \boldsymbol{i}^{\mathrm{g}}_{\mathrm{t}_\zeta} \tag{3.24}$$

where $R_{\mathrm{com}_\zeta} = R_{\mathrm{c}_\zeta} + R_{\mathrm{t}_\zeta}$ and $L_{\mathrm{com}_\zeta} = L_{\mathrm{c}_\zeta} + L_{\mathrm{t}_\zeta}$.

Thus, the state-space model for the L-filtered converter is defined using the following state-space matrices:

$$\boldsymbol{A}^{\mathrm{loc}}_{\mathrm{E}_\zeta} = \begin{bmatrix} -\dfrac{R_{\mathrm{com}_\zeta}}{L_{\mathrm{com}_\zeta}} & \omega_0 \\ -\omega_0 & -\dfrac{R_{\mathrm{com}_\zeta}}{L_{\mathrm{com}_\zeta}} \end{bmatrix}; \quad \boldsymbol{B}^{\mathrm{loc}}_{\mathrm{E}_\zeta} = \begin{bmatrix} 1/L_{\mathrm{com}_\zeta} & 0 \\ 0 & 1/L_{\mathrm{com}_\zeta} \end{bmatrix} \tag{3.25}$$

$$\boldsymbol{C}_{\mathrm{E}_\zeta}^{\mathrm{loc}} = \begin{bmatrix} e_{\zeta\mathrm{d},0}^{\mathrm{g}} & e_{\zeta\mathrm{q},0}^{\mathrm{g}} & i_{\mathrm{t}_\zeta\mathrm{d},0}^{\mathrm{g}} & i_{\mathrm{t}_\zeta\mathrm{q},0}^{\mathrm{g}} \\ 0 & 0 & \dfrac{e_{\zeta\mathrm{d},0}^{\mathrm{g}}}{E_{\zeta,0}} & \dfrac{e_{\zeta\mathrm{q},0}^{\mathrm{g}}}{E_{\zeta,0}} \\ 1 & 0 & 0 & 0 \\ 0 & 1 & 0 & 0 \\ 0 & 0 & 1 & 0 \\ 0 & 0 & 0 & 1 \end{bmatrix} \begin{bmatrix} 1 & 0 \\ 0 & 1 \\ f & 0 \\ 0 & f \end{bmatrix} \tag{3.26}$$

where $f = L_{\mathrm{c}_\zeta} L_{\mathrm{t}_\zeta} \left(R_{\mathrm{t}_\zeta}/L_{\mathrm{t}_\zeta} - R_{\mathrm{c}_\zeta}/L_{\mathrm{c}_\zeta} \right) / L_{\mathrm{com}_\zeta}$. For this filter, $\boldsymbol{x}_{\mathrm{E}}^{\mathrm{loc}} = \Delta \boldsymbol{i}_\zeta^{\mathrm{g}}$ and $\boldsymbol{z}_{\mathrm{E}}^{\mathrm{loc}}$ and $\boldsymbol{z}_{\mathrm{E}}^{\mathrm{lin}}$ are as before, giving the same equation form as seen in equation 3.1.

Finally, the feed-forward matrices, one acting on $\boldsymbol{z}_{\mathrm{E}}^{\mathrm{loc}}$ and the other on $\boldsymbol{z}_{\mathrm{E}}^{\mathrm{lin}}$, are given as follows:

$$\boldsymbol{D}_{\mathrm{E}_\zeta}^{\mathrm{loc}} = \frac{L_{\mathrm{t}_\zeta}}{L_{\mathrm{com}_\zeta}} \begin{bmatrix} i_{\mathrm{t}_\zeta\mathrm{d},0}^{\mathrm{g}} & i_{\mathrm{t}_\zeta\mathrm{q},0}^{\mathrm{g}} \\ e_{\zeta\mathrm{d},0}^{\mathrm{g}}/E_{\zeta,0} & e_{\zeta\mathrm{q},0}^{\mathrm{g}}/E_{\zeta,0} \\ 0 & 0 \\ 0 & 0 \\ 1 & 0 \\ 0 & 1 \end{bmatrix}; \quad \boldsymbol{D}_{\mathrm{E}_\zeta}^{\mathrm{lin}_1} = \frac{L_{\mathrm{c}_\zeta}}{L_{\mathrm{com}_\zeta}} \begin{bmatrix} i_{\mathrm{t}_\zeta\mathrm{d},0}^{\mathrm{g}} & i_{\mathrm{t}_\zeta\mathrm{q},0}^{\mathrm{g}} \\ e_{\zeta\mathrm{d},0}^{\mathrm{g}}/E_{\zeta,0} & e_{\zeta\mathrm{q},0}^{\mathrm{g}}/E_{\zeta,0} \\ 0 & 0 \\ 0 & 0 \\ 1 & 0 \\ 0 & 1 \end{bmatrix} \tag{3.27}$$

Note - the output and feed-forward matrices shown above assume that the output contains voltage magnitude and not reactive power.

As with the LC filter analysis, if the system comprises only one converter, the $\boldsymbol{D}_{\mathrm{E}_\zeta}^{\mathrm{lin}}$ matrix can be omitted.

3.2.3 Frequency response

The matrices are then used to calculate $\boldsymbol{G}(s)$ using equation 3.4. $\boldsymbol{G}(s)$ needs evaluating at each complex frequency, $s = j\omega$. From inspection, $\boldsymbol{G}(s)$ is an six-by-four matrix. The elements in the top row connect $\Delta \boldsymbol{v}_\zeta^{\mathrm{g}}$ to changes in the real power; the elements of the second row connect $\Delta \boldsymbol{v}_\zeta^{\mathrm{g}}$ to changes in the filter bus voltage/reactive power (depending on the control strategy); the elements of the third row connect $\Delta \boldsymbol{v}_\zeta^{\mathrm{g}}$ to changes in the d component of the converter current in

the grid dq frame; the elements of the fourth row connect $\Delta \boldsymbol{v}_{\zeta}^{\mathrm{g}}$ to changes in the q component of the converter current in the grid dq frame; the elements of the fifth row connect $\Delta \boldsymbol{v}_{\zeta}^{\mathrm{g}}$ to changes in the d component of the filter bus voltage in the grid dq frame; and the elements of the sixth row connect $\Delta \boldsymbol{v}_{\zeta}^{\mathrm{g}}$ to changes in the q component of the filter bus voltage in the grid dq frame.

Note - increased predictive capability can be obtained by setting $R_{\mathrm{f}_{\zeta}} \rightarrow f_1(s)$, $C_{\mathrm{f}_{\zeta}} \rightarrow f_2(s)$, $L_{\mathrm{f}_{\zeta}} \rightarrow f_3(s)$, etc., such that the resistance, inductance and capacitance terms vary with frequency, as they would in reality. This can, if desired, then be combined with subspace algorithms to form an effective state-space model of the power system into which frequency dependent characteristics is naturally embedded.

Chapter 4

Analysis of dq-axis vector current control

In this chapter, an analysis of dq-axis vector current control is presented. Linear and non-linear simulations are presented, with the latter being used to assess the correctness of the former. A range of topologies are considered, covering different AC filters, different PLLs, and outer loop controllers. Attention is given to second order PLLs so as to include topologies that could be applied to systems where the system frequency is not necessarily constant.

The linear models are given both in frequency response form and state-unified space form.. By utilising sub-space algorithms, the former can be used to extract poles and zeros of the combined system (controller, plant and feedback). In the second method, the component state-space models of the various elements of the controller and plant are combined into a unified state-space model (which is essentially what a sub-space algorithm determines), which is then used to calculate the poles and zeros. While its derivation may be more involved, the latter approach allows the reader to easily construct models in compiled languages, which is useful for integration into larger programmes and also for speed reasons.

4.1 Overview of dq-axis vector current control

A popular control algorithm is dq-axis vector current control [1]. Control is carried out in a dq frame established by a PLL[1]. The PLL is provided with the voltage $\boldsymbol{e}_{\zeta}^{\mathrm{abc}}$, and estimates the phase of said voltage. Using this phase estimation, the current flowing through the phase reactor is converted to the PLL dq frame. In addition, so too is the voltage which was used as an input to the PLL.

Current components (d and q) are compared against reference values which correspond to desired power output (d reference) and reactive power output/AC voltage (q reference). The error signals, one for the d component and one for the q component, go through PI controllers, the output of which are reference dq values for the bridge voltage; the reference dq values are then converted back to the abc frame by an inverse Park transform. This reference signal then goes through a PWM process, which sets the switching of the IGBT devices. Accordingly, dq-axis vector current control can be summarised by figure 4.1:

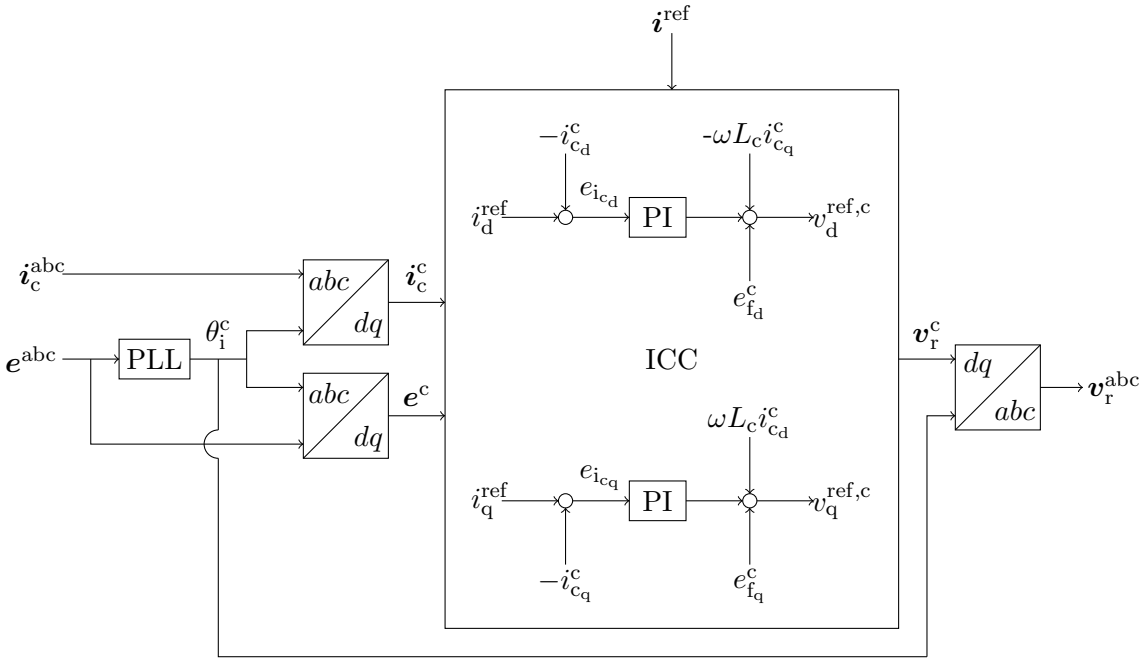

Figure 4.1: Overview of the dq-axis vector current control scheme including the frame transformations and PLL. The inner current controller block, ICC, contains two control loops, each with their own PI controller. The outer loop controllers are omitted in this block diagram.

[1]The dq frame for the converter is denoted by superscript c.

In reality, dq-axis vector current control is implemented twice: once for positive-sequence components, and once for zero and negative sequence components. This is required for effective performance during faults and/or unbalanced loads.

4.1.1 Reference current values

As stated in chapter 2, the d-component current reference value is set either by an active power controller or a DC bus voltage controller. In this work, an active power controller is introduced in section 4.5.3.

The q-component current reference value is set either by a reactive power controller or an AC voltage controller; thus, since AC voltage control is seen as preferable to reactive power control in weak AC systems, the controller adopted for setting $\Im\left\{\boldsymbol{i}_\zeta^{\text{ref}}\right\}$ in this work is as shown in figure 4.2 in section 4.5.3.

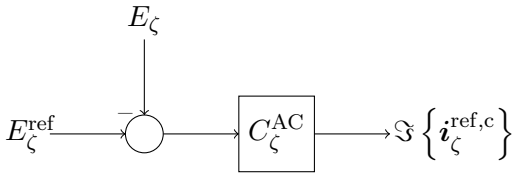

Figure 4.2: AC droop control in the dq-axis vector current control scheme when reactive power is directly controlled. The C_ζ^{AC} block refers to the reactive power control loop.

Since reactive power goes as the negative of $\Im\left\{\boldsymbol{i}_\zeta^{\text{ref,c}}\right\}$, and voltage is linked to reactive power, the controller, C_ζ^{AC}, should have a negative gain.

4.2 Relationship between PLL dq frames and grid dq frame

The two PLL algorithms to be considered in this work are the first-order and second-order PLLs. The former is illustrated in figure 4.3, while the latter is illustrated in figure 4.4.

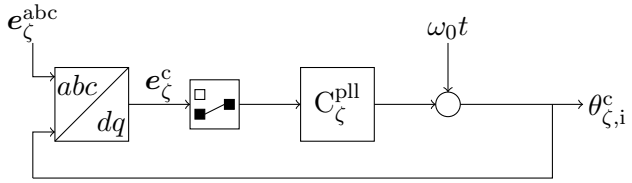

Figure 4.3: Simple PLL control system. $\mathrm{C}_\zeta^{\mathrm{pll}}$ is the PI controller.

The abc to dq transformation of the voltage $\boldsymbol{e}_\zeta^{\mathrm{abc}}$ is achieved using the standard Park transformation:

$$\boldsymbol{P}^{\mathrm{c}}\boldsymbol{e}_\zeta^{\mathrm{abc}} = E_\zeta \begin{bmatrix} \cos\theta_{\zeta,\mathrm{i}}^{\mathrm{c}} & \cos(\theta_{\zeta,\mathrm{i}}^{\mathrm{c}} - 2\pi/3) & \cos(\theta_{\zeta,\mathrm{i}}^{\mathrm{c}} + 2\pi/3) \\ -\sin\theta_{\zeta,\mathrm{i}}^{\mathrm{c}} & -\sin(\theta_{\zeta,\mathrm{i}}^{\mathrm{c}} - 2\pi/3) & -\sin(\theta_{\zeta,\mathrm{i}}^{\mathrm{c}} + 2\pi/3) \end{bmatrix} \begin{bmatrix} \cos\theta_{\zeta,\mathrm{i}} \\ \cos(\theta_{\zeta,\mathrm{i}} - 2\pi/3) \\ \cos(\theta_{\zeta,\mathrm{i}} + 2\pi/3) \end{bmatrix} \tag{4.1}$$

where $\theta_{\zeta,\mathrm{i}}^{\mathrm{c}}$ is the PLL estimation of the instantaneous phase of $\boldsymbol{e}_\zeta^{\mathrm{abc}}$ (whose real instantaneous phase is $\theta_{\zeta,\mathrm{i}}$) and E_ζ is the magnitude of $\boldsymbol{e}_\zeta^{\mathrm{abc}}$. Considering equation 3.5, the voltage vector in the converter dq frame can be expressed by equation 4.2:

$$\boldsymbol{e}_\zeta^{\mathrm{c}} = \frac{3E_\zeta}{2} \begin{bmatrix} \cos\theta_{\zeta,\mathrm{i}}^{\mathrm{c}}\cos\theta_{\zeta,\mathrm{i}} + \sin\theta_{\zeta,\mathrm{i}}^{\mathrm{c}}\sin\theta_{\zeta,\mathrm{i}} \\ \cos\theta_{\zeta,\mathrm{i}}^{\mathrm{c}}\sin\theta_{\zeta,\mathrm{i}} - \sin\theta_{\zeta,\mathrm{i}}^{\mathrm{c}}\cos\theta_{\zeta,\mathrm{i}} \end{bmatrix} \tag{4.2}$$

Referring to figure 4.3, it follows that the estimation of the instantaneous phase may be expressed as $\theta_{\zeta,\mathrm{i}}^{\mathrm{c}} = \omega_0 t + \theta_\zeta^{\mathrm{c}}$, where $\theta_\zeta^{\mathrm{c}}$ (which is the output of the PLL) can be interpreted as the estimation of the phase difference between the filter bus voltage and the voltage at the slack bus. Hence, equation 4.2 may be expressed as follows:

$$\boldsymbol{e}_\zeta^{\mathrm{c}} = \frac{3E_\zeta}{2} \begin{bmatrix} (\cos(\omega_0 t)\cos\theta_{\zeta,\mathrm{i}} + \sin(\omega_0 t)\sin\theta_{\zeta,\mathrm{i}})\cos\theta_\zeta^{\mathrm{c}} + \dots \\ \qquad (\cos(\omega_0 t)\sin\theta_{\zeta,\mathrm{i}} - \sin(\omega_0 t)\cos\theta_{\zeta,\mathrm{i}})\sin\theta_\zeta^{\mathrm{c}} \\ \\ (\cos(\omega_0 t)\sin\theta_{\zeta,\mathrm{i}} - \sin(\omega_0 t)\cos\theta_{\zeta,\mathrm{i}})\cos\theta_\zeta^{\mathrm{c}} - \dots \\ \qquad (\sin(\omega_0 t)\sin\theta_{\zeta,\mathrm{i}} + \cos(\omega_0 t)\cos\theta_{\zeta,\mathrm{i}})\sin\theta_\zeta^{\mathrm{c}} \end{bmatrix} \tag{4.3}$$

Applying equation 3.5 again, it follows that

$$\boldsymbol{e}_{\zeta}^{\mathrm{c}} = \begin{bmatrix} \cos\theta_{\zeta}^{\mathrm{c}} & \sin\theta_{\zeta}^{\mathrm{c}} \\ -\sin\theta_{\zeta}^{\mathrm{c}} & \cos\theta_{\zeta}^{\mathrm{c}} \end{bmatrix} \boldsymbol{e}_{\zeta}^{\mathrm{g}} \tag{4.4}$$

where $\boldsymbol{e}_{\zeta}^{\mathrm{g}}$ is the vector containing the dq components of the filter bus voltage in the grid dq frame. Equation 4.4 allows the connection of a system whose dynamics are expressed in the PLL dq frame with a system whose dynamics are expressed in the grid dq frame.

If a second-order SRF-PLL is used, the output of the PI controller in the PLL is $\Delta\omega$, which is then added to the nominal frequency, before being integrated to give the phase.

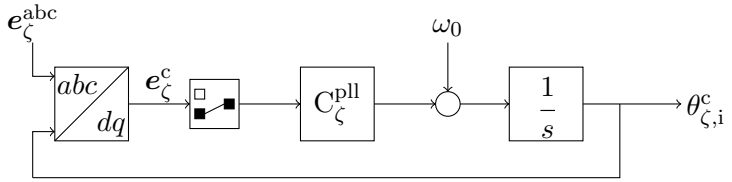

Figure 4.4: Simple PLL control system. $\mathrm{C}_{\zeta}^{\mathrm{pll}}$ is the PI controller.

Mathematically,

$$\boldsymbol{e}_{\zeta}^{\mathrm{c}} = \begin{bmatrix} \cos\left(\int \Delta\omega \mathrm{d}t\right) & \sin\left(\int \Delta\omega \mathrm{d}t\right) \\ -\sin\left(\int \Delta\omega \mathrm{d}t\right) & \cos\left(\int \Delta\omega \mathrm{d}t\right) \end{bmatrix} \boldsymbol{e}_{\zeta}^{\mathrm{g}} \tag{4.5}$$

The integral term may still be interpreted as the estimation of the phase difference between the filter bus and slack bus, with the steady-state phase difference being the constant of integration. However, it is important to note that higher-order models experience greater sensitivity, which may introduce errors and/or decrease the range of validity of a linear model constructed around some operating point.

4.3 Linear analysis of the controller

4.3.1 Phase-tracking errors in the PLL

The objective of the PLL is to track the phase of whatever input signal it is provided with. To do so, using the definition of the Park transformation used in this work, the PLL seeks to create a reference dq frame in which the q component of the input signal transformed into the PLL dq frame is zero. With reference to figure 4.3 and the definition of the grid dq frame, the PLL only seeks to determine θ i.e. the phase of the voltage at the filter bus relative to the slack bus.

4.3.2 First-order PLL

Referring to figure 4.3 it follows that a simple first order PLL has the following control action:

$$\theta_{\zeta}^{\mathrm{c}} = G_{\zeta}^{\mathrm{pll}} * \Im\left\{\boldsymbol{e}_{\zeta}^{\mathrm{c}}\right\} \tag{4.6}$$

where G_{ζ}^{pll} represents a PI controller. The $*$ sign denotes the convolution of G_{ζ}^{pll} and $\Im\left\{\boldsymbol{e}_{\zeta}^{\mathrm{c}}\right\}$. In the frequency domain, the convolution theorem states that convolution actions become multipliers; that is,

$$\theta_{\zeta}^{\mathrm{c}}(s) = G_{\zeta}^{\mathrm{pll}}(s).\Im\left\{\boldsymbol{e}_{\zeta}^{\mathrm{c}}(s)\right\} \tag{4.7}$$

For small signal stability analysis, the focus will be constrained to perturbations in the signals; hence, it is desirable to work towards an expression based on equation 4.8:

$$\Delta\theta_{\zeta}^{\mathrm{c}}(s) = G_{\zeta}^{\mathrm{pll}}(s).\Im\left\{\Delta\boldsymbol{e}_{\zeta}^{\mathrm{c}}(s)\right\} \tag{4.8}$$

Starting in the time domain, let us perturb all the variables and linearise the system. For example, $\theta_{\zeta}^{\mathrm{c}} \rightarrow \theta_{\zeta,0} + \Delta\theta_{\zeta}^{\mathrm{c}}$ The superscript 'c' has been omitted from $\theta_{\zeta,0}$ since in steady-state $\theta_{\zeta,0}^{\mathrm{c}} = \theta_{\zeta,0}$.

Applying this expression to the trigonometric functions,

$$\begin{aligned}\cos\theta_\zeta^{\mathrm{c}} &= \cos(\theta_{\zeta,0} + \Delta\theta_\zeta^{\mathrm{c}}) \\ &\approx \cos\theta_{\zeta,0} - \Delta\theta_\zeta^{\mathrm{c}} \sin\theta_{\zeta,0} \qquad (4.9)\\ \sin\theta_\zeta^{\mathrm{c}} &= \sin(\theta_{\zeta,0} + \Delta\theta_\zeta^{\mathrm{c}}) \\ &\approx \sin\theta_{\zeta,0} + \Delta\theta_\zeta^{\mathrm{c}} \cos\theta_{\zeta,0} \qquad (4.10)\end{aligned}$$

Considering figure 4.3 and equation 4.6, perturbations in $\boldsymbol{e}_\zeta^{\mathrm{abc}}$ map directly onto phase-tracking errors in the PLL. By taking equation 4.4 into account, it follows that for the PLL

$$\begin{aligned}\Im\left\{\boldsymbol{e}_\zeta^{\mathrm{c}}\right\} &= \Im\left\{\boldsymbol{e}_{\zeta,0}^{\mathrm{c}} + \Delta\boldsymbol{e}_\zeta^{\mathrm{c}}\right\} \\ &= \begin{bmatrix}-\sin(\theta_{\zeta,0} + \Delta\theta_\zeta^{\mathrm{c}}) & \cos(\theta_{\zeta,0} + \Delta\theta_\zeta^{\mathrm{c}})\end{bmatrix}\left(\boldsymbol{e}_{\zeta,0}^{\mathrm{g}} + \Delta\boldsymbol{e}_\zeta^{\mathrm{g}}\right) \qquad (4.11)\end{aligned}$$

Thus, expanding equation 4.11 and removing the steady-state components and only leaving those terms with first order perturbations yields

$$\Im\left\{\Delta\boldsymbol{e}_\zeta^{\mathrm{c}}\right\} = \begin{bmatrix}-\sin\theta_{\zeta,0} & \cos\theta_{\zeta,0}\end{bmatrix}\Delta\boldsymbol{e}_\zeta^{\mathrm{g}} - E_{\zeta,0}\Delta\theta_\zeta^{\mathrm{c}} \qquad (4.12)$$

Thus, taking the Laplace transform of equation 4.12 and substituting into equation 4.8 yields the following result:

$$\Delta\theta_\zeta^{\mathrm{c}}(s) = \frac{G_\zeta^{\mathrm{pll}}(s)}{1 + G_\zeta^{\mathrm{pll}}(s)E_{\zeta,0}}\begin{bmatrix}-\sin\theta_{\zeta,0} & \cos\theta_{\zeta,0}\end{bmatrix}\Delta\boldsymbol{e}_\zeta^{\mathrm{g}}(s) \qquad (4.13)$$

In order to be easily integrated with the network model, equation 4.13 is modified such that $\boldsymbol{y}_{\mathrm{E}_\zeta}$ is acted upon rather than $\Delta\boldsymbol{e}_\zeta^{\mathrm{g}}(s)$ alone. Accordingly,

$$\Delta\theta_\zeta^{\mathrm{c}} = \underbrace{\frac{G_\zeta^{\mathrm{pll}}(s)}{1 + G_\zeta^{\mathrm{pll}}(s)E_{\zeta,0}}\begin{bmatrix}-\sin\theta_{\zeta,0} & \cos\theta_{\zeta,0}\end{bmatrix}\boldsymbol{T}_1^{\mathrm{vcc}}}_{\boldsymbol{G}_\zeta^a(s)}\Delta\boldsymbol{e}_\zeta^{\mathrm{g}}(s) \qquad (4.14)$$

where

$$\boldsymbol{T}_1^{\text{vcc}} = \begin{bmatrix} \boldsymbol{O}(2,4) & \boldsymbol{I}_2 \end{bmatrix}$$

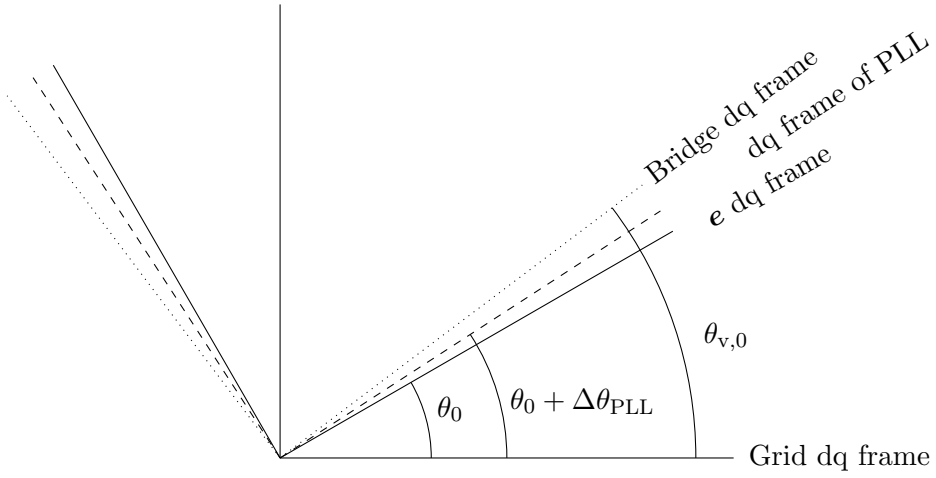

Figure 4.5: Four dq frames: grid dq frame (solid), filter bus voltage dq frame (solid), PLL dq frame (dashed), converter dq frame (dotted)

Contribution to the unified linear state-space model

In order to facilitate the development of the unified linear state-space model, equation 4.14 must be expressed in state-space form. Let us begin by expressing equation 4.14 as follows:

$$\Delta\theta_\zeta^{\text{c}} = \frac{a_{\text{pll}}s + b_{\text{pll}}}{s + c_{\text{pll}}} \begin{bmatrix} -\sin\theta_{\zeta,0} & \cos\theta_{\zeta,0} \end{bmatrix} \Delta\boldsymbol{e}_\zeta^{\text{g}} \tag{4.15}$$

Such a transfer function can be represented by the following state-space model:

$$\frac{\mathrm{d}\boldsymbol{x}_\zeta^{\mathrm{pll}}}{\mathrm{d}t} = \underbrace{\left[-\frac{k_{\zeta,\mathrm{i}}^{\mathrm{pll}}}{1+k_{\zeta,\mathrm{p}}^{\mathrm{pll}}E_{\zeta,0}}\right]}_{\boldsymbol{A}_\zeta^{\mathrm{pll}}}\boldsymbol{x}_\zeta^{\mathrm{pll}} + \dots$$
$$\underbrace{\left(\frac{k_{\mathrm{i}}^{\mathrm{pll}}}{1+E_{\zeta,0}k_{\mathrm{p}}^{\mathrm{pll}}} - \frac{k_{\mathrm{p}}^{\mathrm{pll}}k_{\mathrm{i}}^{\mathrm{pll}}E_{\zeta,0}}{(1+k_{\mathrm{p}}^{\mathrm{pll}}E_{\zeta,0})^2}\right)\begin{bmatrix}\boldsymbol{O}(1,4) & -\sin\theta_{\zeta,0} & \cos\theta_{\zeta,0}\end{bmatrix}}_{\boldsymbol{B}_\zeta^{\mathrm{pll}}}\boldsymbol{y}_{\mathrm{E}_\zeta}^{\mathrm{loc}} \tag{4.16}$$

$$\Delta\theta_\zeta^{\mathrm{c}} = \underbrace{\begin{bmatrix}1\end{bmatrix}}_{\boldsymbol{C}_\zeta^{\mathrm{pll}}}\boldsymbol{x}_\zeta^{\mathrm{pll}} + \underbrace{\left[\frac{k_{\zeta,\mathrm{p}}^{\mathrm{pll}}}{(1+k_{\zeta,\mathrm{p}}^{\mathrm{pll}}E_{\zeta,0})}\right]\begin{bmatrix}\boldsymbol{O}(1,4) & -\sin\theta_{\zeta,0} & \cos\theta_{\zeta,0}\end{bmatrix}}_{\boldsymbol{D}_\zeta^{\mathrm{pll}}}\boldsymbol{y}_{\mathrm{E}_\zeta}^{\mathrm{loc}} \tag{4.17}$$

4.3.3 Second-order PLL

For a second order PLL, the output of the PI controller is added to the nominal grid frequency, which is then integrated up to give the instantaneous phase. Due to linearity of the integral, one could imagine the phase as follows:

$$\theta_\zeta^{\mathrm{c}} = \int \Delta\omega\mathrm{d}t + \underbrace{\int \omega_0\mathrm{d}t}_{\omega_0 t} \tag{4.18}$$

The first term could be imagined as a higher-order controller, $G_{\zeta,\mathrm{fic}}^{\mathrm{pll}}$ where

$$G_{\zeta,\mathrm{fic}}^{\mathrm{pll}} = (k_{\zeta,\mathrm{p}}^{\mathrm{pll}}s^2 + k_{\zeta,\mathrm{i}}^{\mathrm{pll}}s)/s^2 \tag{4.19}$$
$$= G_\zeta^{\mathrm{pll}}/s \tag{4.20}$$

In which case, it can be shown that the $\boldsymbol{G}_\zeta^{\mathrm{a}}$ matrix should be as given in equation 4.21:

$$\boldsymbol{G}_\zeta^a(s) = \frac{G_\zeta^{\mathrm{pll}}(s)}{s+G_\zeta^{\mathrm{pll}}(s)E_{\zeta,0}}\begin{bmatrix}-\sin\theta_{\zeta,0} & \cos\theta_{\zeta,0}\end{bmatrix}\boldsymbol{T}_1^{\mathrm{vcc}} \tag{4.21}$$

Contribution to unified linear state-space model

To create a linearised state-space model, equation 4.21 may be viewed in the following form:

$$\Delta\theta_{\zeta}^{\mathrm{c}}(s) = \left[\frac{a_{\mathrm{PLL}}s + b_{\mathrm{PLL}}}{s^2 + c_{\mathrm{PLL}}s + d_{\mathrm{PLL}}}\right] \begin{bmatrix} 0 & 0 & 0 & 0 & -\sin\theta_{\zeta,0} & \cos\theta_{\zeta,0} \\ 0 & 0 & 0 & 0 & 0 & 0 \end{bmatrix} \boldsymbol{y}_{\mathrm{E}\zeta}^{\mathrm{loc}} \tag{4.22}$$

From this, the PLL portion may be represented in the following way:

$$\frac{\mathrm{d}}{\mathrm{d}t}\begin{bmatrix} \dot{x}_{\mathrm{ss}\zeta}^{\mathrm{pll}} \\ x_{\mathrm{ss}\zeta}^{\mathrm{pll}} \end{bmatrix} = \underbrace{\begin{bmatrix} -E_{\zeta,0}k_{\zeta,\mathrm{p}}^{\mathrm{pll}} & -E_{\zeta,0}k_{\zeta,\mathrm{i}}^{\mathrm{pll}} \\ 1 & 0 \end{bmatrix}}_{\boldsymbol{A}_{\mathrm{ss}\zeta}^{\mathrm{pll}}} \underbrace{\begin{bmatrix} \dot{x}_{\mathrm{ss}\zeta}^{\mathrm{pll}} \\ x_{\mathrm{ss}\zeta}^{\mathrm{pll}} \end{bmatrix}}_{\boldsymbol{x}_{\mathrm{ss}\zeta}^{\mathrm{pll}}} + \underbrace{\begin{bmatrix} 0 & 0 & 0 & 0 & -\sin\theta_{\zeta,0} & \cos\theta_{\zeta,0} \\ 0 & 0 & 0 & 0 & 0 & 0 \end{bmatrix}}_{\boldsymbol{B}_{\mathrm{ss}\zeta}^{\mathrm{pll}}} \boldsymbol{y}_{\mathrm{E}\zeta}^{\mathrm{loc}} \tag{4.23}$$

$$\Delta\theta_{\zeta}^{\mathrm{c}} = \underbrace{\begin{bmatrix} k_{\zeta,\mathrm{p}}^{\mathrm{pll}} & k_{\zeta,\mathrm{i}}^{\mathrm{pll}} \end{bmatrix}}_{\boldsymbol{C}_{\mathrm{ss}\zeta}^{\mathrm{pll}}} \begin{bmatrix} \dot{x}_{\mathrm{ss}\zeta}^{\mathrm{pll}} \\ x_{\mathrm{ss}\zeta}^{\mathrm{pll}} \end{bmatrix} \tag{4.24}$$

where the fact that $\Delta\boldsymbol{e}_{\zeta}^{\mathrm{g}}$ belongs to $\boldsymbol{y}_{\mathrm{E}\zeta}^{\mathrm{loc}}$ has been exploited.

4.3.4 Frame transformations (abc→dq)

The controller's inputs are measurements of the converter current and filter bus voltage in the PLL dq frame.

By operating in a dq frame synchronised with the filter bus voltage, $i_{\mathrm{d}}^{\mathrm{ref}}$ is used solely to regulate active power output and $i_{\mathrm{q}}^{\mathrm{ref}}$ is used solely to regulate AC voltage/reactive power output in dq-axis vector current control.

However, perturbations in the filter bus voltage cause phase tracking errors in the PLL and so the PLL dq frame and the filter bus voltage dq frame are *not* one and the same. These errors in the PLL result in improper calculation of the d and q components (the d and q components are not truly aligned with the filter bus voltage dq frame).

By extension, changes in the converter currents are miscalculated due to misalignment of the PLL dq frame with the filter bus voltage frame.

Considering equation 4.4, the converter current expressed in the PLL dq frame is given as follows:

$$\boldsymbol{i}^{\mathrm{c}}_{\mathrm{c}_\zeta} = \begin{bmatrix} \cos\theta^{\mathrm{c}}_\zeta & \sin\theta^{\mathrm{c}}_\zeta \\ -\sin\theta^{\mathrm{c}}_\zeta & \cos\theta^{\mathrm{c}}_\zeta \end{bmatrix} \boldsymbol{i}^{\mathrm{g}}_{\mathrm{c}_\zeta} \tag{4.25}$$

Applying the perturbation and linearisation technique as before,

$$\Delta\boldsymbol{i}^{\mathrm{c}}_{\mathrm{c}_\zeta}(s) = \underbrace{\begin{bmatrix} \cos\theta_{\zeta,0} & \sin\theta_{\zeta,0} \\ -\sin\theta_{\zeta,0} & \cos\theta_{\zeta,0} \end{bmatrix} \boldsymbol{T}^{\mathrm{vcc}}_2}_{\boldsymbol{G}^{\mathrm{b}}_\zeta(s)} \boldsymbol{y}^{\mathrm{loc}}_{\mathrm{E}_\zeta}(s) + \underbrace{\begin{bmatrix} -\sin\theta_{\zeta,0} & \cos\theta_{\zeta,0} \\ -\cos\theta_{\zeta,0} & -\sin\theta_{\zeta,0} \end{bmatrix} \boldsymbol{i}^{\mathrm{g}}_{\mathrm{c}_\zeta,0}}_{\boldsymbol{G}^{\mathrm{c}}_\zeta(s)} \left[\Delta\theta^{\mathrm{c}}_\zeta(s)\right] \tag{4.26}$$

where

$$\boldsymbol{T}^{\mathrm{vcc}}_2 = \begin{bmatrix} \boldsymbol{O}(2,2) & \boldsymbol{I}_2 & \boldsymbol{O}(2,2) \end{bmatrix}$$

That is, $\Delta\boldsymbol{i}^{\mathrm{g}}_{\mathrm{c}_\zeta} = \boldsymbol{T}^{\mathrm{vcc}}_2 \boldsymbol{y}^{\mathrm{loc}}_{\mathrm{E}_\zeta}$.This is so as to allow easy integration with the network model.

Similar expressions are obtained for $\Delta\boldsymbol{e}^{\mathrm{c}}_\zeta$:

$$\Delta\boldsymbol{e}^{\mathrm{c}}_\zeta(s) = \underbrace{\begin{bmatrix} \cos\theta_{\zeta,0} & \sin\theta_{\zeta,0} \\ -\sin\theta_{\zeta,0} & \cos\theta_{\zeta,0} \end{bmatrix} \boldsymbol{T}^{\mathrm{vcc}}_1}_{\boldsymbol{G}^{\mathrm{d}}_\zeta(s)} \boldsymbol{y}^{\mathrm{loc}}_{\mathrm{E}_\zeta} + \underbrace{\begin{bmatrix} -\sin\theta_{\zeta,0} & \cos\theta_{\zeta,0} \\ -\cos\theta_{\zeta,0} & -\sin\theta_{\zeta,0} \end{bmatrix} \boldsymbol{e}^{\mathrm{g}}_{\zeta,0}}_{\boldsymbol{G}^{\mathrm{e}}_\zeta(s)} \left[\Delta\theta^{\mathrm{c}}_\zeta(s)\right] \tag{4.27}$$

Contribution to unified linear state-space model

Since there is no explicit dependence on s in this section, including these components in a combined linearised state-space model is a trivial process. That is,

$$\boldsymbol{y}^{\mathrm{g}\to\mathrm{c}}_\zeta = \underbrace{\begin{bmatrix} \boldsymbol{G}^{\mathrm{b}}_\zeta \\ \boldsymbol{G}^{\mathrm{d}}_\zeta \end{bmatrix}}_{\boldsymbol{C}^{\mathrm{abc},1}_\zeta} \boldsymbol{y}^{\mathrm{loc}}_{\mathrm{E}_\zeta} + \underbrace{\begin{bmatrix} \boldsymbol{G}^{\mathrm{c}}_\zeta \\ \boldsymbol{G}^{\mathrm{e}}_\zeta \end{bmatrix} \boldsymbol{C}^{\mathrm{pll}}_\zeta}_{\boldsymbol{C}^{\mathrm{abc},2}_\zeta} \boldsymbol{x}^{\mathrm{pll}}_\zeta \tag{4.28}$$

with an additional term being present for the first-order PLL:

$$\boldsymbol{y}_{\zeta}^{\mathrm{g}\to\mathrm{c}} = \underbrace{\left(\begin{bmatrix} \boldsymbol{G}_{\zeta}^{\mathrm{b}} \\ \boldsymbol{G}_{\zeta}^{\mathrm{d}} \end{bmatrix} + \begin{bmatrix} \boldsymbol{G}_{\zeta}^{\mathrm{c}} \\ \boldsymbol{G}_{\zeta}^{\mathrm{e}} \end{bmatrix} \boldsymbol{D}_{\zeta}^{\mathrm{pll}} \right)}_{\boldsymbol{C}_{\zeta}^{\mathrm{abc},1}} \boldsymbol{y}_{\mathrm{E}_{\zeta}}^{\mathrm{loc}} + \underbrace{\begin{bmatrix} \boldsymbol{G}_{\zeta}^{\mathrm{c}} \\ \boldsymbol{G}_{\zeta}^{\mathrm{e}} \end{bmatrix} \boldsymbol{C}_{\zeta}^{\mathrm{pll}}}_{\boldsymbol{C}_{\zeta}^{\mathrm{abc},2}} \boldsymbol{x}_{\zeta}^{\mathrm{pll}} \tag{4.29}$$

4.3.5 The current controller

Analysing first in the frequency domain, the control law for a dq-axis vector current PI controller tuned using the Internal Model Control principle is given by equation 4.30 [22]:

$$\boldsymbol{v}_{\zeta}^{\mathrm{ref,c}}(s) = \underbrace{\alpha_{\mathrm{c}_{\zeta}} \left[L_{\mathrm{c}_{\zeta}} + \frac{R_{\mathrm{c}_{\zeta}}}{s} \right]}_{G_{\zeta}^{\mathrm{cc}}} (\boldsymbol{i}_{\zeta}^{\mathrm{ref,c}}(s) - \boldsymbol{i}_{\mathrm{c}_{\zeta}}^{\mathrm{c}}(s)) + \omega_0 L_{\mathrm{c}_{\zeta}} \begin{bmatrix} 0 & -1 \\ 1 & 0 \end{bmatrix} \boldsymbol{i}_{\mathrm{c}_{\zeta}}^{\mathrm{c}}(s) + H_{\zeta}^{\mathrm{lp}}(s) \boldsymbol{e}_{\zeta}^{\mathrm{c}}(s) \tag{4.30}$$

where $\alpha_{\mathrm{c}_{\zeta}}$ is the bandwidth of the closed-loop system at the current control level, typically chosen to be 20% of the switching frequency, f_{s}, of the converter to avoid undesirable interactions between the current controller and the PWM process [3][6]. Alternative tuning algorithms give very similar transfer functions for the current controller (this is due to the simplistic nature of the model of the grid upon which almost all converter stability is assessed).

A first-order low pass filter of the form given in equation 4.31 is applied to $\boldsymbol{e}_{\zeta}^{\mathrm{c}}$ to improve disturbance rejection. $\alpha_{\mathrm{f}_{\zeta}}$ being the bandwidth (in rad/s) of the low pass filter.

$$H_{\zeta}^{\mathrm{lp}}(s) = \alpha_{\mathrm{f}_{\zeta}} / (s + \alpha_{\mathrm{f}_{\zeta}}) \tag{4.31}$$

As with the network transfer function matrix, for mathematical reasons it is convenient to represent linear model of the current controller as the sum of three individual actions: that due to the changes in $\boldsymbol{i}_{\zeta}^{\mathrm{ref,c}}$; that due to the changes in $\boldsymbol{i}_{\mathrm{c}_{\zeta}}^{\mathrm{c}}$, and that due to changes in $\boldsymbol{e}_{\zeta}^{\mathrm{c}}$.

In matrix form,

$$\Delta \boldsymbol{v}_{\zeta}^{\mathrm{ref,c}}(s) = \underbrace{\begin{bmatrix} G_{\zeta}^{\mathrm{cc}} & 0 \\ 0 & G_{\zeta}^{\mathrm{cc}} \end{bmatrix}}_{\boldsymbol{G}_{\zeta}^{\mathrm{f}}(s)} \Delta \boldsymbol{i}_{\zeta}^{\mathrm{ref,c}}(s) + \underbrace{\begin{bmatrix} -G_{\zeta}^{\mathrm{cc}} & -\omega_0 L_{\mathrm{c}_1} \\ \omega_0 L_{\mathrm{c}_{\zeta}} & -G_{\zeta}^{\mathrm{cc}} \end{bmatrix}}_{\boldsymbol{G}_{\zeta}^{\mathrm{g}}(s)} \Delta \boldsymbol{i}_{\mathrm{c}_{\zeta}}^{\mathrm{c}}(s) + \underbrace{\begin{bmatrix} H_{\zeta}^{\mathrm{lp}}(s) & 0 \\ 0 & H_{\zeta}^{\mathrm{lp}}(s) \end{bmatrix}}_{\boldsymbol{G}_{\zeta}^{\mathrm{h}}(s)} \Delta \boldsymbol{e}_{\zeta}^{\mathrm{c}}(s) \tag{4.32}$$

Contribution to unified linear state-space model

One could express the linearised model of the current controller in state-space form as shown:

$$\frac{\Delta \mathrm{d}\boldsymbol{e}_{\mathrm{f}_{\zeta}}^{\mathrm{c}}}{\mathrm{d}t} = \underbrace{\begin{bmatrix} -\alpha_{\mathrm{f}_{\zeta}} & 0 \\ 0 & -\alpha_{\mathrm{f}_{\zeta}} \end{bmatrix}}_{\boldsymbol{A}_{\zeta}^{\mathrm{lp}}} \underbrace{\Delta \boldsymbol{e}_{\mathrm{f}_{\zeta}}^{\mathrm{c}}}_{\boldsymbol{x}_{\zeta}^{\mathrm{lp}}} + \underbrace{\begin{bmatrix} 0 & 0 & \alpha_{\mathrm{f}_{\zeta}} & 0 \\ 0 & 0 & 0 & \alpha_{\mathrm{f}_{\zeta}} \end{bmatrix} \boldsymbol{C}_{\zeta}^{\mathrm{abc,1}}}_{\boldsymbol{B}_{\zeta}^{\mathrm{lp,1}}} \boldsymbol{y}_{\mathrm{E}_{\zeta}}^{\mathrm{loc}} + \underbrace{\begin{bmatrix} 0 & 0 & \alpha_{\mathrm{f}_{\zeta}} & 0 \\ 0 & 0 & 0 & \alpha_{\mathrm{f}_{\zeta}} \end{bmatrix} \boldsymbol{C}_{\zeta}^{\mathrm{abc,2}}}_{\boldsymbol{B}_{\zeta}^{\mathrm{lp,2}}} \boldsymbol{x}_{\zeta}^{\mathrm{pll}} \tag{4.33}$$

$$\boldsymbol{y}_{\zeta}^{\mathrm{lp}} = \underbrace{\begin{bmatrix} 0 & 0 & 1 & 0 \\ 0 & 0 & 0 & 1 \end{bmatrix}^{\mathrm{T}}}_{\boldsymbol{C}_{\zeta}^{\mathrm{lp}}} \Delta \boldsymbol{e}_{\mathrm{f}_{\zeta}}^{\mathrm{c}} \tag{4.34}$$

such that

$$\boldsymbol{z}_\zeta^{\mathrm{cc}} = \underbrace{\begin{bmatrix} 1 & 0 & 0 & 0 \\ 0 & 1 & 0 & 0 \\ 0 & 0 & 0 & 0 \\ 0 & 0 & 0 & 0 \end{bmatrix} \boldsymbol{C}_\zeta^{\mathrm{abc},1}}_{\boldsymbol{M}_\zeta^{\mathrm{cc},1}} \boldsymbol{y}_{\mathrm{E}_\zeta}^{\mathrm{loc}} + \underbrace{\begin{bmatrix} 1 & 0 & 0 & 0 \\ 0 & 1 & 0 & 0 \\ 0 & 0 & 0 & 0 \\ 0 & 0 & 0 & 0 \end{bmatrix} \boldsymbol{C}_\zeta^{\mathrm{abc},2}}_{\boldsymbol{M}_\zeta^{\mathrm{cc},2}} \boldsymbol{x}_\zeta^{\mathrm{pll}} + \boldsymbol{C}_\zeta^{\mathrm{lp}} \boldsymbol{x}_\zeta^{\mathrm{lp}} \tag{4.35}$$

$$\frac{\mathrm{d}\boldsymbol{x}_\zeta^{\mathrm{cc}}}{\mathrm{d}t} = \underbrace{\begin{bmatrix} 1 & 0 \\ 0 & 1 \end{bmatrix}}_{\boldsymbol{B}_\zeta^{\mathrm{cc,ref}}} \underbrace{\left[\Delta \boldsymbol{i}_\zeta^{\mathrm{ref,c}}\right]}_{\boldsymbol{z}_\zeta^{\mathrm{ref}}} + \underbrace{\begin{bmatrix} -1 & 0 & 0 & 0 \\ 0 & -1 & 0 & 0 \end{bmatrix}}_{\boldsymbol{B}_\zeta^{\mathrm{cc}}} \underbrace{\begin{bmatrix} \Delta \boldsymbol{i}_{\mathrm{c}_\zeta}^{\mathrm{c}} \\ \Delta \boldsymbol{e}_\zeta^{\mathrm{c}} \end{bmatrix}}_{\boldsymbol{z}_\zeta^{\mathrm{cc}}} \tag{4.36}$$

$$\begin{aligned} \underbrace{\Delta \boldsymbol{v}_\zeta^{\mathrm{ref,c}}}_{\boldsymbol{y}_\zeta^{\mathrm{cc}}} = {} & \underbrace{\begin{bmatrix} \alpha_{\mathrm{c}_\zeta} R_{\mathrm{c}_\zeta} & 0 \\ 0 & \alpha_{\mathrm{c}_\zeta} R_{\mathrm{c}_\zeta} \end{bmatrix}}_{\boldsymbol{C}_\zeta^{\mathrm{cc}}} \underbrace{\left[\Delta \boldsymbol{i}_\zeta^{\mathrm{ref}} - \Delta \boldsymbol{i}_{\mathrm{c}_\zeta}^{\mathrm{c}}\right]}_{\boldsymbol{x}_\zeta^{\mathrm{cc}}} + \underbrace{\begin{bmatrix} \alpha_{\mathrm{c}_\zeta} L_{\mathrm{c}_\zeta} & 0 \\ 0 & \alpha_{\mathrm{c}_\zeta} L_{\mathrm{c}_\zeta} \end{bmatrix}}_{\boldsymbol{D}_\zeta^{\mathrm{cc,ref}}} \underbrace{\left[\Delta \boldsymbol{i}_{\mathrm{c}_\zeta}^{\mathrm{ref,c}}\right]}_{\boldsymbol{z}_\zeta^{\mathrm{ref}}} + \dots \\ & \underbrace{\begin{bmatrix} -\alpha_{\mathrm{c}_\zeta} L_{\mathrm{c}_\zeta} & -\omega_0 L_{\mathrm{c}_\zeta} & 1 & 0 \\ \omega_0 L_{\mathrm{c}_\zeta} & -\alpha_{\mathrm{c}_\zeta} L_{\mathrm{c}_\zeta} & 0 & 1 \end{bmatrix}}_{\boldsymbol{D}_\zeta^{\mathrm{cc}}} \underbrace{\begin{bmatrix} \Delta \boldsymbol{i}_{\mathrm{c}_\zeta}^{\mathrm{c}} \\ \Delta \boldsymbol{e}_{\mathrm{f}_\zeta}^{\mathrm{c}} \end{bmatrix}}_{\boldsymbol{z}_\zeta^{\mathrm{cc}}} \end{aligned} \tag{4.37}$$

That is,

$$\frac{\mathrm{d}\boldsymbol{x}_\zeta^{\mathrm{cc}}}{\mathrm{d}t} = \boldsymbol{B}_\zeta^{\mathrm{cc}} \boldsymbol{z}_\zeta^{\mathrm{cc}} + \boldsymbol{B}_\zeta^{\mathrm{ref}} \boldsymbol{z}_\zeta^{\mathrm{ref}} \tag{4.38}$$

$$\boldsymbol{y}_\zeta^{\mathrm{cc}} = \boldsymbol{C}_\zeta^{\mathrm{cc}} \boldsymbol{x}_\zeta^{\mathrm{cc}} + \boldsymbol{E}_\zeta^{\mathrm{cc}} \boldsymbol{z}_\zeta^{\mathrm{cc}} + \boldsymbol{D}_\zeta^{\mathrm{ref}} \boldsymbol{z}_\zeta^{\mathrm{ref}} \tag{4.39}$$

4.3.6 Voltage signals for PWM

The PLL dq frame then connects back to the grid frame by an inverse process, which, after accounting for the delays associated with the PWM process, provides the values for $\Delta \boldsymbol{v}_\zeta^{\mathrm{g}}(s)$. In an almost

identical fashion to that seen in the voltage $\boldsymbol{e}_{\zeta}^{\mathrm{g}}$ being transformed into the converter dq frame,

$$\Delta\boldsymbol{v}_{\zeta}^{\mathrm{ref,g}}(s) = \underbrace{\begin{bmatrix}\cos\theta_{\zeta,0} & -\sin\theta_{\zeta,0}\\ \sin\theta_{\zeta,0} & \cos\theta_{\zeta,0}\end{bmatrix}}_{\boldsymbol{G}_{\zeta}^{\mathrm{i}}(s)}\Delta\boldsymbol{v}_{\zeta}^{\mathrm{ref,c}}(s) + \underbrace{\begin{bmatrix}-\sin\theta_{\zeta,0} & -\cos\theta_{\zeta,0}\\ \cos\theta_{\zeta,0} & -\sin\theta_{\zeta,0}\end{bmatrix}\boldsymbol{v}_{\zeta,0}^{\mathrm{c}}}_{\boldsymbol{G}_{\zeta}^{\mathrm{j}}(s)}\left[\Delta\theta_{\zeta}^{\mathrm{c}}(s)\right] \tag{4.40}$$

Essentially, the sign of $\theta_{\zeta}^{\mathrm{c}}$ has changed to reflect the inverse Park transformation being applied here.

Note, the steady-state values of the bridge voltage in the PLL dq frame are related to the converter voltage in the grid dq frame by the following:

$$\begin{aligned}\boldsymbol{v}_{\zeta,0}^{\mathrm{c}} &= v_{\mathrm{d},0}^{\mathrm{g}}\cos\theta_0 + v_{\mathrm{q},0}^{\mathrm{g}}\sin\theta_0 + j(v_{\mathrm{q},0}^{\mathrm{g}}\cos\theta_0 - v_{\mathrm{d},0}^{\mathrm{g}}\sin\theta_0)\\ &= \underbrace{V_{\zeta,0}\cos(\theta_{\mathrm{v}_{\zeta},0}-\theta_{\zeta,0})}_{\Re\left\{\boldsymbol{v}_{\zeta,0}^{\mathrm{c}}\right\}} + j\underbrace{V_{\zeta,0}\sin(\theta_{\mathrm{v}_{\zeta},0}-\theta_{\zeta,0})}_{\Im\left\{\boldsymbol{v}_{\zeta,0}^{\mathrm{c}}\right\}}\end{aligned} \tag{4.41}$$

where $V_{\zeta,0}$ is the converter terminal voltage magnitude. This means that $\boldsymbol{G}_{\zeta}^{\mathrm{j}}$ can be simplified to the following:

$$\boldsymbol{G}_{\zeta}^{\mathrm{j}}(s) = \begin{bmatrix}-V_{\zeta,0}\sin\theta_{\mathrm{v}_{\zeta},0} & V_{\zeta,0}\cos\theta_{\mathrm{v}_{\zeta},0}\end{bmatrix}^{\mathrm{T}} \tag{4.42}$$

Contribution to unified linear state-space model

For the unified linear state-space model for quick time-domain simulations, assuming a second-order PLL, the component state-space model is as follows:

$$\boldsymbol{y}_\zeta^{\mathrm{c}\to\mathrm{g}} = \boldsymbol{G}_\zeta^{\mathrm{i}}\boldsymbol{y}_\zeta^{\mathrm{cc}} + \boldsymbol{G}_\zeta^{\mathrm{j}}\boldsymbol{y}_\zeta^{\mathrm{pll}} \tag{4.43}$$

$$= \underbrace{\begin{bmatrix} \boldsymbol{O}(2, N_{\mathrm{E}}) & \overbrace{\begin{bmatrix} \left(\boldsymbol{G}_\zeta^{\mathrm{i}}\boldsymbol{D}_\zeta^{\mathrm{cc}}\boldsymbol{M}_\zeta^{\mathrm{cc},2} + \boldsymbol{G}_\zeta^{\mathrm{j}}\boldsymbol{C}_\zeta^{\mathrm{pll}}\right) & \boldsymbol{G}_\zeta^{\mathrm{i}}\boldsymbol{D}_\zeta^{\mathrm{cc}}\boldsymbol{C}_\zeta^{\mathrm{lp}} & \boldsymbol{G}_\zeta^{\mathrm{i}}\boldsymbol{C}_\zeta^{\mathrm{cc}} \end{bmatrix}}^{\boldsymbol{\rho}_\zeta^{\mathrm{vcc}}} \end{bmatrix}}_{\boldsymbol{C}_\zeta^{\mathrm{dq}}} \underbrace{\begin{bmatrix} \boldsymbol{x}_{\mathrm{E}}^{\mathrm{loc}} \\ \boldsymbol{x}_\zeta^{\mathrm{pll}} \\ \boldsymbol{x}_\zeta^{\mathrm{lp}} \\ \boldsymbol{x}_\zeta^{\mathrm{cc}} \end{bmatrix}}_{\boldsymbol{x}_\zeta^{\mathrm{uni}}} + \ldots$$

$$\underbrace{\left[\boldsymbol{G}_\zeta^{\mathrm{i}}\boldsymbol{D}_\zeta^{\mathrm{cc,ref}}\right]}_{\boldsymbol{D}_\zeta^{\mathrm{dq}}}\boldsymbol{z}_\zeta^{\mathrm{ref}} + \underbrace{\left[\boldsymbol{G}_\zeta^{\mathrm{i}}\boldsymbol{D}_\zeta^{\mathrm{cc}}\boldsymbol{M}_\zeta^{\mathrm{cc},1}\right]}_{\boldsymbol{E}_\zeta^{\mathrm{dq}}}\boldsymbol{y}_{\mathrm{E}\zeta}^{\mathrm{loc}} \tag{4.44}$$

where N_{E} covers the number of states due to the electrical part of the system.

If a first-order PLL is modelled, the $\boldsymbol{E}_\zeta^{\mathrm{dq}}$ term requires a small modification:

$$\boldsymbol{E}_\zeta^{\mathrm{dq}} = \boldsymbol{G}_\zeta^{\mathrm{i}}\boldsymbol{D}_\zeta^{\mathrm{cc}}\boldsymbol{M}_\zeta^{\mathrm{cc},1} + \boldsymbol{G}_\zeta^{\mathrm{j}}\boldsymbol{D}_\zeta^{\mathrm{pll}} \tag{4.45}$$

For the single converter system, $N_{\mathrm{E}} = 4$ or 6, depending on whether an L or LC filter is adopted[2]. To permit extending the model to multi-converter systems, the states for a given converter, ζ, using dq-axis vector current control in a multi-converter system will be defined as

$$\boldsymbol{x}_\zeta^{\mathrm{vcc}} = \begin{bmatrix} \left(\boldsymbol{x}_\zeta^{\mathrm{pll}}\right)^{\mathrm{T}} & \left(\boldsymbol{x}_\zeta^{\mathrm{lp}}\right)^{\mathrm{T}} & \left(\boldsymbol{x}_\zeta^{\mathrm{cc}}\right)^{\mathrm{T}} \end{bmatrix}^{\mathrm{T}} \tag{4.46}$$

The author would also like to stress that for the multi-converter system, $\boldsymbol{G}_\zeta^{\mathrm{i}}$, $\boldsymbol{D}_\zeta^{\mathrm{ref}}$, $\boldsymbol{G}_\zeta^{\mathrm{j}}$, $\boldsymbol{C}_\zeta^{\mathrm{pll}}$ and $\boldsymbol{D}_\zeta^{\mathrm{cc}}$, etc. will vary from converter to converter i.e. these component matrices need re-evaluation when moving through the converters in the model construction.

[2]Different filter topologies would have a different value of N_{E}.

4.4 Combined system of plant and controller

Combining all the sections except for those which relate to the calculation of reference current values, the following block diagram is derived when the PLL is applied.

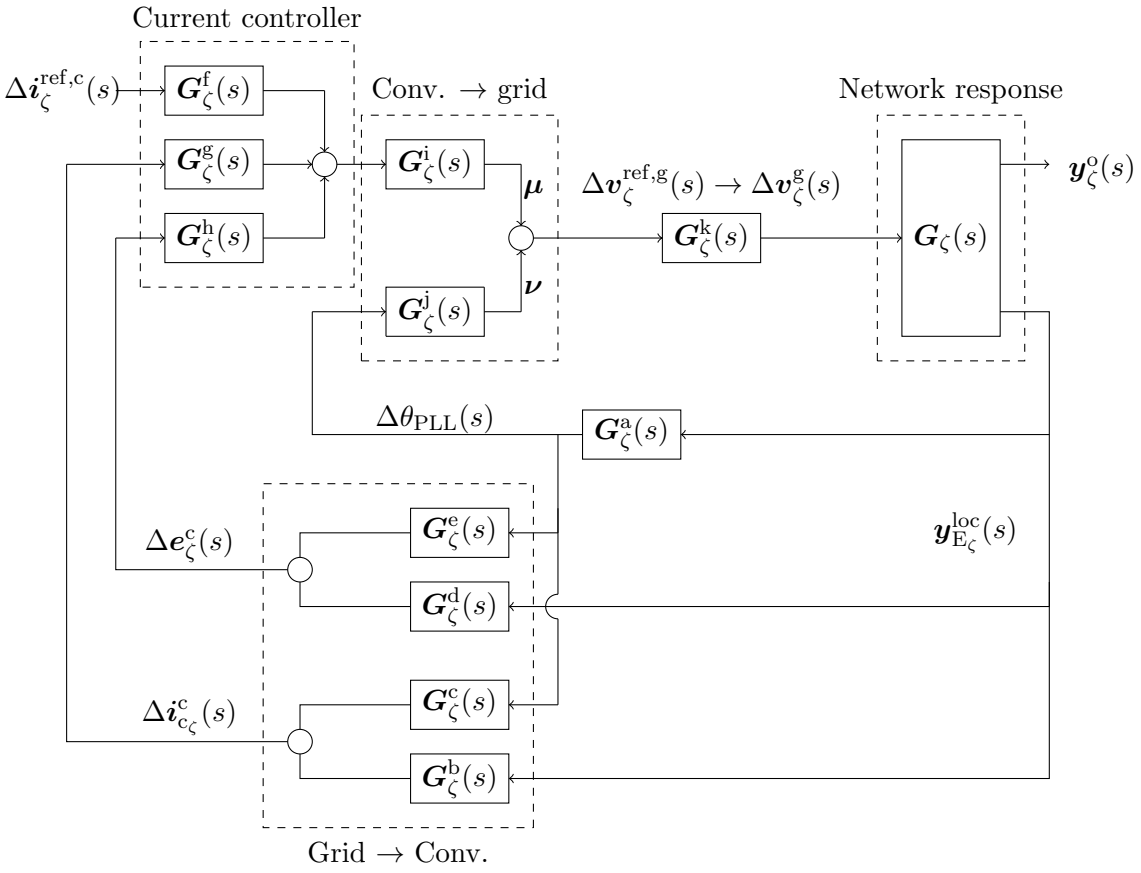

Figure 4.6: Complete linearised model for frequency domain analysis of a single converter system.

If one were to include the effects of delays during the PWM process, a Padé approximant could be used, which would feature in the $\boldsymbol{G}_\zeta^{\mathrm{k}}$ matrix; otherwise, $\boldsymbol{G}_\zeta^{\mathrm{k}}$ is just the identity matrix. In general, it was found that the delay had little impact on the stability, presumably due to the fact that it had a most pronounced effect in the high frequency region, beyond the frequencies where issues have historically been reported [3].

In this case, simply joining the connecting the blocks (because there are no convolution integrals

left in the model), it follows that

$$\begin{aligned}\Delta\boldsymbol{v}_{\zeta}^{\mathrm{g}} &= \boldsymbol{\mu}+\boldsymbol{\nu}\\ &= \boldsymbol{G}_{\zeta}^{\mathrm{k}}\left[\boldsymbol{G}_{\zeta}^{\mathrm{i}}\boldsymbol{G}_{\zeta}^{\mathrm{f}}\Delta\boldsymbol{i}_{\zeta}^{\mathrm{ref}}+\left[\boldsymbol{G}_{\zeta}^{\mathrm{i}}\left(\boldsymbol{G}_{\zeta}^{\mathrm{g}}\left(\boldsymbol{G}_{\zeta}^{\mathrm{c}}\boldsymbol{G}_{\zeta}^{\mathrm{a}}+\boldsymbol{G}_{\zeta}^{\mathrm{b}}\right)+\boldsymbol{G}_{\zeta}^{\mathrm{h}}\left(\boldsymbol{G}_{\zeta}^{\mathrm{e}}\boldsymbol{G}_{\zeta}^{\mathrm{a}}+\boldsymbol{G}_{\zeta}^{\mathrm{d}}\right)\right)+\boldsymbol{G}_{\zeta}^{\mathrm{j}}\boldsymbol{G}_{\zeta}^{\mathrm{a}}\right]\boldsymbol{y}_{\mathrm{E}_{\zeta}}^{\mathrm{loc}}\right]\end{aligned}$$

While the author stated that PWM delays have negligible influence on the stability in the weak AC systems, the $\boldsymbol{G}_{\zeta}^{\mathrm{k}}$ matrix has been included so as to allow users/readers to investigate such impacts if so desired.

Noting that $\boldsymbol{y}_{\mathrm{E}_{\zeta}}^{\mathrm{loc}}=\boldsymbol{G}_{\zeta}\Delta\boldsymbol{v}_{\zeta}^{\mathrm{g}}$,

$$\boldsymbol{y}_{\mathrm{E}_{\zeta}}^{\mathrm{loc}}=\boldsymbol{G}_{\zeta}\boldsymbol{G}_{\zeta}^{\mathrm{k}}\boldsymbol{G}_{\zeta}^{\mathrm{h}}\boldsymbol{G}_{\zeta}^{\mathrm{e}}\Delta\boldsymbol{i}_{\zeta}^{\mathrm{ref}}+\boldsymbol{G}_{\zeta}\boldsymbol{\kappa}_{\zeta}^{\mathrm{cc}}\boldsymbol{y}_{\mathrm{E}_{\zeta}}^{\mathrm{loc}}$$

where

$$\boldsymbol{\kappa}_{\zeta}^{\mathrm{cc}}=\boldsymbol{G}_{\zeta}^{\mathrm{k}}\left[\boldsymbol{G}_{\zeta}^{\mathrm{i}}\left(\boldsymbol{G}_{\zeta}^{\mathrm{g}}\left(\boldsymbol{G}_{\zeta}^{\mathrm{c}}\boldsymbol{G}_{\zeta}^{\mathrm{a}}+\boldsymbol{G}_{\zeta}^{\mathrm{b}}\right)+\boldsymbol{G}_{\zeta}^{\mathrm{h}}\left(\boldsymbol{G}_{\zeta}^{\mathrm{e}}\boldsymbol{G}_{\zeta}^{\mathrm{a}}+\boldsymbol{G}_{\zeta}^{\mathrm{d}}\right)\right)+\boldsymbol{G}_{\zeta}^{\mathrm{j}}\boldsymbol{G}_{\zeta}^{\mathrm{a}}\right]$$

Thus, it follows that the closed-loop frequency response of the inner current controller is as follows:

$$\boldsymbol{y}_{\zeta}^{\mathrm{o}}=\underbrace{\boldsymbol{\Omega}\left(\boldsymbol{I}-\boldsymbol{G}_{\zeta}\boldsymbol{\kappa}_{\zeta}^{\mathrm{cc}}\right)^{-1}\boldsymbol{G}_{\zeta}\boldsymbol{G}_{\zeta}^{\mathrm{k}}\boldsymbol{G}_{\zeta}^{\mathrm{i}}\boldsymbol{G}_{\zeta}^{\mathrm{f}}}_{\boldsymbol{H}^{\mathrm{vcc}}(s)}\Delta\boldsymbol{i}_{\zeta}^{\mathrm{ref}} \tag{4.47}$$

where

$$\boldsymbol{y}_{\zeta}^{\mathrm{o}}=\begin{bmatrix}\Delta P_{\zeta} & \Delta E_{\zeta}\end{bmatrix}^{\mathrm{T}} \tag{4.48}$$

The $\boldsymbol{\Omega}$ term is just to ensure that only the response of ΔP_{ζ} and ΔE_{ζ} to $\Delta\boldsymbol{i}_{\zeta}^{\mathrm{ref}}$ are considered. Thus,

$$\boldsymbol{\Omega}=\begin{bmatrix}1 & 0 & 0 & 0 & 0 & 0\\ 0 & 1 & 0 & 0 & 0 & 0\end{bmatrix} \tag{4.49}$$

Note - equation 4.47 is valid only for single-converter systems.

Unified linear state-space model for single converter system

Now let us complete the unified linear state-space model for the single converter system, which contains the dynamics of both the controller and plant in one single state-space model. For simplicity, let us ignore the switching delays.

Before substituting for $\boldsymbol{y}_\zeta^{\mathrm{c}\to\mathrm{g}}$ and $\boldsymbol{y}_{\mathrm{E}_\zeta}^{\mathrm{loc}}$, the state-equation reads as follows:

$$\frac{\mathrm{d}\boldsymbol{x}_\zeta^{\mathrm{uni}}}{\mathrm{d}t} = \begin{bmatrix} \boldsymbol{A}_{\mathrm{E}_\zeta}^{\mathrm{loc}} & \boldsymbol{O}(N_{\mathrm{E}}, N_{\mathrm{c}}) \\ \boldsymbol{O}(N_{\mathrm{c}}, N_{\mathrm{E}}) & \underbrace{\begin{bmatrix} \boldsymbol{A}_\zeta^{\mathrm{pll}} & \boldsymbol{O}(2, N_{\mathrm{pll}}) & \boldsymbol{O}(2,2) \\ \boldsymbol{B}_\zeta^{\mathrm{lp},2} & \boldsymbol{A}_\zeta^{\mathrm{lp}} & \boldsymbol{O}(N_{\mathrm{pll}}, N_{\mathrm{pll}}) \\ \boldsymbol{B}_\zeta^{\mathrm{cc}}\boldsymbol{M}_\zeta^{\mathrm{cc},2} & \boldsymbol{B}_\zeta^{\mathrm{cc}}\boldsymbol{C}_\zeta^{\mathrm{lp}} & \boldsymbol{O}(2,2) \end{bmatrix}}_{\boldsymbol{A}_\zeta^{\mathrm{vcc}}} \end{bmatrix} \underbrace{\begin{bmatrix} \boldsymbol{x}_{\mathrm{E}_\zeta}^{\mathrm{loc}} \\ \boldsymbol{x}_\zeta^{\mathrm{vcc}} \end{bmatrix}}_{\boldsymbol{x}_\zeta^{\mathrm{uni}}} + \dots$$
$$\begin{bmatrix} \boldsymbol{O}(N_{\mathrm{E}}, 6) \\ \underbrace{\begin{bmatrix} \boldsymbol{B}_\zeta^{\mathrm{pll}} \\ \boldsymbol{B}_\zeta^{\mathrm{lp},1} \\ \boldsymbol{B}_\zeta^{\mathrm{cc}}\boldsymbol{M}_\zeta^{\mathrm{cc},1} \end{bmatrix}}_{\boldsymbol{B}_\zeta^{\mathrm{vcc,a}}} \end{bmatrix} \boldsymbol{y}_{\mathrm{E}_\zeta}^{\mathrm{loc}} + \begin{bmatrix} \boldsymbol{B}_{\mathrm{E}_\zeta}^{\mathrm{loc}} \\ \boldsymbol{O}(N_{\mathrm{c}}, 2) \end{bmatrix} \boldsymbol{y}_\zeta^{\mathrm{c}\to\mathrm{g}} + \begin{bmatrix} \boldsymbol{O}(N_{\mathrm{E}}, N_{\mathrm{ref}}) \\ \underbrace{\begin{bmatrix} \boldsymbol{O}(N_{\mathrm{pll}}, N_{\mathrm{ref}}) \\ \boldsymbol{O}(2, N_{\mathrm{ref}}) \\ \boldsymbol{B}_\zeta^{\mathrm{cc,ref}} \end{bmatrix}}_{\boldsymbol{B}_\zeta^{\mathrm{vcc,b}}} \end{bmatrix} \boldsymbol{z}_\zeta^{\mathrm{ref}} \tag{4.50}$$

where N_{pll} refers to the order of the PLL being used and, for a single-converter system, $N_{\mathrm{ref}} = 2$ (one for each component of $\Delta\boldsymbol{i}_\zeta^{\mathrm{ref,c}}$). The total number of states due to the controller is N_{c}. For simulations only covering the PLL and the inner current controller, $N_{\mathrm{c}} = N_{\mathrm{pll}}+4$: in addition to the state-variables associated with the PLL, there are two state-variables for the action of the low-pass filter and two for the action of the PI controllers in the inner current controller). If no filtering is applied to the voltage, $N_{\mathrm{c}} = N_{\mathrm{pll}} + 2$.

This is actually a convenient form to work with when assessing multi-converter systems, which will be covered in chapter 7.

For a *single* converter system,

$$\boldsymbol{y}_{\zeta}^{\mathrm{c}\to\mathrm{g}} = \underbrace{\left(\boldsymbol{I}_2 - \boldsymbol{E}_{\zeta}^{\mathrm{dq}}\boldsymbol{D}_{\mathrm{E}\zeta}^{\mathrm{loc}}\right)^{-1}}_{\boldsymbol{\Lambda}}\left(\boldsymbol{C}_{\zeta}^{\mathrm{dq}}\boldsymbol{x}_{\zeta}^{\mathrm{uni}} + \boldsymbol{D}_{\zeta}^{\mathrm{dq}}\boldsymbol{z}_{\zeta}^{\mathrm{ref}} + \boldsymbol{E}_{\zeta}^{\mathrm{dq}}\boldsymbol{C}_{\mathrm{E}\zeta}^{\mathrm{loc}}\boldsymbol{x}_{\mathrm{E}\zeta}^{\mathrm{loc}}\right) \tag{4.51}$$

$$\boldsymbol{y}_{\mathrm{E}\zeta}^{\mathrm{loc}} = \boldsymbol{C}_{\mathrm{E}\zeta}^{\mathrm{loc}}\boldsymbol{x}_{\mathrm{E}\zeta}^{\mathrm{loc}} + \boldsymbol{D}_{\mathrm{E}\zeta}^{\mathrm{loc}}\boldsymbol{y}_{\zeta}^{\mathrm{c}\to\mathrm{g}} \tag{4.52}$$

Thus, the state equation can easily be expressed in terms of only state vectors, $\boldsymbol{x}_{\zeta}^{\mathrm{uni}}$, and the control vector, $\boldsymbol{z}_{\zeta}^{\mathrm{ref}}$; that is,

$$\frac{\mathrm{d}\boldsymbol{x}_{\zeta}^{\mathrm{uni}}}{\mathrm{d}t} = \boldsymbol{A}_{\zeta}^{\mathrm{uni}}\boldsymbol{x}_{\zeta}^{\mathrm{uni}} + \boldsymbol{B}_{\zeta}^{\mathrm{uni}}\boldsymbol{z}_{\zeta}^{\mathrm{ref}} \tag{4.53}$$

If a first order PLL is used, the system has five states from the controller side, and either four or six from the plant, depending on whether an L or LC filter is applied. If a second order PLL is used, the system has six states from the controller side, and either four or six from the plant, depending on whether an L or LC filter is applied.

Each component matrix is small, and so the cost of the matrix multiplications is small, as is the cost of determining $\boldsymbol{\Lambda}$. The unified state-space formulation can easily be coded in C++, which gives rise to significant speed gains, and removes the need for licensed software such as MATLAB/Simulink.

Even if the unified state-space model were not used, it is good to know how many states there are in order to allow effective operation of a sub-space algorithm.

For convenience, the output vector of the unified model, $\boldsymbol{y}_{\zeta}^{\mathrm{uni}}$, is defined to be $\boldsymbol{y}_{\zeta}^{\mathrm{o}}$.

The frequency response data can be obtained from the unified state-space model using 3.4. Since the state-space model unifies the controller and plant, the state matrices can be used to *directly* calculate the poles and zeros of the combined system. The poles of the overall system are just the eigenvalues of $\boldsymbol{A}_{\zeta}^{\mathrm{uni}}$. The zeros require a little more effort. The QZ method is suitable for this problem. Alternatively, if the reader uses MATLAB, one can use built in commands as shown in the Appendices.

4.4.1 Linear models including outer controllers

An extension of the linear model described earlier to include outer controllers is presented in figure 4.7:

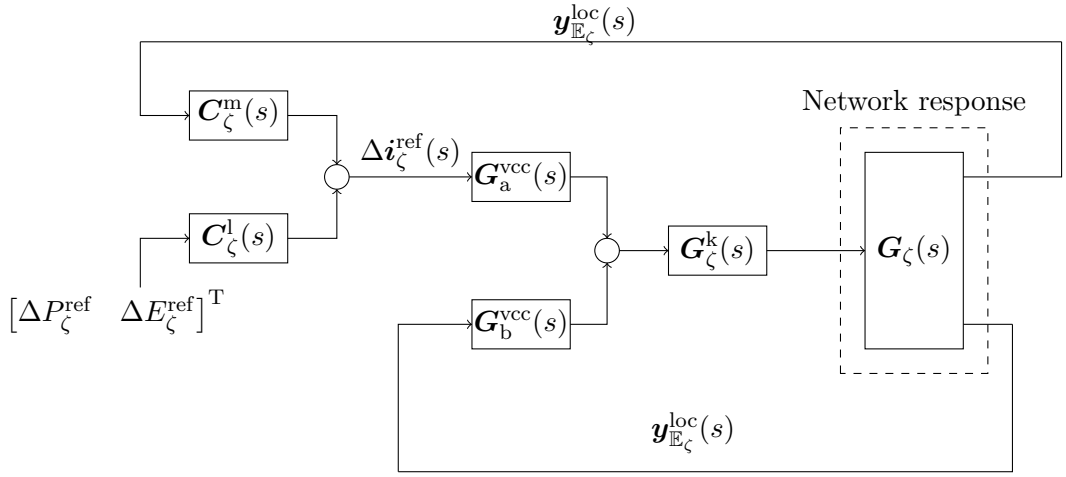

Figure 4.7: Simplified linear model of dq-axis vector current control including outer controllers.

However, this assumes that there is a perfect measurement of the voltage magnitude and power output. Considering [5], the voltage magnitude is sometimes determined from the PLL by equation 4.54:

$$E_\zeta = |\boldsymbol{e}^{\mathrm{g}}_{\zeta}| \tag{4.54}$$

To a first order,

$$\Delta E_\zeta = \left(\frac{\left(\boldsymbol{e}^{\mathrm{g}}_{\zeta,0}\right)^{\mathrm{T}}}{E_{\zeta,0}} \right) \Delta\boldsymbol{e}^{\mathrm{g}}_{\zeta} \tag{4.55}$$

Equation 4.55 may be simplified by simply noting that $\Re\left\{\boldsymbol{e}^{\mathrm{g}}_{\zeta,0}\right\} = E_{\zeta,0}$ and $\Im\left\{\boldsymbol{e}^{\mathrm{g}}_{\zeta,0}\right\} = 0$.

Similarly, if the power output of the converter were calculated from dq quantities, there is a connection to the PLL. Even if they were not, a connection to the PLL would probably exist through a frequency droop mechanism.

First order perturbations in the power output are given by equation 4.56:

$$\Delta P_\zeta = \left(\boldsymbol{i}^{\mathrm{c}}_{\mathrm{c}_\zeta,0}\right)^{\mathrm{T}} \Delta \boldsymbol{e}^{\mathrm{c}}_\zeta + \left(\boldsymbol{e}^{\mathrm{c}}_{\zeta,0}\right)^{\mathrm{T}} \Delta \boldsymbol{i}^{\mathrm{c}}_{\mathrm{c}_\zeta} \tag{4.56}$$

Thus,

$$\begin{bmatrix} \Delta P_\zeta \\ \Delta E_\zeta \end{bmatrix} = \begin{bmatrix} \left(\boldsymbol{i}^{\mathrm{c}}_{\mathrm{c}_\zeta,0}\right)^{\mathrm{T}} \\ \begin{bmatrix} 1 & 0 \end{bmatrix} \end{bmatrix} \Delta \boldsymbol{e}^{\mathrm{c}}_\zeta + \begin{bmatrix} E_{\zeta,0} & 0 \\ 0 & 0 \end{bmatrix} \Delta \boldsymbol{i}^{\mathrm{c}}_{\mathrm{c}_\zeta} \tag{4.57}$$

Hence, it is possible to connect the outer loop voltage measurement with the inner level model. If so desired, one could add in the effect of frequency droop by linking the output of the PLL to the outer controllers. However, the author feels that sufficient insight will be given by having the PLL used to calculate the power output of the converter.

Referring to figure 4.8, it can be deduced that the closed-loop frequency response is as follows:

$$\begin{aligned} \Delta \boldsymbol{v}^{\mathrm{g}}_\zeta = \boldsymbol{G}^{\mathrm{k}}_\zeta \Big[\boldsymbol{G}^{\mathrm{j}}_\zeta \boldsymbol{G}^{\mathrm{a}}_\zeta + \boldsymbol{G}^{\mathrm{i}}_\zeta \Big[\boldsymbol{G}^{\mathrm{g}}_\zeta \left(\boldsymbol{G}^{\mathrm{b}}_\zeta + \boldsymbol{G}^{\mathrm{c}}_\zeta \boldsymbol{G}^{\mathrm{a}}_\zeta \right) + \boldsymbol{G}^{\mathrm{h}}_\zeta \left(\boldsymbol{G}^{\mathrm{d}}_\zeta + \boldsymbol{G}^{\mathrm{e}}_\zeta \boldsymbol{G}^{\mathrm{a}}_\zeta \right) + \dots \\ \boldsymbol{G}^{\mathrm{f}}_\zeta \left(\boldsymbol{G}^{\mathrm{m}}_\zeta \left(\boldsymbol{G}^{\mathrm{b}}_\zeta + \boldsymbol{G}^{\mathrm{c}}_\zeta \boldsymbol{G}^{\mathrm{a}} \right) + \boldsymbol{G}^{\mathrm{n}}_\zeta \left(\boldsymbol{G}^{\mathrm{d}}_\zeta + \boldsymbol{G}^{\mathrm{e}}_\zeta \boldsymbol{G}^{\mathrm{a}}_\zeta \right) \right) \Big] \Big] \boldsymbol{G}_\zeta \Delta \boldsymbol{v}^{\mathrm{g}}_\zeta + \boldsymbol{G}^{\mathrm{k}}_\zeta \boldsymbol{G}^{\mathrm{i}}_\zeta \boldsymbol{G}^{\mathrm{f}}_\zeta \boldsymbol{G}^{\mathrm{l}}_\zeta \begin{bmatrix} \Delta P^{\mathrm{ref}}_\zeta \\ \Delta E^{\mathrm{ref}}_\zeta \end{bmatrix} \end{aligned} \tag{4.58}$$

Following the same approach as before, it can be shown that

$$\boldsymbol{y}^{\mathrm{o}}_\zeta = \boldsymbol{G}_\zeta \left[\boldsymbol{I} - \boldsymbol{\kappa}^{\mathrm{out}}_\zeta \right]^{-1} \boldsymbol{G}^{\mathrm{k}}_\zeta \boldsymbol{G}^{\mathrm{i}}_\zeta \boldsymbol{G}^{\mathrm{f}}_\zeta \boldsymbol{G}^{\mathrm{l}}_\zeta \begin{bmatrix} \Delta P^{\mathrm{ref}}_\zeta \\ \Delta E^{\mathrm{ref}}_\zeta \end{bmatrix} \tag{4.59}$$

where $\boldsymbol{\kappa}^{\mathrm{out}}_\zeta$ is defined through equation 4.58.

Contribution to the unified state-space model

The contribution of the outer controllers to the linearised state-space model is given as follows:

$$\frac{\mathrm{d}\boldsymbol{x}_\zeta^{\mathrm{oc}}}{\mathrm{d}t} = \underbrace{\begin{bmatrix} 1 & 0 \\ 0 & 1 \end{bmatrix}}_{\boldsymbol{B}_\zeta^{\mathrm{oc,ref}}} \begin{bmatrix} \Delta P_\zeta^{\mathrm{ref}} \\ \Delta E_\zeta^{\mathrm{ref}} \end{bmatrix} + \underbrace{\begin{bmatrix} -E_{\zeta,0} & 0 & -\Re\left\{\boldsymbol{i}_{\mathrm{c}\zeta,0}^{\mathrm{c}}\right\} & -\Im\left\{\boldsymbol{i}_{\mathrm{c}\zeta,0}^{\mathrm{c}}\right\} \\ 0 & 0 & -1 & 0 \end{bmatrix}}_{\boldsymbol{B}_\zeta^{\mathrm{oc}}} \boldsymbol{y}_\zeta^{\mathrm{g}\to\mathrm{c}} \tag{4.60}$$

$$\begin{aligned} \Delta\boldsymbol{i}_\zeta^{\mathrm{ref,c}} = {} & \underbrace{\begin{bmatrix} k_{\mathrm{i}}^{\mathrm{apc}} & 0 \\ 0 & k_{\mathrm{i}}^{\mathrm{avc}} \end{bmatrix}}_{\boldsymbol{C}_\zeta^{\mathrm{oc}}} \underbrace{\begin{bmatrix} \Delta P_\zeta^{\mathrm{ref}} - \Delta P_\zeta \\ \Delta E_\zeta^{\mathrm{ref}} - \Delta E_\zeta \end{bmatrix}}_{\boldsymbol{x}_\zeta^{\mathrm{oc}}} + \underbrace{\begin{bmatrix} k_{\mathrm{p}}^{\mathrm{apc}} & 0 \\ 0 & k_{\mathrm{p}}^{\mathrm{avc}} \end{bmatrix}}_{\boldsymbol{D}_\zeta^{\mathrm{oc,ref}}} \begin{bmatrix} \Delta P_\zeta^{\mathrm{ref}} \\ \Delta E_\zeta^{\mathrm{ref}} \end{bmatrix} + \dots \\ & \underbrace{\begin{bmatrix} -k_{\mathrm{p}}^{\mathrm{apc}} & 0 \\ 0 & -k_{\mathrm{p}}^{\mathrm{avc}} \end{bmatrix} \begin{bmatrix} E_{\zeta,0} & 0 & \Re\left\{\boldsymbol{i}_{\mathrm{c}\zeta,0}^{\mathrm{c}}\right\} & \Im\left\{\boldsymbol{i}_{\mathrm{c}\zeta,0}^{\mathrm{c}}\right\} \\ 0 & 0 & 1 & 0 \end{bmatrix}}_{\boldsymbol{D}_\zeta^{\mathrm{oc}}} \boldsymbol{y}_\zeta^{\mathrm{g}\to\mathrm{c}} \end{aligned} \tag{4.61}$$

Thus, there are two additional states to add to N_{c}. Equations 4.50 and 4.60 may be united as follows:

$$\begin{aligned} \frac{\mathrm{d}}{\mathrm{d}t}\begin{bmatrix} \boldsymbol{x}_\zeta^{\mathrm{uni}} \\ \boldsymbol{x}_\zeta^{\mathrm{oc}} \end{bmatrix} = {} & \begin{bmatrix} \boldsymbol{A}_{\mathrm{E}\zeta}^{\mathrm{loc}} & \boldsymbol{O}(N_{\mathrm{E}}, N_{\mathrm{c}}-2) & \boldsymbol{O}(N_{\mathrm{E}}, 2) \\ \boldsymbol{O}(N_{\mathrm{c}}-2, N_{\mathrm{E}}) & \boldsymbol{A}_\zeta^{\mathrm{vcc}} & \boldsymbol{B}_\zeta^{\mathrm{vcc,b}}\boldsymbol{C}_\zeta^{\mathrm{oc}} \\ \boldsymbol{O}(2, N_{\mathrm{E}}) & \begin{bmatrix} \boldsymbol{B}_\zeta^{\mathrm{oc}}\boldsymbol{C}_\zeta^{\mathrm{abc},2} & \boldsymbol{O}(2,4) \end{bmatrix} & \boldsymbol{O}(2,2) \end{bmatrix} \begin{bmatrix} \boldsymbol{x}_\zeta^{\mathrm{uni}} \\ \boldsymbol{x}_\zeta^{\mathrm{oc}} \end{bmatrix} + \dots \\ & \begin{bmatrix} \boldsymbol{O}(N_{\mathrm{E}}, 6) \\ \boldsymbol{B}_\zeta^{\mathrm{vcc,a}} \\ \boldsymbol{B}_\zeta^{\mathrm{oc}}\boldsymbol{C}_\zeta^{\mathrm{abc,1}} \end{bmatrix} \boldsymbol{y}_{\mathrm{E}\zeta}^{\mathrm{loc}} + \begin{bmatrix} \boldsymbol{O}(N_{\mathrm{E}}+N_{\mathrm{c}}-2, N_{\mathrm{ref}}) \\ \boldsymbol{B}_\zeta^{\mathrm{oc,ref}} \end{bmatrix} \begin{bmatrix} \Delta P_\zeta^{\mathrm{ref}} \\ \Delta E_\zeta^{\mathrm{ref}} \end{bmatrix} + \dots \\ & \begin{bmatrix} \boldsymbol{B}_{\mathrm{E}\zeta}^{\mathrm{loc}} \\ \boldsymbol{O}(N_{\mathrm{c}}, 2) \end{bmatrix} \boldsymbol{y}_\zeta^{\mathrm{c}\to\mathrm{g}} \end{aligned} \tag{4.62}$$

Considering equations 4.44 and 4.61,

$$\begin{aligned}\boldsymbol{y}_{\zeta}^{\mathrm{c}\to\mathrm{g}} = &\Bigg(\begin{bmatrix}\boldsymbol{O}(2,N_{\mathrm{E}}) & \boldsymbol{\rho}_{\zeta}^{\mathrm{vcc}} & \boldsymbol{O}(2,2)\end{bmatrix} + \boldsymbol{G}_{\zeta}^{\mathrm{i}}\boldsymbol{D}_{\zeta}^{\mathrm{cc,ref}}\boldsymbol{C}_{\zeta}^{\mathrm{oc}}\begin{bmatrix}\boldsymbol{O}(2,N_{\mathrm{E}}+N_{\mathrm{c}}-2) & \boldsymbol{I}_2\end{bmatrix} + \dots \\ &\boldsymbol{G}_{\zeta}^{\mathrm{i}}\boldsymbol{D}_{\zeta}^{\mathrm{cc,ref}}\boldsymbol{D}_{\zeta}^{\mathrm{oc}}\boldsymbol{C}_{\zeta}^{\mathrm{abc,2}}\begin{bmatrix}\boldsymbol{O}(N_{\mathrm{pll}},N_{\mathrm{E}}) & \boldsymbol{I}_{N_{\mathrm{pll}}} & \boldsymbol{O}(N_{\mathrm{pll}},N_{\mathrm{c}}-N_{\mathrm{pll}})\end{bmatrix}\Bigg)\begin{bmatrix}\boldsymbol{x}_{\zeta}^{\mathrm{uni}} \\ \boldsymbol{x}_{\zeta}^{\mathrm{oc}}\end{bmatrix} + \dots \\ &\left(\boldsymbol{G}_{\zeta}^{\mathrm{i}}\boldsymbol{D}_{\zeta}^{\mathrm{cc,ref}}\boldsymbol{D}_{\zeta}^{\mathrm{oc}}\boldsymbol{C}_{\zeta}^{\mathrm{abc,1}} + \boldsymbol{G}_{\zeta}^{\mathrm{i}}\boldsymbol{E}_{\zeta}^{\mathrm{cc}}\boldsymbol{M}_{\zeta}^{\mathrm{cc,1}}\right)\boldsymbol{y}_{\mathrm{E}_{\zeta}}^{\mathrm{loc}} + \boldsymbol{G}_{\zeta}^{\mathrm{i}}\boldsymbol{D}_{\zeta}^{\mathrm{cc,ref}}\boldsymbol{D}_{\zeta}^{\mathrm{oc,ref}}\begin{bmatrix}\Delta P_{\zeta}^{\mathrm{ref}} \\ \Delta E_{\zeta}^{\mathrm{ref}}\end{bmatrix} \\ = &\boldsymbol{C}_{\zeta}^{\mathrm{dq}'}\begin{bmatrix}\boldsymbol{x}_{\zeta}^{\mathrm{uni}} \\ \boldsymbol{x}_{\zeta}^{\mathrm{oc}}\end{bmatrix} + \boldsymbol{D}_{\zeta}^{\mathrm{dq}'}\begin{bmatrix}\Delta P_{\zeta}^{\mathrm{ref}} \\ \Delta E_{\zeta}^{\mathrm{ref}}\end{bmatrix} + \boldsymbol{E}_{\zeta}^{\mathrm{dq}'}\boldsymbol{y}_{\mathrm{E}_{\zeta}}^{\mathrm{loc}} \qquad (4.63)\end{aligned}$$

Using equation 4.52, it is possible to express $\boldsymbol{y}_{\zeta}^{\mathrm{c}\to\mathrm{g}}$ in terms of only the state vector, $\begin{bmatrix}\left(\boldsymbol{x}_{\zeta}^{\mathrm{uni}}\right)^{\mathrm{T}} & \left(\boldsymbol{x}_{\zeta}^{\mathrm{oc}}\right)^{\mathrm{T}}\end{bmatrix}^{\mathrm{T}}$, and the control vector, $\begin{bmatrix}\Delta P_{\zeta}^{\mathrm{ref}} & \Delta E_{\zeta}^{\mathrm{ref}}\end{bmatrix}^{\mathrm{T}}$.

which means that a unified state-equation featuring only the state and control vectors can be derived.

The purpose of presenting some simulation results where outer loop is included is to simply illustrate the knock-on effect of the poor dynamics at the current control and PLL level on outer loop control.

However, it should be noted that the linear model including outer controllers presented here is far more specific than that presented for the inner current level only. A large amount of variation can be found in the outer controllers. For example, DC bus voltage regulators could be applied instead of an active power controller, or the PLL might not be used to calculate either the voltage magnitude or the active power output. Thus, in order to to remain as generic as possible, multi-converter system analyses will ignore the outer loop. If the inner loop is functioning well, it is reasonable to assume that the outer loop controllers, whatever their topology, should not introduce issues in and of themselves, so long as they are well-tuned.

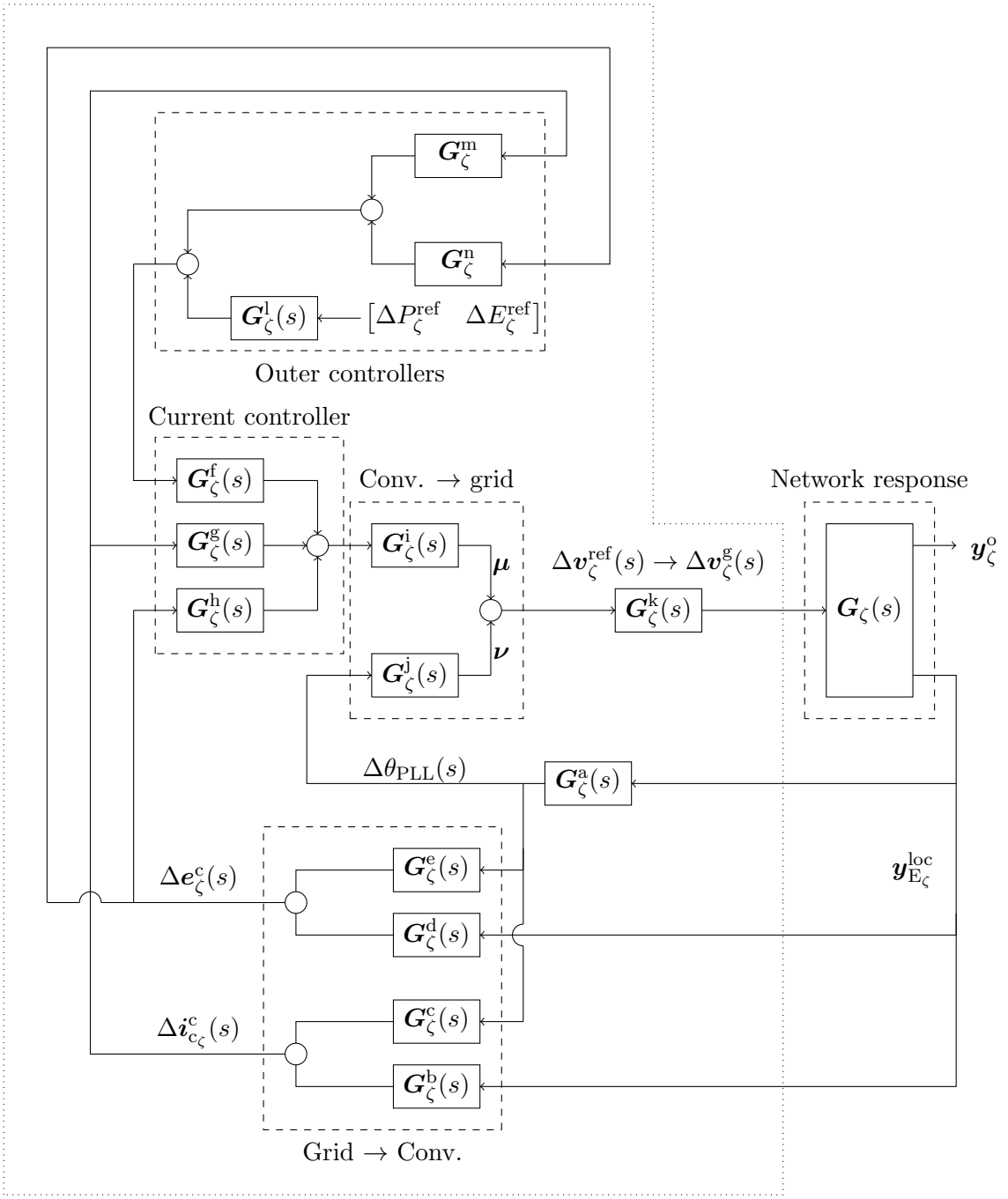

Figure 4.8: Linearised model including outer control where outer loop feedback signals are determined from quantities in PLL dq frame.

If the reader wishes to embed frequency dependent component values i.e. $R_{\mathrm{c}_1} \rightarrow R_{\mathrm{c}_1}(\omega)$, the block diagram approach is more appropriate as it can be paired with the sub-space algorithms.

4.4.2 Condensed models for upgrading to multi-converter system analyses

For convenience, particularly when considering multi-converter systems as done in chapter 7, the dq-axis vector current control system for converter ζ may be condensed into two blocks as shown:

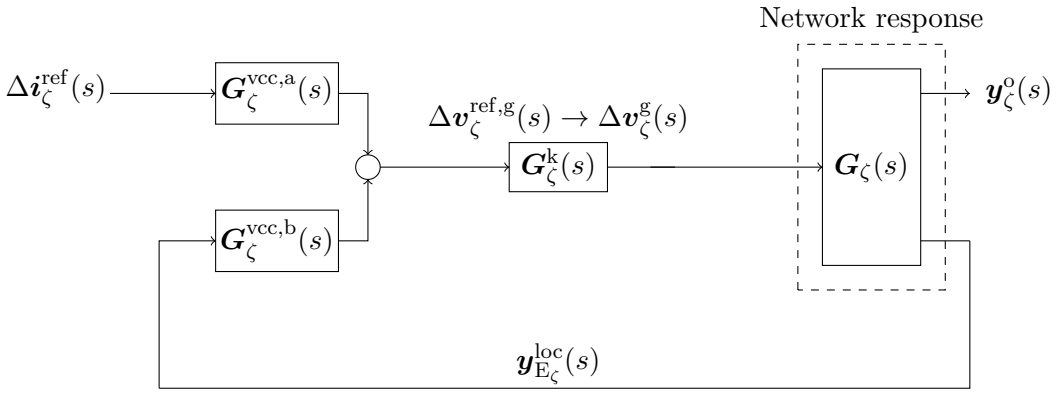

Figure 4.9: Fully condensed linearised model suitable for adapting to more complex systems

That is,

$$\Delta \boldsymbol{v}_\zeta^{\mathrm{ref,g}}(s) = \boldsymbol{G}_\zeta^{\mathrm{vcc,a}}(s)\Delta \boldsymbol{i}_\zeta^{\mathrm{ref}}(s) + \boldsymbol{G}_\zeta^{\mathrm{vcc,b}}(s)\boldsymbol{y}_{\mathrm{E}_\zeta}^{\mathrm{loc}} \tag{4.64}$$

Such a representation can then be easily integrated into a larger model comprising multiple converters, which are covered in chapter 7. However, the structure embedded in $\boldsymbol{G}_\zeta^{\mathrm{vcc,b}}$ will change with the PLL, thus requiring re-evaluation.

Unified state-space model

For an n converter system, equation 4.50 would be recycled in the following manner:

$$\frac{\mathrm{d}}{\mathrm{d}t}\begin{bmatrix}\boldsymbol{x}_{\mathrm{E}}\\ \boldsymbol{x}_1^{\mathrm{vcc}}\\ \boldsymbol{x}_2^{\mathrm{vcc}}\\ \vdots\\ \boldsymbol{x}_{\mathrm{n}}^{\mathrm{vcc}}\end{bmatrix} = \begin{bmatrix}\boldsymbol{A}_{\mathrm{E}} & & & & \\ & \boldsymbol{A}_1^{\mathrm{vcc}} & & & \\ & & \boldsymbol{A}_2^{\mathrm{vcc}} & & \\ & & & \ddots & \\ & & & & \boldsymbol{A}_{\mathrm{n}}^{\mathrm{vcc}}\end{bmatrix}\begin{bmatrix}\boldsymbol{x}_{\mathrm{E}}\\ \boldsymbol{x}_1^{\mathrm{vcc}}\\ \boldsymbol{x}_2^{\mathrm{vcc}}\\ \vdots\\ \boldsymbol{x}_{\mathrm{n}}^{\mathrm{vcc}}\end{bmatrix} + \begin{bmatrix}\boldsymbol{B}_{\mathrm{E}}\\ \boldsymbol{O}(N_{\mathrm{E}}, 2n)\end{bmatrix}\underbrace{\begin{bmatrix}\boldsymbol{y}_1^{\mathrm{c}\to\mathrm{g}}\\ \boldsymbol{y}_2^{\mathrm{c}\to\mathrm{g}}\\ \vdots\\ \boldsymbol{y}_{\mathrm{n}}^{\mathrm{c}\to\mathrm{g}}\end{bmatrix}}_{\boldsymbol{z}_{\mathrm{E}}^{\mathrm{loc}}} + \dots$$

$$\underbrace{\begin{bmatrix}\boldsymbol{O}(N_{\mathrm{E}}, 6n)\\ \begin{bmatrix}\boldsymbol{B}_1^{\mathrm{vcc,a}} & & & \\ & \boldsymbol{B}_2^{\mathrm{vcc,a}} & & \\ & & \ddots & \\ & & & \boldsymbol{B}_{\mathrm{ss,a_n}}^{\mathrm{vcc}}\end{bmatrix}\end{bmatrix}}_{\boldsymbol{B}^{\mathrm{vcc,a}}}\begin{bmatrix}\boldsymbol{y}_{\mathrm{E}_1}^{\mathrm{loc}}\\ \boldsymbol{y}_{\mathrm{E}_2}^{\mathrm{loc}}\\ \vdots\\ \boldsymbol{y}_{\mathrm{E}_{\mathrm{n}}}^{\mathrm{loc}}\end{bmatrix} + \dots$$

$$\underbrace{\begin{bmatrix}\boldsymbol{O}(N_{\mathrm{E}}, 2n)\\ \begin{bmatrix}\boldsymbol{B}_1^{\mathrm{vcc,b}} & & & \\ & \boldsymbol{B}_2^{\mathrm{vcc,b}} & & \\ & & \ddots & \\ & & & \boldsymbol{B}_{\mathrm{n}}^{\mathrm{vcc,b}}\end{bmatrix}\end{bmatrix}}_{\boldsymbol{B}^{\mathrm{vcc,b}}}\begin{bmatrix}\boldsymbol{z}_1^{\mathrm{ref}}\\ \boldsymbol{z}_2^{\mathrm{ref}}\\ \vdots\\ \boldsymbol{z}_{\mathrm{n}}^{\mathrm{ref}}\end{bmatrix} \tag{4.65}$$

where $\boldsymbol{y}_{\mathrm{E}_\zeta}^{\mathrm{loc}}$ is as defined in equation 3.15. The vector $\boldsymbol{y}_\zeta^{\mathrm{c}\to\mathrm{g}}$ contains the bridge voltages set by the controller for converter ζ.

Note also that the superscript has been dropped from $\boldsymbol{A}_{\mathrm{E}}$ and $\boldsymbol{B}_{\mathrm{E}}$. This is because the electrical system will encompass more than just the local system. Embedded in these terms are the coupling terms. The controller matrices remain unchanged since the controllers just react to the network dynamics but do not directly communicate with other controllers. The final source of coupling is accounted for through substitution for $\boldsymbol{y}_{\mathrm{E}}^{\mathrm{loc}}$. In chapter 7, these matrices will be derived.

4.5 Linear & non-linear simulations involving dq-axis vector current control

For single converter systems, $\zeta = 1$ only. A range of operating points are considered, covering different short-circuit ratios and different power set points to identify problematic areas.

A study revealed that if delays were ignored from the block diagram model and $R_{c_1} \neq R_{c_1}(\omega)$ (and also for all other components), the unified state-space model and block diagram approach agreed perfectly (as they should if implemented correctly). Sample MATLAB codes demonstrating such can be found in the Appendices.

The baseline model to be investigated is one where the converter has only the inner current controller and uses a simple PLL to synchronise with the grid. The converter uses an LC filter in these simulations. The filter characteristics are based on [3] and are given in table 4.1. These values are chosen for two reasons: first, the filter characteristics found in [3] are those found in the Caprivi link, making the choice of values realistic; second, by taking the same values, direct comparisons can be made with the results presented in [3], which could then be used to provide additional confidence in the validity of the models outlined in this work. The second point is subject to the control algorithms being kept the same in the comparison.

$\omega_0 L_{c_1}$	R_{c_1}	$\omega_0 C_{f_1}$
0.20	0.01	1/0.17

Table 4.1: Filter characteristics in p.u. values

The per unit system used is based on a system with a base power, S_{base} of 350 MVA, and a base voltage of 195 kV.

4.5.1 Using a first-order PLL

While comparisons between the non-linear and linear models could be used as a means of validating the linear model, a first-order PLL with the same gains as found in [3] was adopted to begin with to allow a direct comparison with results presented in [3] to be made. This in turn would provide

additional confidence in the model, before proceeding to new territory. In other words, to avoid confusion, the author would like to stress that the subsection (Baseline case studies (LC filter) 4.5.1) is primarily for validation purposes. The reader is referred to [3] for an extended comparison (covering an alternative simulation software PSCAD).

The author would also like to draw the reader to the fact that controller set up given in [3] is one where the PLL is not only 1st order, but of low bandwidth. Through a reverse engineering approach, it was found that the bandwidth of the PLL adopted in [3] must be below 20 rad/s. Given the feedback provided by manufacturers and transmission system operators, a 2nd order PLL with a bandwidth over 120 rad/s should be tested also. This is covered in subsequent sections.

Baseline case studies (LC filter)

Figures 4.10-4.12 show the performance of the dq-axis vector current controller for three different power set points, P_0, when the short-circuit ratio (SCR) is 3: $P_0 = 0.0,\ 0.50$ and 0.90 p.u. For each power set point, a set of four Bode plots are presented. Starting at the top left and moving clockwise, the first Bode plot shows the response of active power output to a change in $i_{\mathrm{d}}^{\mathrm{ref}}$, the second Bode plot shows the response of active power output to a change in $i_{\mathrm{q}}^{\mathrm{ref}}$, the third shows the response of reactive power output to a change in $i_{\mathrm{q}}^{\mathrm{ref}}$, and the fourth shows the response of reactive power output to a change in $i_{\mathrm{d}}^{\mathrm{ref}}$. For each Bode plot, there are two curves: the solid line is that predicted by the linear model; the dotted red line illustrates the results of frequency scanning a non-linear model. In addition to the Bode plots, for each power set point, time domain results from simulations using the non-linear model are included. These show the per unit voltage, active power and reactive power levels during a step change (of 0.1 per unit) in either $i_{\mathrm{d}}^{\mathrm{ref}}$ (solid lines) or $i_{\mathrm{q}}^{\mathrm{ref}}$. Specifically, the blue lines show the voltage, the orange lines show the active power output, and the yellow lines show the reactive power output.

A strong system is defined as one having a short circuit ratio (SCR) of 3 or higher. When the short circuit ratio is 3, the power system is on the border of no longer being defined as strong. However, it can be seen from figures 4.10-4.12 that dq-axis vector current control algorithm still performs satisfactorily.

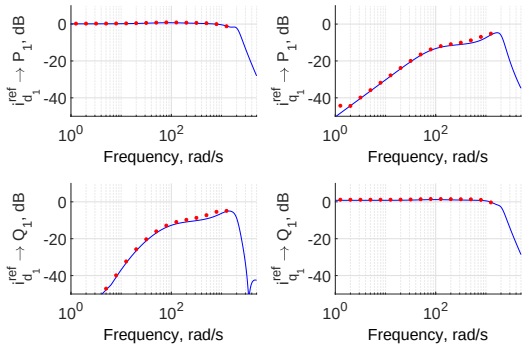

(a) Solid line - linear model; dotted - frequency scanning.

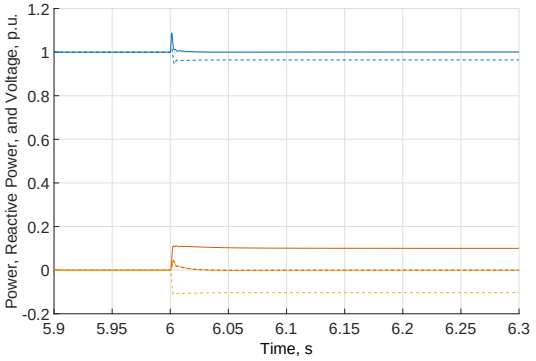

(b) Time domain simulation of non-linear model of vcc. Solid - $\Delta \boldsymbol{i}_1^{\mathrm{ref,c}} = 0.1, 0$; dashed - $\Delta \boldsymbol{i}_1^{\mathrm{ref}} = 0, 0.1$

Figure 4.10: Performance of the dq-axis vector current controller. SCR = 3, $P_{1,0} = 0.0$pu.

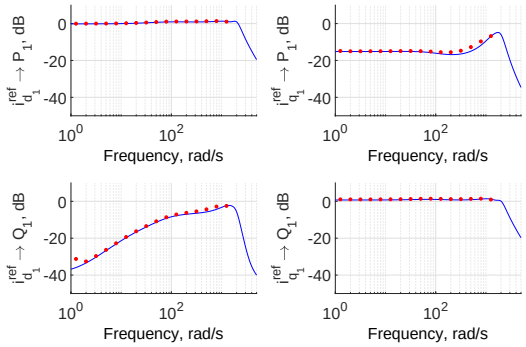

(a) Solid line - linear model; dotted - frequency scanning.

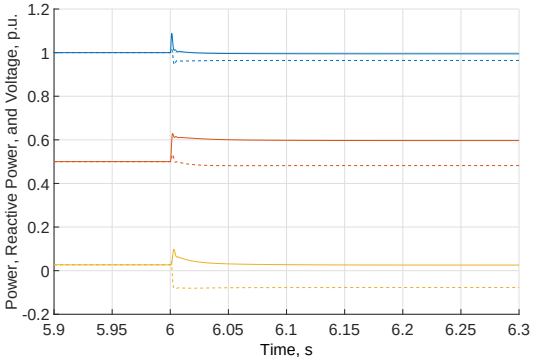

(b) Time domain simulation of non-linear model of vcc. Solid - $\Delta \boldsymbol{i}_1^{\mathrm{ref,c}} = 0.1, 0$; dashed - $\Delta \boldsymbol{i}_1^{\mathrm{ref,c}} = 0, 0.1$

Figure 4.11: Performance of the dq-axis vector current controller. SCR = 3, $P_{1,0} = 0.50$pu.

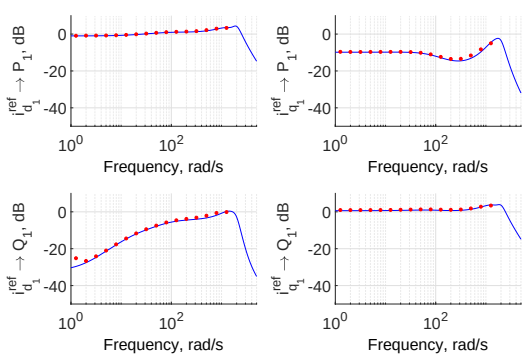

(a) Solid line - linear model; dotted - frequency scanning.

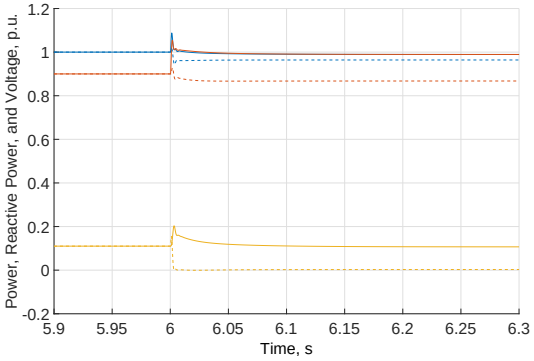

(b) Time domain simulation of non-linear model of vcc. Solid - $\Delta \boldsymbol{i}_1^{\text{ref,c}} = 0.1, 0$; dashed - $\Delta \boldsymbol{i}_1^{\text{ref,c}} = 0, 0.1$.

Figure 4.12: Performance of the dq-axis vector current controller. SCR = 3, $P_{1,0} = 0.90$pu.

Figures 4.13-4.15 show the performance of the dq-axis vector current controller for three different power set points, P_0, when the short-circuit ratio (SCR) is 1: $P_0 = 0.0,\ 0.50$ and 0.70 p.u. For each power set point, a set of four Bode plots are presented. Starting at the top left and moving clockwise, the first Bode plot shows the response of active power output to a change in $i_{\text{d}}^{\text{ref}}$, the second Bode plot shows the response of active power output to a change in $i_{\text{q}}^{\text{ref}}$, the third shows the response of AC voltage magnitude at the filter bus to a change in $i_{\text{q}}^{\text{ref}}$, and the fourth shows the response of AC voltage magnitude at the filter bus to a change in $i_{\text{d}}^{\text{ref}}$. As before, for each Bode plot, there are two curves: the solid line is that predicted by the linear model; the dotted red line illustrates the results of frequency scanning a non-linear model. In addition to the Bode plots, for each power set point, time domain results from simulations using the non-linear model are included. These show the per unit voltage and active power levels during a step change (of 0.1 per unit) in either $i_{\text{d}}^{\text{ref}}$ (solid lines) or $i_{\text{q}}^{\text{ref}}$. Specifically, the blue lines show the voltage and the red lines show the active power output.

For a short circuit ratio of 1, the system is regarded as very weak. In this scenario, it can be seen that performance is not as desired. This is due to the strong influence that changes in $i_{\text{q}}^{\text{ref}}$ have on the power output, which can be seen from the Bode plots. The issue becomes more significant as the converter is operating closer to rated power.

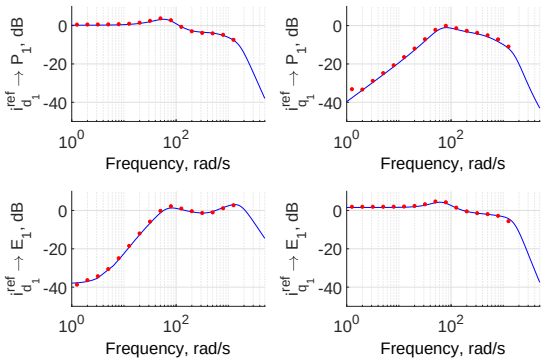

(a) Solid line - linear model; dotted - frequency scanning.

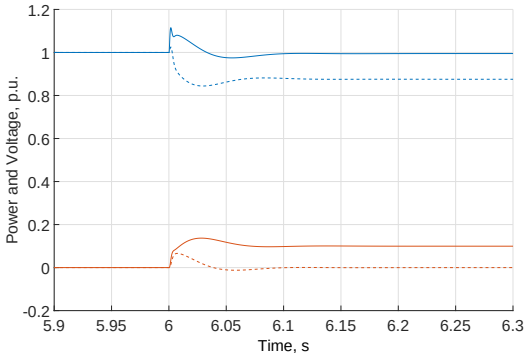

(b) Time domain simulation of non-linear model. Solid - $\Delta \boldsymbol{i}_1^{\mathrm{ref,c}} = 0.1, 0$; dashed - $\Delta \boldsymbol{i}_1^{\mathrm{ref,c}} = 0, 0.1$.

Figure 4.13: Performance of the dq-axis vector current controller. SCR = 1, $P_{1,0} = 0.0$pu.

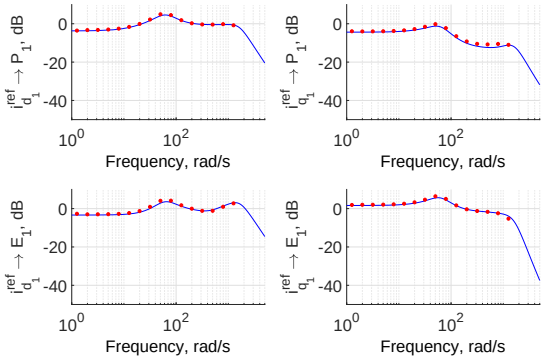

(a) Solid line - linear model; dotted - frequency scanning.

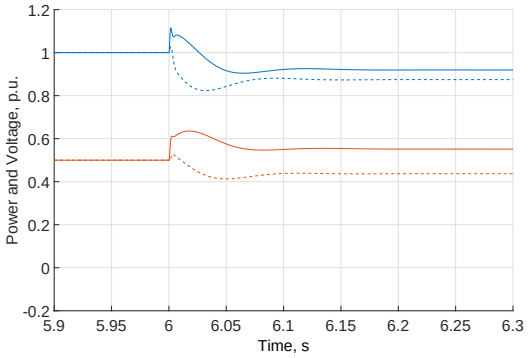

(b) Time domain simulation of non-linear model. Solid - $\Delta \boldsymbol{i}_1^{\mathrm{ref,c}} = 0.1, 0$; dashed - $\Delta \boldsymbol{i}_1^{\mathrm{ref,c}} = 0, 0.1$.

Figure 4.14: Performance of the dq-axis vector current controller. SRC = 1, $P_{1,0} = 0.50$pu.

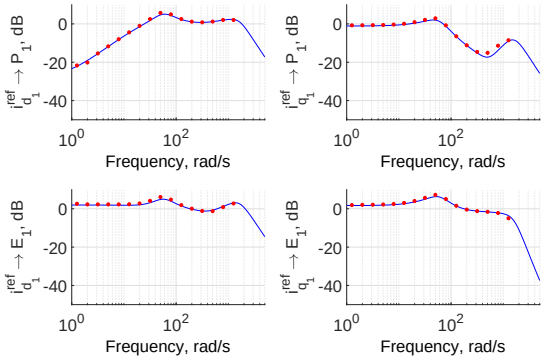

(a) Solid line - linear model; dotted - frequency scanning.

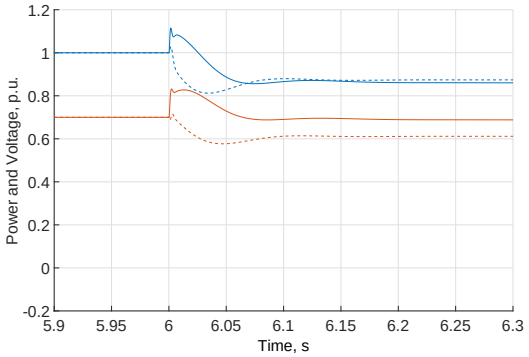

(b) Time domain simulation of non-linear model. Solid - $\Delta \boldsymbol{i}_1^{\mathrm{ref,c}} = 0.1, 0$; dashed - $\Delta \boldsymbol{i}_1^{\mathrm{ref,c}} = 0, 0.1$.

Figure 4.15: Performance of the dq-axis vector current controller. SCR = 1, $P_{1,0} = 0.70$pu.

At the highest power set point considered, high frequency content can be observed in the initial aftermath of the step change. This can also be observed at lower power set points, but to a lesser extent. One contributor to this behaviour was internal delays in the PWM process.

Figure 4.16 shows the poles and zeros for a variety of active power set points when the short-circuit ratio is one. Active power set points vary from 0p.u. to 0.7p.u. At the highest power set point, the transmission zeros are closest to the origin. Note, while the system is coupled, it is not unstable, as no poles are in the right half plane. However, the high degree of coupling does imply that instability could occur if outer feedback control is introduced.

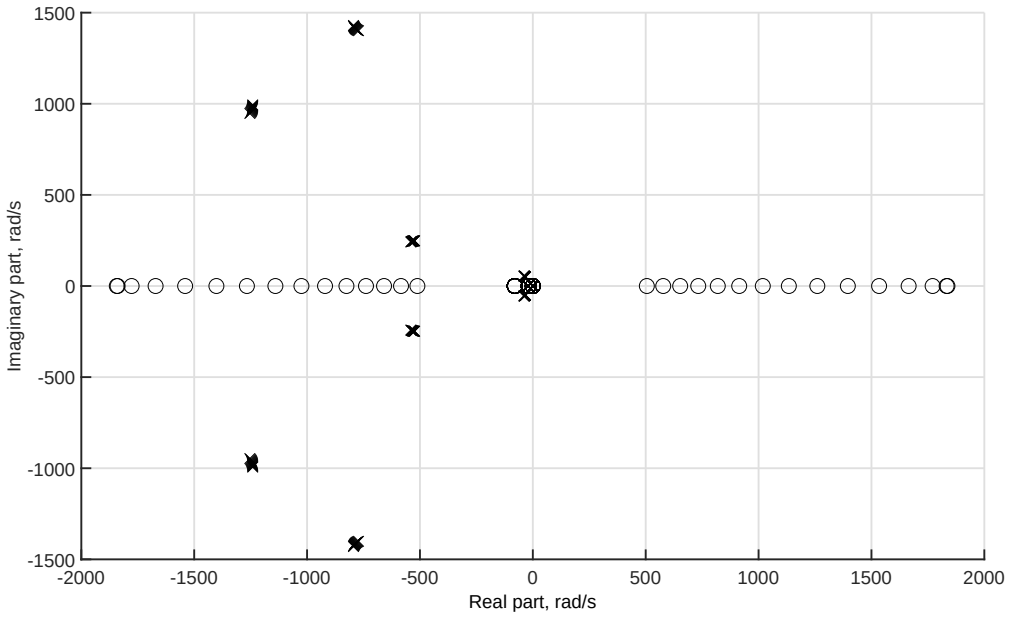

Figure 4.16: Poles and zeros for the controller in a system with a short-circuit ratio of 1 as evaluated at a range of active power set points.

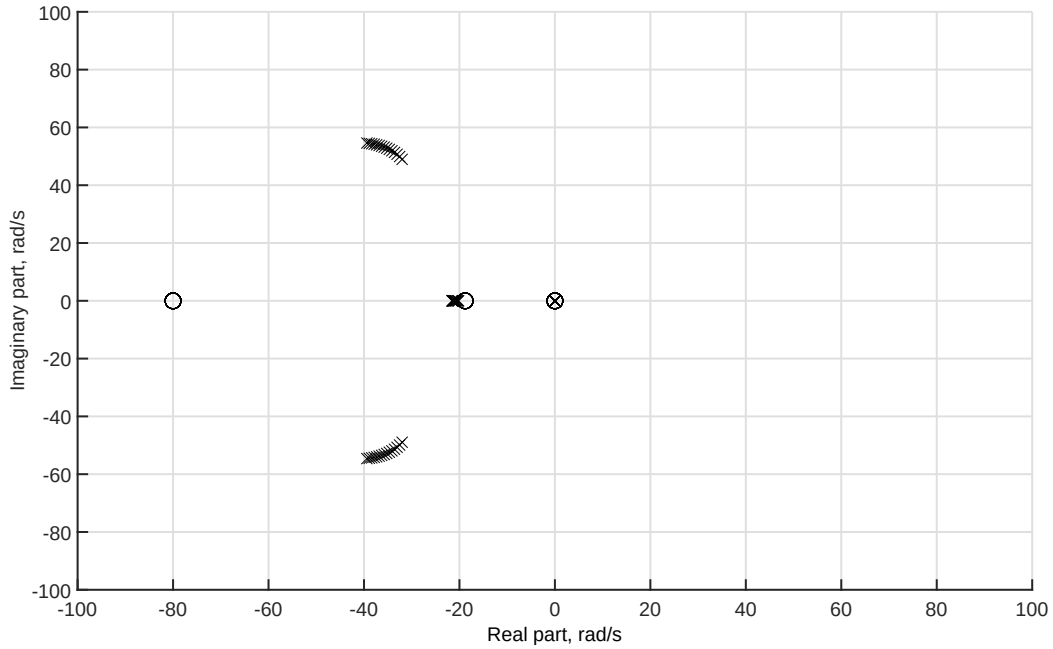

Figure 4.17: Zoom on low frequency poles and zeros for the controller in a system with a short-circuit ratio of 1 as evaluated at a range of active power set points.

Using an L filter

In this section, the capacitor bank is removed and the phase reactor inductance is scaled down accordingly; thus, the system becomes equivalent to a simple model of an MCC-HVDC system.

If the internal model control principle is recycled, i.e. the gains are set according to Harnefors, the bandwidth of the inner current controller becomes too great when the short-circuit ratio is one and the power loading is 0.5pu or greater. This means that an additional source of coupling could be introduced: that between the current controller and the switching process (of the IGBTs).

Again, cross-coupling is also observed, which is undesirable from the perspective of the outer controllers. That being said, the lack of a low-frequency pole in the system may relax some of the constraints that would be imposed on the outer controllers.

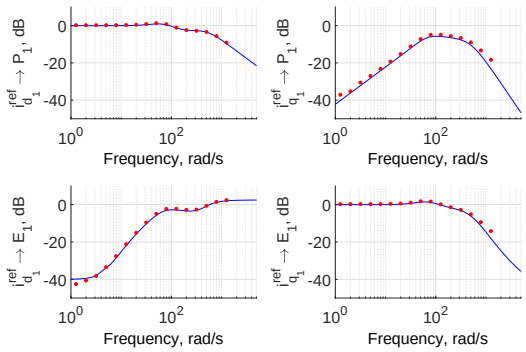

(a) Solid line - linear model; dotted - frequency scanning.

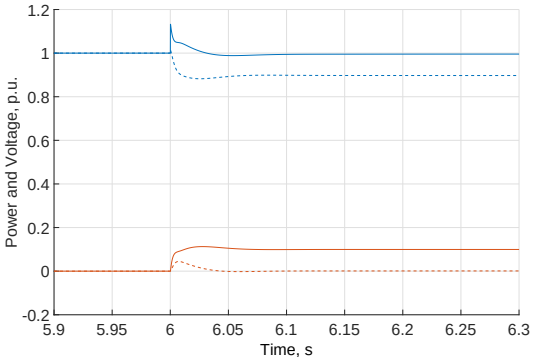

(b) Time domain simulation of non-linear model. Solid - $\Delta \boldsymbol{i}_1^{\mathrm{ref,c}} = 0.1, 0$; dashed - $\Delta \boldsymbol{i}_1^{\mathrm{ref,c}} = 0, 0.1$.

Figure 4.18: Performance of the dq-axis vector current controller. SCR = 1, $P_{1,0} = 0.0$pu.

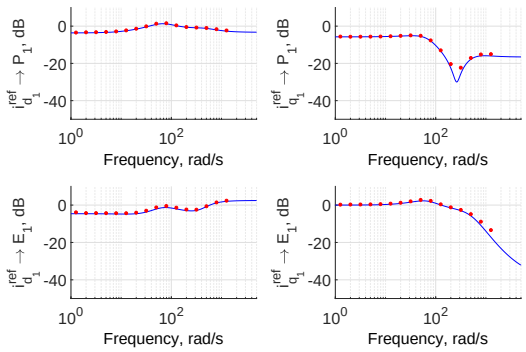

(a) Solid line - linear model; dotted - frequency scanning.

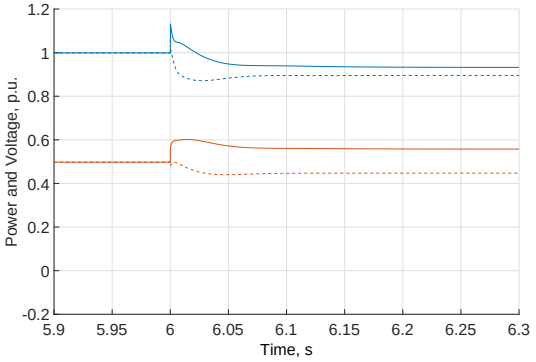

(b) Time domain simulation of non-linear model. Solid - $\Delta \boldsymbol{i}_1^{\mathrm{ref,c}} = 0.1, 0$; dashed - $\Delta \boldsymbol{i}_1^{\mathrm{ref,c}} = 0, 0.1$.

Figure 4.19: Performance of the dq-axis vector current controller. SCR = 1, $P_{1,0} = 0.50$pu.

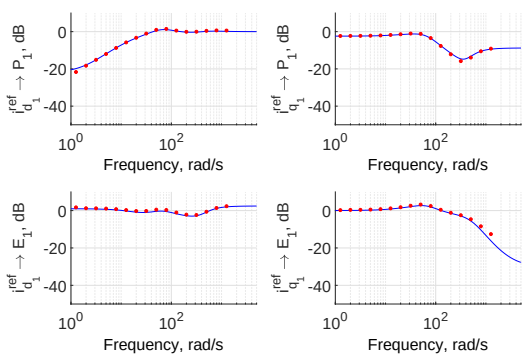

(a) Solid line - linear model; dotted - frequency scanning.

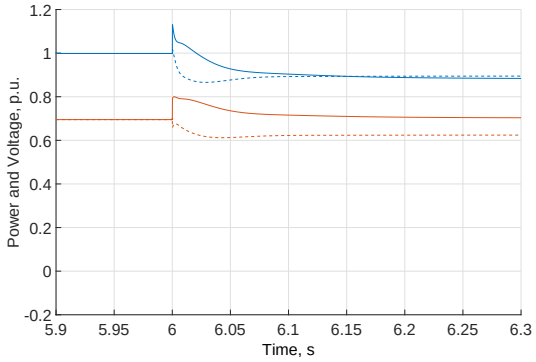

(b) Time domain simulation of non-linear model. Solid - $\Delta \boldsymbol{i}_1^{\text{ref,c}} = 0.1, 0$; dashed - $\Delta \boldsymbol{i}_1^{\text{ref,c}} = 0, 0.1$.

Figure 4.20: Performance of the dq-axis vector current controller. SCR = 1, $P_{1,0} = 0.70$pu.

4.5.2 Using a second-order PLL

In reality, a second-order PLL would be employed to make it possible for the PLL to track frequency variations, which could then be used in droop control systems. The PLL applied in this section was tuned such that it was critically damped and had a bandwidth of 100 rad/s, which is in line with both the literature and feedback from manufacturers and transmission system operators.

Since dq-axis vector current control experienced difficulties at a short circuit ratio of one, this section will focus on said value.

LC filter

The following figures show the performance of the controller when a second order PLL (right) is applied. It can be observed that the cross-coupling is not only present but worse. Without even considering outer loop control, the converter becomes unstable when the active power set point is over 0.5 p.u. This result should be taken as more reflective of the true limitations of dq-axis vector current control given the topology of the PLL that was used.

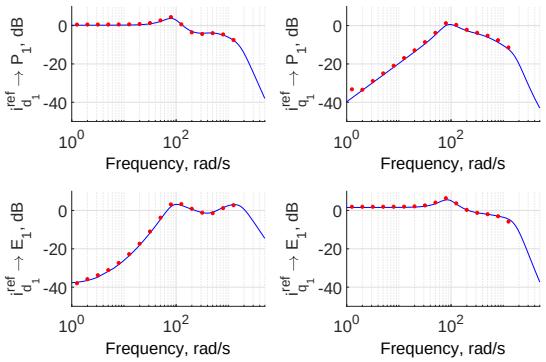

(a) Solid line - linear model; dotted - frequency scanning.

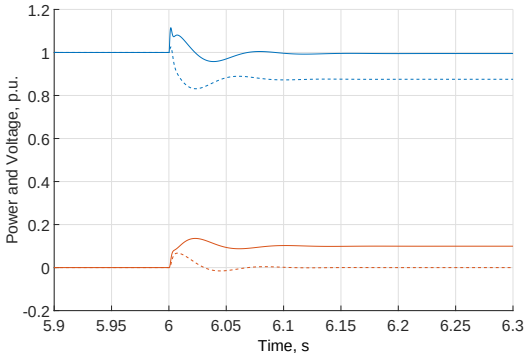

(b) Time domain simulation of non-linear model. Solid - $\Delta \boldsymbol{i}_1^{\mathrm{ref,c}} = 0.1, 0$; dashed - $\Delta \boldsymbol{i}_1^{\mathrm{ref,c}} = 0, 0.1$.

Figure 4.21: Performance of the dq-axis vector current controller. SCR = 1, $P_{1,0} = 0.0$pu.

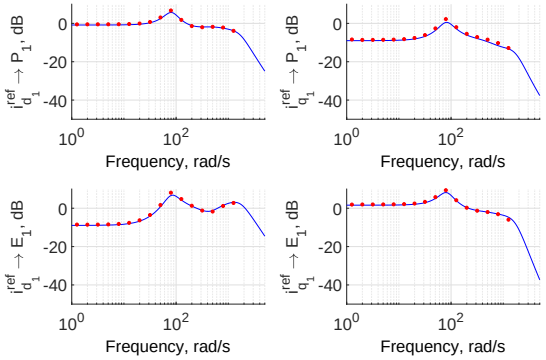

(a) Solid line - linear model; dotted - frequency scanning.

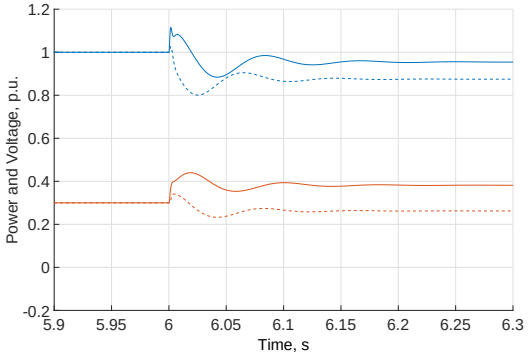

(b) Time domain simulation of non-linear model. Solid - $\Delta \boldsymbol{i}_1^{\mathrm{ref,c}} = 0.1, 0$; dashed - $\Delta \boldsymbol{i}_1^{\mathrm{ref,c}} = 0, 0.1$.

Figure 4.22: Performance of the dq-axis vector current controller. SRC = 1, $P_{1,0} = 0.30$pu.

Figure 4.23 shows a discrepancy appearing between the linear and non-linear models. This can be explained by considering the time domain simulation featuring a step, where it can be observed that the system is marginally stable i.e. on the brink of becoming highly non-linear. For higher power set points, it was found that the inner current controller was unstable, with a pole moving to the right half plane. This could be avoided by reducing the gains of the PLL; however, this may lead to other issues already mentioned.

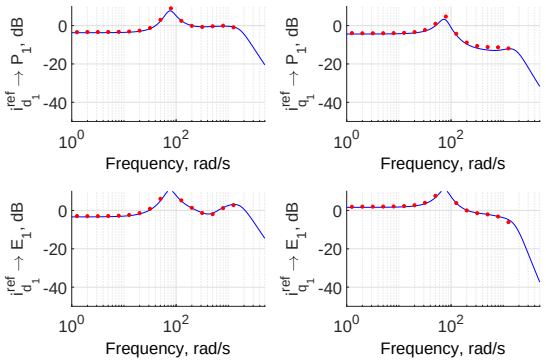

(a) Solid line - linear model; dotted - frequency scanning.

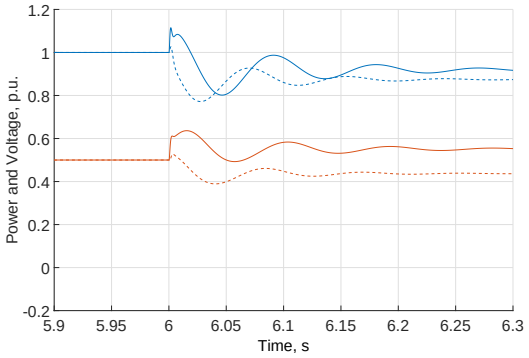

(b) Time domain simulation of non-linear model. Solid - $\Delta \boldsymbol{i}_1^{\mathrm{ref,c}} = 0.1, 0$; dashed - $\Delta \boldsymbol{i}_1^{\mathrm{ref,c}} = 0, 0.1$.

Figure 4.23: Performance of the dq-axis vector current controller. SCR = 1, $P_{1,0} = 0.50$pu.

Figures 4.24 and 4.25 show the poles and zeros as predicted by the unified linear state-space model. No pole moves over to the right half-plane; however, a pair of poles can be seen to move close to the y-axis as power set point increases. Coupled with delays, this would probably create an unstable system.

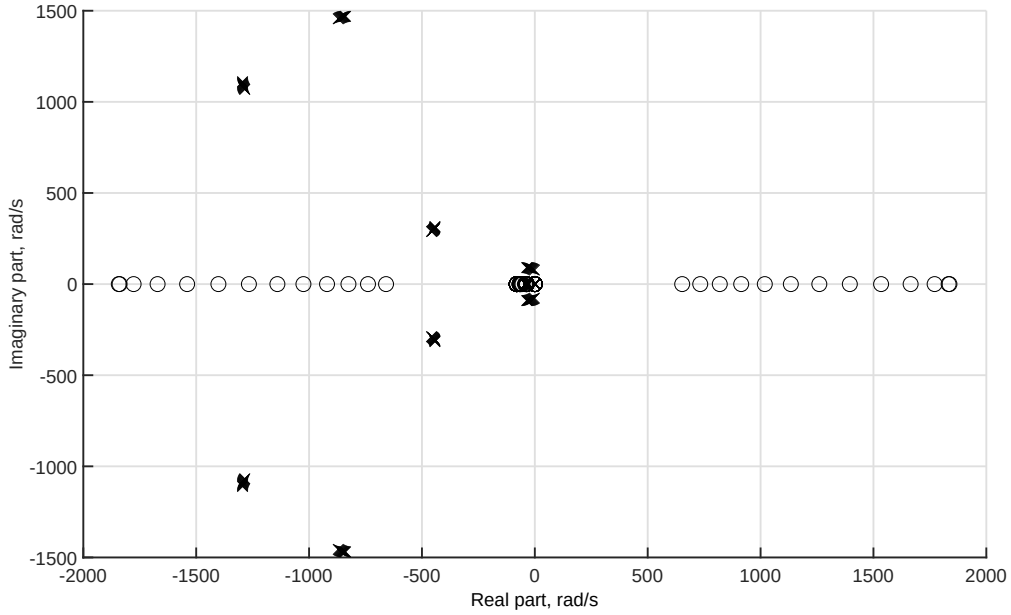

Figure 4.24: Pole-zero map for the dq-axis vector current control system when a second order PLL is applied. System evaluated across a range of active power set points ($0 \rightarrow 0.6$p.u.).

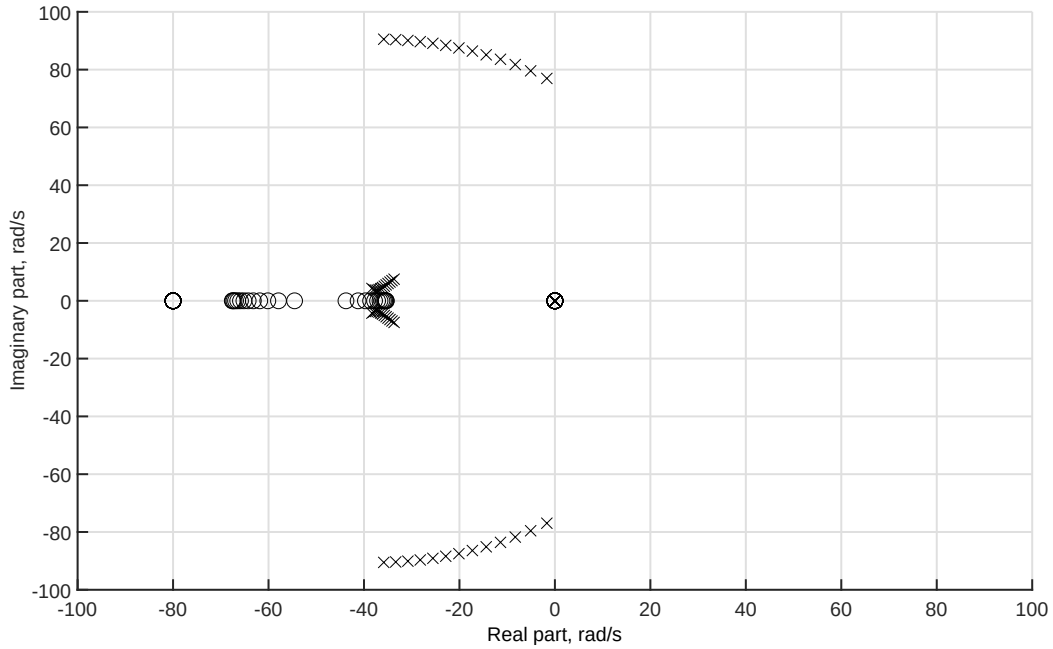

Figure 4.25: Close up of low frequency poles and zeros for the dq-axis vector current control system when a second order PLL is applied. System evaluated across a range of active power set points ($0 \rightarrow 0.6$p.u.).

L filter

In the case of the L filter, there is no system resonance that can combine with the PLL to form a highly problematic system. This can be seen in figures 4.26 - 4.28. In other words, there is no strong oscillatory behaviour at the inner current control level as seen in the LC filter case.

Even so, the beginning of the voltage collapse due to $\Re\left\{\Delta \boldsymbol{i}_1^{\mathrm{ref,c}}\right\}$ seen in the studies with the first order PLL can be observed, which complicates the role of the outer controllers.

An additional issue can also be seen in figure 4.26. Specifically, there is significant power in the high frequency region in the transmittance from $\Re\left\{\Delta \boldsymbol{i}_1^{\mathrm{ref,c}}\right\} \rightarrow \Delta E$. This could lead to undesirable coupling between the PWM process and the current controller. This issue is not observed in the non-linear model due to the average value model being applied. Nevertheless, the presence of this issue should be noted, particularly when considering fault performance.

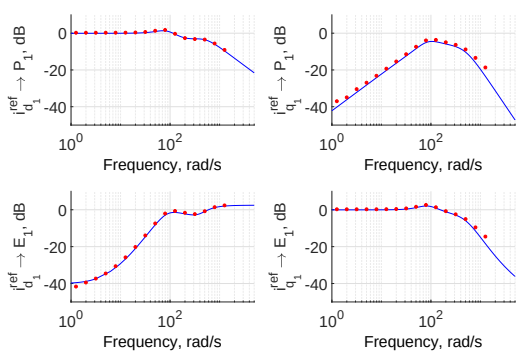

(a) Solid line - linear model; dotted - frequency scanning.

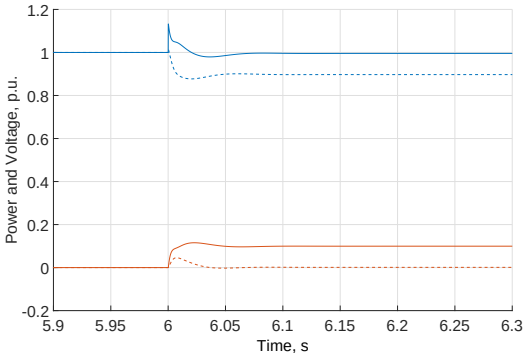

(b) Solid - $\Delta i_{\mathrm{d}}^{\mathrm{r}} = 0.1$; dashed - $\Delta i_{\mathrm{q}}^{\mathrm{r}} = 0.1$

Figure 4.26: Performance of the dq-axis vector current controller. SCR = 1, $P_{1,0} = 0.0$pu.

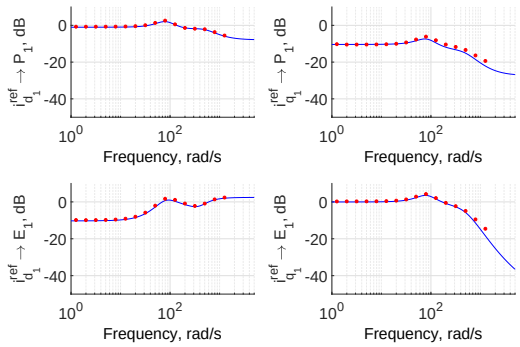

(a) Solid line - linear model; dotted - frequency scanning.

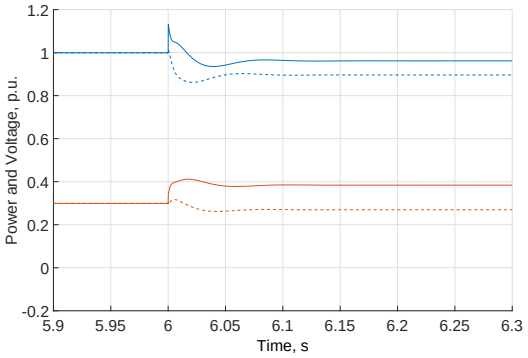

(b) Solid - $\Delta i_{\mathrm{d}}^{\mathrm{r}} = 0.1$; dashed - $\Delta i_{\mathrm{q}}^{\mathrm{r}} = 0.1$

Figure 4.27: Performance of the dq-axis vector current controller. SRC = 1, $P_{1,0} = 0.30$pu.

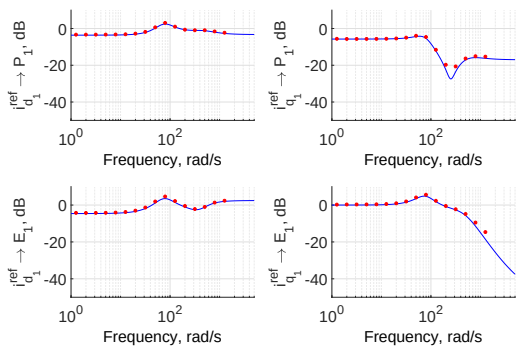

(a) Solid line - linear model; dotted - frequency scanning.

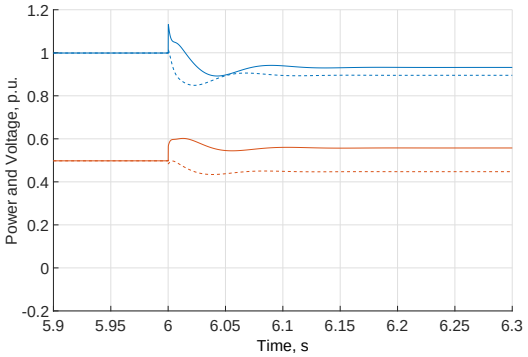

(b) Solid - $\Delta i_{\mathrm{d}}^{\mathrm{r}} = 0.1$; dashed - $\Delta i_{\mathrm{q}}^{\mathrm{r}} = 0.1$

Figure 4.28: Performance of the dq-axis vector current controller. SCR = 1, $P_{1,0} = 0.50$pu.

Similar results were obtained when dropping the integral term completely. In other words, when transitioning to a high-gain first-order PLL, associated with which is a moderately high bandwidth, stability is compromised in the low short-circuit ratio system.

Considering these results and those presented in section 4.5.2, it is possible to attribute a large portion of the poor performance to the dynamics associated with the PLL specifically.

In general, the 2nd order filter, particularly when coupled with an LC filter with a low resonant frequency, suggests dq-axis vector current control may have issues achieving power outputs above 0.5p.u.

4.5.3 Adding outer loop and/or droop controllers

Considering figure 4.15, if a change in $\Re\left\{\Delta\boldsymbol{i}_1^{\text{ref,c}}\right\}$ causes a drop in the voltage at the filter bus, a voltage droop controller would respond to this by changing $\Im\left\{\Delta\boldsymbol{i}_1^{\text{ref,c}}\right\}$; however, considering figure 4.15, this would impact on the power output, which would trigger the frequency droop controller to act, which ultimately re-enforce the original drop in voltage. The end result is an unstable system.

Even if droop control were not employed, there would still be outer controllers as discussed in section 4.1.1.

Due to the poor dynamics at the current control level, stability only occurs when the bandwidth of the outer controllers is very low, at which point response time becomes unacceptable. The only 'simple' option available to try and improve the response time would be to increase the gains of the controller(s); however, this produces an unstable system.

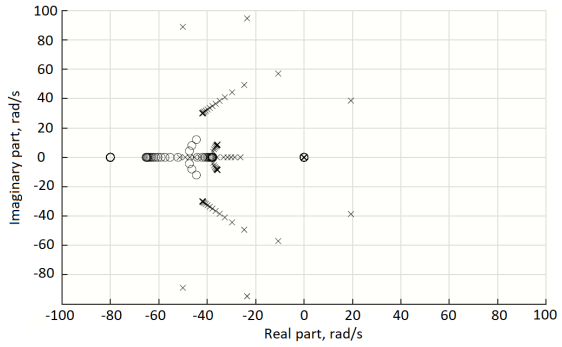

(a) Zoom on low frequency poles and zeros for the controller in a system with a short-circuit ratio of 1 as evaluated at a range of active power set points.

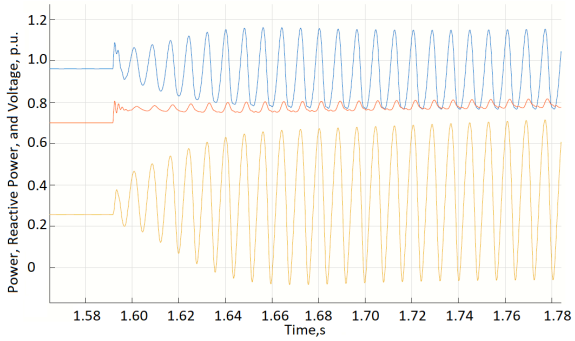

(b) Time domain simulation of non-linear model of vcc during an attempt to change active power set point.

Figure 4.29: Performance of the dq-axis vector current controller. SCR = 1, $P_{1,0} = 0.70$pu.

4.5.4 An investigation on the specific influence of the PLL

In the previous sections, it was shown that, at the current control level, the system is ill-conditioned, which would pose a significant problem for outer controllers, consistent with the work of Egea-Alvarez [5]. All relevant literature indicates that a major contributor to the ill-conditioning is the PLL. However, it would be preferable to be more specific. PLLs are known to be stable when operating in isolation in weak AC systems. Thus, the negative effects of the PLL on dq-axis vector current control scheme must be in the application of the PLL output. There are three applications of the PLL: the first two are found in the abc→dq frame transformations acting on currents and voltages respectively; the third is found in the dq→abc frame transformation. Using the linear model, it is possible to remove eliminate the dynamics associated with various parts of the controller. This is not possible with the non-linear time domain model since all elements must be active during a simulation.

Figure 4.30 shows the influence of ignoring the PLL dynamics on the final frame transformation i.e. ignoring the $\boldsymbol{C}_{\zeta}^{\mathrm{j}}$ matrix. Particularly in the low frequency region, which is where the outer controllers will be most active, the main diagonal elements have significantly more power than before. By discarding the relevant parts of the unified state-space model, a reduced state-space model can be produced which omits the influence of the PLL, giving the results also shown in figure 4.30. The associated time domain results are shown in figure 4.31.

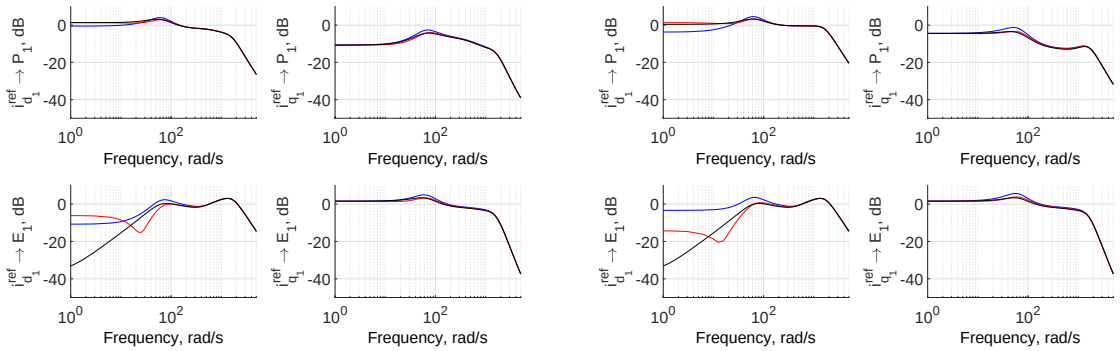

(a) $\boldsymbol{H}^{\text{vcc}}(s)$ when $P_0 = 0.25$p.u.

(b) $\boldsymbol{H}^{\text{vcc}}(s)$ when $P_0 = 0.5$p.u.

(c) $\boldsymbol{H}^{\text{vcc}}(s)$ when $P_0 = 0.60$p.u.

(d) $\boldsymbol{H}^{\text{vcc}}(s)$ when $P_0 = 0.75$p.u.

Figure 4.30: $\boldsymbol{H}^{\text{vcc}}$ when (1) all elements of the controller are included (blue), (2) the effect of PLL dynamics on the final frame transformation are removed (red) and (3) when all effects of the PLL dynamics are removed (black). Response evaluated at a variety of power set points when the short-circuit ratio is one.

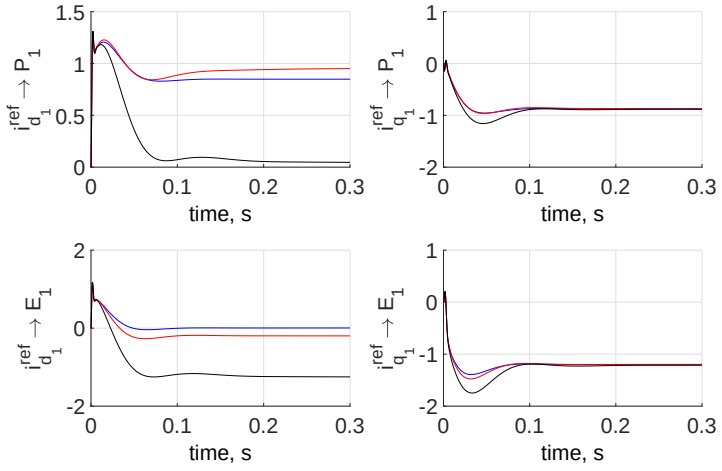

Figure 4.31: Influence of the PLL dynamics evaluated when SCR = 1, $P_0 = 0.7$pu. The black lines are results from running the unified state-space model when all PLL dynamics are included; the red lines are results from when the effect of $\Delta\theta$ on the final frame transformation have been omitted; the blue lines are from when the effect of $\Delta\theta$ has been omitted from all frame transformations. All results have been normalised.

Of course, there is still strong power from $\Delta i_{\mathrm{q}}^{\mathrm{ref}}$ to ΔP. This is discussed later. Also, note that the right hand plot shows slightly improved performance in terms of final steady-state error in power output compared to previous plots. This will be due to the non-linear nature of the combined system being omitted in figure 4.31.

Note how figure 4.30 is similar to the linearised model when *all* PLL dynamics have been removed. This implies that the overwhelming detrimental impact of the PLL is created by the presence of a frame transformation after the current controller. Why might this be the case?

Let us treat the current reference values as fixed; this would be equivalent to studying dq-axis vector current control when network perturbations are applied, perhaps at some voltage source in the system, rather than the perturbation being (conventionally) applied to the current reference components. In this scenario, dq-axis vector current control may, 'loosely speaking', be viewed as a cascaded control system where the 'outer loop' reference variable becomes the target q component for the voltage transformed into the dq frame (which is zero).

The general rule of cascaded control is that the bandwidth of the outer controller should be less than that of an inner controller. For completeness, dq-axis vector current control is not a conventional cascaded control system for three reasons: first, the presence (and location) of the reference current values; second, the dual application of the PLL phase angle i.e. before and after the current controller; and third, the application of the output of the PLL in its internal Park transformation. Nevertheless, the general rule still has relevance, particularly if we continue to treat the current reference values as fixed (for hypothetical purposes). For this reason, let us focus on the second point. The second observation of the control architecture produces two criteria: first, the bandwidth of the PLL should be lower than that of the current controller; and second, the final frame transformation should contain no major dynamics in the frequency range covered by the bandwidth of the current controller. It is not possible to achieve both criteria unless the voltage at the point of common coupling is stiff. If this voltage is not stiff, only one criterion can be satisfied at any one time. Given that the PLL is a low-bandwidth system, one would expect the final frame transformation to be problematic if the voltage is weak. This would create a system which, from the perspective of the active power and AC voltage magnitude controllers, would be difficult to control.

4.6 Summary

It has been shown that the stability of a single converter using dq-axis vector current control in the small-signal domain is governed by the following parameters: the line inductance, or more appropriately the electrical proximity of the PCC to a stiff voltage source; the power loading; the filter topology; the PLL, and the outer loop controllers. In the weak system (SCR = 1), the coupling between the two current control loops is strongly dependent on power loading. It has been observed that operating beyond $P = 0.5$p.u. may be unachievable in such a system. This would, in one way or another, severely limit the economic viability of such a system.

An approach to modelling based predominantly in the frequency domain has been outlined. This can be coupled with experimental data which describes the behaviour of the resistance, capacitance and inductance of the components across a range of frequencies. This can then be converted to an effective state-space model using sub-space algorithms. Alternatively, one can use the unified state-space model to calculate the performance directly, at the cost of losing frequency dependence in components. Both algorithms can be implemented in compiled languages, but the former requires additional algorithms (sub-space) in order to extract poles and zeros. This makes the latter algorithm preferable for speed (both in terms of development and programme run times) reasons, which is important when considering multi-converter systems.

Chapter 5

Analysis of proportional resonant control

In this chapter, the proportional resonant controller is assessed, both through linear and non-linear models. In so doing, a linear model of proportional resonant control is developed, which may be of use to developers and/or researchers. To the author's best knowledge, no linear model of proportional resonant control which includes PLL dynamics has previously been presented and validated in low SCR systems.

While proportional resonant control avoids the application of the PLL angle after a current regulator, it is shown that damping of low-frequency system resonances is poor, making proportional resonant control (in its basic form) unsuitable for LC-filtered systems, and possibly even L-filtered systems if the wider network carries with it a low frequency resonance.

5.1 Development of the linear model of proportional resonant control including PLL dynamics

Let us now consider another control algorithm which has experienced interest: proportional resonant control. In this work, figure 5.1 illustrates the proportional resonant controller adopted in this work.

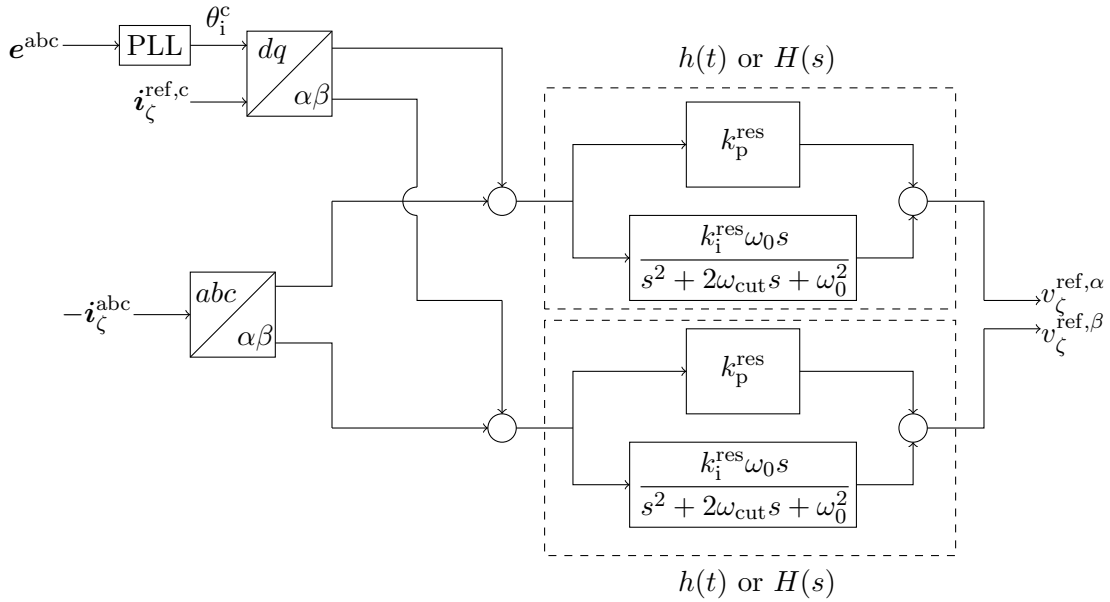

Figure 5.1: Block diagram illustrating the proportional resonant controller. The $\alpha\beta$ output signals are converted to abc signals by a simple inverse Clarke transform.

As can be observed from figure 5.1, the $\alpha\beta$ frame is used extensively. It is therefore much more convenient to express the frame transformations as abc$\rightarrow \alpha\beta$, $\alpha\beta \rightarrow$abc, dq$\rightarrow \alpha\beta$ and $\alpha\beta \rightarrow$dq.

Considering section 4.2, the relevant frame transformations are as follows:

$$\boldsymbol{T}^{\alpha\beta\rightarrow g} = \begin{bmatrix} \cos(\omega_0 t) & \sin(\omega_0 t) \\ -\sin(\omega_0 t) & \cos(\omega_0 t) \end{bmatrix}; \quad \boldsymbol{T}^{c\rightarrow\alpha\beta} = \begin{bmatrix} \cos(\omega_0 t + \theta_\zeta^c) & -\sin(\omega_0 t + \theta_\zeta^c) \\ \sin(\omega_0 t + \theta_\zeta^c) & \cos(\omega_0 t + \theta_\zeta^c) \end{bmatrix} \tag{5.1}$$

Let us note that, to a first-order approximation,

$$\begin{aligned}\boldsymbol{T}^{\mathrm{c}\to\alpha\beta} &= \begin{bmatrix}\cos(\omega_0 t) & \sin(\omega_0 t)\\ -\sin(\omega_0 t) & \cos(\omega_0 t)\end{bmatrix}\begin{bmatrix}\cos(\theta^{\mathrm{c}}_{\zeta,0}+\Delta\theta^{\mathrm{c}}_{\zeta}) & \sin(\theta^{\mathrm{c}}_{\zeta,0}+\Delta\theta^{\mathrm{c}}_{\zeta})\\ -\sin(\theta^{\mathrm{c}}_{\zeta,0}+\Delta\theta^{\mathrm{c}}_{\zeta}) & \cos(\theta^{\mathrm{c}}_{\zeta,0}+\Delta\theta^{\mathrm{c}}_{\zeta})\end{bmatrix}\\ &= \begin{bmatrix}\cos(\omega_0 t) & -\sin(\omega_0 t)\\ \sin(\omega_0 t) & \cos(\omega_0 t)\end{bmatrix}\begin{bmatrix}\cos(\theta^{\mathrm{c}}_{\zeta,0}) & -\sin(\theta^{\mathrm{c}}_{\zeta,0})\\ \sin(\theta^{\mathrm{c}}_{\zeta,0}) & \cos(\theta^{\mathrm{c}}_{\zeta,0})\end{bmatrix}\begin{bmatrix}1 & -\Delta\theta^{\mathrm{c}}_{\zeta}\\ \Delta\theta^{\mathrm{c}}_{\zeta} & 1\end{bmatrix}\end{aligned} \tag{5.2}$$

Proceeding to analyse the system in the time domain, the voltage reference set by the proportional resonant controller may be expressed as follows:

$$\begin{aligned}\boldsymbol{v}^{\mathrm{ref},\alpha\beta}_{\zeta} &= h(t) * \left(\boldsymbol{i}^{\mathrm{ref},\alpha\beta}_{\zeta} - \boldsymbol{i}^{\alpha\beta}_{\mathrm{c}_\zeta}\right)\\ &= h(t) * \left[\boldsymbol{T}^{\mathrm{c}}_{\mathrm{dq}\to\alpha\beta}\boldsymbol{i}^{\mathrm{ref,c}}_{\zeta} - \boldsymbol{T}^{\mathrm{g}}_{\mathrm{dq}\to\alpha\beta}\boldsymbol{i}^{\mathrm{g}}_{\mathrm{c}_\zeta}\right]\\ &= h(t) * \left[\begin{bmatrix}\cos(\omega_0 t) & -\sin(\omega_0 t)\\ \sin(\omega_0 t) & \cos(\omega_0 t)\end{bmatrix}\begin{bmatrix}\cos(\theta^{\mathrm{c}}_{\zeta,0}) & -\sin(\theta^{\mathrm{c}}_{\zeta,0})\\ \sin(\theta^{\mathrm{c}}_{\zeta,0}) & \cos(\theta^{\mathrm{c}}_{\zeta,0})\end{bmatrix}\begin{bmatrix}1 & -\Delta\theta^{\mathrm{c}}_{\zeta}\\ \Delta\theta^{\mathrm{c}}_{\zeta} & 1\end{bmatrix}\times\dots\right.\\ &\qquad\left.\left(\boldsymbol{i}^{\mathrm{ref,c}}_{\zeta,0}+\Delta\boldsymbol{i}^{\mathrm{ref,c}}_{\zeta}\right) - \begin{bmatrix}\cos(\omega_0 t) & -\sin(\omega_0 t)\\ \sin(\omega_0 t) & \cos(\omega_0 t)\end{bmatrix}\left(\boldsymbol{i}^{\mathrm{g}}_{\mathrm{c}_\zeta,0}+\Delta\boldsymbol{i}^{\mathrm{g}}_{\mathrm{c}_\zeta}\right)\right]\end{aligned} \tag{5.3}$$

where $h(t)$ is the proportional-resonant controller.

Note how the output of the resonant controller is the $\alpha\beta$ signal. A consequence of this is that a mixture of multiplication and convolution will be present at the same time during the analysis. This, can instantly be observed when both sides are multiplied by $\boldsymbol{T}^{\alpha\beta\to\mathrm{g}}$ such that the output of the controller may be linked with the model of the network. That is,

$$\begin{aligned}\boldsymbol{v}^{\mathrm{g}}_{\zeta} = \begin{bmatrix}\cos(\omega_0 t) & \sin(\omega_0 t)\\ -\sin(\omega_0 t) & \cos(\omega_0 t)\end{bmatrix}\Bigg[h(t) * \Bigg[\begin{bmatrix}\cos(\theta^{\mathrm{c}}_{\zeta,0}) & -\sin(\theta^{\mathrm{c}}_{\zeta,0})\\ \sin(\theta^{\mathrm{c}}_{\zeta,0}) & \cos(\theta^{\mathrm{c}}_{\zeta,0})\end{bmatrix}\times\dots\\ \Bigg[\begin{bmatrix}\cos(\omega_0 t) & -\sin(\omega_0 t)\\ \sin(\omega_0 t) & \cos(\omega_0 t)\end{bmatrix}\Delta\boldsymbol{i}^{\mathrm{ref,c}}_{\zeta} + \begin{bmatrix}-\sin(\omega_0 t) & -\cos(\omega_0 t)\\ -cos(\omega_0 t) & \sin(\omega_0 t)\end{bmatrix}\boldsymbol{i}^{\mathrm{ref,c}}_{\zeta,0}\Delta\theta^{\mathrm{c}}_{\zeta}\Bigg] - \dots\\ \begin{bmatrix}\cos(\omega_0 t) & -\sin(\omega_0 t)\\ \sin(\omega_0 t) & \cos(\omega_0 t)\end{bmatrix}\Delta\boldsymbol{i}^{\mathrm{g}}_{\mathrm{c}_\zeta}\Bigg]\Bigg]\end{aligned} \tag{5.4}$$

From Zmood [24],

$$
\begin{aligned}
L\left\{\cos(\omega_0 t)\left[h(t) * \left[g(t)\cos(\omega_0 t)\right]\right]\right\} &= \frac{1}{4}[H(s+j\omega_0)G(s+2j\omega_0) + H(s-j\omega_0)G(s) + \dots \\
&\quad H(s+j\omega_0)G(s) + H(s-j\omega_0)G(s-2j\omega_0)] \\
L\left\{\sin(\omega_0 t)\left[h(t) * \left[g(t)\sin(\omega_0 t)\right]\right]\right\} &= \frac{1}{4}[-H(s+j\omega_0)G(s+2j\omega_0) + H(s-j\omega_0)G(s) + \dots \\
&\quad H(s+j\omega_0)G(s) - H(s-j\omega_0)G(s-2j\omega_0)] \\
L\left\{\cos(\omega_0 t)\left[h(t) * \left[g(t)\sin(\omega_0 t)\right]\right]\right\} &= \frac{j}{4}[[H(s-j\omega_0) - H(s+j\omega_0)]\,G(s) + \dots \\
&\quad H(s+j\omega_0)G(s+2j\omega_0) - H(s-j\omega_0)G(s-2j\omega_0)] \\
L\left\{\sin(\omega_0 t)\left[h(t) * \left[g(t)\cos(\omega_0 t)\right]\right]\right\} &= \frac{j}{4}[[H(s-j\omega_0) - H(s+j\omega_0)]\,G(s) + \dots \\
&\quad -H(s+j\omega_0)G(s+2j\omega_0) + H(s-j\omega_0)G(s-2j\omega_0)] \quad (5.5)
\end{aligned}
$$

where $g(t)$ is some signal, which in this case could be a current signal or phase from the PLL, and $H(s)$ is, in this work, the transfer function of the resonant controller.

Hence,

$$
\boldsymbol{H}^{\mathrm{res}} = L\left\{\begin{bmatrix} \cos(\omega_0 t) & \sin(\omega_0 t) \\ -\sin(\omega_0 t) & \cos(\omega_0 t) \end{bmatrix}\left(h(t) * \begin{bmatrix} \cos(\omega_0 t) & -\sin(\omega_0 t) \\ \sin(\omega_0 t) & \cos(\omega_0 t) \end{bmatrix}\right)\right\} \quad (5.6)
$$

$$
= \frac{1}{2}\begin{bmatrix} \{H(s+j\omega_0) + H(s-j\omega_0)\} & j\{H(s+j\omega_0) - H(s-j\omega_0)\} \\ j\{H(s+j\omega_0) - H(s-j\omega_0)\} & \{H(s+j\omega_0) + H(s-j\omega_0)\} \end{bmatrix} \quad (5.7)
$$

Taking the Laplace transform of equation 5.4 yields the following result:

$$
\Delta\boldsymbol{v}_{\zeta}^{\mathrm{g}}(s) = \underbrace{\begin{bmatrix} \cos\theta_{\zeta,0}^{\mathrm{c}} & -\sin\theta_{\zeta,0}^{\mathrm{c}} \\ \sin\theta_{\zeta,0}^{\mathrm{c}} & \cos\theta_{\zeta,0}^{\mathrm{c}} \end{bmatrix}}_{\boldsymbol{G}_{\zeta}^{\mathrm{b}}}\left(\underbrace{\boldsymbol{H}^{\mathrm{res}}}_{\boldsymbol{G}_{\zeta}^{\mathrm{c}}}\left(\Delta\boldsymbol{i}_{\zeta}^{\mathrm{ref,c}} + \underbrace{\begin{bmatrix} 0 & -1 \\ 1 & 0 \end{bmatrix}}_{\boldsymbol{G}_{\zeta}^{\mathrm{e}}}\boldsymbol{i}_{\mathrm{c}\varsigma,0}^{\mathrm{ref,c}}\,\Delta\theta_{\zeta}^{\mathrm{c}}\right)\right) + \underbrace{(-\boldsymbol{H}^{\mathrm{res}}\boldsymbol{T}_2)}_{\boldsymbol{G}_{\zeta}^{\mathrm{d}}}\boldsymbol{y}_{\mathrm{E}\zeta}^{\mathrm{loc}} \quad (5.8)
$$

5.1.1 Block diagrams and transfer function matrix extraction

Perturbations in the phase angle are linked to the perturbations in the voltage at the PCC through the linearised model of the PLL almost completely described in the analysis of dq-axis vector current control. The phase reactor current and PCC voltage perturbations are then linked to the bridge voltage perturbations by the network response matrix, $\boldsymbol{G}_\zeta$. Thus,

$$\boldsymbol{y}_\zeta^{\mathrm{o}} = \boldsymbol{\Omega}\boldsymbol{G}_\zeta \left[\boldsymbol{I} - \boldsymbol{G}_\zeta^{\mathrm{b}}\boldsymbol{G}_\zeta^{\mathrm{c}}\boldsymbol{G}_\zeta^{\mathrm{e}}\boldsymbol{G}_\zeta^{\mathrm{a}}\boldsymbol{G}_\zeta + \boldsymbol{G}_\zeta^{\mathrm{d}}\boldsymbol{G}_\zeta\right]^{-1} \boldsymbol{G}_\zeta^{\mathrm{b}}\boldsymbol{G}_\zeta^{\mathrm{c}}\boldsymbol{G}_\zeta \Delta\boldsymbol{i}_\zeta^{\mathrm{ref,c}} \tag{5.9}$$

$\boldsymbol{G}_\zeta^{\mathrm{a}}$ is the frequency response of the PLL, details of which may be found in the previous chapter.

The $\boldsymbol{\Omega}$ term is just to ensure that only the response of ΔP_ζ and ΔE_ζ to $\Delta\boldsymbol{i}_\zeta^{\mathrm{ref,c}}$ are considered. Thus,

$$\boldsymbol{\Omega} = \begin{bmatrix} 1 & 0 & 0 & 0 & 0 & 0 \\ 0 & 1 & 0 & 0 & 0 & 0 \end{bmatrix} \tag{5.10}$$

The outer loop controllers were simple PI controllers, with the outputs being passed through low-pass filters (with a cut-off frequency of α_{f}) to improve disturbance rejection. Including these in the linear model is achieved through the inclusion of $\boldsymbol{G}_\zeta^{\mathrm{g}}$ and $\boldsymbol{G}_\zeta^{\mathrm{h}}$ as shown 5.2:

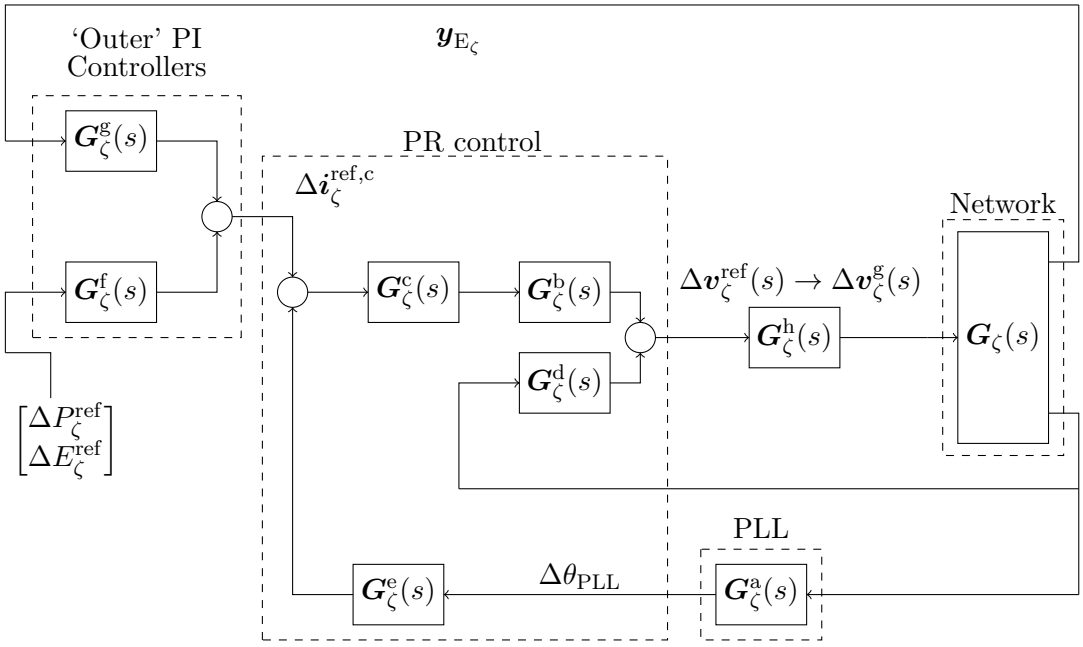

Figure 5.2: Block diagram illustrating the linearised model

5.2 Linear & non-linear simulations involving proportional resonant control

For single converter systems, $\zeta = 1$ only. In this section, attention is paid to systems where the short-circuit ratio is 1 and 3. The former is to assess the performance in very weak systems, while the latter is to assess any coupling issues that may be present as the system strength increases. To make a fair comparison, the component values are the same as provided in table 4.1.

For each operating point, a Bode-plot figure comprising four Bode sub-plots will be presented. The four sub-plots form the transfer function matrix, $\boldsymbol{H}_1^{\mathrm{prc}}$, evaluated across a large frequency range. $H_1^{\mathrm{prc}}(1,1)$ captures the response of power output to changes in P_1^{ref}; $H_1^{\mathrm{prc}}(1,2)$ captures the response of power output to changes in E_1^{ref}; $H_1^{\mathrm{prc}}(2,1)$ captures the response of reactive power output/voltage magnitude (depending on the system strength) to changes in P_1^{ref}; and $H_1^{\mathrm{prc}}(2,2)$ captures the response of reactive power output/voltage magnitude (depending on the system strength) to changes in E_1^{ref}.

In addition, for each operating point, time domain simulations using the non-linear model are presented showing step changes of $\Delta P_{\zeta}^{\text{ref}} = 0.1$p.u. and $\Delta P_1 = P_{1,0}$ where $P_{1,0}$ is the steady-state power set point around which the given linearisation has been applied. For example, considering the operating point SCR = 1, $P_{1,0} = 0.5$p.u. The top left plot features the Bode plots evaluated at $P_{1,0} = 0.5$p.u. The top right plot features the time domain plots showing the active power output (red), reactive power output (yellow) and PCC voltage (blue) over a period of time during which a step change of $\Delta P_1 = 0.5$p.u. is introduced, after which a step change is $\Delta P_1 = 0.1$p.u introduced. The currents during both step changes are shown in the bottom two plots, covering both small and large disturbances. The zooms show the current of a single phase compared against its effective reference (calculated by inverse Clarke transform). If the SCR = 1, step changes in E_1^{ref} are also presented; these can be seen in the top right plot with the dashed lines.

The proportional term in the resonant controller has a gain that is the same as that found in the dq-axis vector current controller; however, the integral gain was adjusted to give the desired resonant response. To produce currents at the grid frequency, the resonant frequency of the controller is set at the grid frequency. A small amount of damping was included to reduce sensitivities to variations in the grid frequency, but also to remove numerical issues associated with undamped resonances (which can produce infinities).

For LC filtered systems, it was found that moderate bandwidth 2nd order PLLs had adverse interactions with the capacitor bank. While not presented here, the reader can easily confirm such a statement through the models provided in the Appendices.

If a low bandwidth 1st-order PLL is used, such as that used in [3], it was possible to achieve stable operation in power systems with short circuit ratios of one; however, in order to do so, significant effort was required so that the outer controllers could (a) compensate for improper performance of the inner level controller (current regulator becomes coupled) (b) provide damping.

The main controller settings are given in table 5.1:

$k_{\text{p}}^{\text{res}}$	$k_{\text{i}}^{\text{res}}$	ω_{cut}	$k_{\text{p}}^{\text{pow}}$	$k_{\text{i}}^{\text{pow}}$	$k_{\text{p}}^{\text{vol}}$	$k_{\text{i}}^{\text{vol}}$	α_{f}
$\alpha_{\text{c}} L_{\text{c}}$	$13 k_{\text{p}}^{\text{res}}$	15 rad/s	0	50	0	60	100

Table 5.1: Parameters for the proportional resonant controller for LC systems

For the L-filtered cases, the gains were boosted and the cut-off frequency for the low-pass filters could also be increased. The author acknowledges that this may result in an overly fine-tuned controller. However, this is done to simply assess the potential for proportional resonant control if all the resonant frequencies are high, at which point, active damping techniques such as those found in [33][34][35].

$k_{\mathrm{p}}^{\mathrm{res}}$	$k_{\mathrm{i}}^{\mathrm{res}}$	ω_{cut}	$k_{\mathrm{p}}^{\mathrm{pow}}$	$k_{\mathrm{i}}^{\mathrm{pow}}$	$k_{\mathrm{p}}^{\mathrm{vol}}$	$k_{\mathrm{i}}^{\mathrm{vol}}$	α_{f_1}
$\alpha_{\mathrm{c}_1} L_{\mathrm{c}_1}$	$13 k_{\mathrm{p}}^{\mathrm{res}}$	15 rad/s	0	70	0	70	180

Table 5.2: Parameters for the proportional resonant controller for L systems

Depending on the order, the following settings were adopted for the PLL:

	$k_{\mathrm{p}}^{\mathrm{pll}}$	$k_{\mathrm{i}}^{\mathrm{pll}}$
1st order	20	20
2nd order	100	7

Table 5.3: Parameters for the PLL.

The gain associated with the resonant controller yields an error of approximately 0.55% in current magnitude (phases were significantly more accurate). That being said, the steady-state errors in the active power output and AC voltage magnitude are eliminated by the outer controllers.

5.2.1 Using a first-order PLL

Baseline case studies (LC filter)

For the LC-filtered converter, an outer control loop topology as shown was adopted:

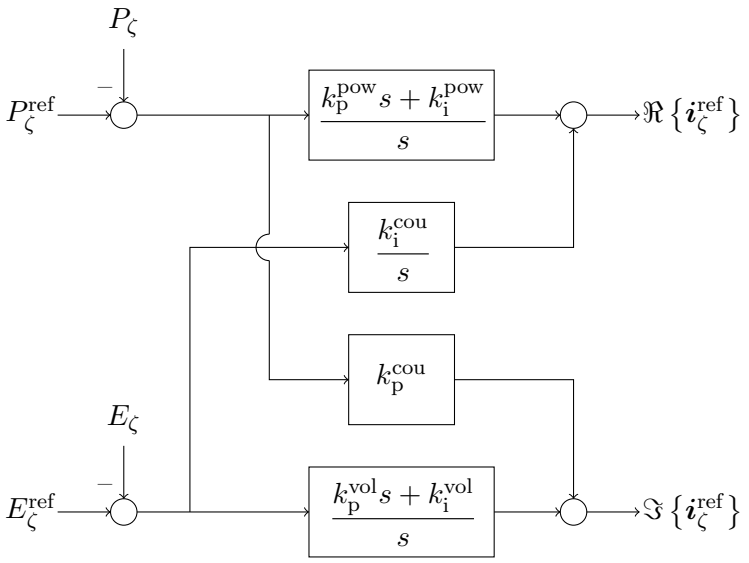

Figure 5.3: Illustration of the coupling controller.

A non-linear gain-scheduled control approach may improve performance further; however, for implementation reasons similar to those discussed in chapter two, it was decided that gain-scheduling would not be applied. Moreover, improved tuning techniques for the main diagonal controllers may yield sufficient performance in their own right.

k_p^cou	k_i^cou
-40	-25

Table 5.4: Parameters for the cross-coupling controllers

Figures 5.4 to 5.6 illustrate the performance of proportional resonant control when the short-circuit ratio is three. In general, the main diagonal terms are dominant. However, the transmittance from E^ref to P does carry power around 30 rad/s; this is mainly the result of the integral cross-coupling controller, which has deliberately not been gain-scheduled for simplicity and because it might be difficult to infer what the system short-circuit ratio is in practice (which would be required for effective gain scheduling). As a result, in some operating points it boosts performance, while in others it degrades it. The choice of the gain was ultimately set such that it had a greater positive influence on weak systems than it did negatively affect performance in strong systems.

The transmittance from P^ref to E has very little power; hence, when a small change in power set

point is introduced, there is very little response in the voltage level as can be seen from the time traces. Contrary to power synchronization control, for systems with short-circuit ratios of three, the transmittances from E^{ref} to P and P^{ref} to E actually decrease as the converter operates closer to rated power.

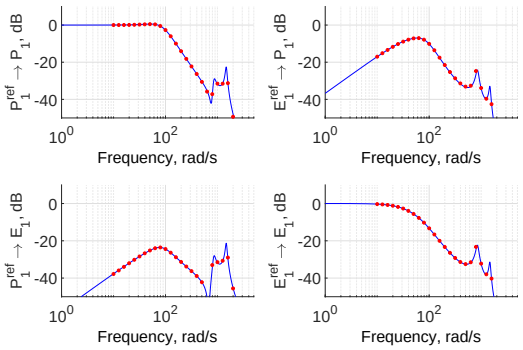

(a) $\boldsymbol{H}_1^{\text{prc}}$. Solid line - linear model; dotted - frequency scanning.

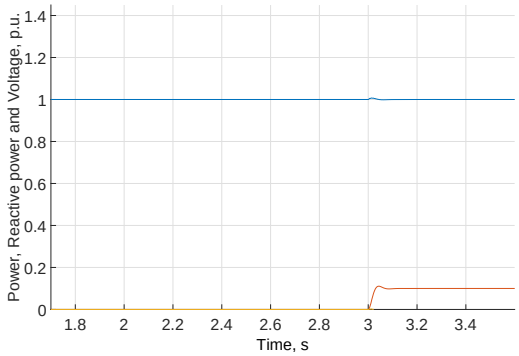

(b) Time domain simulation of non-linear model. Solid - change in P_1^{ref}; dashed - change in E_1^{ref}

Figure 5.4: Performance of the proportional resonant controller. SCR = 3, $P_{1,0} = 0.0$pu.

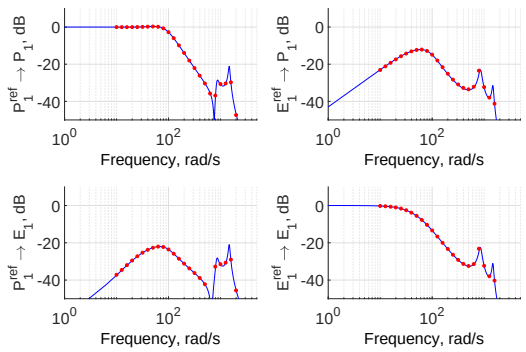

(a) $\boldsymbol{H}_1^{\text{prc}}$. Solid line - linear model; dotted - frequency scanning.

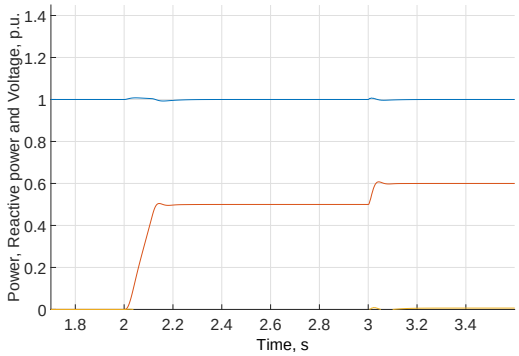

(b) Time domain simulation of non-linear model. Solid - change in P_1^{ref}; dashed - change in E_1^{ref}

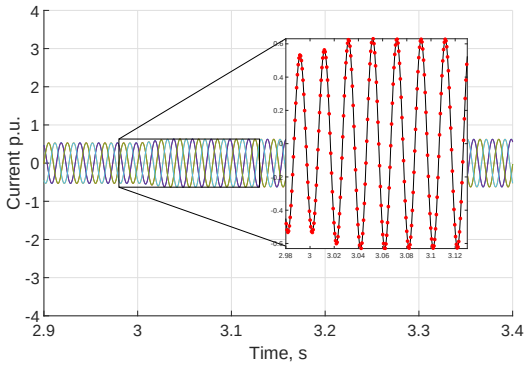

(c) Current tracking capability of controller when $\Delta P_1 = 0.1$p.u. and $P_{1,0} = 0.5$p.u.

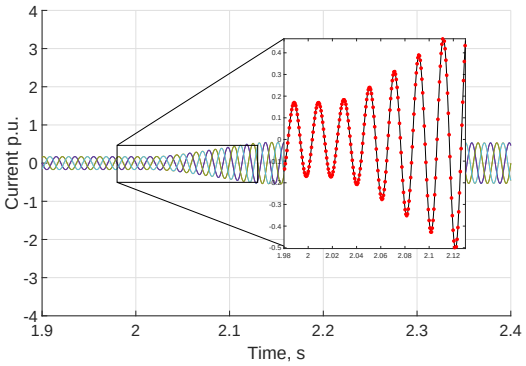

(d) Current tracking capability of controller when $\Delta P_1 = 0.5$p.u. and $P_{1,0} = 0.0$p.u.

Figure 5.5: Performance of the proportional resonant controller. SCR = 3, $P_{1,0} = 0.5$pu.

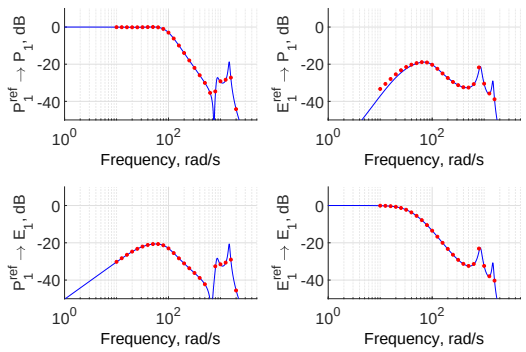

(a) $\boldsymbol{H}_1^{\text{prc}}$. Solid line - linear model; dotted - frequency scanning.

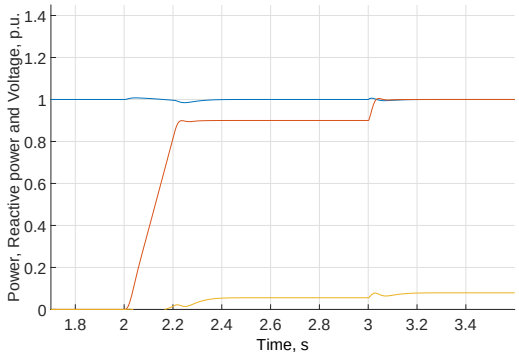

(b) Time domain simulation of non-linear model. Solid - change in P_1^{ref}; dashed - change in E_1^{ref}

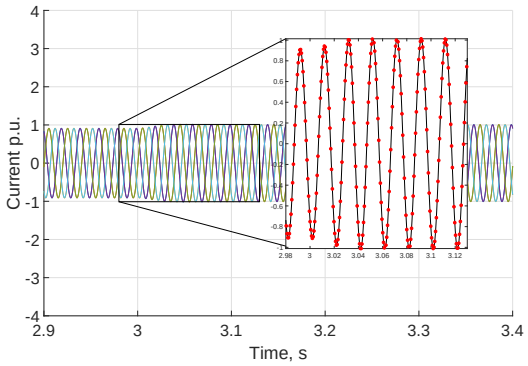

(c) Current tracking capability of controller when $\Delta P_1 = 0.1$p.u. and $P_{1,0} = 0.9$p.u.

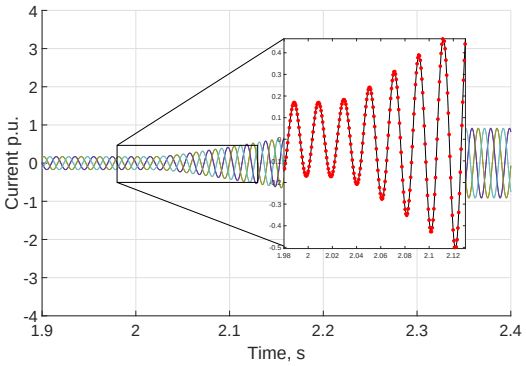

(d) Current tracking capability of controller when $\Delta P_1 = 0.9$p.u. and $P_{1,0} = 0.0$p.u.

Figure 5.6: Performance of the proportional resonant controller. SCR = 3, $P_{1,0} = 0.90$pu.

Figures 5.7 to 5.9 show the performance of proportional resonant control when the short-circuit ratio is one. When the short-circuit ratio is one, there is significantly more power in the transmittances $E_1^{\text{ref}} \rightarrow P_1$ and $P_1^{\text{ref}} \rightarrow E_1$. This is similar to what was observed in dq-axis vector current control, with coupling tending to increase with power set point. In addition, the high frequency resonances are poorly damped, which is an undesirable trait.

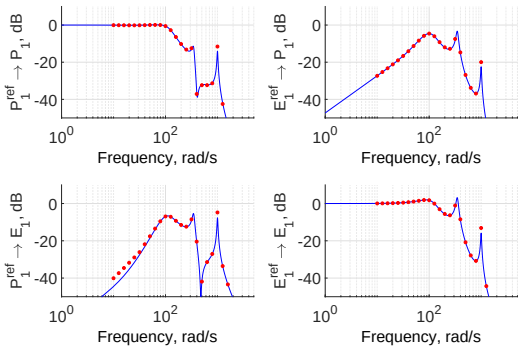

(a) $\boldsymbol{H}_1^{\text{prc}}$. Solid line - linear model; dotted - frequency scanning.

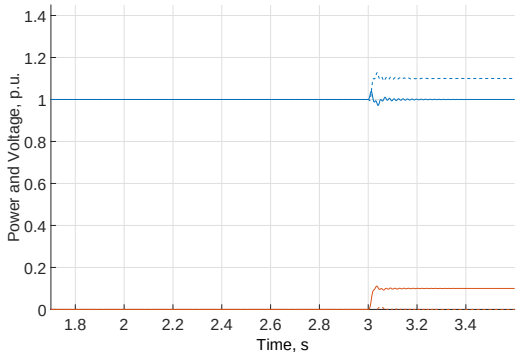

(b) Time domain simulation of non-linear model. Solid - change in P_1^{ref}; dashed - change in E_1^{ref}

Figure 5.7: Performance of the proportional resonant controller. SCR = 1, $P_{1,0} = 0.0$pu.

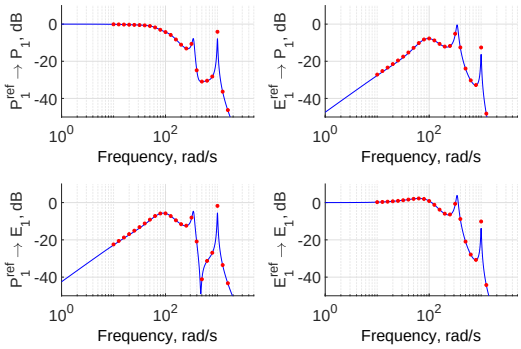

(a) $\boldsymbol{H}_1^{\text{prc}}$. Solid line - linear model; dotted - frequency scanning.

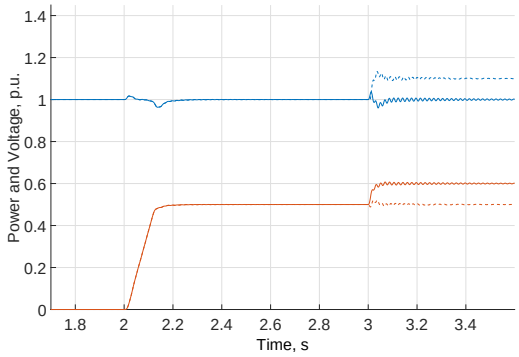

(b) Time domain simulation of non-linear model. Solid - change in P_1^{ref}; dashed - change in E_1^{ref}

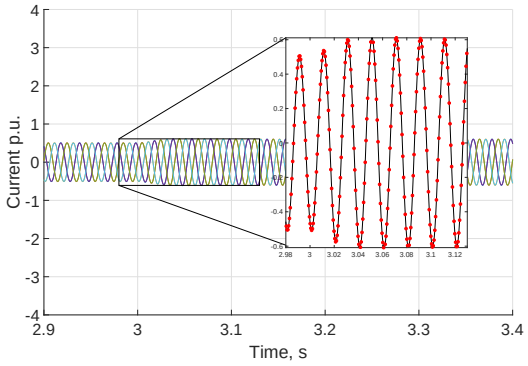

(c) Current tracking capability of controller when $\Delta P_1 = 0.1$p.u. and $P_{1,0} = 0.5$p.u.

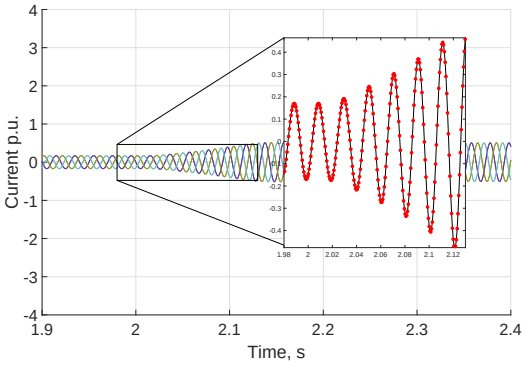

(d) Current tracking capability of controller when $\Delta P_1 = 0.5$p.u. and $P_{1,0} = 0.0$p.u.

Figure 5.8: Performance of the proportional resonant controller. SCR = 1, $P_0 = 0.5$pu.

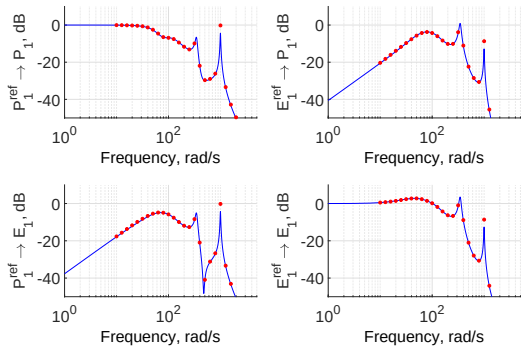

(a) $\boldsymbol{H}_1^{\text{prc}}$. Solid line - linear model; dotted - frequency scanning.

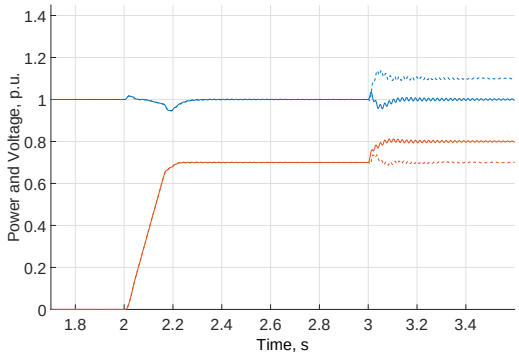

(b) Time domain simulation of non-linear model. Solid - change in P_1^{ref}; dashed - change in E_1^{ref}

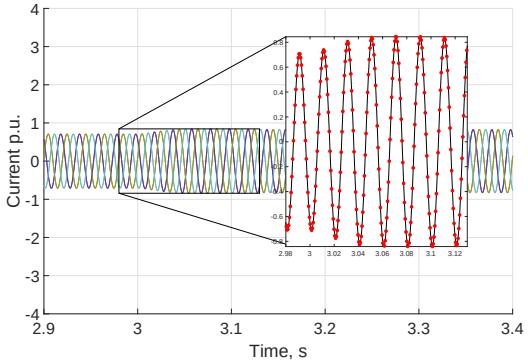

(c) Current tracking capability of controller when $\Delta P_1 = 0.1$p.u. and $P_{1,0} = 0.7$p.u.

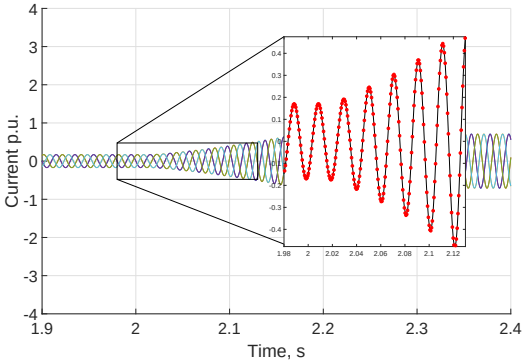

(d) Current tracking capability of controller when $\Delta P_1 = 0.7$p.u. and $P_{1,0} = 0.0$p.u.

Figure 5.9: Performance of the proportional resonant controller. SCR = 1, $P_{1,0} = 0.70$pu.

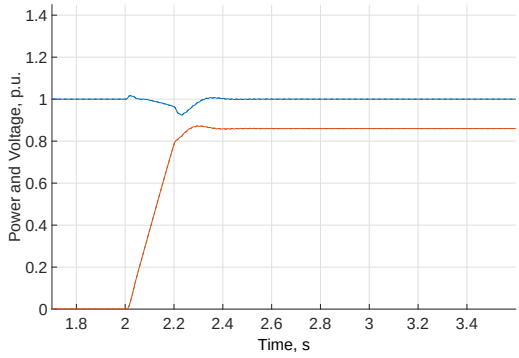

(a) Time domain simulation of non-linear model when a large disturbance, $\Delta P_1 = 0.86$p.u., is introduced.

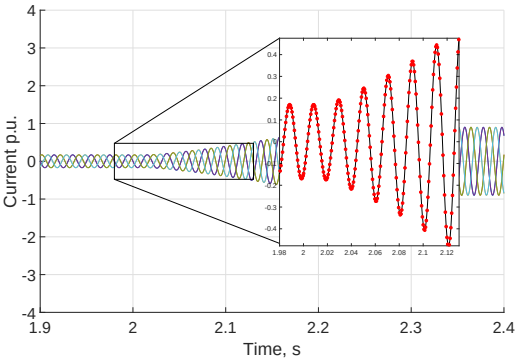

(b) Current tracking capability of controller when $\Delta P_1 = 0.80$p.u. and $P_{1,0} = 0.0$p.u.

Figure 5.10: Performance of the proportional resonant controller. SCR = 1, $\Delta P_1 = 0.86$pu.

An inspection of the poles and zeros of the transfer function matrix, $\boldsymbol{H}_1^{\text{prc}}$ shows that all the poles are in the left half plane; however, two pairs of poles are close to the origin and poorly damped. This is probably due to improper filtering techniques. Future studies could involve developing a controller with improved filtering. This may also remove the need for one (or even both) of the cross-coupling controllers.

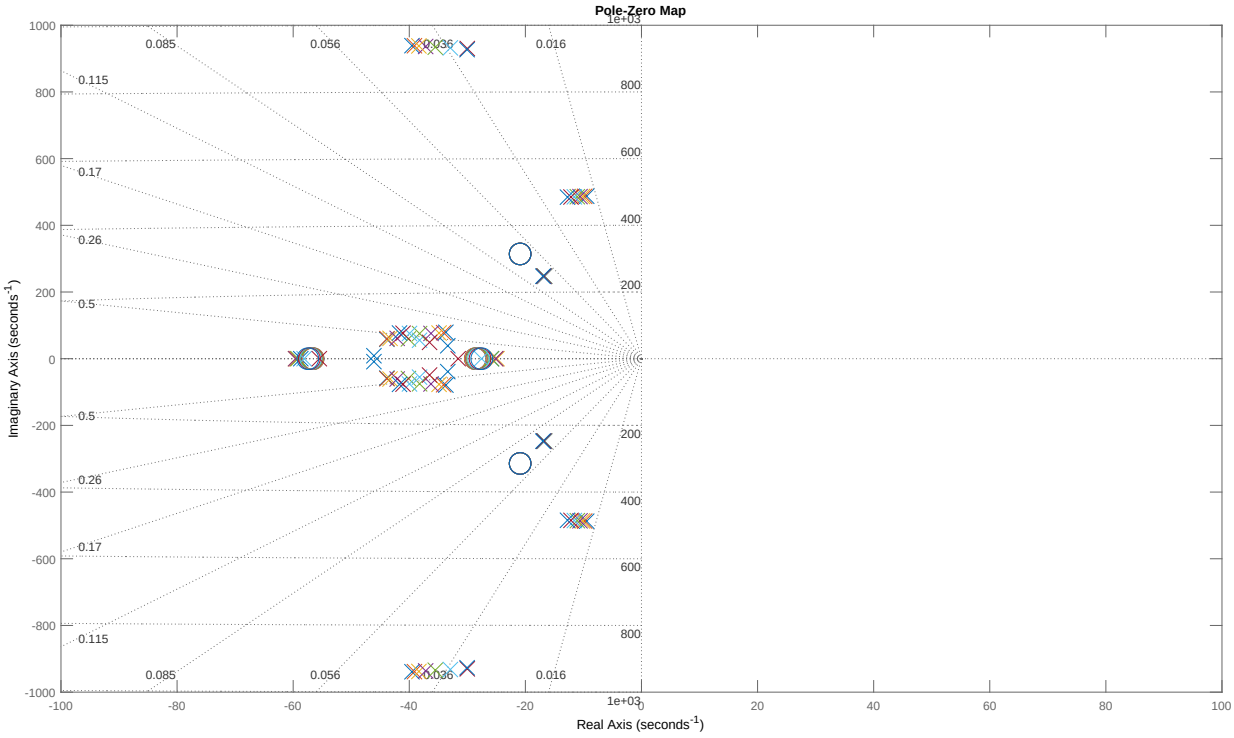

Figure 5.11: Poles and zeros for the controller in a system with a short-circuit ratio of 1 as evaluated at a range of active power set points. Each colour corresponds to a different active power set point.

Active power set points vary from 0p.u. to 07p.u. The associated colours are blue, orange, yellow-ochre, purple, green, cerulean, red and blue.

Using an L filter

Figures 5.12 to 5.14 show the performance of proportional resonant control when the short-circuit ratio is one. it can be seen that there is significantly more power in the transmittances $E_1^{\text{ref}} \rightarrow P_1$ and $P_1^{\text{ref}} \rightarrow E_1$. As with dq-axis vector current control, the coupling tends to increase with power

set point.

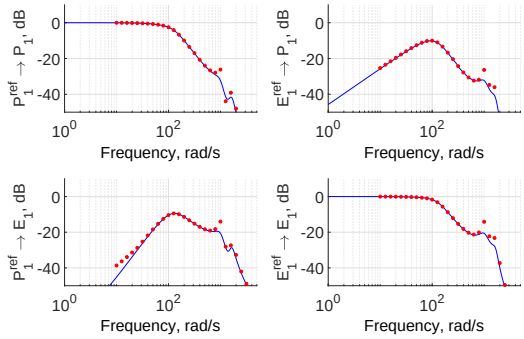

(a) $\boldsymbol{H}_1^{\text{prc}}$. Solid line - linear model; dotted - frequency scanning.

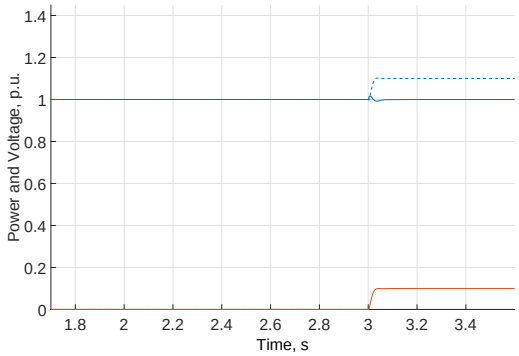

(b) Time domain simulation of non-linear model. Solid - change in P_1^{ref}; dashed - change in E_1^{ref}

Figure 5.12: Performance of the proportional resonant controller. SCR = 1, $P_{1,0} = 0.0$pu.

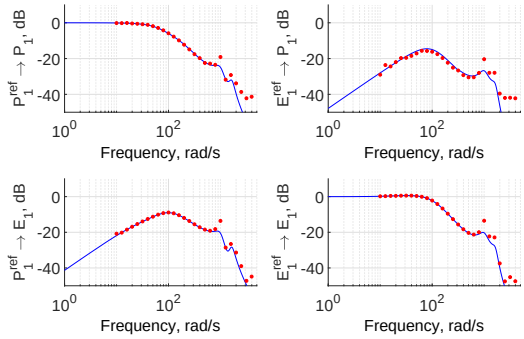

(a) $\boldsymbol{H}_1^{\text{prc}}$. Solid line - linear model; dotted - frequency scanning.

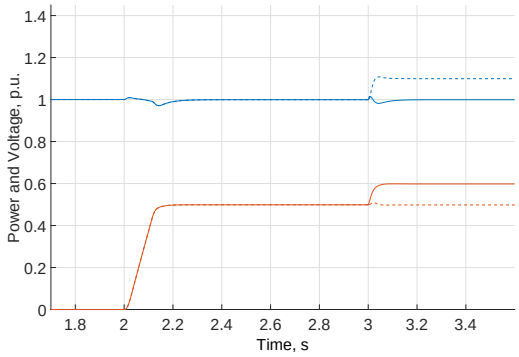

(b) Time domain simulation of non-linear model. Solid - change in P_1^{ref}; dashed - change in E_1^{ref}

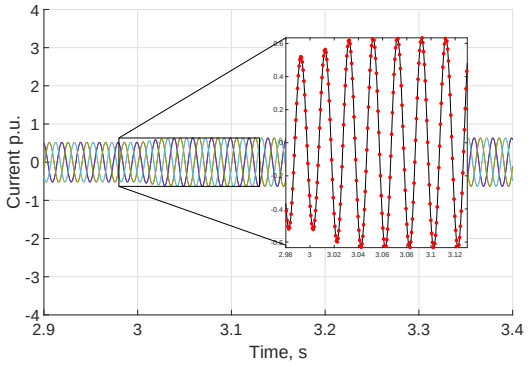

(c) Current tracking capability of controller when $\Delta P_1 = 0.1$p.u. and $P_{1,0} = 0.5$p.u.

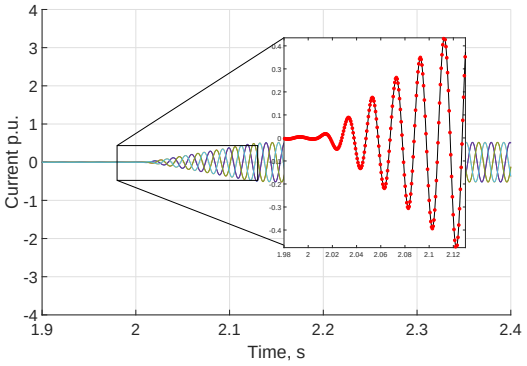

(d) Current tracking capability of controller when $\Delta P_1 = 0.5$p.u. and $P_{1,0} = 0.0$p.u.

Figure 5.13: Performance of the proportional resonant controller. SCR = 1, $P_{1,0} = 0.5$pu.

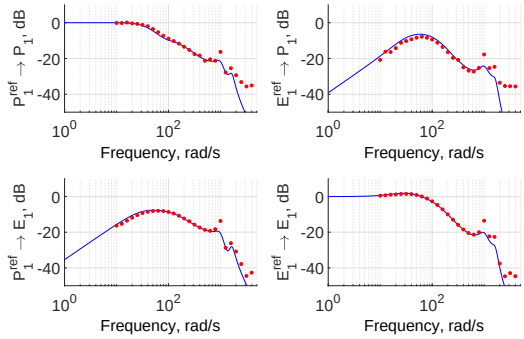

(a) $\boldsymbol{H}_1^{\text{prc}}$. Solid line - linear model; dotted - frequency scanning.

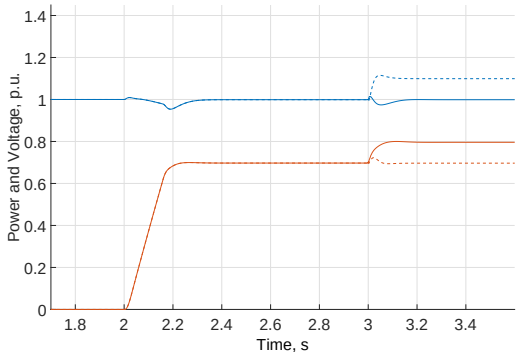

(b) Time domain simulation of non-linear model. Solid - change in P_1^{ref}; dashed - change in E_1^{ref}

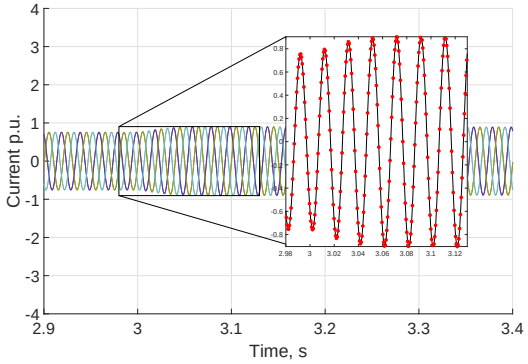

(c) Current tracking capability of controller when $\Delta P_1 = 0.1$p.u. and $P_{1,0} = 0.7$p.u.

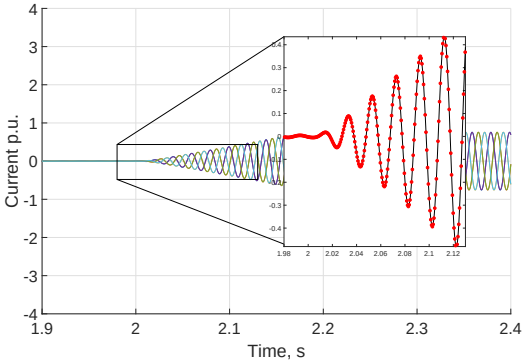

(d) Current tracking capability of controller when $\Delta P_1 = 0.7$p.u. and $P_{1,0} = 0.0$p.u.

Figure 5.14: Performance of the proportional resonant controller. SCR = 1, $P_{1,0} = 0.70$pu.

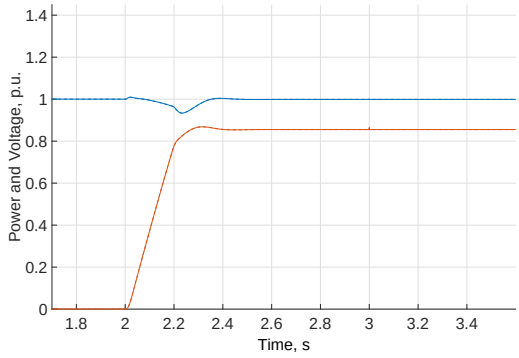

(a) Time domain simulation of non-linear model when a large disturbance, $\Delta P_1 = 0.86$p.u., is introduced.

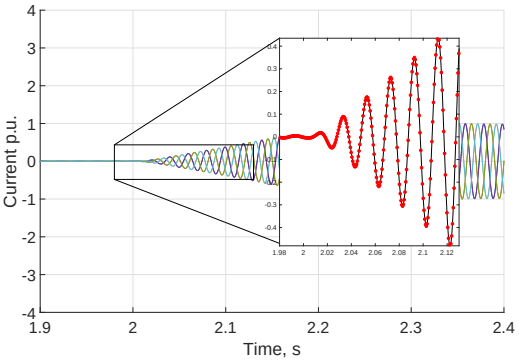

(b) Current tracking capability of controller when $\Delta P_1 = 0.86$p.u. and $P_{1,0} = 0.0$p.u.

Figure 5.15: Performance of the proportional resonant controller. SCR = 1, $\Delta P_1 = 0.86$pu.

5.2.2 Using a second-order PLL

Using an L filter

In this section, results are presented only for the case where the short-circuit ratio is one when a 2nd order PLL is applied. As can be seen, the controller encounters issues at high power set points in weak AC systems.

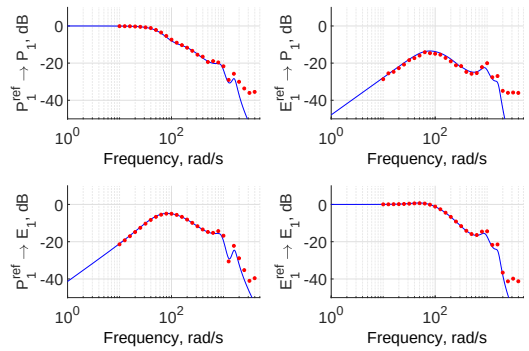

(a) $\boldsymbol{H}_1^{\text{prc}}$. Solid line - linear model; dotted - frequency scanning.

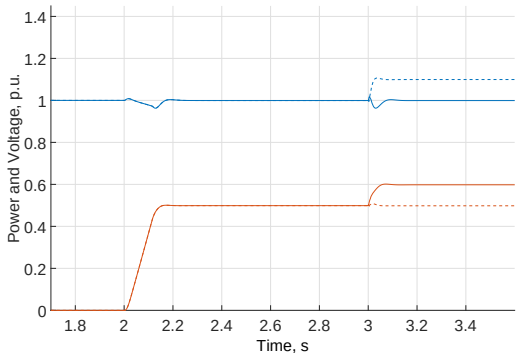

(b) Time domain simulation of non-linear model. Solid - change in P_1^{ref}; dashed - change in E_1^{ref}

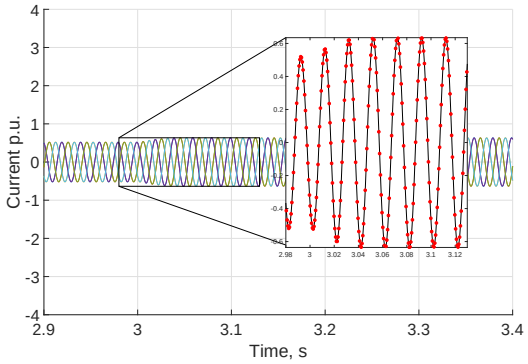

(c) Current tracking ability of the resonant controller when $\Delta P_1 = 0.1$p.u. and $P_{1,0} = 0.5$p.u.

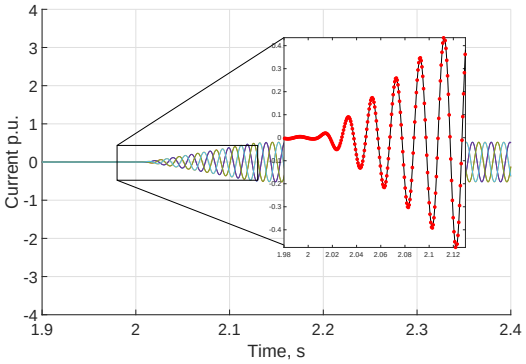

(d) Current tracking ability of the resonant controller when $\Delta P_1 = 0.5$p.u. and $P_{1,0} = 0.0$p.u.

Figure 5.16: Performance of the proportional resonant controller. SCR = 1, $P_{1,0} = 0.5$pu.

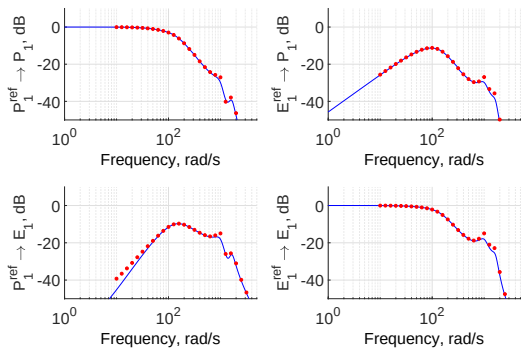

(a) $\boldsymbol{H}_1^{\text{prc}}$. Solid line - linear model; dotted - frequency scanning.

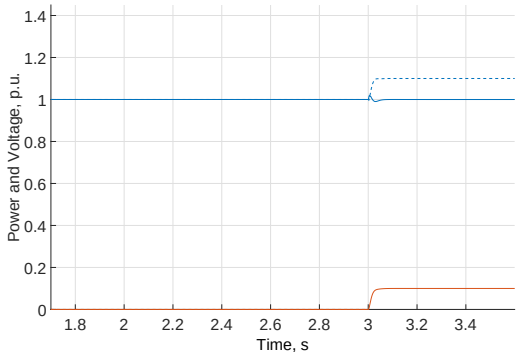

(b) Time domain simulation of non-linear model. Solid - change in P_1^{ref}; dashed - change in E_1^{ref}

Figure 5.17: Performance of the proportional resonant controller. SCR = 1, $P_{1,0} = 0.0$pu.

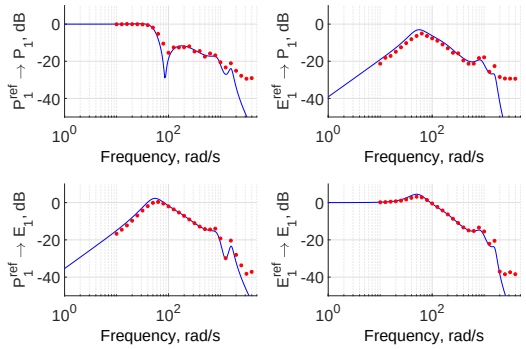

(a) $\boldsymbol{H}_1^{\text{prc}}$. Solid line - linear model; dotted - frequency scanning.

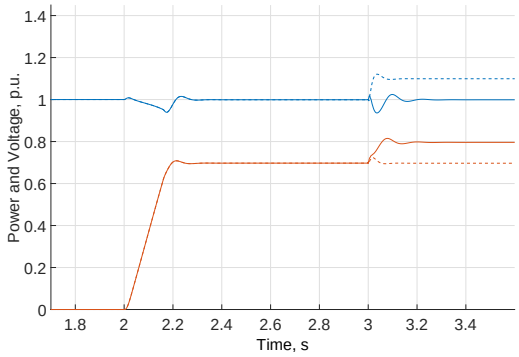

(b) Time domain simulation of non-linear model. Solid - change in P_1^{ref}; dashed - change in E_1^{ref}

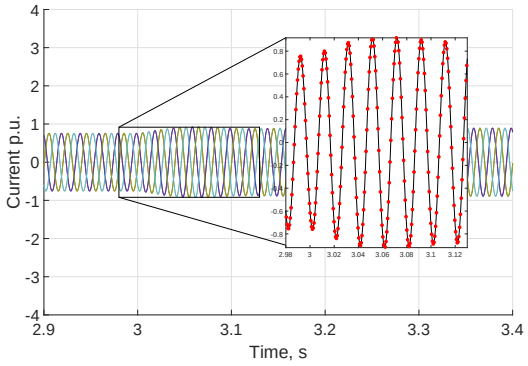

(c) Current tracking capability of controller when $\Delta P_1 = 0.1$p.u. and $P_{1,0} = 0.7$p.u.

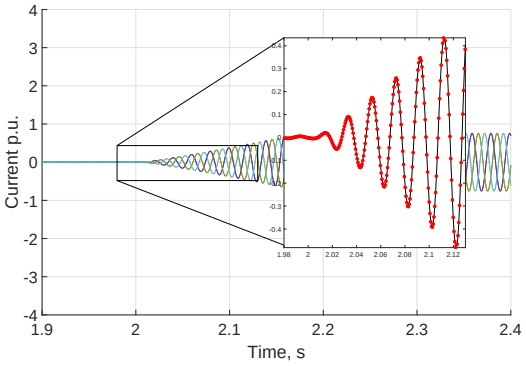

(d) Current tracking capability of controller when $\Delta P_1 = 0.7$p.u. and $P_{1,0} = 0.0$p.u.

Figure 5.18: Performance of the proportional resonant controller. SCR = 1, $P_{1,0} = 0.70$pu.

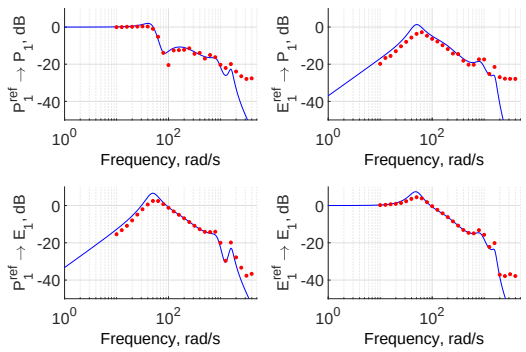

(a) $\boldsymbol{H}_1^{\text{prc}}$. Solid line - linear model; dotted - frequency scanning.

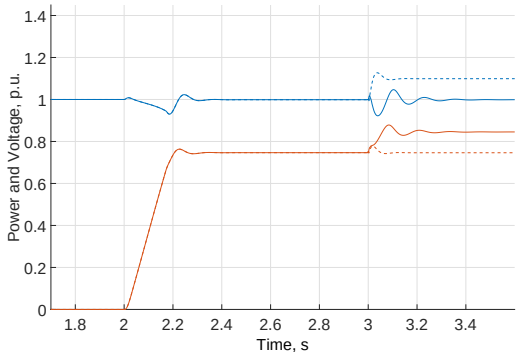

(b) Time domain simulation of non-linear model. Solid - change in P_1^{ref}; dashed - change in E_1^{ref}

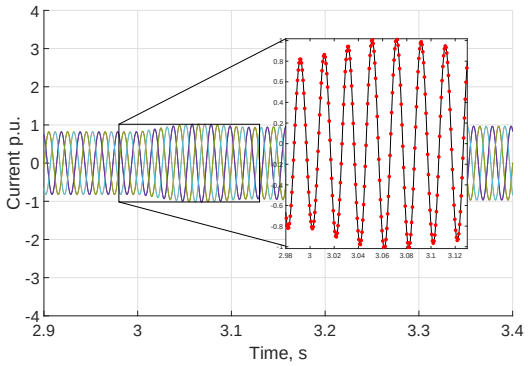

(c) Current tracking capability of controller when $\Delta P_1 = 0.1$p.u. and $P_{1,0} = 0.75$p.u.

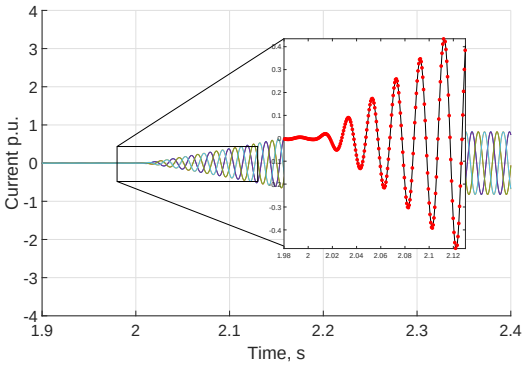

(d) Current tracking capability of controller when $\Delta P_1 = 0.75$p.u. and $P_{1,0} = 0.0$p.u.

Figure 5.19: Performance of the proportional resonant controller. SCR = 1, $P_{1,0} = 0.75$pu.

5.3 Summary

In general, it was found that proportional resonant control was less effective at damping system resonances, which restricts its ability to function well in weak systems. Compensating action was achieved through a mixture of low-pass filters and cross-coupling controllers. In other words, the controller design was relatively complex.

A linear model of proportional resonant control which can be easily integrated into large systems has been developed. It includes PLL dynamics. The linear model predicted the dynamics in the low and medium frequency ranges fairly well. However, in the high frequency range, the resonance was under-predicted by the linear model, highlighting the need for appropriate gain and phase margins

and damping. By attempting to achieve these criteria, the bandwidth of the outer controller was compromised, yielding a slow system at the high power set points.

Chapter 6

Analysis of power synchronization control

The third control algorithm considered in this work is the power synchronization controller. As with dq-axis vector current control and proportional resonant control, the mathematical analysis is presented for converters which use either an L or an LC filter.

6.1 Overview of power synchronization control

As previously mentioned, in contrast to the dq-axis vector current control algorithm, the power synchronization control algorithm has no PLL. Synchronization is achieved through power flow considerations. Changes in the measured power output and/or changes in the phase angle of the bridge voltage. The AC voltage is supported by a second control loop. A high-pass filter is combined with a measurement of the current flowing through the phase reactor in order to provide damping of a resonance. This is summarised in figure 6.1:

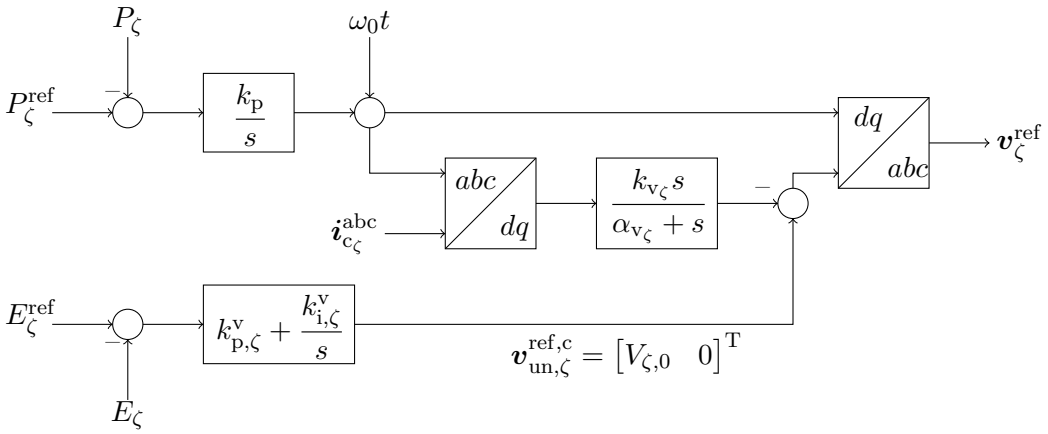

Figure 6.1: Combined power synchronization control system with damping

Note that the output of the AC voltage controller is defined to be the d-component of the bridge voltage reference in the converter dq frame. That is, synchronization is with the bridge voltage and not the PCC voltage. This lines up with the expression for power flow across a reactance.

Mathematically, the voltage reference (for the PWM process) as expressed in the converter dq frame is set according to

$$\boldsymbol{v}_\zeta^{\mathrm{ref,c}}(s) = \boldsymbol{v}_{\mathrm{un},\zeta}^{\mathrm{ref,c}}(s) - H_\zeta^{\mathrm{hp}}(s)\boldsymbol{i}_{\mathrm{c}_\zeta}^{\mathrm{c}}(s) \tag{6.1}$$

The power reference could be set by a DC voltage controller.

6.2 Linear analysis of the controller

6.2.1 The PI controllers

Referring to figure 6.1, the control laws could be expressed in the following matrix form:

$$\begin{bmatrix} \theta_{\mathrm{v}\zeta}(s) \\ V_{\mathrm{un},\zeta}(s) \end{bmatrix} = \begin{bmatrix} G_\zeta^{\mathrm{psl}}(s) & 0 \\ 0 & G_\zeta^{\mathrm{avl}}(s) \end{bmatrix} \begin{bmatrix} P_\zeta^{\mathrm{ref}}(s) \\ E_\zeta^{\mathrm{ref}}(s) \end{bmatrix} + \begin{bmatrix} -G_\zeta^{\mathrm{psl}}(s) & 0 \\ 0 & -G_\zeta^{\mathrm{avl}}(s) \end{bmatrix} \begin{bmatrix} P_\zeta(s) \\ E_\zeta(s) \end{bmatrix} \tag{6.2}$$

where $G_\zeta^{\mathrm{psl}}(s)$ and $G_\zeta^{\mathrm{avl}}(s)$ are the PI controllers for the two loops.

In order to be easily combined with the state-space model of the power system, let us express equation 6.2 as follows:

$$\begin{bmatrix} \theta_{\mathrm{v}\zeta}(s) \\ V_{\mathrm{un},\zeta}(s) \end{bmatrix} = \underbrace{\begin{bmatrix} G_\zeta^{\mathrm{psl}}(s) & 0 \\ 0 & G_\zeta^{\mathrm{avl}}(s) \end{bmatrix}}_{\boldsymbol{G}_\zeta^{\mathrm{a}}(s)} \begin{bmatrix} P_\zeta^{\mathrm{ref}}(s) \\ E_\zeta^{\mathrm{ref}}(s) \end{bmatrix} + \underbrace{\begin{bmatrix} -C_{\mathrm{PSL}}(s) & 0 & 0 & 0 & 0 & 0 \\ 0 & -C_{\mathrm{AVL}}(s) & 0 & 0 & 0 & 0 \end{bmatrix}}_{\boldsymbol{G}_\zeta^{\mathrm{b}}(s)} \boldsymbol{y}_{\mathrm{E}\zeta}^{\mathrm{loc}} \tag{6.3}$$

If load compensation techniques are to be applied, something which will be of importance for multi-converter systems (see chapter 4), the measurement fed into the voltage controller should be as follows:

$$E_\zeta \rightarrow |\boldsymbol{e}_\zeta^{\mathrm{g}} + k_{\mathrm{c}_\zeta}(R_{\mathrm{c}_\zeta} + jX_{\mathrm{c}_\zeta})\boldsymbol{i}_{\mathrm{c}_\zeta}^{\mathrm{g}}| \tag{6.4}$$

where

$$X_{\mathrm{c}_\zeta} = \omega_0 L_{\mathrm{c}_\zeta} \tag{6.5}$$

Let

$$\boldsymbol{w}_\zeta = \begin{bmatrix} w_{\zeta,\mathrm{d}} \\ w_{\zeta,\mathrm{q}} \end{bmatrix} = \begin{bmatrix} e_{\mathrm{d}}^{\mathrm{g}} + k_{\mathrm{c}}(R_{\mathrm{c}} i_{\mathrm{cd}}^{\mathrm{g}} - \omega_0 L_{\mathrm{c}_\zeta} i_{\mathrm{cq}}^{\mathrm{g}}) \\ e_{\mathrm{q}}^{\mathrm{g}} + k_{\mathrm{c}}(R_{\mathrm{c}} i_{\mathrm{cq}}^{\mathrm{g}} + \omega_0 L_{\mathrm{c}} i_{\mathrm{cd}}^{\mathrm{g}}) \end{bmatrix} \tag{6.6}$$

To a first order,

$$\Delta W_\zeta = \frac{1}{W_0}(w_{\mathrm{d},0}\Delta w_\mathrm{d} + w_{\mathrm{q},0}\Delta w_\mathrm{q}) \tag{6.7}$$

In other words, with load compensation applied,

$$\begin{aligned}\boldsymbol{G}_\zeta^\mathrm{b}(s) \to &\begin{bmatrix} -G_\zeta^\mathrm{psl} & 0 \\ 0 & -G_\zeta^\mathrm{avl} \end{bmatrix} \times \dots \\ &\begin{bmatrix} 1 & 0 & 0 & 0 & 0 & 0 \\ 0 & 0 & \dfrac{k_\mathrm{c}(R_{\mathrm{c}_\zeta} + \omega_0 L_{\mathrm{c}_\zeta})w_{\zeta,\mathrm{d}0}}{W_{\zeta,0}} & \dfrac{w_{\zeta,\mathrm{q}0}k_\mathrm{c}(R_{\mathrm{c}_\zeta} - \omega_0 L_{\mathrm{c}_\zeta})}{W_{\zeta,0}} & \dfrac{w_{\zeta,\mathrm{d}0}}{W_{\zeta,0}} & \dfrac{w_{\zeta,\mathrm{q}0}}{W_{\zeta,0}} \end{bmatrix}\end{aligned} \tag{6.8}$$

Contribution to the unified state-space model

For the unified state-space model, let us repeat previously outlined approaches:

$$\begin{aligned}\frac{\mathrm{d}\boldsymbol{x}_\zeta^\mathrm{ol}}{\mathrm{d}t} = &\underbrace{\begin{bmatrix} 1 & 0 \\ 0 & 1 \end{bmatrix}}_{\boldsymbol{B}_\zeta^\mathrm{ref}} \underbrace{\begin{bmatrix} \Delta P_\zeta^\mathrm{ref} \\ \Delta E_\zeta^\mathrm{ref} \end{bmatrix}}_{\boldsymbol{z}_\zeta^\mathrm{ref}} + \dots \\ &\underbrace{-\begin{bmatrix} 1 & 0 & 0 & 0 & 0 & 0 \\ 0 & 0 & \dfrac{k_{\mathrm{c}_\zeta}(R_{\mathrm{c}_\zeta} + \omega_0 L_{\mathrm{c}_\zeta})w_{\mathrm{d},0}}{W_0} & \dfrac{w_{\mathrm{q},0}k_\mathrm{c}(R_\mathrm{c} - \omega_0 L_\mathrm{c})}{W_0} & \dfrac{w_{\mathrm{d},0}}{W_0} & \dfrac{w_{\mathrm{q},0}}{W_0} \end{bmatrix}}_{\boldsymbol{B}_\zeta^\mathrm{ol}} \underbrace{\boldsymbol{y}_{\mathrm{E}_\zeta}^\mathrm{loc}}_{\boldsymbol{z}_\zeta^\mathrm{ol}}\end{aligned} \tag{6.9}$$

$$\begin{bmatrix} \theta_\mathrm{v} \\ V_\mathrm{un} \end{bmatrix} = \underbrace{\begin{bmatrix} k_\mathrm{i}^\mathrm{apc} & 0 \\ 0 & k_\mathrm{i}^\mathrm{avc} \end{bmatrix}}_{\boldsymbol{C}_\zeta^\mathrm{ol}} \underbrace{\begin{bmatrix} \Delta P_\zeta^\mathrm{ref} - \Delta P_\zeta \\ \Delta E_\zeta^\mathrm{ref} - \Delta E_\zeta \end{bmatrix}}_{\boldsymbol{x}_\zeta^\mathrm{ol}} + \underbrace{\begin{bmatrix} k_\mathrm{p}^\mathrm{apc} & 0 \\ 0 & k_\mathrm{p}^\mathrm{avc} \end{bmatrix}}_{\boldsymbol{D}_\zeta^\mathrm{ref}} \underbrace{\begin{bmatrix} \Delta P_\zeta^\mathrm{ref} \\ \Delta E_\zeta^\mathrm{ref} \end{bmatrix}}_{\boldsymbol{z}_\zeta^\mathrm{ref}} + \underbrace{-\boldsymbol{D}_\zeta^\mathrm{ref}\boldsymbol{B}_\zeta^\mathrm{ol}}_{\boldsymbol{D}_\zeta^\mathrm{ol}} \boldsymbol{y}_{\mathrm{E}_\zeta}^\mathrm{loc} \tag{6.10}$$

6.2.2 Voltage reference signals in the converter dq frame

Perturbing equation 6.1 yields

$$\Delta \boldsymbol{v}_{\zeta}^{\mathrm{ref,c}}(s) = \Delta \boldsymbol{v}_{\mathrm{un},\zeta}^{\mathrm{ref,c}}(s) - H_{\zeta}^{\mathrm{hp}}(s)\Delta \boldsymbol{i}_{\mathrm{c}\zeta}^{\mathrm{c}}(s) \tag{6.11}$$

In a similar fashion to section 4.3.4, perturbations in the current components, as expressed in the converter dq frame, may be related to perturbations in the phase angle of the converter dq frame and perturbations in the current components, as expressed in the grid dq frame, as shown:

$$\begin{aligned}\Delta \boldsymbol{i}_{\mathrm{c}\zeta}^{\mathrm{c}}(s) = &\underbrace{\begin{bmatrix} \cos\theta_{\mathrm{v}\zeta,0} & \sin\theta_{\mathrm{v}\zeta,0} \\ -\sin\theta_{\mathrm{v}\zeta,0} & \cos\theta_{\mathrm{v}\zeta,0} \end{bmatrix}}_{\boldsymbol{C}_{\zeta}^{\mathrm{c}}(s)} \boldsymbol{T}_1^{\mathrm{psc}} \Delta \boldsymbol{i}_{\mathrm{c}\zeta}^{\mathrm{g}}(s) + \ldots \\ &\underbrace{\begin{bmatrix} \begin{bmatrix} -\sin\theta_{v_\zeta,0} & \cos\theta_{v_\zeta,0} \\ -\cos\theta_{v_\zeta,0} & \sin\theta_{v_\zeta,0} \end{bmatrix} \boldsymbol{i}_{\mathrm{c}\zeta,0}^{\mathrm{g}} & \boldsymbol{O}(2,1) \end{bmatrix}}_{\boldsymbol{G}_{\zeta}^{\mathrm{d}}(s)} \begin{bmatrix} \Delta\theta_{\mathrm{v}\zeta}^{\mathrm{c}}(s) \\ \Delta V_{\mathrm{un},\zeta}(s) \end{bmatrix}\end{aligned} \tag{6.12}$$

where the linking matrix, $\boldsymbol{T}_1^{\mathrm{psc}}$, is introduced to enable easy connection to the network model. $\boldsymbol{T}_1^{\mathrm{psc}}$ is defined as follows:

$$\boldsymbol{T}_1^{\mathrm{psc}} = \begin{bmatrix} 0 & 0 & 1 & 0 & 0 & 0 \\ 0 & 0 & 0 & 1 & 0 & 0 \end{bmatrix} \tag{6.13}$$

Thus, first-order perturbations in the voltage reference, as expressed in the converter dq frame, are given as follows:

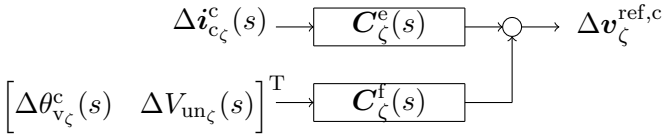

where

$$\boldsymbol{G}_{\zeta}^{\mathrm{e}}(s) = -H_{\zeta}^{\mathrm{hp}}(s) \begin{bmatrix} 1 & 0 \\ 0 & 1 \end{bmatrix}; \quad \boldsymbol{G}_{\zeta}^{\mathrm{f}}(s) = \begin{bmatrix} 0 & 1 \\ 0 & 0 \end{bmatrix} \tag{6.14}$$

$\boldsymbol{C}_{\zeta}^{\mathrm{f}}$ contains two columns, including one for $\Delta\theta_{\mathrm{v}\zeta}^{\mathrm{c}}$, so that it can easily be linked to the collective output of the PI controllers. In addition, it comprises two rows so that a dq vector for the voltage reference is formed; this is because the PI controller acting on $(E_{\zeta}^{\mathrm{ref}} - E_{\zeta})$ only sets the magnitude (of the d component) of the unfiltered voltage reference signal.

Contribution to the unified linear state-space model

As with dq-axis vector current control, the initial frame transformation process is easily embedded into the unified state-space model by simply recycling $\boldsymbol{G}_{\zeta}^{\mathrm{c}}$ and $\boldsymbol{G}_{\zeta}^{\mathrm{d}}$.

$$\boldsymbol{y}_{\zeta}^{\mathrm{abc}\to\mathrm{dq}} = \boldsymbol{G}_{\zeta}^{\mathrm{c}} \boldsymbol{y}_{\mathrm{E}\zeta}^{\mathrm{loc}} + \boldsymbol{G}_{\zeta}^{\mathrm{d}} \boldsymbol{y}_{\zeta}^{\mathrm{ol}} \tag{6.15}$$

Let us note that a state-space form of a high-pass filter with unity gain, which takes as an input z_{ζ}^{hp}, is as follows:

$$\frac{\mathrm{d}x_{\zeta}^{\mathrm{hp}}}{\mathrm{d}t} = -\alpha_{\mathrm{v}\zeta} x_{\zeta}^{\mathrm{hp}} + z_{\zeta}^{\mathrm{hp}} \tag{6.16}$$

$$y_{\zeta}^{\mathrm{hp}} = -\alpha_{\mathrm{v}\zeta} x_{\zeta}^{\mathrm{hp}} + z_{\zeta}^{\mathrm{hp}} \tag{6.17}$$

where y_ζ^{hp} is the output, which in this case is being fed into the final stages of the controller. In other words, the state-space representation of the action $-H_\zeta^{\mathrm{hp}}(s)\Delta \boldsymbol{i}_{\mathrm{c}\zeta}^{\mathrm{c}}$ is as follows:

$$\frac{\mathrm{d}\boldsymbol{x}_\zeta^{\mathrm{hp}}}{\mathrm{d}t} = \underbrace{\begin{bmatrix} -\alpha_{\mathrm{v}\zeta} & 0 \\ 0 & -\alpha_{\mathrm{v}\zeta} \end{bmatrix}}_{\boldsymbol{A}_\zeta^{\mathrm{hp}}} \boldsymbol{x}_\zeta^{\mathrm{hp}} + \underbrace{\begin{bmatrix} k_{\mathrm{v}\zeta} & 0 \\ 0 & k_{\mathrm{v}\zeta} \end{bmatrix}}_{\boldsymbol{B}_\zeta^{\mathrm{hp}}} \Delta \boldsymbol{i}_{\mathrm{c}\zeta}^{\mathrm{c}} \tag{6.18}$$

$$\boldsymbol{y}_\zeta^{\mathrm{hp}} = \underbrace{\begin{bmatrix} \alpha_{\mathrm{v}\zeta} & 0 \\ 0 & \alpha_{\mathrm{v}\zeta} \end{bmatrix}}_{\boldsymbol{C}_\zeta^{\mathrm{hp}}} \boldsymbol{x}_\zeta^{\mathrm{hp}} + \underbrace{\begin{bmatrix} -k_{\mathrm{v}\zeta} & 0 \\ 0 & -k_{\mathrm{v}\zeta} \end{bmatrix}}_{\boldsymbol{D}_\zeta^{\mathrm{hp}}} \Delta \boldsymbol{i}_{\mathrm{c}\zeta}^{\mathrm{c}} \tag{6.19}$$

which, when combined with the unfiltered signal, may be expressed as follows:

$$\boldsymbol{z}_\zeta^{\mathrm{dq}\to\mathrm{abc}} = \boldsymbol{y}_\zeta^{\mathrm{hp}} + \boldsymbol{G}_\zeta^{\mathrm{f}} \boldsymbol{y}_\zeta^{\mathrm{ol}} \tag{6.20}$$

6.2.3 Voltage signals for the PWM

The converter dq frame then connects back to the grid frame by an inverse process, which provides the values for $\Delta \boldsymbol{v}_\zeta^{\mathrm{ref}}$. Hence, the dynamics associated with the inverse Park transformation are as follows:

$$\begin{aligned} \Delta v_{\mathrm{d}}^{\mathrm{g}} &= \cos\theta_{\mathrm{v},0}\Delta v_{\mathrm{d}}^{\mathrm{ref,c}} - \sin\theta_{\mathrm{v},0}\Delta v_{\mathrm{q}}^{\mathrm{ref,c}} - (v_{\mathrm{d},0}^{\mathrm{c}}\sin\theta_{\mathrm{v},0} + v_{\mathrm{q},0}^{\mathrm{c}}\cos\theta_{\mathrm{v},0})\Delta\theta_{\mathrm{v}}^{\mathrm{c}} \\ \Delta v_{\mathrm{q}}^{\mathrm{g}} &= \sin\theta_{\mathrm{v},0}\Delta v_{\mathrm{d}}^{\mathrm{ref,c}} + \cos\theta_{\mathrm{v},0}\Delta v_{\mathrm{q}}^{\mathrm{ref,c}} + (v_{\mathrm{d},0}^{\mathrm{c}}\cos\theta_{\mathrm{v},0} - v_{\mathrm{q},0}^{\mathrm{c}}\sin\theta_{\mathrm{v},0})\Delta\theta_{\mathrm{v}}^{\mathrm{c}} \end{aligned} \tag{6.21}$$

Given that the converter dq frame is, in steady-state, aligned with the bridge voltage, it follows that

$$\begin{aligned} \begin{bmatrix} v_{\mathrm{d},0}^{\mathrm{c}} \\ v_{\mathrm{q},0}^{\mathrm{c}} \end{bmatrix} &= \begin{bmatrix} \cos\theta_{\mathrm{v},0} & -\sin\theta_{\mathrm{v},0} \\ \sin\theta_{\mathrm{v},0} & \cos\theta_{\mathrm{v},0} \end{bmatrix} \begin{bmatrix} v_{\mathrm{d},0}^{\mathrm{g}} \\ v_{\mathrm{q},0}^{\mathrm{g}} \end{bmatrix} \\ &= \begin{bmatrix} \cos\theta_{\mathrm{v},0}v_{\mathrm{d},0}^{\mathrm{g}} + \sin\theta_{\mathrm{v},0}v_{\mathrm{q},0}^{\mathrm{g}} \\ -\sin\theta_{\mathrm{v},0}v_{\mathrm{d},0}^{\mathrm{g}} + \cos\theta_{\mathrm{v},0}v_{\mathrm{q},0}^{\mathrm{g}} \end{bmatrix} \end{aligned} \tag{6.22}$$

Hence, it can be shown that

$$\boldsymbol{G}_{\zeta}^{\mathrm{h}} = \begin{bmatrix} -\Im\left\{\boldsymbol{v}_{\zeta,0}^{\mathrm{g}}\right\} & 0 \\ +\Re\left\{\boldsymbol{v}_{\zeta,0}^{\mathrm{g}}\right\} & 0 \end{bmatrix} \tag{6.23}$$

Expressed in matrix form, the frame transformation process is as follows:

$$\Delta\boldsymbol{v}_{\zeta}^{\mathrm{ref,g}} = \underbrace{\begin{bmatrix} \cos\theta_{\mathrm{v}_\zeta,0} & -\sin\theta_{\mathrm{v}_\zeta,0} \\ \sin\theta_{\mathrm{v}_\zeta,0} & \cos\theta_{\mathrm{v}_\zeta,0} \end{bmatrix}}_{\boldsymbol{G}_{\zeta}^{\mathrm{g}}(s)} \Delta\boldsymbol{v}_{\zeta}^{\mathrm{ref,c}}(s) + \underbrace{\begin{bmatrix} -\Im\left\{\boldsymbol{v}_{\zeta,0}^{\mathrm{g}}\right\} & 0 \\ +\Re\left\{\boldsymbol{v}_{\zeta,0}^{\mathrm{g}}\right\} & 0 \end{bmatrix}}_{\boldsymbol{G}_{\zeta}^{\mathrm{h}}(s)} \begin{bmatrix} \Delta\theta_{\mathrm{v}_\zeta}^{\mathrm{c}}(s) \\ \Delta V_{\mathrm{un},\zeta}(s) \end{bmatrix} \tag{6.24}$$

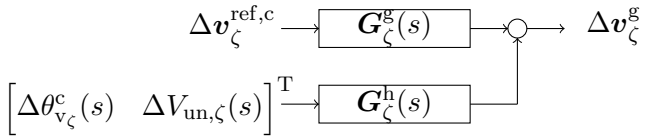

Figure 6.2: Section of controller where the drive voltages are converted to the grid frame.

Contribution to unified state-space model

A useful result that will be applied in chapter 7 is one which links the bridge voltage to the state-vector, output vector

$$\begin{aligned} \boldsymbol{y}_{\zeta}^{\mathrm{dq}\to\mathrm{abc}} = & \underbrace{\begin{bmatrix} \boldsymbol{O}(2,N_{\mathrm{E}}) & \overbrace{\begin{bmatrix}\left(\boldsymbol{G}_{\zeta}^{\mathrm{g}}\left(\boldsymbol{D}_{\zeta}^{\mathrm{hp}}\boldsymbol{G}_{\zeta}^{\mathrm{d}}+\boldsymbol{G}_{\zeta}^{\mathrm{f}}\right)+\boldsymbol{G}_{\zeta}^{\mathrm{h}}\right)\boldsymbol{G}_{\zeta}^{\mathrm{ol}} & \boldsymbol{G}_{\zeta}^{\mathrm{g}}\boldsymbol{C}_{\zeta}^{\mathrm{hp}}\end{bmatrix}}^{\boldsymbol{\rho}_{\mathrm{dq}}^{\mathrm{psc}}} \end{bmatrix}}_{\boldsymbol{C}_{\zeta}^{\mathrm{dq}}} \boldsymbol{x}_{\zeta}^{\mathrm{uni}} + \dots \\ & \underbrace{\left[\left(\boldsymbol{G}_{\zeta}^{\mathrm{g}}\left(\boldsymbol{D}_{\zeta}^{\mathrm{hp}}\boldsymbol{G}_{\zeta}^{\mathrm{d}}+\boldsymbol{G}_{\zeta}^{\mathrm{f}}\right)+\boldsymbol{G}_{\zeta}^{\mathrm{h}}\right)\boldsymbol{D}_{\zeta}^{\mathrm{ol,ref}}\right]}_{\boldsymbol{D}_{\zeta}^{\mathrm{dq}}} \boldsymbol{z}_{\zeta}^{\mathrm{ref}} + \dots \\ & \underbrace{\left[\left(\boldsymbol{G}_{\zeta}^{\mathrm{g}}\left(\left(\boldsymbol{D}_{\zeta}^{\mathrm{hp}}\boldsymbol{G}_{\zeta}^{\mathrm{d}}+\boldsymbol{G}_{\zeta}^{\mathrm{f}}\right)+\boldsymbol{G}_{\zeta}^{\mathrm{h}}\right)\boldsymbol{D}_{\zeta}^{\mathrm{ol}}+\boldsymbol{D}_{\zeta}^{\mathrm{hp}}\boldsymbol{G}_{\zeta}^{\mathrm{c}}\right)\right]}_{\boldsymbol{E}_{\zeta}^{\mathrm{dq}}} \boldsymbol{y}_{\mathrm{E}_\zeta}^{\mathrm{loc}} \end{aligned} \tag{6.25}$$

where

$$\boldsymbol{x}_{\zeta}^{\mathrm{uni}} = \left[\left(\boldsymbol{x}_{\mathrm{E}_{\zeta}}^{\mathrm{loc}} \right)^{\mathrm{T}} \quad \left(\boldsymbol{x}_{\zeta}^{\mathrm{ol}} \right)^{\mathrm{T}} \quad \left(\boldsymbol{x}_{\zeta}^{\mathrm{hp}} \right)^{\mathrm{T}} \right]^{\mathrm{T}} \tag{6.26}$$

For the single converter system, $N_{\mathrm{E}} = 6$ (see chapter 3). To permit extending the model to multi-converter systems, the states for a given converter, ζ, using power synchronization control in a multi-converter system will be defined as

$$\boldsymbol{x}_{\zeta}^{\mathrm{psc}} = \left[\left(\boldsymbol{x}_{\zeta}^{\mathrm{ol}} \right)^{\mathrm{T}} \quad \left(\boldsymbol{x}_{\zeta}^{\mathrm{hp}} \right)^{\mathrm{T}} \right]^{\mathrm{T}} \tag{6.27}$$

Again, the component state-space matrices will vary from converter to converter i.e. these component matrices need re-evaluation when moving through the converters in the model construction.

6.3 Block diagrams and transfer function matrix extraction

Combining the blocks for the control system with the block diagram for the network, a global block diagram is obtained:

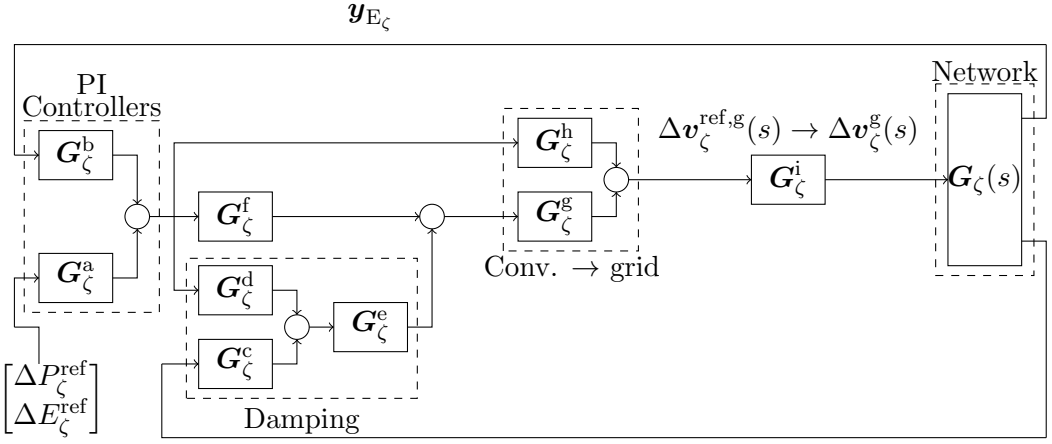

Figure 6.3: Block diagram illustrating the linearised model

From inspection,

$$\Delta \boldsymbol{v}_{\zeta}^{\mathrm{g}} = \boldsymbol{G}_{\zeta}^{\mathrm{i}} \left[\left(\left(\boldsymbol{G}_{\zeta}^{\mathrm{h}} + \boldsymbol{G}_{\zeta}^{\mathrm{g}} \left(\boldsymbol{G}_{\zeta}^{\mathrm{f}} + \boldsymbol{G}_{\zeta}^{\mathrm{e}} \boldsymbol{G}_{\zeta}^{\mathrm{d}} \right) \right) \boldsymbol{G}_{\zeta}^{\mathrm{b}} \boldsymbol{G}_{\zeta} + \boldsymbol{G}_{\zeta}^{\mathrm{g}} \boldsymbol{G}_{\zeta}^{\mathrm{e}} \boldsymbol{G}_{\zeta}^{\mathrm{c}} \boldsymbol{G}_{\zeta} \right) \Delta \boldsymbol{v}_{\zeta}^{\mathrm{g}} + \ldots \right.$$
$$\left. \left(\boldsymbol{G}_{\zeta}^{\mathrm{h}} + \boldsymbol{G}_{\zeta}^{\mathrm{g}} \left(\boldsymbol{G}_{\zeta}^{\mathrm{e}} \boldsymbol{G}_{\zeta}^{\mathrm{d}} + \boldsymbol{G}_{\zeta}^{\mathrm{f}} \right) \right) \boldsymbol{G}_{\zeta}^{\mathrm{a}} \boldsymbol{z}_{\mathrm{E}_{\zeta}}^{\mathrm{loc}} \right] \tag{6.28}$$

Since $\boldsymbol{y}_{\mathrm{E}_{\zeta}}^{\mathrm{loc}} = \boldsymbol{G}_{\zeta} \Delta \boldsymbol{v}_{\zeta}^{\mathrm{g}}$, it follows that

$$\boldsymbol{y}_{\zeta}^{\mathrm{o}} = \boldsymbol{H}_{\zeta}^{\mathrm{psc}} \boldsymbol{z}_{\mathrm{E}_{\zeta}}^{\mathrm{loc}} \tag{6.29}$$

where

$$\boldsymbol{y}_{\mathrm{o}} = \begin{bmatrix} \Delta P_{\zeta} & \Delta E_{\zeta} \end{bmatrix}^{\mathrm{T}} \tag{6.30}$$

and

$$\boldsymbol{H}_{\zeta}^{\mathrm{psc}} = \boldsymbol{\Omega} \boldsymbol{G} \left[\boldsymbol{I}_2 - \left(\left(\boldsymbol{G}_{\zeta}^{\mathrm{h}} + \boldsymbol{G}_{\zeta}^{\mathrm{g}} \left(\boldsymbol{G}_{\zeta}^{\mathrm{f}} + \boldsymbol{G}_{\zeta}^{\mathrm{e}} \boldsymbol{G}_{\zeta}^{\mathrm{d}} \right) \right) \boldsymbol{G}_{\zeta}^{\mathrm{b}} \boldsymbol{G}_{\zeta} + \boldsymbol{G}_{\zeta}^{\mathrm{g}} \boldsymbol{G}_{\zeta}^{\mathrm{e}} \boldsymbol{C}_3 \boldsymbol{G}_{\zeta} \right) \right]^{-1} \times \ldots$$
$$\left(\boldsymbol{G}_{\zeta}^{\mathrm{h}} + \boldsymbol{G}_{\zeta}^{\mathrm{g}} \left(\boldsymbol{G}_{\zeta}^{\mathrm{e}} \boldsymbol{G}_{\zeta}^{\mathrm{d}} + \boldsymbol{G}_{\zeta}^{\mathrm{f}} \right) \right) \boldsymbol{G}_{\zeta}^{\mathrm{a}} \tag{6.31}$$

$$\boldsymbol{y}_{\mathrm{o}} = \boldsymbol{\Omega} \boldsymbol{y}_{\mathrm{E}_{\zeta}}^{\mathrm{loc}} \tag{6.32}$$

The $\boldsymbol{\Omega}$ term is just to ensure that only the response of ΔP_{ζ} and ΔE_{ζ} to $\begin{bmatrix} \Delta P_{\zeta}^{\mathrm{ref}} & \Delta E_{\zeta}^{\mathrm{ref}} \end{bmatrix}^{\mathrm{T}}$ are considered. Thus,

$$\boldsymbol{\Omega} = \begin{bmatrix} 1 & 0 & 0 & 0 & 0 & 0 \\ 0 & 1 & 0 & 0 & 0 & 0 \end{bmatrix} \tag{6.33}$$

Unified linear state-space model

Now let us complete the unified linear state-space model, which contains the dynamics of both the controller and plant in one single state-space model. For simplicity, let us ignore the switching delays.

Before substituting for $\boldsymbol{y}_{\zeta}^{\mathrm{c}\to\mathrm{g}}$ and $\boldsymbol{y}_{\mathrm{E}_{\zeta}}^{\mathrm{loc}}$, the state-equation reads as follows:

$$\frac{\mathrm{d}\boldsymbol{x}_{\zeta}^{\mathrm{uni}}}{\mathrm{d}t} = \begin{bmatrix} \boldsymbol{A}_{\mathrm{E}_{\zeta}}^{\mathrm{loc}} & \boldsymbol{O}(N_{\mathrm{E}}, N_{\mathrm{c}}) \\ \boldsymbol{O}(N_{\mathrm{c}}, N_{\mathrm{E}}) & \underbrace{\begin{bmatrix} \boldsymbol{A}_{\zeta}^{\mathrm{ol}} & \boldsymbol{O}(2,2) \\ \boldsymbol{B}_{\zeta}^{\mathrm{hp}}\boldsymbol{G}_{\zeta}^{\mathrm{d}}\boldsymbol{C}_{\zeta}^{\mathrm{ol}} & \boldsymbol{A}_{\zeta}^{\mathrm{hp}} \end{bmatrix}}_{\boldsymbol{A}_{\zeta}^{\mathrm{psc}}} \end{bmatrix} \underbrace{\begin{bmatrix} \boldsymbol{x}_{\mathrm{E}_{\zeta}}^{\mathrm{loc}} \\ \boldsymbol{x}_{\zeta}^{\mathrm{psc}} \end{bmatrix}}_{\boldsymbol{x}_{\zeta}^{\mathrm{uni}}} + \begin{bmatrix} \boldsymbol{O}(N_{\mathrm{E}}, N_{\mathrm{ref}}) \\ \underbrace{\begin{bmatrix} \boldsymbol{B}_{\zeta}^{\mathrm{ref}} \\ \boldsymbol{B}_{\zeta}^{\mathrm{hp}}\boldsymbol{G}_{\zeta}^{\mathrm{d}}\boldsymbol{D}_{\zeta}^{\mathrm{ref}} \end{bmatrix}}_{\boldsymbol{B}_{\zeta}^{\mathrm{psc,b}}} \end{bmatrix} \boldsymbol{z}_{\zeta}^{\mathrm{ref}} + \ldots$$

$$\begin{bmatrix} \boldsymbol{B}_{\mathrm{E}_{\zeta}}^{\mathrm{loc}} \\ \boldsymbol{O}(N_{\mathrm{c}}, 2) \end{bmatrix} \boldsymbol{y}_{\zeta}^{\mathrm{c}\to\mathrm{g}} + \begin{bmatrix} \boldsymbol{O}(N_{\mathrm{E}}, 6) \\ \underbrace{\begin{bmatrix} \boldsymbol{B}_{\zeta}^{\mathrm{ol}} \\ \boldsymbol{B}_{\zeta}^{\mathrm{hp}}(\boldsymbol{G}_{\zeta}^{\mathrm{c}} + \boldsymbol{G}_{\zeta}^{\mathrm{d}}\boldsymbol{D}_{\zeta}^{\mathrm{ol}}) \end{bmatrix}}_{\boldsymbol{B}_{\zeta}^{\mathrm{psc,a}}} \end{bmatrix} \boldsymbol{y}_{\mathrm{E}_{\zeta}}^{\mathrm{loc}} \tag{6.34}$$

where $N_{\mathrm{ref}} = 2$, one for the power reference and one for the PCC voltage reference. The number of states associated with the controller, N_{c}, is four.

Equation 6.34 is actually a convenient form to work with when assessing multi-converter systems, which will be covered in chapter 7.

Since

$$\boldsymbol{y}_{\zeta}^{\mathrm{c}\to\mathrm{g}} = \underbrace{\left(\boldsymbol{I}_2 - \boldsymbol{D}_{\zeta}^{\mathrm{dq}}\boldsymbol{D}_{\mathrm{E}_{\zeta}}^{\mathrm{loc}}\right)^{-1}}_{\boldsymbol{\Lambda}} \left(\boldsymbol{C}_{\zeta}^{\mathrm{dq}}\boldsymbol{x}_{\zeta}^{\mathrm{uni}} + \boldsymbol{E}_{\zeta}^{\mathrm{dq}}\boldsymbol{z}_{\zeta}^{\mathrm{ref}} + \boldsymbol{D}_{\zeta}^{\mathrm{dq}}\boldsymbol{C}_{\mathrm{E}_{\zeta}}^{\mathrm{loc}}\boldsymbol{x}_{\mathrm{E}_{\zeta}}^{\mathrm{loc}}\right) \tag{6.35}$$

$$\boldsymbol{y}_{\mathrm{E}_{\zeta}}^{\mathrm{loc}} = \boldsymbol{C}_{\mathrm{E}_{\zeta}}^{\mathrm{loc}}\boldsymbol{x}_{\mathrm{E}_{\zeta}}^{\mathrm{loc}} + \boldsymbol{D}_{\mathrm{E}_{\zeta}}\boldsymbol{y}_{\zeta}^{\mathrm{c}\to\mathrm{g}} \tag{6.36}$$

a unified linear state-space model (plant and controller) can be constructed i.e.

$$\frac{\mathrm{d}\boldsymbol{x}_{\zeta}^{\mathrm{uni}}}{\mathrm{d}t} = \boldsymbol{A}_{\zeta}^{\mathrm{uni}}\boldsymbol{x}_{\zeta}^{\mathrm{uni}} + \boldsymbol{B}_{\zeta}^{\mathrm{uni}}\boldsymbol{z}_{\zeta}^{\mathrm{ref}} \tag{6.37}$$

Assuming an LC filter, the resulting system has ten states (six due to the plant and four due to the controller). For an L filter, the number of states is reduced to eight. From a purely programming perspective, this makes power synchronization control a simpler algorithm which can be assessed more rapidly than dq-axis vector current control.

The frequency response data can be obtained using 3.4. Since the state-space model unifies the

controller and plant, the state matrices can be used to *directly* calculate the poles and zeros of the combined system. The poles of the overall system are just the eigenvalues of $\boldsymbol{A}_{\zeta}^{\mathrm{uni}}$. The zeros require a little more effort. The QZ method is suitable for this problem. Alternatively, one can use built in MATLAB commands.

6.3.1 Condensed models for multi-converter system analyses

As with the linear model of dq-axis vector current control, the model may be condensed as shown below:

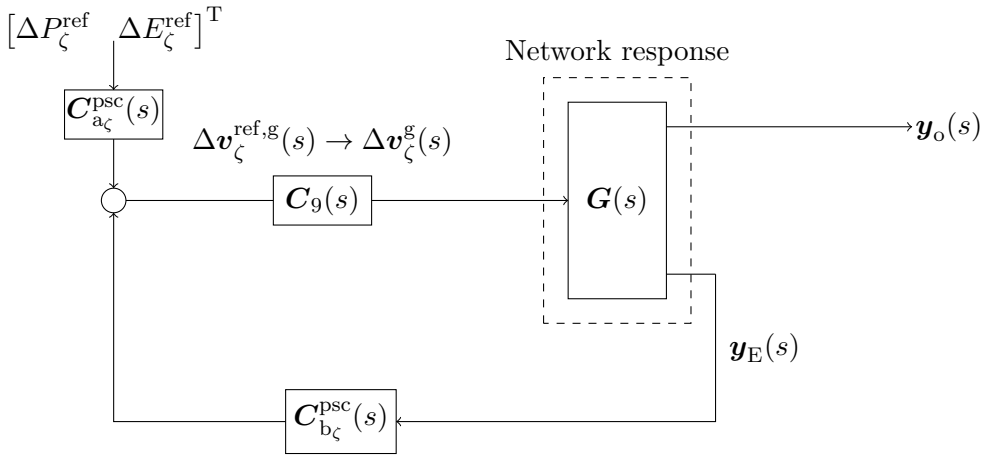

Figure 6.4: Fully condensed linearised model suitable for adapting to more complex systems

In this case, it follows that

$$\Delta \boldsymbol{v}_{\zeta}^{\mathrm{ref,g}}(s) = \boldsymbol{C}_{\zeta}^{\mathrm{psc,b}} \boldsymbol{y}_{\mathrm{E}_{\zeta}}(s) + \boldsymbol{C}_{\zeta}^{\mathrm{psc,a}} \begin{bmatrix} \Delta P_{\zeta}^{\mathrm{ref}} \\ \Delta E_{\zeta}^{\mathrm{ref}} \end{bmatrix} \tag{6.38}$$

which is a result that will be used in chapter 7.

Unified state-space model

For an n converter system, equation 4.50 would be recycled in the following manner:

$$\frac{\mathrm{d}}{\mathrm{d}t}\begin{bmatrix}\boldsymbol{x}_{\mathrm{E}}\\ \boldsymbol{x}_1^{\mathrm{psc}}\\ \boldsymbol{x}_2^{\mathrm{psc}}\\ \vdots\\ \boldsymbol{x}_{\mathrm{n}}^{\mathrm{psc}}\end{bmatrix} = \begin{bmatrix}\boldsymbol{A}_{\mathrm{E}} & & & & \\ & \boldsymbol{A}_1^{\mathrm{psc}} & & & \\ & & \boldsymbol{A}_2^{\mathrm{psc}} & & \\ & & & \ddots & \\ & & & & \boldsymbol{A}_{\mathrm{n}}^{\mathrm{psc}}\end{bmatrix}\begin{bmatrix}\boldsymbol{x}_{\mathrm{E}}\\ \boldsymbol{x}_1^{\mathrm{psc}}\\ \boldsymbol{x}_2^{\mathrm{psc}}\\ \vdots\\ \boldsymbol{x}_{\mathrm{n}}^{\mathrm{psc}}\end{bmatrix} + \begin{bmatrix}\boldsymbol{B}_{\mathrm{E}}\\ \boldsymbol{O}(4n,2n)\end{bmatrix}\underbrace{\begin{bmatrix}\boldsymbol{y}_1^{\mathrm{c\to g}}\\ \boldsymbol{y}_2^{\mathrm{c\to g}}\\ \vdots\\ \boldsymbol{y}_{\mathrm{n}}^{\mathrm{c\to g}}\end{bmatrix}}_{\boldsymbol{z}_{\mathrm{E}}} + \dots$$

$$\begin{bmatrix}\boldsymbol{O}(N_{\mathrm{E}},6n)\\ \underbrace{\begin{bmatrix}\boldsymbol{B}_1^{\mathrm{psc,a}} & & & \\ & \boldsymbol{B}_2^{\mathrm{psc,a}} & & \\ & & \ddots & \\ & & & \boldsymbol{B}_{\mathrm{n}}^{\mathrm{psc,a}}\end{bmatrix}}_{\boldsymbol{B}^{\mathrm{psc,a}}}\end{bmatrix}\underbrace{\begin{bmatrix}\boldsymbol{y}_{\mathrm{E}_1}\\ \boldsymbol{y}_{\mathrm{E}_2}\\ \vdots\\ \boldsymbol{y}_{\mathrm{E}_{\mathrm{n}}}\end{bmatrix}}_{\boldsymbol{y}_{\mathrm{E}}} + \dots$$

$$\begin{bmatrix}\boldsymbol{O}(N_{\mathrm{E}},2n)\\ \underbrace{\begin{bmatrix}\boldsymbol{B}_1^{\mathrm{psc,b}} & & & \\ & \boldsymbol{B}_2^{\mathrm{psc,b}} & & \\ & & \ddots & \\ & & & \boldsymbol{B}_{\mathrm{n}}^{\mathrm{psc,b}}\end{bmatrix}}_{\boldsymbol{B}^{\mathrm{psc,b}}}\end{bmatrix}\underbrace{\begin{bmatrix}\boldsymbol{z}_1^{\mathrm{ref}}\\ \boldsymbol{z}_2^{\mathrm{ref}}\\ \vdots\\ \boldsymbol{z}_{\mathrm{n}}^{\mathrm{ref}}\end{bmatrix}}_{\boldsymbol{z}^{\mathrm{ref}}} \tag{6.39}$$

where $\boldsymbol{y}_{\mathrm{E}_\zeta}$ is as defined in equation 3.15. The vector $\boldsymbol{y}_\zeta^{\mathrm{c\to g}}$ contains the bridge voltages set by the controller for converter ζ.

6.4 Linear & non-linear simulations involving power synchronization control

For all simulations, the same diagonal controller (with the same gains is used), along with the same filter for the current components. The values used are given in table 6.1 [3]:

$k_{\mathrm{p}}^{\mathrm{psl}}$	$k_{\mathrm{i}}^{\mathrm{psl}}$	$k_{\mathrm{p}}^{\mathrm{avl}}$	$k_{\mathrm{i}}^{\mathrm{avl}}$	k_{if}	α_{if}
0	50	0	60	0.45	40

Table 6.1: Settings for the power synchronization controller.

These were as given by Zhang in [3]. This was done to ensure that the controller was not tuned in a manner to make other controllers appear superior by comparison, which would lead to biased and unfair comparisons.

In the following subsections, a range of operating points are considered, covering different filter topologies, different short-circuit ratio values and different power set points. For each operating point considered, four Bode plots are presented such as can be seen in figure 6.5. Starting from the top left and moving clockwise, the first Bode plot shows the frequency response of active power output to a change in P_{ζ}^{ref}, the second Bode plot shows the frequency response of active power output to a change in E_{ζ}^{ref}, the third Bode plot shows the frequency response of the AC voltage magnitude at the filter bus to a change in E_{ζ}^{ref}, and the fourth Bode plot shows the frequency response of the AC voltage magnitude at the filter bus to a change in P_{ζ}^{ref}. Each Bode plot has two curves: the solid curve shows results obtained from the linear model, while the dotted curve shows results obtained from frequency scanning of a non-linear model. In addition, time domain plots are shown for each operating point considered. The solid lines show the response of the system to a 0.1 p.u. step change in power set point, while the dashed lines show the response to a 0.1 p.u. step change in the reference AC voltage magnitude at the filter bus, E_{ζ}^{ref}. The blue lines show the AC voltage magnitude at the filter bus, the red-orange lines show the active power output, and the yellow lines show the reactive power output.

6.4.1 Baseline case studies (LC filter)

In this section, two short-circuit ratio values are considered: three and one. The former is to illustrate the performance of the control algorithm in moderate strength systems, while the latter is to illustrate the performance of the control algorithm when the converter is highly isolated electrically speaking.

Figures 6.5 to 6.7 illustrate the performance of the controller in a system with a short-circuit ratio

of three for three different power set points: $P_0 = 0.0$ p.u., 0.50 p.u. and 0.9 p.u.

It can be seen that there is a strong response in the off-main diagonal elements at around 100 rad/s. This can be thought of as the converter 'swinging' with and against the slack bus. As more converters with controllers which mimic synchronous machine dynamics are installed, the effective short-circuit ratio is boosted, which will lead to greater swinging. In addition, as can be observed, the oscillatory behaviour increases with power set point.

While this may suggest a weakness in the power synchronization control algorithm, decoupling could be boosted by incorporating a power system stabiliser, much as would be done in a real synchronous generator.

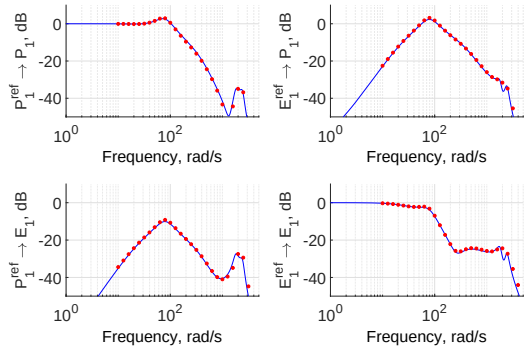

(a) Solid line - linear model; dotted - frequency scanning.

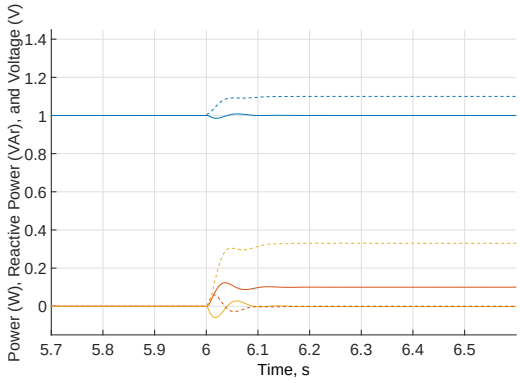

(b) Time domain simulation of non-linear model featuring a change in P^{ref}.

Figure 6.5: Performance of the power synchronization controller. SCR = 3, $P_0 = 0.0$pu.

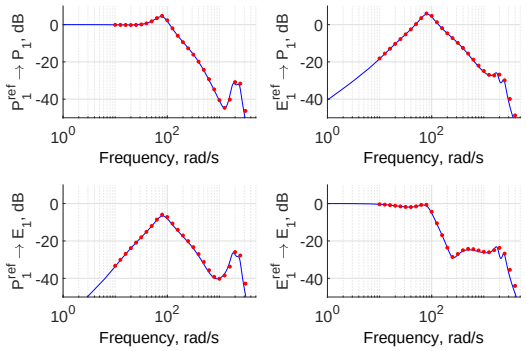

(a) Solid line - linear model; dotted - frequency scanning.

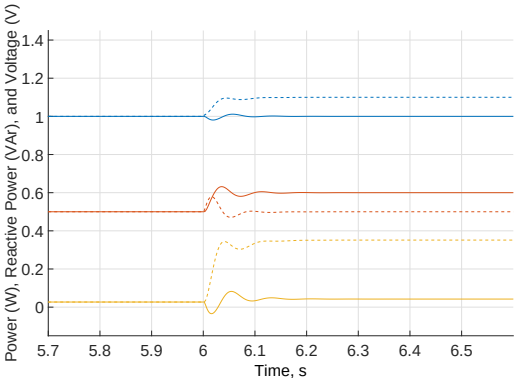

(b) Time domain simulation of non-linear model featuring a change in P^{ref}.

Figure 6.6: Performance of the power synchronization controller. SCR = 3, $P_0 = 0.50$pu.

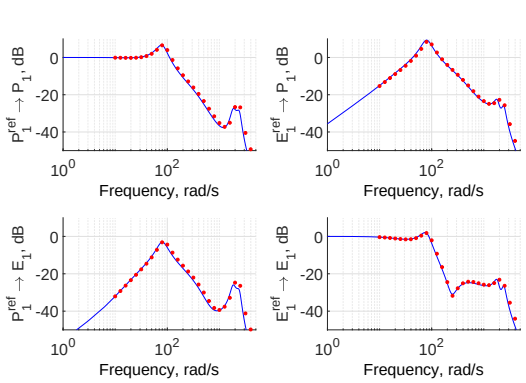

(a) Solid line - linear model; dotted - frequency scanning.

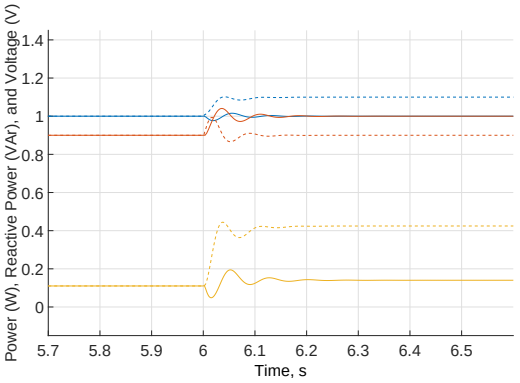

(b) Time domain simulation of non-linear model featuring a change in P^{ref}.

Figure 6.7: Performance of the power synchronization controller. SCR = 3, $P_0 = 0.90$pu.

Figures 6.8 to 6.10 show the performance of the power synchronization control scheme when the short-circuit ratio is one. It can be seen that cross-coupling between the control loops is relatively minor, with most coupling again occurring at frequencies around 100 rad/s. That is to say, the system properties have a secondary role in the location of the peak i.e. the controller is the primary driver of the location. This is desirable since it reduces the need to know about system topology in order to effectively compensate for the coupling.

As can be seen, the linear model developed in this thesis is in good agreement with the frequency scanning results. This gives confidence that the dynamics predicted by the linear model are accurate.

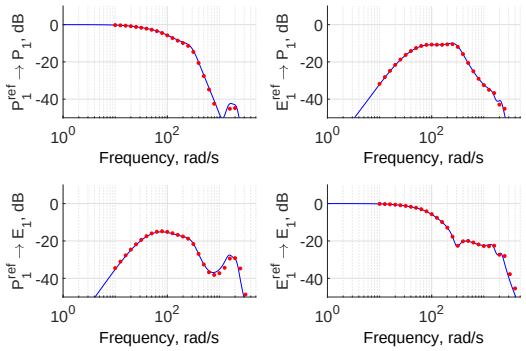

(a) Bode magnitude plots for power synchronization control. Solid line - linear model; dotted - frequency scanning.

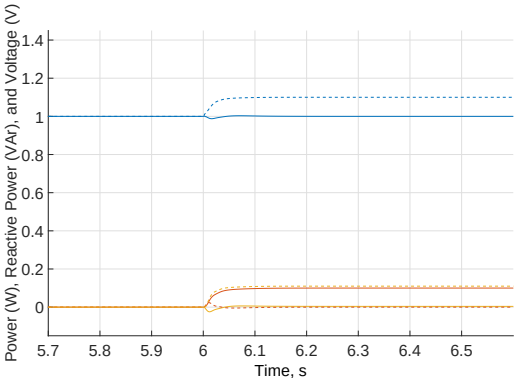

(b) Time domain simulation of non-linear model. Solid - change in P^{ref}; dashed - change in E^{ref}

Figure 6.8: Performance of the power synchronization controller. SCR = 1, $P_0 = 0.0$pu.

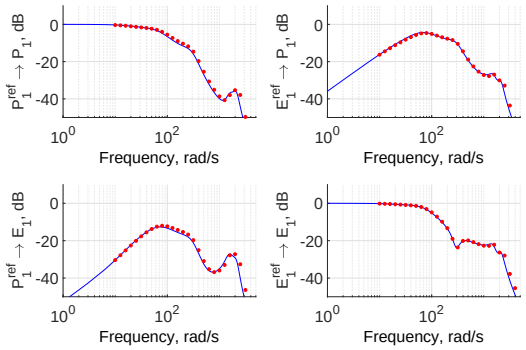

(a) Bode magnitude plots for power synchronization control. Solid line - linear model; dotted - frequency scanning.

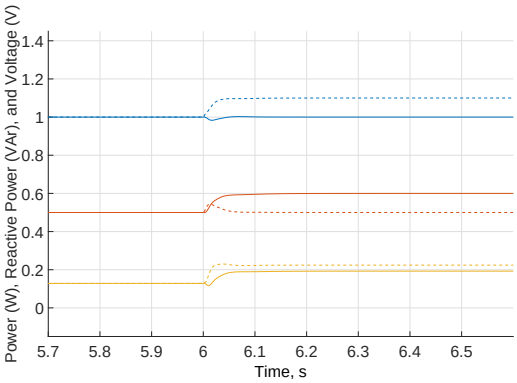

(b) Time domain simulation of non-linear model. Solid - change in P^{ref}; dashed - change in E^{ref}

Figure 6.9: Performance of the dq-axis vector current controller. SCR = 1, $P_0 = 0.50$pu.

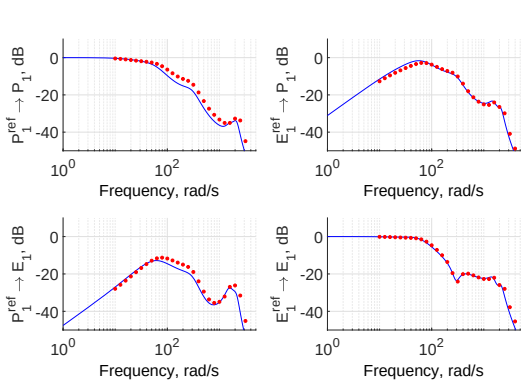

(a) Bode magnitude plots for power synchronization control. Solid line - linear model; dotted - frequency scanning.

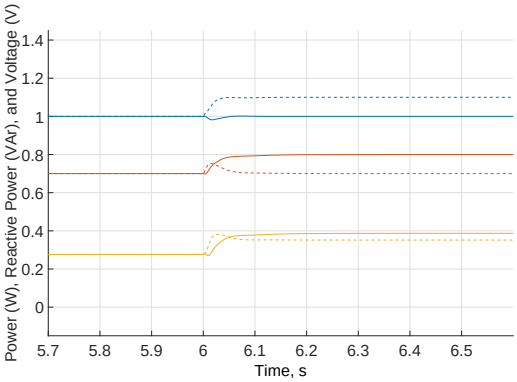

(b) Time domain simulation of non-linear model. Solid - change in P^{ref}; dashed - change in E^{ref}

Figure 6.10: Performance of the power synchronization controller. SCR = 1, $P_0 = 0.70$pu.

At $P_0 = 0.7$pu, it can be observed that there is a significant discrepancy developing between the linear and non-linear models. Specifically, the predicted response, from the linear model, of power output to changes in P^{ref} is lower than observed in the non-linear model in the mid-to-high frequency range. This is probably partly due to a combination of the size of the amplitude of the disturbance to which the system was subjected, and the high load angle, which would result in high order terms becoming more powerful. To understand this, consider perturbing $\sin\theta_{\text{v}}$:

$$\begin{aligned}\sin(\theta_{\text{v},0} + \Delta\theta_{\text{v}}) &= \sin\theta_{\text{v},0}\cos(\Delta\theta_{\text{v}}) + \cos\theta_{\text{v},0}\sin(\Delta\theta_{\text{v}}) \\ &= \sin\theta_{\text{v},0}\left(1 - \frac{(\Delta\theta_{\text{v}})^2}{2} + \ldots\right) + \cos\theta_{\text{v},0}\left(\Delta\theta_{\text{v}} + \frac{(\Delta\theta_{\text{v}})^3}{6} + \ldots\right) \end{aligned} \tag{6.40}$$

If P_0 is high, $\theta_{\text{v},0}$ will be high also. As a result, $\sin\theta_{\text{v},0}$ will not be very small. As a result, the coefficient in front of $(\Delta\theta_{\text{v}_\zeta})^2$ term may be sufficiently large to accommodate for the small size of $(\Delta\theta_{\text{v}})^2$ on its own. The weighting of this effect would be dependent on the control topology, the filter topology, and would also have a frequency bias by virtue of the present of PI controllers and the high-pass filter.

Figure 6.11 and 6.12 show the poles and zeros of the combined system (plant and controller with feedback) for a range of power set points. As can be seen, there are no right half plane poles. Active

power set points vary from 0p.u. to 0.85p.u. At the highest power set point, the transmission zeros are closest to the origin. Relative to the transmission zeros, the poles exhibit lower sensitivity to the power set point.

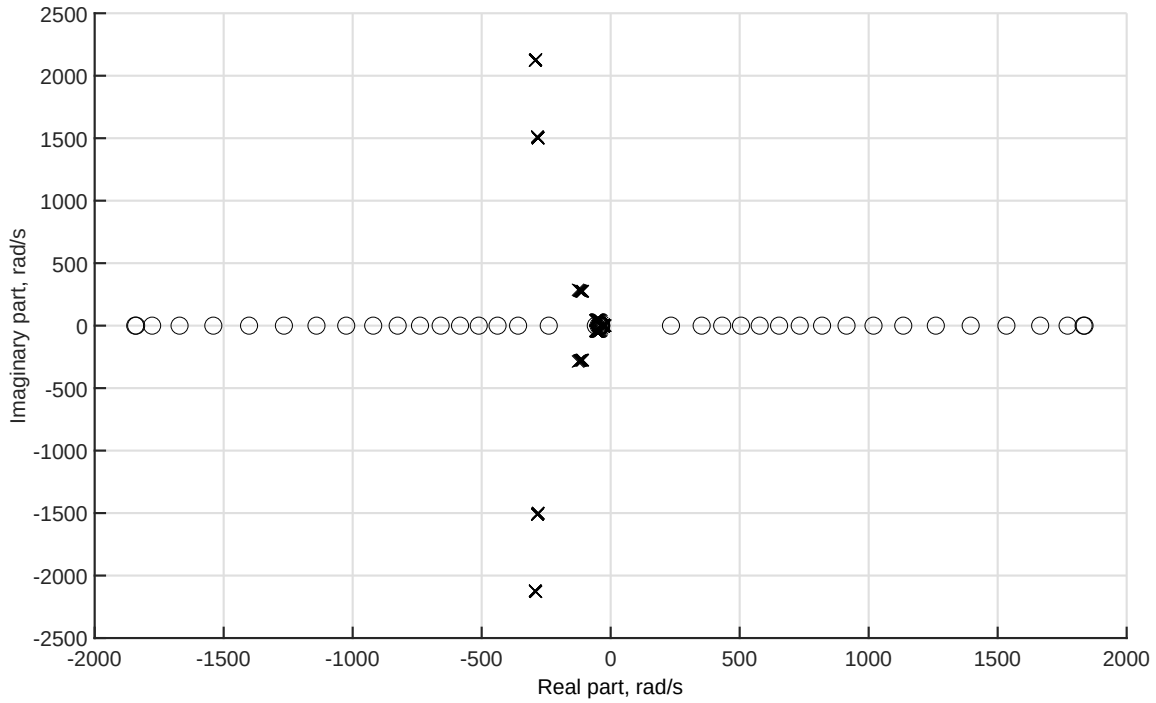

Figure 6.11: Poles and zeros for the controller the combined system when the short-circuit ratio is 1 as evaluated at a range of active power set points.

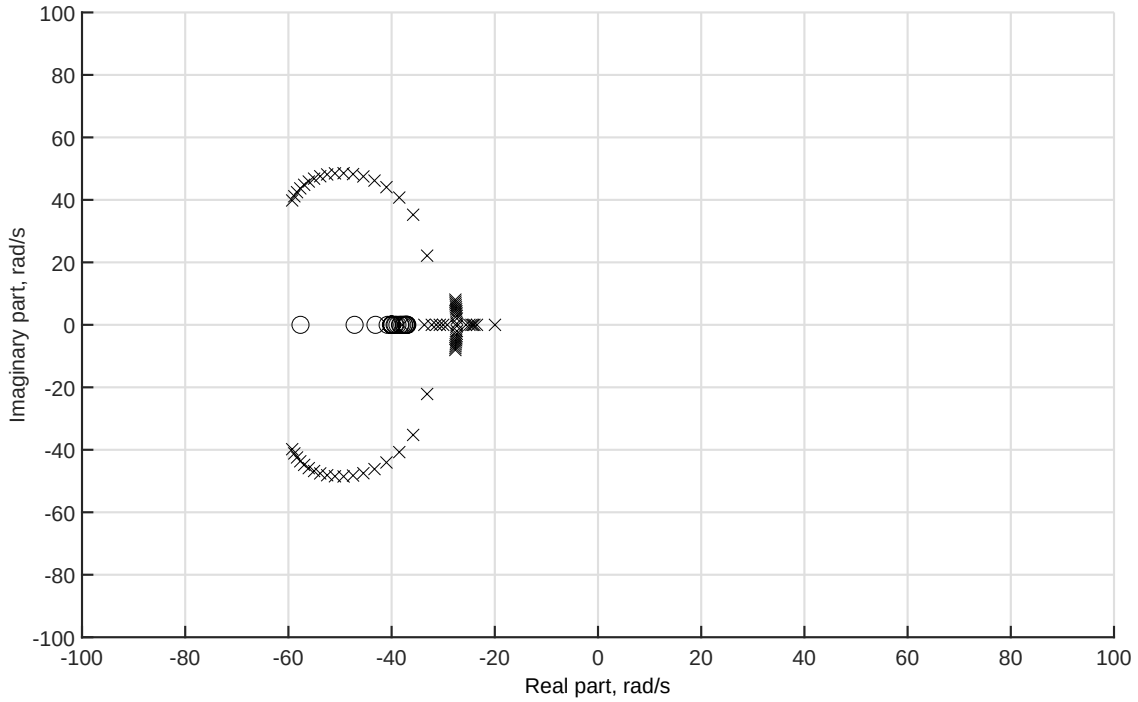

Figure 6.12: Close up of low frequency poles and zeros for the combined system when the short-circuit ratio is 1 as evaluated at a range of active power set points.

6.4.2 Using an L filter

In this section, results are presented only for the case where the short-circuit ratio is one. It can be observed that the performance of the power synchronization controller does not exhibit strong sensitivity to the filter topology. It would thus be suitable for application to MMC systems.

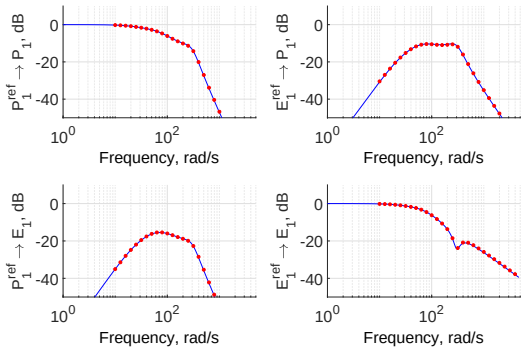

(a) Bode magnitude plots for power synchronization control. Solid line - linear model; dotted - frequency scanning.

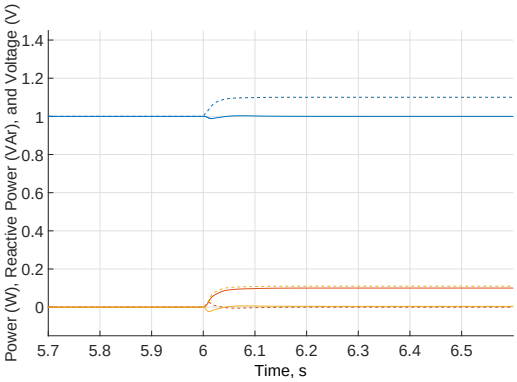

(b) Time domain simulation of non-linear model. Solid - change in P^{ref}; dashed - change in E^{ref}

Figure 6.13: Performance of the power synchronization controller. SCR = 1, $P_0 = 0.0$pu.

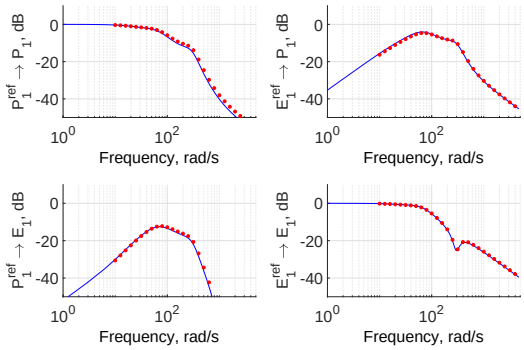

(a) Bode magnitude plots for power synchronization control. Solid line - linear model; dotted - frequency scanning.

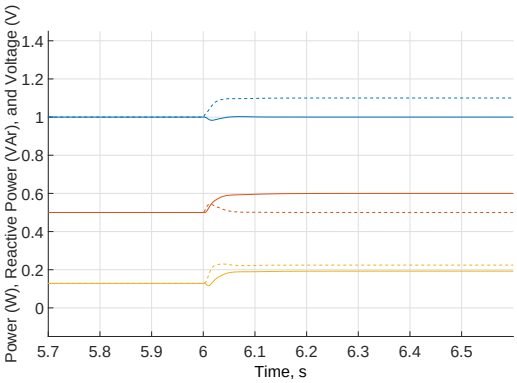

(b) Time domain simulation of non-linear model. Solid - change in P^{ref}; dashed - change in E^{ref}

Figure 6.14: Performance of the power synchronization controller. SCR = 1, $P_0 = 0.5$pu.

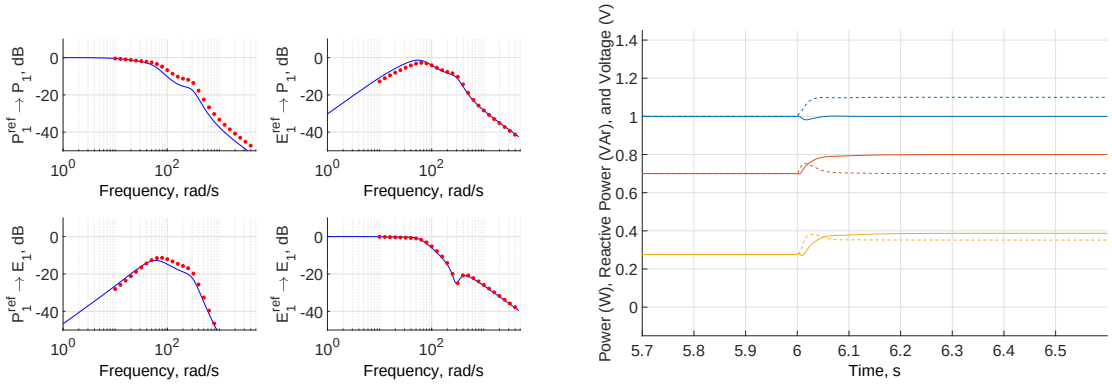

(a) Bode magnitude plots for power synchronization control. Solid line - linear model; dotted - frequency scanning.

(b) Time domain simulation of non-linear model. Solid - change in P^{ref}; dashed - change in E^{ref}

Figure 6.15: Performance of the power synchronization controller. SCR = 1, $P_0 = 0.7$pu.

6.5 Summary

A pole-zero analysis revealed power synchronization control had superior damping capabilities. In addition, the relative simplicity of such a controller (or similar such algorithms) makes it appealing for developers. Importantly, the controller was able to make the converter behave as a voltage source.

A re-formulation of the linear model of power synchronization control has been presented and thoroughly validated. By containing all control elements in the control part of the combined model (controller and plant with feedback), the model can easily be integrated into larger systems comprising multiple converters. In the next chapter, studies involving multiple converters where some use power synchronization control and others use dq-axis vector current control will be presented.

Chapter 7

Small-signal stability in multiple-converter systems

In reality, power systems will comprise numerous converters. Not only is it possible for coupling to occur within a converter's numerous control loops, it is also possible for interactions to occur between the control loops of different converters. That is to say, in an n converter system, it is of interest to know how converter 1 influences converter 2, 3, 4, and so on, and also the influence of all converters on converter 1 (and every other converter for that matter).

In this chapter, the models developed in the previous chapters are extended to allow investigations of high-impedance systems comprising multiple converters. Moreover, the linear models herein developed are formulated in such a way as to be sufficiently flexible to model an arbitrary number of converters. Readers should be able to easily implement the state-space models herein developed in their desired programming language with relative ease. Additionally, the models are such that a single simulation comprising multiple converters may be such that each converter has its own unique controller may be studied. As a representative example, converter 1 may use dq-axis vector current control, while converter 2 may use power synchronization control.

Given the multivariate nature of the system, the exact stability margins would highly be specific to the system under consideration. Thus, it is the author's belief that it is more appropriate to outline an algorithm which can be used to quickly evaluate an extensive range of scenarios.

7.1 Power system modelling

Let us consider power systems in which there are parallel lines linking at some global point of common coupling, which then links to a wider network through a simple RL line. For each parallel line, there is a converter with a filter and local transmission line as described in chapter 3. This forms a system as shown in figure 7.1:

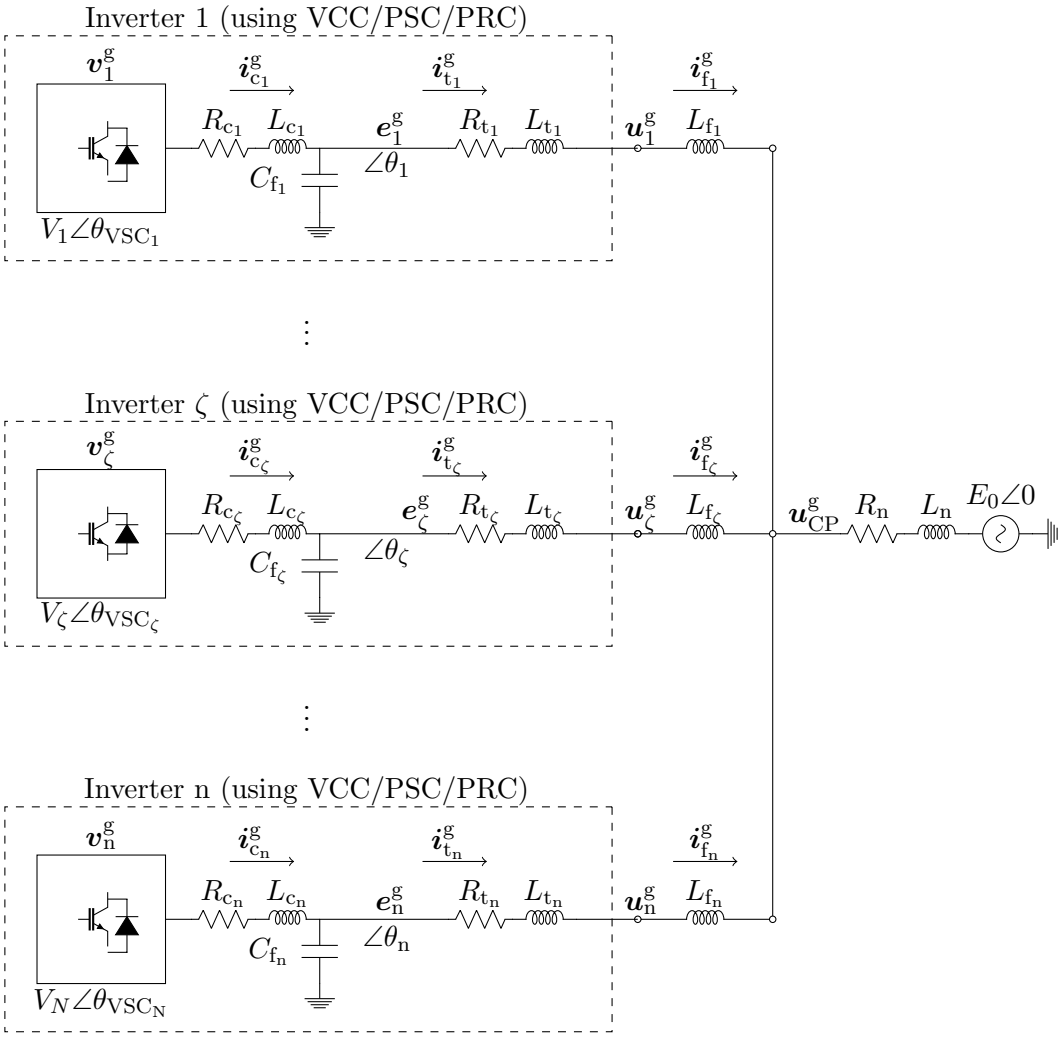

Figure 7.1: Circuit diagram (single-line representation) of a simple multi-converter power system. $\boldsymbol{u}_{\mathrm{CP}}^{\mathrm{g}}$ is the voltage at the 'global' connection point, as expressed in the grid dq frame.

Note that there are no local loads in this topology. To account for such, a second system is defined as shown in figure 7.2

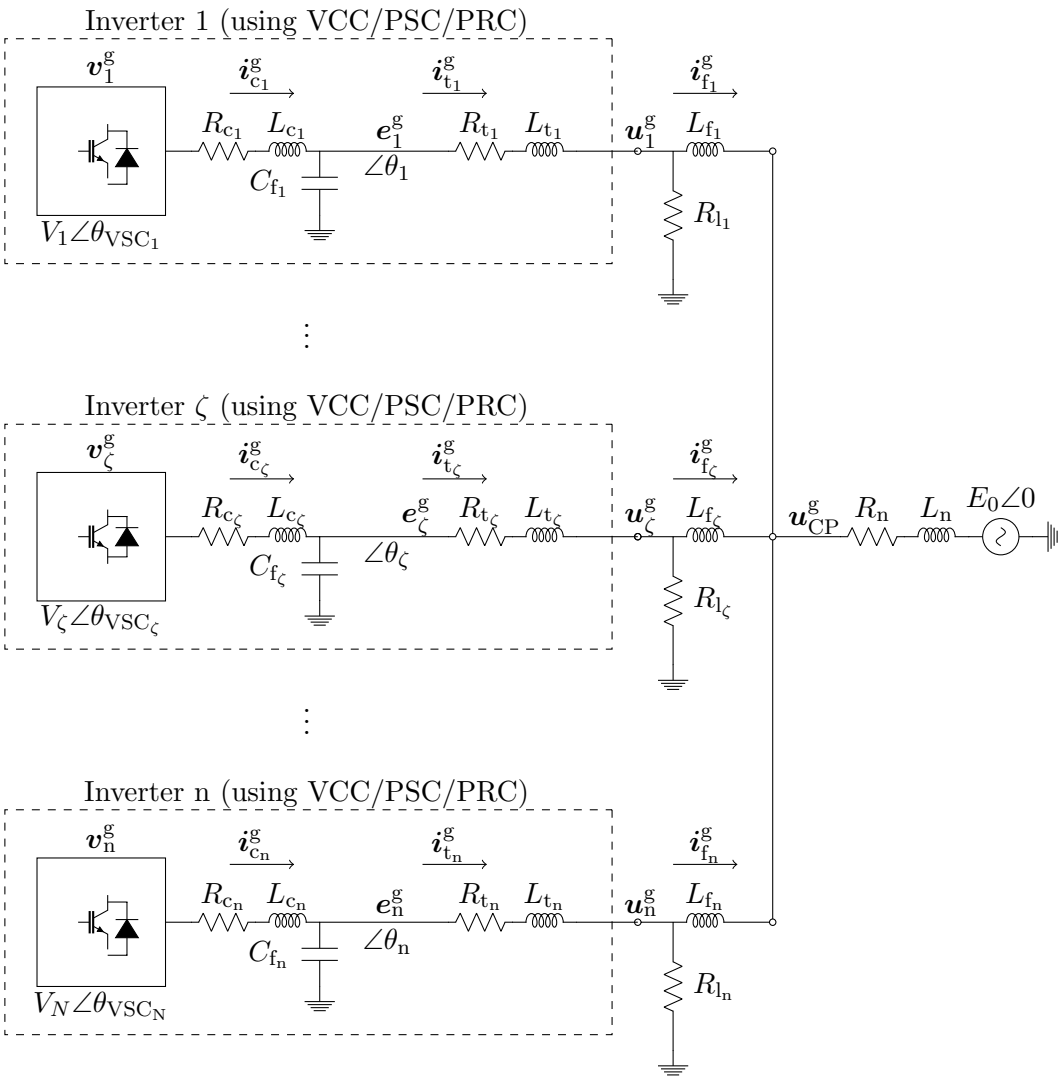

Figure 7.2: Circuit diagram (single-line representation) of a simple multi-converter power system where each converter has its own local load. $\boldsymbol{u}_{\mathrm{CP}}^{\mathrm{g}}$ is the voltage at the 'global' connection point, as expressed in the grid dq frame.

For analysing these systems, the grid dq frame is now defined such that it is aligned with the slack bus at the end of the network line. As a result, the voltages at the end of the each local transmission line, $\boldsymbol{u}_\zeta^{\mathrm{g}}$, are no longer guaranteed to be aligned with the d axis of the grid dq frame.

The system may be split into three sections: one section which represents the dynamics of the inverter filters and their local transmission lines; one which represents the linking of the inverters to a common point; and one which represents the remainder of the system.

The part of the network model which represents the wider power system is a simple transmission line with a slack bus. The dynamics of this section are given as follows:

$$L_{\mathrm{n}}\frac{\mathrm{d}\sum_{\zeta}\Delta\boldsymbol{i}_{\mathrm{f}_{\zeta}}^{\mathrm{g}}}{\mathrm{d}t}=\Delta\boldsymbol{u}_{\mathrm{CP}}^{\mathrm{g}}-R_{\mathrm{n}}\sum_{\zeta}\Delta\boldsymbol{i}_{\mathrm{f}_{\zeta}}^{\mathrm{g}}+\omega_{0}L_{\mathrm{n}}\begin{bmatrix}0 & 1\\ -1 & 0\end{bmatrix}\sum_{\zeta}\Delta\boldsymbol{i}_{\mathrm{f}_{\zeta}}^{\mathrm{g}} \tag{7.1}$$

7.1.1 No local loads

To begin with, let us consider a network comprising n converters as shown in figure 7.1. This could be a local network corresponding to a cluster of wind turbines, or a set of solar panels, or even a very simplified model of a system comprising a collection of HVDC systems.

From inspection, it can be observed that $\boldsymbol{i}_{\mathrm{f}_{\zeta}}^{\mathrm{g}}=\boldsymbol{i}_{\mathrm{t}_{\zeta}}^{\mathrm{g}}$. In addition, by Kirchoff's law,

$$\boldsymbol{i}_{\mathrm{n}}^{\mathrm{g}}=\sum_{\zeta}\boldsymbol{i}_{\mathrm{f}_{\zeta}}^{\mathrm{g}} \tag{7.2}$$

where $\boldsymbol{i}_{\mathrm{n}}^{\mathrm{g}}$ is the current flowing through the transmission line with inductance L_{n}, which represents the wider network.

Derivation of the linear model of the power system

Consider a single instance of the local system first. In this chapter, the voltages at the ends of local transmission lines are not necessarily stiff; thus, the $\boldsymbol{B}_{\mathrm{E}}^{\mathrm{lin}_1}\boldsymbol{z}_{\mathrm{E}}^{\mathrm{lin}}$ are not neglected and so the dynamics are no longer expressed in the standard state-space form, but in the form of equation 3.1, which is shown below for convenience:

$$\frac{\mathrm{d}\boldsymbol{x}_{\mathrm{E}_{\zeta}}^{\mathrm{loc}}}{\mathrm{d}t}=\boldsymbol{A}_{\mathrm{E}_{\zeta}}^{\mathrm{loc}}\boldsymbol{x}_{\mathrm{E}_{\zeta}}^{\mathrm{loc}}+\boldsymbol{B}_{\mathrm{E}_{\zeta}}^{\mathrm{loc}}\boldsymbol{z}_{\mathrm{E}_{\zeta}}^{\mathrm{loc}}+\boldsymbol{B}_{\mathrm{E}_{\zeta}}^{\mathrm{lin}_1}\boldsymbol{z}_{\mathrm{E}_{\zeta}}^{\mathrm{lin}} \tag{7.3}$$

where the superscript 'loc' is to denote that the matrix/matrices and associated vectors are referring to local, single converter systems (see Fig. 3.1 and 7.1). The superscript 'lin' describes the voltages at the ends of the local transmission lines.

For the n converter case, let us define

$$\begin{aligned}
\boldsymbol{x}_{\mathrm{E}}^{\mathrm{loc}} &= \begin{bmatrix} \left(\boldsymbol{x}_{\mathrm{E}_1}^{\mathrm{loc}}\right)^{\mathrm{T}} & \left(\boldsymbol{x}_{\mathrm{E}_2}^{\mathrm{loc}}\right)^{\mathrm{T}} & \left(\boldsymbol{x}_{\mathrm{E}_3}^{\mathrm{loc}}\right)^{\mathrm{T}} & \dots & \left(\boldsymbol{x}_{\mathrm{E}_n}^{\mathrm{loc}}\right)^{\mathrm{T}} \end{bmatrix}^{\mathrm{T}} \\
\boldsymbol{z}_{\mathrm{E}}^{\mathrm{loc}} &= \begin{bmatrix} \left(\Delta\boldsymbol{v}_1^{\mathrm{g}}\right)^{\mathrm{T}} & \left(\Delta\boldsymbol{v}_2^{\mathrm{g}}\right)^{\mathrm{T}} & \left(\Delta\boldsymbol{v}_3^{\mathrm{g}}\right)^{\mathrm{T}} & \dots & \left(\Delta\boldsymbol{v}_n^{\mathrm{g}}\right)^{\mathrm{T}} \end{bmatrix}^{\mathrm{T}} \\
\boldsymbol{z}_{\mathrm{E}}^{\mathrm{lin}} &= \begin{bmatrix} \left(\Delta\boldsymbol{u}_1^{\mathrm{g}}\right)^{\mathrm{T}} & \left(\Delta\boldsymbol{u}_2^{\mathrm{g}}\right)^{\mathrm{T}} & \left(\Delta\boldsymbol{u}_3^{\mathrm{g}}\right)^{\mathrm{T}} & \dots & \left(\Delta\boldsymbol{u}_n^{\mathrm{g}}\right)^{\mathrm{T}} \end{bmatrix}^{\mathrm{T}}
\end{aligned} \tag{7.4}$$

where the vectors are as given in chapter 3.

Thus, equation 7.3 becomes

$$\frac{\mathrm{d}\boldsymbol{x}_{\mathrm{E}}^{\mathrm{loc}}}{\mathrm{d}t} = \boldsymbol{A}_{\mathrm{E}}^{\mathrm{loc}}\boldsymbol{x}_{\mathrm{E}}^{\mathrm{loc}} + \boldsymbol{B}_{\mathrm{E}}^{\mathrm{loc}}\boldsymbol{z}_{\mathrm{E}}^{\mathrm{loc}} + \boldsymbol{B}_{\mathrm{E}}^{\mathrm{lin}_1}\boldsymbol{z}_{\mathrm{E}}^{\mathrm{lin}} \tag{7.5}$$

where

$$\boldsymbol{A}_{\mathrm{E}}^{\mathrm{loc}} = \begin{bmatrix} \boldsymbol{A}_{\mathrm{E}_1}^{\mathrm{loc}} & & & & \\ & \boldsymbol{A}_{\mathrm{E}_2}^{\mathrm{loc}} & & & \\ & & \boldsymbol{A}_{\mathrm{E}_3}^{\mathrm{loc}} & & \\ & & & \ddots & \\ & & & & \boldsymbol{A}_{\mathrm{E}_n}^{\mathrm{loc}} \end{bmatrix} \tag{7.6}$$

$$\boldsymbol{B}_{\mathrm{E}}^{\mathrm{loc}} = \begin{bmatrix} \boldsymbol{B}_{\mathrm{E}_1}^{\mathrm{loc}} & & & & \\ & \boldsymbol{B}_{\mathrm{E}_2}^{\mathrm{loc}} & & & \\ & & \boldsymbol{B}_{\mathrm{E}_3}^{\mathrm{loc}} & & \\ & & & \ddots & \\ & & & & \boldsymbol{B}_{\mathrm{E}_n}^{\mathrm{loc}} \end{bmatrix}; \boldsymbol{B}_{\mathrm{E}}^{\mathrm{lin}_1} = \begin{bmatrix} \boldsymbol{B}_{\mathrm{E}_1}^{\mathrm{lin}_1} & & & & \\ & \boldsymbol{B}_{\mathrm{E}_2}^{\mathrm{lin}_1} & & & \\ & & \boldsymbol{B}_{\mathrm{E}_3}^{\mathrm{lin}_1} & & \\ & & & \ddots & \\ & & & & \boldsymbol{B}_{\mathrm{E}_n}^{\mathrm{lin}_1} \end{bmatrix} \tag{7.7}$$

The elements of $\boldsymbol{x}_{\mathrm{E}_\zeta}^{\mathrm{loc}}$ will be set according to the filter of converter ζ.

Since there are no local loads to consider, the local system matrices $\boldsymbol{A}_{\mathrm{E}_\zeta}^{\mathrm{loc}}$, $\boldsymbol{B}_{\mathrm{E}_\zeta}^{\mathrm{loc}}$ and $\boldsymbol{B}_{\mathrm{E}_\zeta}^{\mathrm{lin}_1}$, are as defined in chapter 3.

To facilitate the linking of the local systems with the wider network, a model of the connection point is included which includes a small inductance for each line, L_{f_ζ}; this may be thought of as part of the inductance of the transmission line. The dynamics of said section are thus as follows:

$$L_{\mathrm{f}_\zeta}\frac{\mathrm{d}\Delta\boldsymbol{i}^{\mathrm{g}}_{\mathrm{t}_\zeta}}{\mathrm{d}t} = \Delta\boldsymbol{u}^{\mathrm{g}}_{\zeta} - \Delta\boldsymbol{u}^{\mathrm{g}}_{\mathrm{CP}} + \omega_0 L_{\mathrm{f}_\alpha}\begin{bmatrix}0 & 1\\ -1 & 0\end{bmatrix}\Delta\boldsymbol{i}^{\mathrm{g}}_{\mathrm{t}_\zeta} \qquad \zeta = 1,2,3,\ldots,n \tag{7.8}$$

Therefore, for each line,

$$\begin{aligned}L_{\mathrm{f}_\zeta}\frac{\mathrm{d}\Delta\boldsymbol{i}^{\mathrm{g}}_{\mathrm{t}_\zeta}}{\mathrm{d}t} = \Delta\boldsymbol{u}^{\mathrm{g}}_{\zeta} - \left(L_{\mathrm{n}}\frac{\mathrm{d}\sum_\eta \Delta\boldsymbol{i}^{\mathrm{g}}_{\mathrm{t}_\eta}}{\mathrm{d}t} + R_{\mathrm{n}}\left(\sum_\eta \Delta\boldsymbol{i}^{\mathrm{g}}_{\mathrm{t}_\eta}\right) - \omega_0 L_{\mathrm{n}}\begin{bmatrix}0 & 1\\ -1 & 0\end{bmatrix}\left(\sum_\eta \Delta\boldsymbol{i}^{\mathrm{g}}_{\mathrm{t}_\eta}\right)\right) + \ldots\\ \omega_0 L_{\mathrm{f}_\zeta}\begin{bmatrix}0 & 1\\ -1 & 0\end{bmatrix}\Delta\boldsymbol{i}^{\mathrm{g}}_{\mathrm{t}_\zeta}\end{aligned} \tag{7.9}$$

Let

$$\boldsymbol{x}^{\mathrm{lin}}_{\mathrm{E}} = \begin{bmatrix}(\Delta\boldsymbol{i}^{\mathrm{g}}_{\mathrm{t}_1})^{\mathrm{T}} & (\Delta\boldsymbol{i}^{\mathrm{g}}_{\mathrm{t}_2})^{\mathrm{T}} & (\Delta\boldsymbol{i}^{\mathrm{g}}_{\mathrm{t}_3})^{\mathrm{T}} & \ldots & (\Delta\boldsymbol{i}^{\mathrm{g}}_{\mathrm{t}_{\mathrm{N}}})^{\mathrm{T}}\end{bmatrix}^{\mathrm{T}} \tag{7.10}$$

Therefore, the combined dynamics of all linking sections and the wider network may be expressed as follows:

$$\frac{\mathrm{d}\boldsymbol{x}^{\mathrm{lin}}_{\mathrm{E}}}{\mathrm{d}t} = \boldsymbol{A}^{\mathrm{lin}_1}_{\mathrm{E}}\boldsymbol{x}^{\mathrm{lin}}_{\mathrm{E}} + \boldsymbol{A}^{\mathrm{lin}_2}_{\mathrm{E}}\frac{\mathrm{d}\boldsymbol{x}^{\mathrm{lin}}_{\mathrm{E}}}{\mathrm{d}t} + \boldsymbol{B}^{\mathrm{lin}_2}_{\mathrm{E}}\boldsymbol{z}^{\mathrm{lin}}_{\mathrm{E}} \tag{7.11}$$

The matrices $\boldsymbol{A}_{\mathrm{E}}^{\mathrm{lin_{1a}}}$, $\boldsymbol{A}_{\mathrm{E}}^{\mathrm{lin_{1b}}}$, $\boldsymbol{A}_{\mathrm{E}}^{\mathrm{lin_2}}$ and $\boldsymbol{B}_{\mathrm{E}}^{\mathrm{loc_{1a}}}$ are given as follows:

$$\boldsymbol{A}_{\mathrm{E}}^{\mathrm{lin_{1a}}} = \begin{bmatrix} \begin{bmatrix} 0 & \omega_0 \\ -\omega_0 & 0 \end{bmatrix} & & & \\ & \begin{bmatrix} 0 & \omega_0 \\ -\omega_0 & 0 \end{bmatrix} & & \\ & & \ddots & \\ & & & \begin{bmatrix} 0 & \omega_0 \\ -\omega_0 & 0 \end{bmatrix} \end{bmatrix} \tag{7.12}$$

$$\boldsymbol{A}_{\mathrm{E}}^{\mathrm{lin_{1b}}} = \begin{bmatrix} \begin{bmatrix} -\frac{R_\mathrm{n}}{L_{\mathrm{f}_1}} & \frac{\omega_0 L_\mathrm{n}}{L_{\mathrm{f}_1}} \\ -\frac{\omega_0 L_\mathrm{n}}{L_{\mathrm{f}_1}} & -\frac{R_\mathrm{n}}{L_{\mathrm{f}_1}} \end{bmatrix} & \begin{bmatrix} -\frac{R_\mathrm{n}}{L_{\mathrm{f}_1}} & \frac{\omega_0 L_\mathrm{n}}{L_{\mathrm{f}_1}} \\ -\frac{\omega_0 L_\mathrm{n}}{L_{\mathrm{f}_1}} & -\frac{R_\mathrm{n}}{L_{\mathrm{f}_1}} \end{bmatrix} & \cdots & \begin{bmatrix} -\frac{R_\mathrm{n}}{L_{\mathrm{f}_1}} & \frac{\omega_0 L_\mathrm{n}}{L_{\mathrm{f}_1}} \\ -\frac{\omega_0 L_\mathrm{n}}{L_{\mathrm{f}_1}} & -\frac{R_\mathrm{n}}{L_{\mathrm{f}_1}} \end{bmatrix} \\ \begin{bmatrix} -\frac{R_\mathrm{n}}{L_{\mathrm{f}_2}} & \frac{\omega_0 L_\mathrm{n}}{L_{\mathrm{f}_2}} \\ -\frac{\omega_0 L_\mathrm{n}}{L_{\mathrm{f}_2}} & -\frac{R_\mathrm{n}}{L_{\mathrm{f}_2}} \end{bmatrix} & \begin{bmatrix} -\frac{R_\mathrm{n}}{L_{\mathrm{f}_2}} & \frac{\omega_0 L_\mathrm{n}}{L_{\mathrm{f}_2}} \\ -\frac{\omega_0 L_\mathrm{n}}{L_{\mathrm{f}_2}} & -\frac{R_\mathrm{n}}{L_{\mathrm{f}_2}} \end{bmatrix} & \cdots & \begin{bmatrix} -\frac{R_\mathrm{n}}{L_{\mathrm{f}_2}} & \frac{\omega_0 L_\mathrm{n}}{L_{\mathrm{f}_2}} \\ -\frac{\omega_0 L_\mathrm{n}}{L_{\mathrm{f}_2}} & -\frac{R_\mathrm{n}}{L_{\mathrm{f}_2}} \end{bmatrix} \\ \vdots & \vdots & \ddots & \vdots \\ \begin{bmatrix} -\frac{R_\mathrm{n}}{L_{\mathrm{f}_\mathrm{n}}} & \frac{\omega_0 L_\mathrm{n}}{L_{\mathrm{f}_\mathrm{n}}} \\ -\frac{\omega_0 L_\mathrm{n}}{L_{\mathrm{f}_\mathrm{n}}} & -\frac{R_\mathrm{n}}{L_{\mathrm{f}_\mathrm{n}}} \end{bmatrix} & \begin{bmatrix} -\frac{R_\mathrm{n}}{L_{\mathrm{f}_\mathrm{n}}} & \frac{\omega_0 L_\mathrm{n}}{L_{\mathrm{f}_\mathrm{n}}} \\ -\frac{\omega_0 L_\mathrm{n}}{L_{\mathrm{f}_\mathrm{n}}} & -\frac{R_\mathrm{n}}{L_{\mathrm{f}_\mathrm{n}}} \end{bmatrix} & \cdots & \begin{bmatrix} -\frac{R_\mathrm{n}}{L_{\mathrm{f}_\mathrm{n}}} & \frac{\omega_0 L_\mathrm{n}}{L_{\mathrm{f}_\mathrm{n}}} \\ -\frac{\omega_0 L_\mathrm{n}}{L_{\mathrm{f}_\mathrm{n}}} & -\frac{R_\mathrm{n}}{L_{\mathrm{f}_\mathrm{n}}} \end{bmatrix} \end{bmatrix} \tag{7.13}$$

$$\boldsymbol{A}_{\mathrm{E}}^{\mathrm{lin_2}} = -L_\mathrm{n} \begin{bmatrix} \frac{1}{L_{\mathrm{f}_1}} & 0 & \frac{1}{L_{\mathrm{f}_1}} & 0 & \cdots & \frac{1}{L_{\mathrm{f}_1}} & 0 \\ 0 & \frac{1}{L_{\mathrm{f}_1}} & 0 & \frac{1}{L_{\mathrm{f}_1}} & \cdots & 0 & \frac{1}{L_{\mathrm{f}_1}} \\ \frac{1}{L_{\mathrm{f}_2}} & 0 & \frac{1}{L_{\mathrm{f}_2}} & 0 & \cdots & \frac{1}{L_{\mathrm{f}_2}} & 0 \\ 0 & \frac{1}{L_{\mathrm{f}_2}} & 0 & \frac{1}{L_{\mathrm{f}_2}} & \cdots & 0 & \frac{1}{L_{\mathrm{f}_2}} \\ \vdots & \vdots & \vdots & \vdots & \ddots & \vdots & \vdots \\ \frac{1}{L_{\mathrm{f}_\mathrm{n}}} & 0 & \frac{1}{L_{\mathrm{f}_\mathrm{n}}} & 0 & \cdots & \frac{1}{L_{\mathrm{f}_\mathrm{n}}} & 0 \\ 0 & \frac{1}{L_{\mathrm{f}_\mathrm{n}}} & 0 & \frac{1}{L_{\mathrm{f}_\mathrm{n}}} & \cdots & 0 & \frac{1}{L_{\mathrm{f}_\mathrm{n}}} \end{bmatrix} \tag{7.14}$$

Finally,

$$\boldsymbol{B}_{\mathrm{E}}^{\mathrm{lin}_2} = \begin{bmatrix} \begin{bmatrix} 1/L_{\mathrm{f}_1} & \\ & 1/L_{\mathrm{f}_1} \end{bmatrix} & & & & \\ & \begin{bmatrix} 1/L_{\mathrm{f}_2} & \\ & 1/L_{\mathrm{f}_2} \end{bmatrix} & & & \\ & & \ddots & & \\ & & & \begin{bmatrix} 1/L_{\mathrm{f}_\mathrm{n}} & \\ & 1/L_{\mathrm{f}_\mathrm{n}} \end{bmatrix} \end{bmatrix} \tag{7.15}$$

The above matrices can be very easily coded in MATLAB (using the repmat command) or in C++ by appropriate looping.

Considering equation 7.11

$$\frac{\mathrm{d}\boldsymbol{x}_{\mathrm{E}}^{\mathrm{lin}}}{\mathrm{d}t} = \underbrace{\left(\boldsymbol{I} - \boldsymbol{A}_{\mathrm{E}}^{\mathrm{lin}_2}\right)^{-1} \boldsymbol{A}_{\mathrm{E}}^{\mathrm{lin}_1}}_{\boldsymbol{A}_{\mathrm{E}}^{\mathrm{lin}_3}} \boldsymbol{x}_{\mathrm{E}}^{\mathrm{lin}} + \underbrace{\left(\boldsymbol{I} - \boldsymbol{A}^{\mathrm{lin}_2}\right)^{-1} \boldsymbol{B}_{\mathrm{E}}^{\mathrm{lin}_2}}_{\boldsymbol{B}_{\mathrm{E}}^{\mathrm{lin}_3}} \boldsymbol{z}_{\mathrm{E}}^{\mathrm{lin}} \tag{7.16}$$

Equations 7.5 and 7.16 can be linked through the appropriate substitution for $\boldsymbol{z}_{\mathrm{E}}^{\mathrm{lin}}$. Also, the state vector of the wider network part of the model, $\boldsymbol{x}_{\mathrm{E}}^{\mathrm{lin}}$, can be thought of as a sub-group of the state vector of the converter part, $\boldsymbol{x}_{\mathrm{E}}^{\mathrm{loc}}$. Thus, the two sections can be linked:

$$\begin{aligned} \frac{\mathrm{d}\boldsymbol{x}_{\mathrm{E}}^{\mathrm{loc}}}{\mathrm{d}t} &= \boldsymbol{A}_{\mathrm{E}}^{\mathrm{loc}} \boldsymbol{x}_{\mathrm{E}}^{\mathrm{loc}} + \boldsymbol{B}_{\mathrm{E}}^{\mathrm{loc}} \boldsymbol{z}_{\mathrm{E}}^{\mathrm{loc}} + \ldots \\ &\qquad \boldsymbol{B}_{\mathrm{E}}^{\mathrm{lin}_1} \left(\left(\boldsymbol{B}_{\mathrm{E}}^{\mathrm{lin}_3}\right)^{-1} \frac{\mathrm{d}\boldsymbol{x}_{\mathrm{E}}^{\mathrm{lin}}}{\mathrm{d}t} - \left(\boldsymbol{B}_{\mathrm{E}}^{\mathrm{lin}_3}\right)^{-1} \boldsymbol{A}_{\mathrm{E}}^{\mathrm{lin}_3} \boldsymbol{x}_{\mathrm{E}}^{\mathrm{lin}} \right) \end{aligned} \tag{7.17}$$

$$\boldsymbol{\kappa} \frac{\mathrm{d}\boldsymbol{x}_{\mathrm{E}}^{\mathrm{loc}}}{\mathrm{d}t} = \left(\boldsymbol{A}_{\mathrm{E}}^{\mathrm{loc}} - \boldsymbol{B}_{\mathrm{E}}^{\mathrm{lin}_1} \left(\boldsymbol{B}_{\mathrm{E}}^{\mathrm{lin}_3}\right)^{-1} \boldsymbol{A}_{\mathrm{E}}^{\mathrm{lin}_3} \boldsymbol{\sigma} \right) \boldsymbol{x}_{\mathrm{E}}^{\mathrm{loc}} + \boldsymbol{B}_{\mathrm{E}}^{\mathrm{loc}} \boldsymbol{z}_{\mathrm{E}}^{\mathrm{loc}} \tag{7.18}$$

where

$$\boldsymbol{\kappa} = \boldsymbol{I} - \boldsymbol{B}_{\mathrm{E}}^{\mathrm{lin}_1} \left(\boldsymbol{B}_{\mathrm{E}}^{\mathrm{lin}_3} \right)^{-1} \boldsymbol{\sigma} \tag{7.19}$$

and

$$\boldsymbol{\sigma} = \begin{bmatrix} \boldsymbol{\sigma}_1 & & & & \\ & \boldsymbol{\sigma}_2 & & & \\ & & \boldsymbol{\sigma}_3 & & \\ & & & \ddots & \\ & & & & \boldsymbol{\sigma}_{\mathrm{n}} \end{bmatrix} \tag{7.20}$$

The linking matrices, $\boldsymbol{\sigma}_\zeta$, will depend on the type of converter filter being applied i.e. L or LC:

$$\boldsymbol{\sigma}_\zeta = \begin{cases} \begin{bmatrix} 0 & 0 & 0 & 0 & 1 & 0 \\ 0 & 0 & 0 & 0 & 0 & 1 \end{bmatrix} \text{ for LC} - \text{filtered converters} \\ \begin{bmatrix} 1 & 0 \\ 0 & 1 \end{bmatrix} \text{ for L} - \text{filtered converters} \end{cases} \tag{7.21}$$

Therefore,

$$\frac{\mathrm{d}\boldsymbol{x}_{\mathrm{E}}}{\mathrm{d}t} = \underbrace{\boldsymbol{\kappa}^{-1} \left(\boldsymbol{A}_{\mathrm{E}}^{\mathrm{loc}} - \boldsymbol{B}_{\mathrm{E}}^{\mathrm{lin}_1} \left(\boldsymbol{B}_{\mathrm{E}}^{\mathrm{lin}_3} \right)^{-1} \boldsymbol{A}_{\mathrm{E}}^{\mathrm{lin}_0} \boldsymbol{\sigma} \right)}_{\boldsymbol{A}_{\mathrm{E}}} \boldsymbol{x}_{\mathrm{E}} + \underbrace{\boldsymbol{\kappa}^{-1} \boldsymbol{B}_{\mathrm{E}}^{\mathrm{loc}}}_{\boldsymbol{B}_{\mathrm{E}}} \boldsymbol{z}_{\mathrm{E}} \tag{7.22}$$

where $\boldsymbol{x}_{\mathrm{E}} = \boldsymbol{x}_{\mathrm{E}}^{\mathrm{loc}}$ and $\boldsymbol{z}_{\mathrm{E}} = \boldsymbol{z}_{\mathrm{E}}^{\mathrm{loc}}$ i.e. the dq components of perturbations in the bridge voltages for all converters.

The steady-state solver

To carry out the small signal stability analysis, it is necessary to evaluate the steady-state operating conditions around which the perturbations will be applied. In steady-state, the derivative terms are omitted from the state-equation; thus, to determine the steady-state values, the steady-state

equivalent of equation 7.22 needs solving. This is almost a simple case of swapping perturbation terms for the steady-state values e.g. $\Delta \boldsymbol{e}_1^{\mathrm{g}} \rightarrow \boldsymbol{e}_{1,0}^{\mathrm{g}}$. However, it must be stressed that this involves adding in an additional term in the form of the steady-state slack bus voltage, for which there is no perturbation term. Including the slack bus,

$$\boldsymbol{u}_{\mathrm{CP},0}^{\mathrm{g}} = L_{\mathrm{n}} \frac{d \sum_{\zeta} \boldsymbol{i}_{\mathrm{f}_\zeta,0}^{\mathrm{g}}}{\mathrm{d}t} + R_{\mathrm{n}} \sum_{\zeta} \boldsymbol{i}_{\mathrm{f}_\zeta,0}^{\mathrm{g}} - \omega_0 L_{\mathrm{n}} \begin{bmatrix} 0 & 1 \\ -1 & 0 \end{bmatrix} \sum_{\zeta} \boldsymbol{i}_{\mathrm{f}_\zeta,0}^{\mathrm{g}} + \begin{bmatrix} \epsilon_0 \\ 0 \end{bmatrix} \tag{7.23}$$

Therefore, for each line,

$$\begin{aligned}
\boldsymbol{z}_{\mathrm{E}_\zeta,0}^{\mathrm{lin}} &= \boldsymbol{u}_{\zeta,0}^{\mathrm{g}} \\
&= R_{\mathrm{n}} \sum_{\zeta} \boldsymbol{i}_{\mathrm{t}_\zeta,0}^{\mathrm{g}} - \omega_0 L_{\mathrm{n}} \begin{bmatrix} 0 & 1 \\ -1 & 0 \end{bmatrix} \sum_{\zeta} \boldsymbol{i}_{\mathrm{t}_\zeta,0}^{\mathrm{g}} + \begin{bmatrix} E_0 \\ 0 \end{bmatrix} - \omega_0 L_{\mathrm{f}_\zeta} \begin{bmatrix} 0 & 1 \\ -1 & 0 \end{bmatrix} \boldsymbol{i}_{\mathrm{t}_\zeta,0}^{\mathrm{g}} \\
&= \left[\underbrace{\begin{bmatrix} R_{\mathrm{n}} & -\omega_0 L_{\mathrm{n}} & R_{\mathrm{n}} & -\omega_0 L_{\mathrm{n}} & \dots & R_{\mathrm{n}} & -\omega_0 L_{\mathrm{n}} \\ \omega_0 L_{\mathrm{n}} & R_{\mathrm{n}} & \omega_0 L_{\mathrm{n}} & R_{\mathrm{n}} & \dots & \omega_0 L_{\mathrm{n}} & R_{\mathrm{n}} \end{bmatrix}}_{\boldsymbol{B}_{\zeta,0}^{\mathrm{ss_a}}} \boldsymbol{\sigma}_\zeta \right] \boldsymbol{x}_{\mathrm{E},0} + \dots \\
&\quad \underbrace{\begin{bmatrix} 0 & -\omega_0 L_{\mathrm{f}_\zeta} \\ \omega_0 L_{\mathrm{f}_\zeta} & 0 \end{bmatrix}}_{\boldsymbol{B}_{\zeta,0}^{\mathrm{ss_b}}} \boldsymbol{i}_{\mathrm{t}_\zeta,0}^{\mathrm{g}} + \begin{bmatrix} \epsilon_0 \\ 0 \end{bmatrix}
\end{aligned} \tag{7.24}$$

This may then be substituted into a steady-state form of equation 7.5 to give an equation of the form

$$\begin{aligned}
\boldsymbol{O}(2n,1) = \boldsymbol{A}_{\mathrm{E},0}^{\mathrm{loc}} \boldsymbol{x}_{\mathrm{E},0} + \boldsymbol{B}_{\mathrm{E},0}^{\mathrm{loc}} \boldsymbol{z}_{\mathrm{E},0}^{\mathrm{loc}} + \boldsymbol{B}_{\mathrm{E},0}^{\mathrm{lin_1}} \begin{bmatrix} \epsilon_0 \\ 0 \end{bmatrix} + \dots \\
\boldsymbol{B}_{\mathrm{E},0}^{\mathrm{lin_1}} \left[\begin{bmatrix} \boldsymbol{B}_{1,0}^{\mathrm{ss_a}} \\ \boldsymbol{B}_{1,0}^{\mathrm{ss_a}} \\ \vdots \\ \boldsymbol{B}_{\mathrm{n},0}^{\mathrm{ss_a}} \end{bmatrix} + \begin{bmatrix} \boldsymbol{B}_{1,0}^{\mathrm{ss_b}} & & & \\ & \boldsymbol{B}_{1,0}^{\mathrm{ss_b}} & & \\ & & \ddots & \\ & & & \boldsymbol{B}_{\mathrm{n},0}^{\mathrm{ss_b}} \end{bmatrix} \right] \boldsymbol{\sigma} \boldsymbol{x}_{\mathrm{E},0}
\end{aligned} \tag{7.25}$$

where

$$\boldsymbol{A}_{\mathrm{E},0}^{\mathrm{loc}} = \boldsymbol{A}_{\mathrm{E}}^{\mathrm{loc}} \tag{7.26}$$

$$\boldsymbol{B}_{\mathrm{E},0}^{\mathrm{loc}} = \boldsymbol{B}_{\mathrm{E}}^{\mathrm{loc}} \tag{7.27}$$

$$\boldsymbol{B}_{\mathrm{E},0}^{\mathrm{lin}_1} = \boldsymbol{B}_{\mathrm{E}}^{\mathrm{lin}_1} \tag{7.28}$$

Equation 7.25 cannot be solved on its own since there are too many unknowns for the number of equations. That is, there are $2n$ unknowns which cover the dq components of the steady-state bridge voltages at each converter, and the n_{E} unknowns which are the steady-state state vector elements i.e. $\boldsymbol{x}_{\mathrm{E}}$. There are currently only n_{E} equations.

As before, this issue is resolved by including the expressions for steady-state powers (one for each converter) and steady-state voltage magnitudes at every local point of common coupling (or any other point in the local system). Including these, there is a sufficient number of equations for the system to be solved. As before, due to the non-linear nature of the voltage magnitude expression, an iterative solver is required.

For completeness, the steady-state active power outputs for all converters is given by equation 7.29:

$$\begin{bmatrix} P_{1,0} \\ P_{2,0} \\ P_{3,0} \\ \vdots \\ P_{\mathrm{n},0} \end{bmatrix} = \begin{bmatrix} \boldsymbol{C}_{\mathrm{P}_1} & & & & \\ & \boldsymbol{C}_{\mathrm{P}_2} & & & \\ & & \boldsymbol{C}_{\mathrm{P}_3} & & \\ & & & \ddots & \\ & & & & \boldsymbol{C}_{\mathrm{P}_\mathrm{n}} \end{bmatrix} \boldsymbol{x}_{\mathrm{E},0} \tag{7.29}$$

where

$$\boldsymbol{C}_{\mathrm{P}_\zeta,0} = \begin{cases} \begin{bmatrix} 0 & 0 & i_{\mathrm{t}_\zeta\mathrm{d},0}^{\mathrm{g}} & i_{\mathrm{t}_\zeta\mathrm{q},0}^{\mathrm{g}} & 0 & 0 \end{bmatrix} & \text{for LC-filtered converters} \\ \begin{bmatrix} e_{\zeta\mathrm{d},0}^{\mathrm{g}} & e_{\zeta\mathrm{q},0}^{\mathrm{g}} \end{bmatrix} & \text{for L-filtered converters} \end{cases} \tag{7.30}$$

The steady-state bridge voltage values are described by equation 7.31:

$$\begin{bmatrix} V_{1,0}^2 \\ V_{2,0}^2 \\ \vdots \\ V_{\mathrm{n},0}^2 \end{bmatrix} = \underbrace{\begin{bmatrix} \boldsymbol{C}_{\mathrm{V}_1,0} & & & \\ & \boldsymbol{C}_{\mathrm{V}_2,0} & & \\ & & \ddots & \\ & & & \boldsymbol{C}_{\mathrm{V}_\mathrm{n},0} \end{bmatrix}}_{\boldsymbol{C}_{\mathrm{V},0}} \boldsymbol{z}_{\mathrm{E},0} \tag{7.31}$$

where

$$\boldsymbol{C}_{V_\zeta,0} = \begin{bmatrix} v_{\mathrm{d}_\zeta,0}^{\mathrm{g}} & v_{\mathrm{q}_\zeta,0}^{\mathrm{g}} \end{bmatrix} \tag{7.32}$$

7.1.2 Including local loads

While a system like a wind farm may not have local loads, there are many examples of power systems where there are energy sources and sinks intertwined. To handle this case, the power system model illustrated in figure 7.2 is considered.

Derivation of the linear model of the power system

For simplicity, only resistive loads have been considered, and all converters will be assumed to have an associated local load[1]. In this case, an extra set of equations is introduced:

$$\Delta \boldsymbol{u}_\zeta^{\mathrm{g}} = \Delta \boldsymbol{i}_{\mathrm{l}_\zeta}^{\mathrm{g}} R_{\mathrm{l}_\zeta} \tag{7.33}$$

$$= \left(\Delta \boldsymbol{i}_{\mathrm{t}_\zeta}^{\mathrm{g}} - \Delta \boldsymbol{i}_{\mathrm{f}_\zeta}^{\mathrm{g}} \right) R_{\mathrm{l}_\zeta} \tag{7.34}$$

Consequently, the state-equation for the set of local systems is best expressed as follows:

$$\frac{\mathrm{d}\boldsymbol{x}_{\mathrm{E}}^{\mathrm{loc}}}{\mathrm{d}t} = \boldsymbol{A}_{\mathrm{E}}^{\mathrm{loc}} \boldsymbol{x}_{\mathrm{E}}^{\mathrm{loc}} + \boldsymbol{B}_{\mathrm{E}}^{\mathrm{loc}} \boldsymbol{z}_{\mathrm{E}}^{\mathrm{loc}} + \boldsymbol{B}_{\mathrm{E}}^{\mathrm{lin}_1} \boldsymbol{x}_{\mathrm{E}}^{\mathrm{lin}} \tag{7.35}$$

[1]The second statement is required for stable evaluation of the state-space model in its presented form

where

$$\begin{aligned}
\boldsymbol{x}_{\mathrm{E}}^{\mathrm{loc}} &= \begin{bmatrix} \left(\boldsymbol{x}_{\mathrm{E}_1}^{\mathrm{loc}}\right)^{\mathrm{T}} & \left(\boldsymbol{x}_{\mathrm{E}_2}^{\mathrm{loc}}\right)^{\mathrm{T}} & \left(\boldsymbol{x}_{\mathrm{E}_3}^{\mathrm{loc}}\right)^{\mathrm{T}} & \dots & \left(\boldsymbol{x}_{\mathrm{E}_n}^{\mathrm{loc}}\right)^{\mathrm{T}} \end{bmatrix}^{\mathrm{T}} \\
\boldsymbol{z}_{\mathrm{E}}^{\mathrm{loc}} &= \begin{bmatrix} \left(\Delta\boldsymbol{v}_1^{\mathrm{g}}\right)^{\mathrm{T}} & \left(\Delta\boldsymbol{v}_2^{\mathrm{g}}\right)^{\mathrm{T}} & \left(\Delta\boldsymbol{v}_3^{\mathrm{g}}\right)^{\mathrm{T}} & \dots & \left(\Delta\boldsymbol{v}_n^{\mathrm{g}}\right)^{\mathrm{T}} \end{bmatrix}^{\mathrm{T}} \\
\boldsymbol{x}_{\mathrm{E}}^{\mathrm{lin}} &= \begin{bmatrix} \left(\Delta\boldsymbol{i}_{\mathrm{f}_1}^{\mathrm{g}}\right)^{\mathrm{T}} & \left(\Delta\boldsymbol{i}_{\mathrm{f}_2}^{\mathrm{g}}\right)^{\mathrm{T}} & \left(\Delta\boldsymbol{i}_{\mathrm{f}_3}^{\mathrm{g}}\right)^{\mathrm{T}} & \dots & \left(\Delta\boldsymbol{i}_{\mathrm{f}_n}^{\mathrm{g}}\right)^{\mathrm{T}} \end{bmatrix}^{\mathrm{T}}
\end{aligned} \tag{7.36}$$

and, as with the case with no resistive loads,

$$\boldsymbol{A}_{\mathrm{E}}^{\mathrm{loc}} = \begin{bmatrix} \boldsymbol{A}_{\mathrm{E}_1}^{\mathrm{loc}} & & & & \\ & \boldsymbol{A}_{\mathrm{E}_2}^{\mathrm{loc}} & & & \\ & & \boldsymbol{A}_{\mathrm{E}_3}^{\mathrm{loc}} & & \\ & & & \ddots & \\ & & & & \boldsymbol{A}_{\mathrm{E}_n}^{\mathrm{loc}} \end{bmatrix}; \; \boldsymbol{B}_{\mathrm{E}}^{\mathrm{loc}} = \begin{bmatrix} \boldsymbol{B}_{\mathrm{E}_1}^{\mathrm{loc}} & & & & \\ & \boldsymbol{B}_{\mathrm{E}_2}^{\mathrm{loc}} & & & \\ & & \boldsymbol{B}_{\mathrm{E}_3}^{\mathrm{loc}} & & \\ & & & \ddots & \\ & & & & \boldsymbol{B}_{\mathrm{E}_n}^{\mathrm{loc}} \end{bmatrix} \tag{7.37}$$

$$\boldsymbol{B}_{\mathrm{E}}^{\mathrm{lin}_1} = \begin{bmatrix} \boldsymbol{B}_{\mathrm{E}_1}^{\mathrm{lin}_1} & & & & \\ & \boldsymbol{B}_{\mathrm{E}_2}^{\mathrm{lin}_1} & & & \\ & & \boldsymbol{B}_{\mathrm{E}_3}^{\mathrm{lin}_1} & & \\ & & & \ddots & \\ & & & & \boldsymbol{B}_{\mathrm{E}_n}^{\mathrm{lin}_1} \end{bmatrix} \tag{7.38}$$

For an LC-filtered converter, the component sub-matrices are as follows:

$$\boldsymbol{A}_{\mathrm{E}_\zeta}^{\mathrm{loc}} = \begin{bmatrix} -\frac{R_{\mathrm{c}_\zeta}}{L_{\mathrm{c}_\zeta}} & \omega_0 & -\frac{1}{L_{\mathrm{c}_\zeta}} & 0 & 0 & 0 \\ -\omega_0 & -\frac{R_{\mathrm{c}_\zeta}}{L_{\mathrm{c}_\zeta}} & 0 & -\frac{1}{L_{\mathrm{c}_\zeta}} & 0 & 0 \\ \frac{1}{C_{\mathrm{f}_\zeta}} & 0 & 0 & \omega_0 & -\frac{1}{C_{\mathrm{f}_\zeta}} & 0 \\ 0 & \frac{1}{C_{\mathrm{f}_\zeta}} & -\omega_0 & 0 & 0 & -\frac{1}{C_{\mathrm{f}_\zeta}} \\ 0 & 0 & \frac{1}{L_{\mathrm{t}_\zeta}} & 0 & -\frac{R_{\mathrm{t}_\zeta}+R_{\mathrm{l}_\zeta}}{L_{\mathrm{t}_\zeta}} & \omega_0 \\ 0 & 0 & 0 & \frac{1}{L_{\mathrm{t}_\zeta}} & -\omega_0 & -\frac{R_{\mathrm{t}_\zeta}+R_{\mathrm{l}_\zeta}}{L_{\mathrm{t}_\zeta}} \end{bmatrix}; \; \boldsymbol{B}_{\mathrm{E}_\zeta}^{\mathrm{loc}} = \begin{bmatrix} \frac{1}{L_{\mathrm{c}_\zeta}} & 0 \\ 0 & \frac{1}{L_{\mathrm{c}_\zeta}} \\ 0 & 0 \\ 0 & 0 \\ 0 & 0 \\ 0 & 0 \end{bmatrix}$$

$$\boldsymbol{B}_{\mathrm{E}_\zeta}^{\mathrm{lin}_1} = \begin{bmatrix} 0 & 0 & 0 & 0 & R_{\mathrm{l}_\zeta}/L_{\mathrm{t}_\zeta} & 0 \\ 0 & 0 & 0 & 0 & 0 & R_{\mathrm{l}_\zeta}/L_{\mathrm{t}_\zeta} \end{bmatrix}^{\mathrm{T}} \tag{7.39}$$

While not explicitly presented in this work for brevity reasons, the component sub-matrices for an L-filtered converter have been coded up also (see Appendices) for the reader's interest. The associated sub-matrices are as follows:

$$\boldsymbol{A}_{\mathrm{E}_\zeta}^{\mathrm{loc}} = \begin{bmatrix} -\frac{R_{\mathrm{c}_\zeta}+R_{\mathrm{l}_\zeta}+R_{\mathrm{t}_\zeta}}{\left(L_{\mathrm{c}_\zeta}+L_{\mathrm{t}_\zeta}\right)} & \omega_0 \\ -\omega_0 & -\frac{R_{\mathrm{c}_\zeta}+R_{\mathrm{l}_\zeta}+R_{\mathrm{t}_\zeta}}{\left(L_{\mathrm{c}_\zeta}+L_{\mathrm{t}_\zeta}\right)} \end{bmatrix}; \; \boldsymbol{B}_{\mathrm{E}_\zeta}^{\mathrm{loc}} = \begin{bmatrix} \frac{1}{\left(L_{\mathrm{c}_\zeta}+L_{\mathrm{t}_\zeta}\right)} & 0 \\ 0 & \frac{1}{\left(L_{\mathrm{c}_\zeta}+L_{\mathrm{t}_\zeta}\right)} \end{bmatrix}$$

$$\boldsymbol{B}_{\mathrm{E}_\zeta}^{\mathrm{lin}_1} = \begin{bmatrix} R_{\mathrm{l}_\zeta}/L_{\mathrm{t}_\zeta} & 0 \\ 0 & R_{\mathrm{l}_\zeta}/L_{\mathrm{t}_\zeta} \end{bmatrix}^{\mathrm{T}} \tag{7.40}$$

Equation 7.1 remains unchanged. However, equation 7.8 should be expressed without any explicit

dependence on $\Delta\boldsymbol{u}^{\mathrm{g}}_{\zeta}$; that is,

$$L_{\mathrm{f}_\zeta}\frac{\mathrm{d}\Delta\boldsymbol{i}^{\mathrm{g}}_{\mathrm{f}_\zeta}}{\mathrm{d}t}=\left(\Delta\boldsymbol{i}^{\mathrm{g}}_{\mathrm{t}_\zeta}-\Delta\boldsymbol{i}^{\mathrm{g}}_{\mathrm{f}_\zeta}\right)R_{\mathrm{l}_\zeta}-\Delta\boldsymbol{u}^{\mathrm{g}}_{\mathrm{CP}}+\omega_0 L_{\mathrm{f}_\zeta}\begin{bmatrix}0 & 1\\ -1 & 0\end{bmatrix}\Delta\boldsymbol{i}^{\mathrm{g}}_{\mathrm{f}_\zeta}\qquad \zeta=1,2,3,\ldots,n \tag{7.41}$$

Therefore, for each line,

$$\begin{aligned}L_{\mathrm{f}_\zeta}\frac{\mathrm{d}\Delta\boldsymbol{i}^{\mathrm{g}}_{\mathrm{f}_\zeta}}{\mathrm{d}t}=&\left(\Delta\boldsymbol{i}^{\mathrm{g}}_{\mathrm{t}_\zeta}-\Delta\boldsymbol{i}^{\mathrm{g}}_{\mathrm{f}_\zeta}\right)R_{\mathrm{l}_\zeta}+\omega_0 L_{\mathrm{f}_\zeta}\begin{bmatrix}0 & 1\\ -1 & 0\end{bmatrix}\Delta\boldsymbol{i}^{\mathrm{g}}_{\mathrm{f}_\zeta}-\ldots\\ &\left(L_{\mathrm{n}}\frac{\mathrm{d}\sum_\zeta\Delta\boldsymbol{i}^{\mathrm{g}}_{\mathrm{f}_\zeta}}{\mathrm{d}t}+R_{\mathrm{n}}\sum_\zeta\Delta\boldsymbol{i}^{\mathrm{g}}_{\mathrm{f}_\zeta}-\omega_0 L_{\mathrm{n}}\begin{bmatrix}0 & 1\\ -1 & 0\end{bmatrix}\sum_\zeta\Delta\boldsymbol{i}^{\mathrm{g}}_{\mathrm{f}_\zeta}\right)\end{aligned} \tag{7.42}$$

Since all occurrences of $\Delta\boldsymbol{i}^{\mathrm{g}}_{\mathrm{f}_\zeta}$, i.e. covering all values of ζ, are members of $\boldsymbol{x}^{\mathrm{loc}}_{\mathrm{E}}$, the combined dynamics of all linking sections and the wider network may be expressed as follows:

$$\frac{\mathrm{d}\boldsymbol{x}^{\mathrm{lin}}_{\mathrm{E}}}{\mathrm{d}t}=\underbrace{\left(\boldsymbol{I}-\boldsymbol{A}^{\mathrm{lin}_2}_{\mathrm{E}}\right)^{-1}\left(\boldsymbol{A}^{\mathrm{lin}_{1\mathrm{a}}}_{\mathrm{E}}+\boldsymbol{A}^{\mathrm{lin}_{1\mathrm{b}}}_{\mathrm{E}}\right)}_{\boldsymbol{A}^{\mathrm{lin}_1}_{\mathrm{E}}}\boldsymbol{x}^{\mathrm{lin}}_{\mathrm{E}}+\underbrace{\left(\boldsymbol{I}-\boldsymbol{A}^{\mathrm{lin}_2}_{\mathrm{E}}\right)^{-1}\boldsymbol{B}^{\mathrm{loc}_1\mathrm{a}}_{\mathrm{E}}}_{\boldsymbol{B}^{\mathrm{loc}_1}_{\mathrm{E}}}\boldsymbol{x}^{\mathrm{loc}}_{\mathrm{E}} \tag{7.43}$$

where $n_{\mathrm{E,L}}=n_{\mathrm{E}}-2n$. By extension, if the system comprises no LC-filtered converters, the zero matrix in $\boldsymbol{B}^{\mathrm{loc}_1}_{\mathrm{E}}$ will not be required.

The matrices $\boldsymbol{A}^{\mathrm{lin_{1a}}}$, $\boldsymbol{A}^{\mathrm{lin_{1b}}}$, $\boldsymbol{A}_{\mathrm{E}}^{\mathrm{lin_2}}$ and $\boldsymbol{B}^{\mathrm{loc_{1a}}}$ are given as follows:

$$\boldsymbol{A}_{\mathrm{E}}^{\mathrm{lin_{1a}}} = \begin{bmatrix} \begin{bmatrix} -\frac{R_{\mathrm{l}_1}}{L_{\mathrm{f}_1}} & \omega_0 \\ -\omega_0 & -\frac{R_{\mathrm{l}_1}}{L_{\mathrm{f}_1}} \end{bmatrix} & & & \\ & \begin{bmatrix} -\frac{R_{\mathrm{l}_2}}{L_{\mathrm{f}_2}} & \omega_0 \\ -\omega_0 & -\frac{R_{\mathrm{l}_2}}{L_{\mathrm{f}_2}} \end{bmatrix} & & \\ & & \ddots & \\ & & & \begin{bmatrix} -\frac{R_{\mathrm{l}_\mathrm{n}}}{L_{\mathrm{f}_\mathrm{n}}} & \omega_0 \\ -\omega_0 & -\frac{R_{\mathrm{l}_\mathrm{n}}}{L_{\mathrm{f}_\mathrm{n}}} \end{bmatrix} \end{bmatrix} \tag{7.44}$$

$$\boldsymbol{A}_{\mathrm{E}}^{\mathrm{lin_{1b}}} = \begin{bmatrix} \begin{bmatrix} -\frac{R_\mathrm{n}}{L_{\mathrm{f}_1}} & \frac{\omega_0 L_\mathrm{n}}{L_{\mathrm{f}_1}} \\ -\frac{\omega_0 L_\mathrm{n}}{L_{\mathrm{f}_1}} & -\frac{R_\mathrm{n}}{L_{\mathrm{f}_1}} \end{bmatrix} & \begin{bmatrix} -\frac{R_\mathrm{n}}{L_{\mathrm{f}_1}} & \frac{\omega_0 L_\mathrm{n}}{L_{\mathrm{f}_1}} \\ -\frac{\omega_0 L_\mathrm{n}}{L_{\mathrm{f}_1}} & -\frac{R_\mathrm{n}}{L_{\mathrm{f}_1}} \end{bmatrix} & \cdots & \begin{bmatrix} -\frac{R_\mathrm{n}}{L_{\mathrm{f}_1}} & \frac{\omega_0 L_\mathrm{n}}{L_{\mathrm{f}_1}} \\ -\frac{\omega_0 L_\mathrm{n}}{L_{\mathrm{f}_1}} & -\frac{R_\mathrm{n}}{L_{\mathrm{f}_1}} \end{bmatrix} \\ \begin{bmatrix} -\frac{R_\mathrm{n}}{L_{\mathrm{f}_2}} & \frac{\omega_0 L_\mathrm{n}}{L_{\mathrm{f}_2}} \\ -\frac{\omega_0 L_\mathrm{n}}{L_{\mathrm{f}_2}} & -\frac{R_\mathrm{n}}{L_{\mathrm{f}_2}} \end{bmatrix} & \begin{bmatrix} -\frac{R_\mathrm{n}}{L_{\mathrm{f}_2}} & \frac{\omega_0 L_\mathrm{n}}{L_{\mathrm{f}_2}} \\ -\frac{\omega_0 L_\mathrm{n}}{L_{\mathrm{f}_2}} & -\frac{R_\mathrm{n}}{L_{\mathrm{f}_2}} \end{bmatrix} & \cdots & \begin{bmatrix} -\frac{R_\mathrm{n}}{L_{\mathrm{f}_2}} & \frac{\omega_0 L_\mathrm{n}}{L_{\mathrm{f}_2}} \\ -\frac{\omega_0 L_\mathrm{n}}{L_{\mathrm{f}_2}} & -\frac{R_\mathrm{n}}{L_{\mathrm{f}_2}} \end{bmatrix} \\ \vdots & \vdots & \ddots & \vdots \\ \begin{bmatrix} -\frac{R_\mathrm{n}}{L_{\mathrm{f}_\mathrm{n}}} & \frac{\omega_0 L_\mathrm{n}}{L_{\mathrm{f}_\mathrm{n}}} \\ -\frac{\omega_0 L_\mathrm{n}}{L_{\mathrm{f}_\mathrm{n}}} & -\frac{R_\mathrm{n}}{L_{\mathrm{f}_\mathrm{n}}} \end{bmatrix} & \begin{bmatrix} -\frac{R_\mathrm{n}}{L_{\mathrm{f}_\mathrm{n}}} & \frac{\omega_0 L_\mathrm{n}}{L_{\mathrm{f}_\mathrm{n}}} \\ -\frac{\omega_0 L_\mathrm{n}}{L_{\mathrm{f}_\mathrm{n}}} & -\frac{R_\mathrm{n}}{L_{\mathrm{f}_\mathrm{n}}} \end{bmatrix} & \cdots & \begin{bmatrix} -\frac{R_\mathrm{n}}{L_{\mathrm{f}_\mathrm{n}}} & \frac{\omega_0 L_\mathrm{n}}{L_{\mathrm{f}_\mathrm{n}}} \\ -\frac{\omega_0 L_\mathrm{n}}{L_{\mathrm{f}_\mathrm{n}}} & -\frac{R_\mathrm{n}}{L_{\mathrm{f}_\mathrm{n}}} \end{bmatrix} \end{bmatrix} \tag{7.45}$$

$\boldsymbol{A}_{\mathrm{E}}^{\mathrm{lin}_2}$ is given as follows:

$$\boldsymbol{A}_{\mathrm{E}}^{\mathrm{lin}_2} = -L_{\mathrm{n}} \begin{bmatrix} \frac{1}{L_{\mathrm{f}_1}} & 0 & \frac{1}{L_{\mathrm{f}_1}} & 0 & \dots & \frac{1}{L_{\mathrm{f}_1}} & 0 \\ 0 & \frac{1}{L_{\mathrm{f}_1}} & 0 & \frac{1}{L_{\mathrm{f}_1}} & \dots & 0 & \frac{1}{L_{\mathrm{f}_1}} \\ \frac{1}{L_{\mathrm{f}_2}} & 0 & \frac{1}{L_{\mathrm{f}_2}} & 0 & \dots & \frac{1}{L_{\mathrm{f}_2}} & 0 \\ 0 & \frac{1}{L_{\mathrm{f}_2}} & 0 & \frac{1}{L_{\mathrm{f}_2}} & \dots & 0 & \frac{1}{L_{\mathrm{f}_2}} \\ \vdots & \vdots & \vdots & \vdots & \ddots & \vdots & \vdots \\ \frac{1}{L_{\mathrm{f}_{\mathrm{n}}}} & 0 & \frac{1}{L_{\mathrm{f}_{\mathrm{n}}}} & 0 & \dots & \frac{1}{L_{\mathrm{f}_{\mathrm{n}}}} & 0 \\ 0 & \frac{1}{L_{\mathrm{f}_{\mathrm{n}}}} & 0 & \frac{1}{L_{\mathrm{f}_{\mathrm{n}}}} & \dots & 0 & \frac{1}{L_{\mathrm{f}_{\mathrm{n}}}} \end{bmatrix} \tag{7.46}$$

Finally,

$$\boldsymbol{B}_{\mathrm{E}}^{\mathrm{loc}_1\mathrm{a}} = \begin{bmatrix} \boldsymbol{O}(2,4) & \begin{bmatrix} \frac{R_{\mathrm{l}_1}}{L_{\mathrm{f}_1}} & \\ & \frac{R_{\mathrm{l}_1}}{L_{\mathrm{f}_1}} \end{bmatrix} & & & & \\ & & \boldsymbol{O}(2,4) & \begin{bmatrix} \frac{R_{\mathrm{l}_2}}{L_{\mathrm{f}_2}} & \\ & \frac{R_{\mathrm{l}_2}}{L_{\mathrm{f}_2}} \end{bmatrix} & & \\ & & & & \ddots & \\ & & & & & \boldsymbol{O}(2,4) & \begin{bmatrix} \frac{R_{\mathrm{l}_{\mathrm{n}}}}{L_{\mathrm{f}_{\mathrm{n}}}} & \\ & \frac{R_{\mathrm{l}_{\mathrm{n}}}}{L_{\mathrm{f}_{\mathrm{n}}}} \end{bmatrix} \end{bmatrix} \tag{7.47}$$

The above matrices can be very easily coded in MATLAB (using the repmat command) or in C++ by appropriate looping.

Let the combined state-vector for the electrical part of the system be $\boldsymbol{x}_{\mathrm{E}} = \left[\left(\boldsymbol{x}_{\mathrm{E}}^{\mathrm{loc}}\right)^{\mathrm{T}} \quad \left(\boldsymbol{x}_{\mathrm{E}}^{\mathrm{lin}}\right)^{\mathrm{T}}\right]^{\mathrm{T}}$; thus,

$$\frac{\mathrm{d}\boldsymbol{x}_{\mathrm{E}}}{\mathrm{d}t} = \underbrace{\begin{bmatrix} \boldsymbol{A}_{\mathrm{E}}^{\mathrm{loc}} & \boldsymbol{B}_{\mathrm{E1}}^{\mathrm{lin_1}} \\ \boldsymbol{B}_{\mathrm{E}}^{\mathrm{loc_1}} & \boldsymbol{A}_{\mathrm{E}}^{\mathrm{lin}} \end{bmatrix}}_{\boldsymbol{A}_{\mathrm{E}}} \boldsymbol{x}_{\mathrm{E}} + \underbrace{\begin{bmatrix} \boldsymbol{B}_{\mathrm{E}}^{\mathrm{loc}} \\ \boldsymbol{O}(2n, 2n) \end{bmatrix}}_{\boldsymbol{B}_{\mathrm{E}}} \boldsymbol{z}_{\mathrm{E}} \tag{7.48}$$

The steady-state solver

To carry out the small signal stability analysis, it is necessary to evaluate the steady-state operating conditions around which the perturbations will be applied. In steady-state, the derivative terms are omitted from the state-equation; thus, to determine the steady-state values, the steady-state equivalent of equation 7.48 needs solving. This is almost a simple case of swapping perturbation terms for the steady-state values e.g. $\Delta\boldsymbol{e}_1^{\mathrm{g}} \rightarrow \boldsymbol{e}_{1,0}^{\mathrm{g}}$. However, it must be stressed that this involves adding in an additional term in the form of the steady-state slack bus voltage, for which there is no perturbation term. Including the slack bus,

$$\boldsymbol{u}_{\mathrm{CP},0}^{\mathrm{g}} = L_{\mathrm{n}} \frac{d\sum_{\zeta} \boldsymbol{i}_{\mathrm{f}_\zeta,0}^{\mathrm{g}}}{\mathrm{d}t} + R_{\mathrm{n}} \sum_{\zeta} \boldsymbol{i}_{\mathrm{f}_\zeta,0}^{\mathrm{g}} - \omega_0 L_{\mathrm{n}} \begin{bmatrix} 0 & 1 \\ -1 & 0 \end{bmatrix} \sum_{\zeta} \boldsymbol{i}_{\mathrm{f}_\zeta,0}^{\mathrm{g}} + \begin{bmatrix} E_0 \\ 0 \end{bmatrix} \tag{7.49}$$

Therefore, for each line,

$$\begin{aligned} \boldsymbol{O}(2,1) = \left(\boldsymbol{i}_{\mathrm{t}_\zeta,0}^{\mathrm{g}} - \boldsymbol{i}_{\mathrm{f}_\zeta,0}^{\mathrm{g}}\right) \frac{R_{\mathrm{l}_\zeta}}{L_{\mathrm{f}_\zeta}} + \omega_0 \begin{bmatrix} 0 & 1 \\ -1 & 0 \end{bmatrix} \boldsymbol{i}_{\mathrm{f}_\zeta,0}^{\mathrm{g}} + \left(\omega_0 \frac{L_{\mathrm{n}}}{L_{\mathrm{f}_\zeta}} \begin{bmatrix} 0 & 1 \\ -1 & 0 \end{bmatrix} - \frac{R_{\mathrm{n}}}{L_{\mathrm{f}_\zeta}}\right) \sum_{\zeta} \boldsymbol{i}_{\mathrm{f}_\zeta,0}^{\mathrm{g}} - \ldots \\ \frac{1}{L_{\mathrm{f}_\zeta}} \begin{bmatrix} E_0 \\ 0 \end{bmatrix} \end{aligned} \tag{7.50}$$

The steady-state form of equation 7.43 is thus as follows:

$$\boldsymbol{O}(2n,1) = \underbrace{\left(\boldsymbol{A}_{\mathrm{E},0}^{\mathrm{lin_{1a}}} + \boldsymbol{A}_{\mathrm{E},0}^{\mathrm{lin_{1b}}}\right)}_{\boldsymbol{A}_{\mathrm{E},0}^{\mathrm{lin_1}}} \boldsymbol{x}_{\mathrm{E},0}^{\mathrm{lin}} + \underbrace{\boldsymbol{B}_{\mathrm{E},0}^{\mathrm{loc_1a}}}_{\boldsymbol{B}_{\mathrm{E},0}^{\mathrm{loc_1}}} \boldsymbol{x}_{\mathrm{E},0}^{\mathrm{loc}} + \boldsymbol{B}_{\mathrm{E1},0}^{\mathrm{lin}} \begin{bmatrix} E_0 \\ 0 \end{bmatrix} \tag{7.51}$$

where

$$\boldsymbol{B}_{\mathrm{E1},0}^{\mathrm{lin}} = -\begin{bmatrix} \dfrac{1}{L_{\mathrm{f}_1}} & 0 & \dfrac{1}{L_{\mathrm{f}_2}} & 0 & \dfrac{1}{L_{\mathrm{f}_3}} & 0 & \dots & \dfrac{1}{L_{\mathrm{f}_n}} & 0 \\ 0 & \dfrac{1}{L_{\mathrm{f}_1}} & 0 & \dfrac{1}{L_{\mathrm{f}_2}} & 0 & \dfrac{1}{L_{\mathrm{f}_3}} & \dots & 0 & \dfrac{1}{L_{\mathrm{f}_n}} \end{bmatrix}^{\mathrm{T}} \tag{7.52}$$

Equation 7.53 represents the combined system which needs solving:

$$\boldsymbol{O}(N_{\mathrm{E}}, 1) = \boldsymbol{A}_{\mathrm{E}}\boldsymbol{x}_{\mathrm{E}} + \boldsymbol{B}_{\mathrm{E}}\boldsymbol{z}_{\mathrm{E}} + \begin{bmatrix} \boldsymbol{O}(N_{\mathrm{loc}}, 2) \\ \boldsymbol{B}_{\mathrm{E1}}^{\mathrm{lin}} \end{bmatrix} \begin{bmatrix} E_0 \\ 0 \end{bmatrix} \tag{7.53}$$

As with all previous examples, in order to determine all the unknowns, $2n + N_{\mathrm{E}}$, an additional $2n$ equations are required. These are the bridge voltage magnitudes and active power set points for all converters.

Thus, there is a sufficient number of equations for the number of unknowns, allowing an iterative solver to be developed.

For readers who use MATLAB, the fsolve command can be exploited in order to give a simple solver for obtaining the steady-state values of all terms.

7.2 The unified linear state-space model

Sub-space algorithms are computationally intensive; thus, for system identification and analysis, specifically pole-zero evaluation and simple small-signal time domain simulations, the unified linear state-space model is preferred for multi-converter systems. The block diagram approach may, however, still be used for determining frequency response data, which can then be used to evaluate gain and phase margins.

For the unified linear state-space model, let us first note that the bridge voltages of all converters

may be expressed as follows:

$$\underbrace{\begin{bmatrix}\Delta\boldsymbol{v}_1^{\mathrm{g}}\\ \Delta\boldsymbol{v}_2^{\mathrm{g}}\\ \Delta\boldsymbol{v}_3^{\mathrm{g}}\\ \vdots\\ \Delta\boldsymbol{v}_{\mathrm{n}}^{\mathrm{g}}\end{bmatrix}}_{\boldsymbol{z}_{\mathrm{E}}} = \underbrace{\begin{bmatrix}\boldsymbol{O}(2n,N_{\mathrm{E}}) & \underbrace{\begin{bmatrix}\boldsymbol{\rho}_1^{\mathrm{con}} & & & & \\ & \boldsymbol{\rho}_2^{\mathrm{con}} & & & \\ & & \boldsymbol{\rho}_3^{\mathrm{con}} & & \\ & & & \ddots & \\ & & & & \boldsymbol{\rho}_n^{\mathrm{con}}\end{bmatrix}}_{\boldsymbol{\rho}^{\mathrm{con}}}\end{bmatrix}}_{\boldsymbol{C}^{\mathrm{dq}}} \underbrace{\begin{bmatrix}\boldsymbol{x}_\zeta^{\mathrm{E}}\\ \boldsymbol{x}_1^{\mathrm{con}}\\ \boldsymbol{x}_2^{\mathrm{con}}\\ \vdots\\ \boldsymbol{x}_{\mathrm{n}}^{\mathrm{con}}\end{bmatrix}}_{\boldsymbol{x}_\zeta^{\mathrm{uni}}} + \dots$$

$$\underbrace{\begin{bmatrix}\boldsymbol{D}_1^{\mathrm{dq}} & & & & \\ & \boldsymbol{D}_2^{\mathrm{dq}} & & & \\ & & \boldsymbol{D}_3^{\mathrm{dq}} & & \\ & & & \ddots & \\ & & & & \boldsymbol{D}_{\mathrm{n}}^{\mathrm{dq}}\end{bmatrix}}_{\boldsymbol{D}^{\mathrm{dq}}} \boldsymbol{z}^{\mathrm{ref}} + \underbrace{\begin{bmatrix}\boldsymbol{E}_1^{\mathrm{dq}} & & & & \\ & \boldsymbol{E}_2^{\mathrm{dq}} & & & \\ & & \boldsymbol{E}_3^{\mathrm{dq}} & & \\ & & & \ddots & \\ & & & & \boldsymbol{E}_{\mathrm{n}}^{\mathrm{dq}}\end{bmatrix}}_{\boldsymbol{E}^{\mathrm{dq}}} \boldsymbol{y}_{\mathrm{E}} \tag{7.54}$$

Following on from chapters, let the output of the electrical part of the model, $\boldsymbol{y}_{\mathrm{E}}$ contain

$$\begin{bmatrix}\Delta P_\zeta & \Delta E_\zeta & \left(\Delta\boldsymbol{i}_{\mathrm{c}_\zeta}^{\mathrm{g}}\right)^{\mathrm{T}} & \left(\Delta\boldsymbol{e}_\zeta^{\mathrm{g}}\right)^{\mathrm{T}}\end{bmatrix}^{\mathrm{T}} \tag{7.55}$$

for all converters. Thus,

$$\boldsymbol{y}_{\mathrm{E}} = \boldsymbol{C}_{\mathrm{E}}\boldsymbol{x}^{\mathrm{uni}} + \boldsymbol{D}_{\mathrm{E}}\boldsymbol{z}_{\mathrm{E}} \tag{7.56}$$

where

$$\boldsymbol{C}_{\mathrm{E}} = \begin{bmatrix}\begin{bmatrix}\boldsymbol{C}_{\mathrm{E}_1}^{\mathrm{con}} & & & & \\ & \boldsymbol{C}_{\mathrm{E}_2}^{\mathrm{con}} & & & \\ & & \boldsymbol{C}_{\mathrm{E}_3}^{\mathrm{con}} & & \\ & & & \ddots & \\ & & & & \boldsymbol{C}_{\mathrm{E}_{\mathrm{n}}}^{\mathrm{con}}\end{bmatrix} & \boldsymbol{O}(6n,2n)\end{bmatrix} \tag{7.57}$$

and

$$\boldsymbol{D}_{\mathrm{E}} = \begin{bmatrix} \boldsymbol{D}_{\mathrm{E}_1}^{\mathrm{con}} & & & & \\ & \boldsymbol{D}_{\mathrm{E}_2}^{\mathrm{con}} & & & \\ & & \boldsymbol{D}_{\mathrm{E}_3}^{\mathrm{con}} & & \\ & & & \ddots & \\ & & & & \boldsymbol{D}_{\mathrm{E}_\mathrm{n}}^{\mathrm{con}} \end{bmatrix} \tag{7.58}$$

If there are no local loads, the zero matrix in equation 7.57 should be omitted.

Thus, an expression for $\boldsymbol{z}_{\mathrm{E}}$ in terms of only $\boldsymbol{x}^{\mathrm{uni}}$ and $\boldsymbol{z}^{\mathrm{ref}}$ can be obtained much in the same way as done in previous chapters:

$$\boldsymbol{z}_{\mathrm{E}} = \boldsymbol{C}^{\mathrm{dq}}\boldsymbol{x}^{\mathrm{uni}} + \boldsymbol{D}^{\mathrm{dq}}\boldsymbol{z}^{\mathrm{ref}} + \boldsymbol{E}^{\mathrm{dq}}\left[\boldsymbol{C}_{\mathrm{E}}\boldsymbol{x}_{\mathrm{E}} + \boldsymbol{D}_{\mathrm{E}}\boldsymbol{z}_{\mathrm{E}}\right] \tag{7.59}$$

Note that

$$\boldsymbol{z}_{\mathrm{E}} = \begin{bmatrix} (\boldsymbol{y}_1^{\mathrm{c}\to\mathrm{g}})^{\mathrm{T}} & (\boldsymbol{y}_2^{\mathrm{c}\to\mathrm{g}})^{\mathrm{T}} & (\boldsymbol{y}_3^{\mathrm{c}\to\mathrm{g}})^{\mathrm{T}} & \dots & (\boldsymbol{y}_\mathrm{n}^{\mathrm{c}\to\mathrm{g}})^{\mathrm{T}} \end{bmatrix}^{\mathrm{T}} \tag{7.60}$$

In addition, the state equation with $\boldsymbol{y}_{\mathrm{E}}$, and $\boldsymbol{z}_{\mathrm{E}}$ dependence is given as follows:

$$\frac{\mathrm{d}}{\mathrm{d}t}\begin{bmatrix}\boldsymbol{x}_{\mathrm{E}}\\ \boldsymbol{x}_1^{\mathrm{con}}\\ \boldsymbol{x}_2^{\mathrm{con}}\\ \vdots\\ \boldsymbol{x}_{\mathrm{n}}^{\mathrm{con}}\end{bmatrix} = \begin{bmatrix}\boldsymbol{A}_{\mathrm{E}} & & & & \\ & \boldsymbol{A}_1^{\mathrm{con}} & & & \\ & & \boldsymbol{A}_2^{\mathrm{con}} & & \\ & & & \ddots & \\ & & & & \boldsymbol{A}_{\mathrm{n}}^{\mathrm{con}}\end{bmatrix}\begin{bmatrix}\boldsymbol{x}_{\mathrm{E}}\\ \boldsymbol{x}_1^{\mathrm{con}}\\ \boldsymbol{x}_2^{\mathrm{con}}\\ \vdots\\ \boldsymbol{x}_{\mathrm{n}}^{\mathrm{con}}\end{bmatrix} + \begin{bmatrix}\boldsymbol{B}_{\mathrm{E}}\\ \boldsymbol{O}(N_{\mathrm{c}}, 2n)\end{bmatrix}\underbrace{\begin{bmatrix}\boldsymbol{y}_1^{\mathrm{c}\to\mathrm{g}}\\ \boldsymbol{y}_2^{\mathrm{c}\to\mathrm{g}}\\ \vdots\\ \boldsymbol{y}_{\mathrm{n}}^{\mathrm{c}\to\mathrm{g}}\end{bmatrix}}_{\boldsymbol{z}_{\mathrm{E}}} + \dots$$

$$\begin{bmatrix}\boldsymbol{O}(N_{\mathrm{E}}, 6n)\\ \underbrace{\begin{bmatrix}\boldsymbol{B}_1^{\mathrm{con,a}} & & & \\ & \boldsymbol{B}_2^{\mathrm{con,a}} & & \\ & & \ddots & \\ & & & \boldsymbol{B}_{\mathrm{n}}^{\mathrm{con,a}}\end{bmatrix}}_{\boldsymbol{B}^{\mathrm{con,a}}}\end{bmatrix}\begin{bmatrix}\boldsymbol{y}_{\mathrm{E}_1}\\ \boldsymbol{y}_{\mathrm{E}_2}\\ \vdots\\ \boldsymbol{y}_{\mathrm{E}_{\mathrm{n}}}\end{bmatrix} + \dots$$

$$\begin{bmatrix}\boldsymbol{O}(N_{\mathrm{E}}, 2n)\\ \underbrace{\begin{bmatrix}\boldsymbol{B}_1^{\mathrm{con,b}} & & & \\ & \boldsymbol{B}_2^{\mathrm{con,b}} & & \\ & & \ddots & \\ & & & \boldsymbol{B}_{\mathrm{n}}^{\mathrm{con,b}}\end{bmatrix}}_{\boldsymbol{B}^{\mathrm{con,b}}}\end{bmatrix}\begin{bmatrix}\boldsymbol{z}_1^{\mathrm{ref}}\\ \boldsymbol{z}_2^{\mathrm{ref}}\\ \vdots\\ \boldsymbol{z}_{\mathrm{n}}^{\mathrm{ref}}\end{bmatrix} \tag{7.61}$$

Combining equations 7.54 and 7.61 with the expressions for $\boldsymbol{A}_{\mathrm{E}}$ and $\boldsymbol{B}_{\mathrm{E}}$ from equation 7.22, it is possible to create a unified linear state-space model of the multi-converter system which can easily be coded up in C++.

7.3 Simulations ignoring local loads

In this section, analysis is confined to dq-axis vector current control and power synchronization control. The reason for doing so is that dq-axis vector current control has substantial presence in real applications already, and, out of the three controllers reviewed in the previous chapter, power synchronization control exhibited the best voltage regulating capability. If the reader is interested,

the theory developed in the previous section does allow studies with proportional resonant control to be conducted also.

In addition, each converter is modelled as having an LC filter with per-unit characteristics as given in the previous chapters. The local transmission line is set to 0.1p.u.

7.3.1 DQ-axis vector current control only

Let us consider the two converter case where both converters employ dq-axis vector current control. Let the PLLs used be 1st order. Second-order PLLs can be (and have been) simulated; however, for brevity reasons, results primarily focus on the first-order PLL simulations.

In this system, the outputs can be expressed by equation:

$$\begin{bmatrix} \Delta P_1 \\ \Delta E_1 \\ \Delta P_2 \\ \Delta E_2 \end{bmatrix} = \underbrace{\begin{bmatrix} \frac{\partial P_1}{\partial i_{\mathrm{d}_1}^{\mathrm{ref}}} & \frac{\partial P_1}{\partial i_{\mathrm{q}_1}^{\mathrm{ref}}} & \frac{\partial P_1}{\partial i_{\mathrm{d}_2}^{\mathrm{ref}}} & \frac{\partial P_1}{\partial i_{\mathrm{q}_2}^{\mathrm{ref}}} \\ \frac{\partial E_1}{\partial i_{\mathrm{d}_1}^{\mathrm{ref}}} & \frac{\partial E_1}{\partial i_{\mathrm{q}_1}^{\mathrm{ref}}} & \frac{\partial E_1}{\partial i_{\mathrm{d}_2}^{\mathrm{ref}}} & \frac{\partial E_1}{\partial i_{\mathrm{q}_2}^{\mathrm{ref}}} \\ \frac{\partial P_2}{\partial i_{\mathrm{d}_1}^{\mathrm{ref}}} & \frac{\partial P_2}{\partial i_{\mathrm{q}_1}^{\mathrm{ref}}} & \frac{\partial P_2}{\partial i_{\mathrm{d}_2}^{\mathrm{ref}}} & \frac{\partial P_2}{\partial i_{\mathrm{q}_2}^{\mathrm{ref}}} \\ \frac{\partial E_2}{\partial i_{\mathrm{d}_1}^{\mathrm{ref}}} & \frac{\partial E_2}{\partial i_{\mathrm{q}_1}^{\mathrm{ref}}} & \frac{\partial E_2}{\partial i_{\mathrm{d}_2}^{\mathrm{ref}}} & \frac{\partial E_2}{\partial i_{\mathrm{q}_2}^{\mathrm{ref}}} \end{bmatrix}}_{\boldsymbol{H}^{\mathrm{com}}} \begin{bmatrix} \Delta i_{\mathrm{d}_1}^{\mathrm{ref}} \\ \Delta i_{\mathrm{q}_1}^{\mathrm{ref}} \\ \Delta i_{\mathrm{d}_2}^{\mathrm{ref}} \\ \Delta i_{\mathrm{q}_2}^{\mathrm{ref}} \end{bmatrix} \tag{7.62}$$

For each operating point, Bode and time traces are presented, respectively showing the frequency and time domain results from evaluation of the linear model at this operating point. From left to right, the top row of both figures show the response (either in the frequency domain or time domain) of the active power output, P_1, of converter one to changes in the control variables, $i_{\mathrm{d}_1}^{\mathrm{ref}}$, $i_{\mathrm{q}_1}^{\mathrm{ref}}$, $i_{\mathrm{d}_2}^{\mathrm{ref}}$ and $i_{\mathrm{q}_2}^{\mathrm{ref}}$. From left to right, the second row of both figures show the response (either in the frequency domain or time domain) of the voltage magnitude at the filter bus of converter one, E_1, to changes in the control variables, $i_{\mathrm{d}_1}^{\mathrm{ref}}$, $i_{\mathrm{q}_1}^{\mathrm{ref}}$, $i_{\mathrm{d}_2}^{\mathrm{ref}}$ and $i_{\mathrm{q}_2}^{\mathrm{ref}}$. From left to right, the third row of both figures show the response (either in the frequency domain or time domain) of the active power output of converter two, P_2, to changes in the control variables, $i_{\mathrm{d}_1}^{\mathrm{ref}}$, $i_{\mathrm{q}_1}^{\mathrm{ref}}$, $i_{\mathrm{d}_2}^{\mathrm{ref}}$ and $i_{\mathrm{q}_2}^{\mathrm{ref}}$. Finally, from

left to right, the fourth row of both figures show the response (either in the frequency domain or time domain) of the voltage magnitude at the filter bus of converter two, E_2, to changes in the control variables, $i_{\mathrm{d}_1}^{\mathrm{ref}}$, $i_{\mathrm{q}_1}^{\mathrm{ref}}$, $i_{\mathrm{d}_2}^{\mathrm{ref}}$ and $i_{\mathrm{q}_2}^{\mathrm{ref}}$.

The system strength is set such that the steady-state voltages at the local PCCs have high phases relative to the voltage at the slack bus when the converters operate at $P_{\zeta,0} = 0.7$ p.u..

In figures 7.3 and 7.4, the steady-state power output of converter one is fixed at 0.5pu, while the steady-state power output of converter one is 0.0 p.u.. This translates to the voltage at the filter bus of converter one having a phase of 14.9659 degrees relative to the slack bus, while the equivalent voltage for converter two is 17.4770 degrees. In other words, both converters have relatively low phase differences relative to the slack bus. Considering the findings of [5], [3] and [2] along with chapter 4 of this thesis, it is no surprise that the system, at the current controller level, is well-conditioned at this operating point. In other words, as can be seen in figures 7.3 and 7.4, the diagonal is dominant.

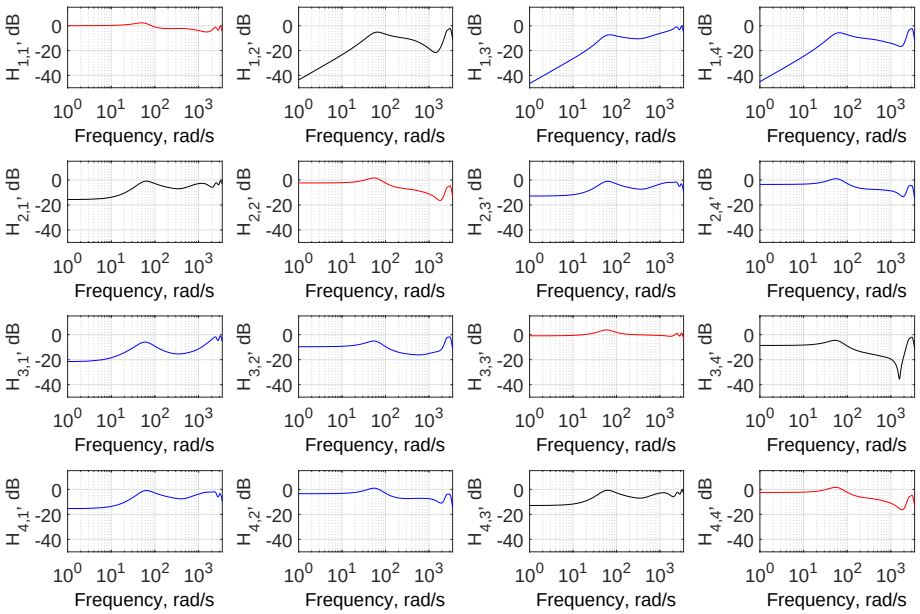

Figure 7.3: $\boldsymbol{H}^{\mathrm{com}}$ evaluated when $P_{1,0} = 0.0$ p.u. and $P_{2,0} = 0.50$ p.u. Bode magnitude response only.

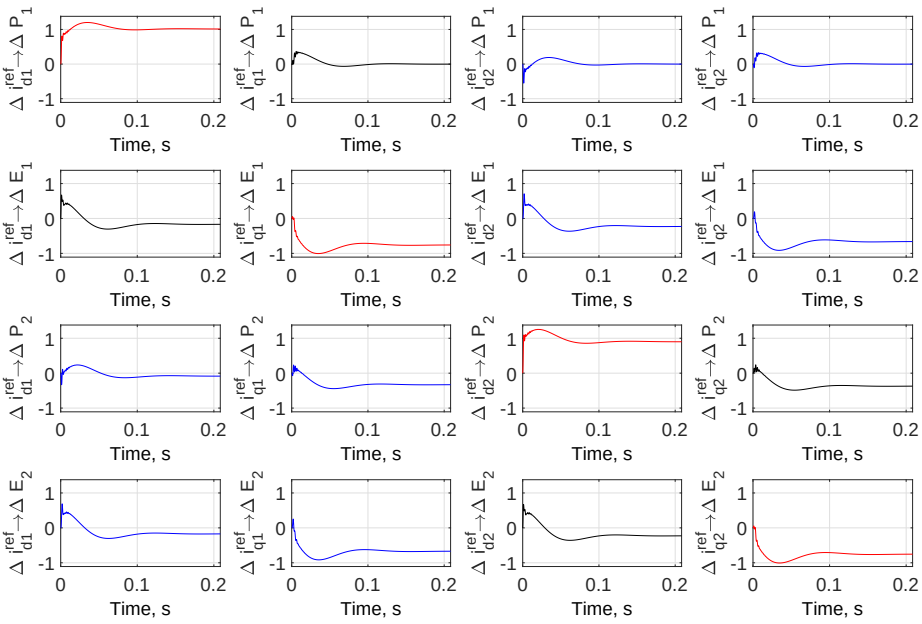

Figure 7.4: Normalised responses to small step changes in the reference values. System evaluated when $P_{1,0} = 0.0$ p.u. and $P_{2,0} = 0.50$ p.u.

When both converters are at $P_{\zeta,0} = 0.5$ p.u., both converters have filter bus voltages that have a phase difference of 34.9104 degrees relative to the slack bus. In the low frequency region, it can be observed in figure 7.5 that $\partial P_1/\partial i_{\mathrm{d}_1}^{\mathrm{ref}}$ is below unity, while at the same time the strengths of $\partial P_1/\partial i_{\mathrm{q}_1}^{\mathrm{ref}}$, $\partial P_1/\partial i_{\mathrm{d}_2}^{\mathrm{ref}}$ and $\partial P_1/\partial i_{\mathrm{q}_2}^{\mathrm{ref}}$ have all increased in the same frequency range. In other words, the system conditioning is deteriorating. It is interesting to note $\partial P_1/\partial i_{\mathrm{d}_2}^{\mathrm{ref}}$. The control variable, $i_{\mathrm{d}_2}^{\mathrm{ref}}$ is set according to a power controller for converter two i.e $i_{\mathrm{d}_2}^{\mathrm{ref}}$ is being manipulated with the intention of controlling P_2. Yet, it can be observed that this control variable is beginning to have an impact on P_1. This can be understood by considering chapter four and/or $\partial E_1/\partial i^{\mathrm{ref}_{\mathrm{d}_2}}$ and $\partial E_2/\partial i^{\mathrm{ref}_{\mathrm{d}_2}}$. In the single converter system, $i_{\mathrm{d}}^{\mathrm{ref}}$ has a significant impact on the voltage (which in the multi-converter system maps to $\partial E_2/\partial i_{\mathrm{d}_2}^{\mathrm{ref}}$ being strong). By disturbing the local voltage, the voltages at other points in the system are also affected (see $\partial E_1/\partial i_{\mathrm{d}_1}^{\mathrm{ref}}$ in figures 7.5 and 7.6). By noting that power flow across a reactance is proportional to the product of the voltages at the ends of the reactance, by disturbing the wider system voltages, $i_{\mathrm{d}_2}^{\mathrm{ref}}$ is able to influence the power output of converter one, which can be seen in figure 7.6. The same is also the case for the influence of $i^{m}athrmref_{\mathrm{d}_1}$ on P_2.

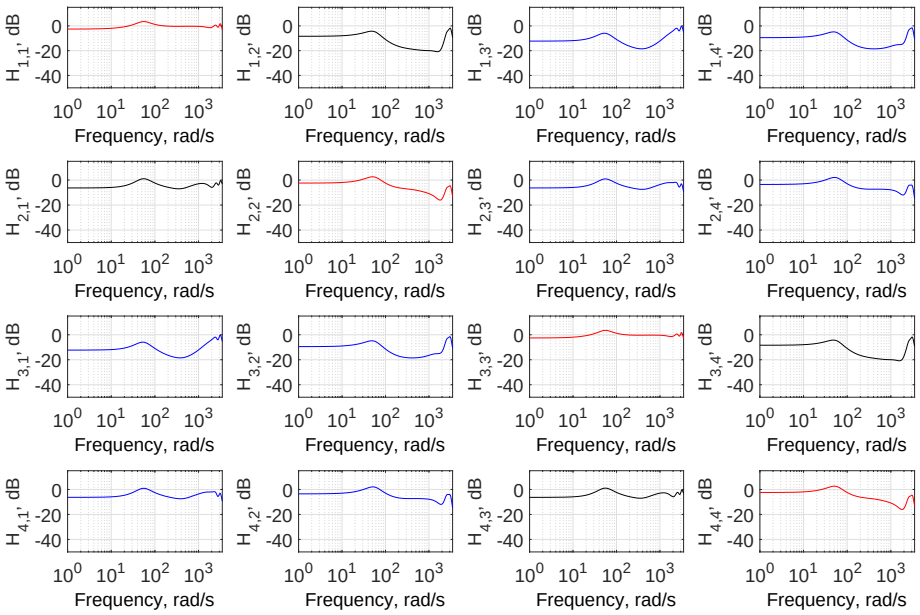

Figure 7.5: $\boldsymbol{H}^{\text{com}}$ evaluated when $P_{1,0} = 0.50$ p.u. and $P_{2,0} = 0.50$ p.u. Bode magnitude response only.

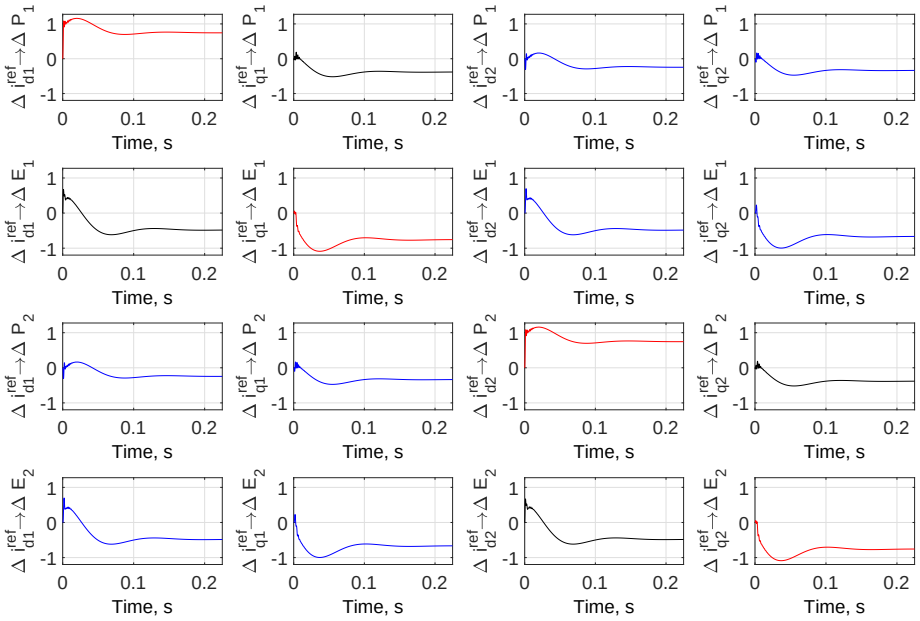

Figure 7.6: Normalised responses to small step changes in the reference values. System evaluated when $P_{1,0} = 0.50$ p.u. and $P_{2,0} = 0.50$ p.u.

In figures 7.8-7.12, the same investigation is carried out, but with converter two having its steady-state active power output fixed at 0.7 pu. Again, it can be observed that when converter one is

operating at $P_{1,0} = 0$ p.u., the performance of converter two's d-component current loop is superior to that seen in chapter 4, even though converter two is operating at 0.7p.u. active power. This is due to the relatively small phase difference between the slack bus voltage and that at the PCC of converter two (approximately 25 degrees).

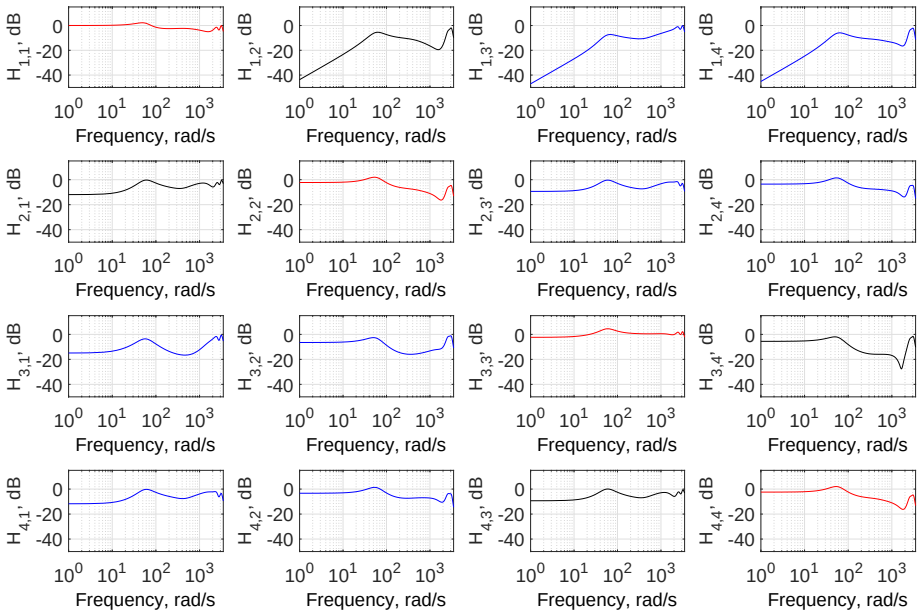

Figure 7.7: $\boldsymbol{H}^{\text{com}}$ evaluated when $P_{1,0} = 0.00$ p.u. and $P_{2,0} = 0.70$ p.u. Bode magnitude response only.

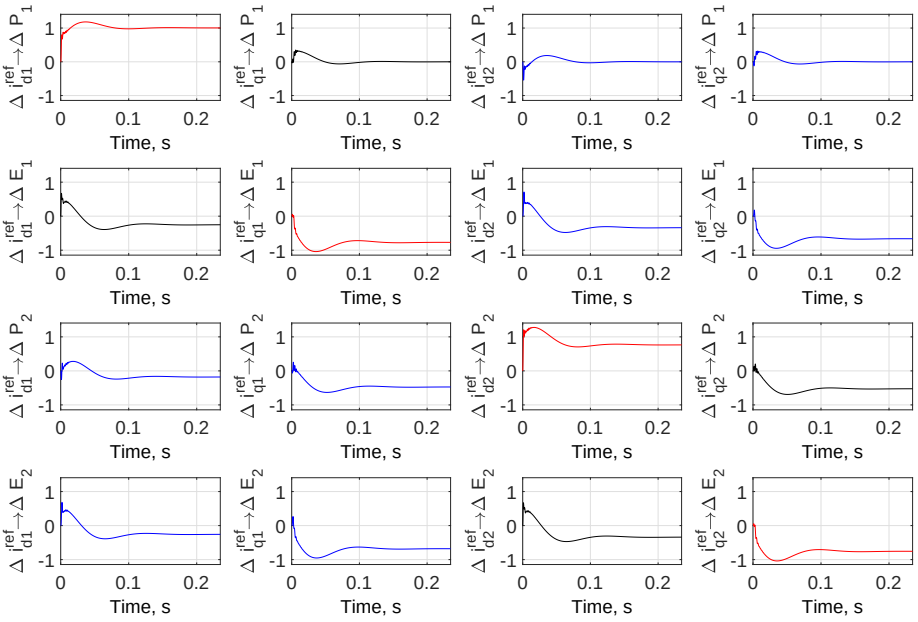

Figure 7.8: Normalised responses to small step changes in the reference values. System evaluated when $P_{1,0} = 0.0$ p.u. and $P_{2,0} = 0.70$ p.u.

However, as the set points of both converters increases, the coupling of the system in the low frequency range re-appears, reaching levels greater than that seen in figures 7.5 and 7.6, in line with an increasing phase angles of the pair of local PCCs relative to the slack bus. Again, the strong connection between $i_{\mathrm{d}_2}^{\mathrm{ref}}$ and P_1 can be observed, and by extension the strong connection between $i_{\mathrm{d}_1}^{\mathrm{ref}}$ and P_2. In other words, there is strong coupling *between converters* in addition to between the control loops in a single converter. This additional coupling introduces an additional degree of freedom to the system which would make the design of outer controllers more complex. More specifically, adopting a gain-scheduled de-coupling scheme such as that presented in [5] may require each controller to have an estimation of the system conditions.

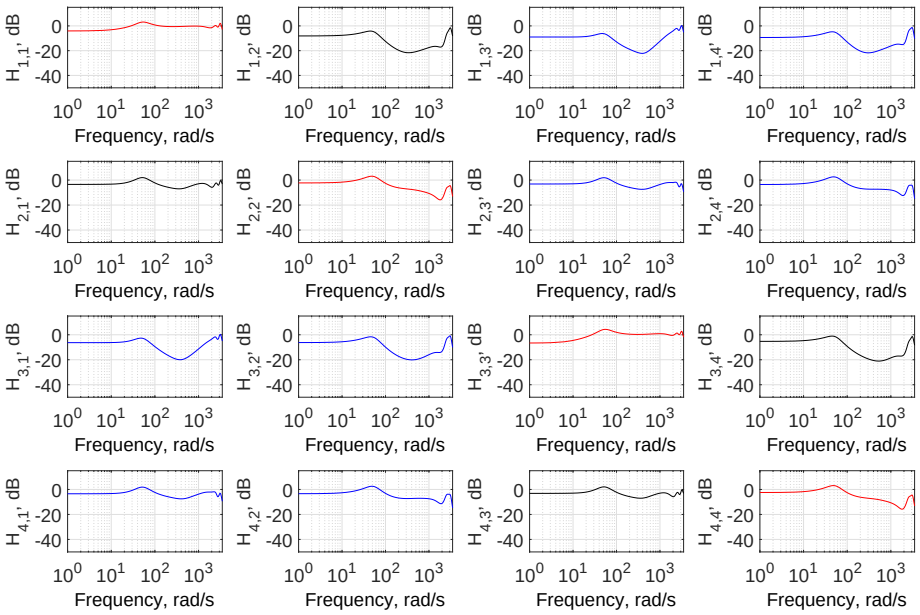

Figure 7.9: $\boldsymbol{H}^{\text{com}}$ evaluated when $P_{1,0} = 0.50$ p.u. and $P_{2,0} = 0.70$ p.u. Bode magnitude response only.

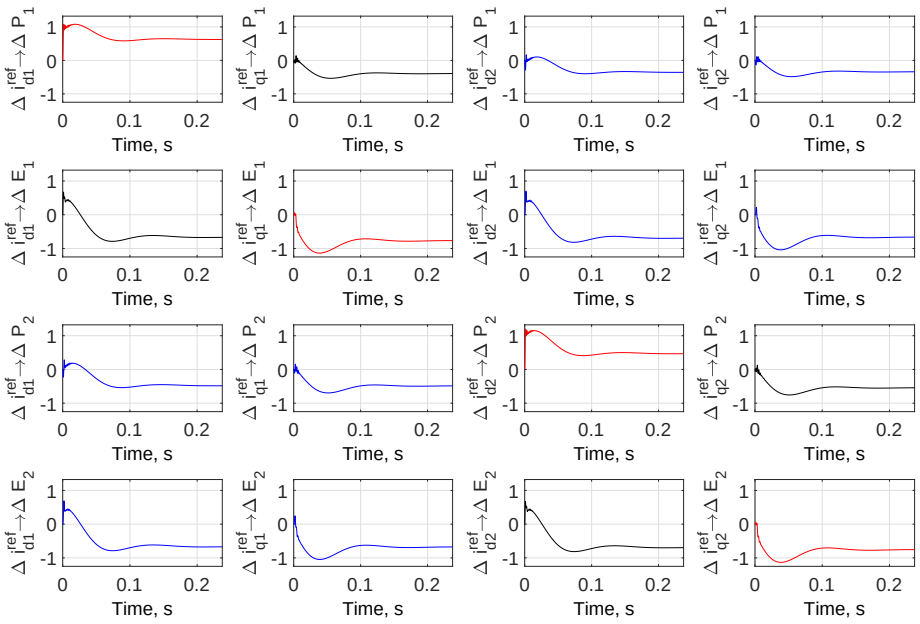

Figure 7.10: Normalised responses to small step changes in the reference values. System evaluated when $P_{1,0} = 0.50$ p.u. and $P_{2,0} = 0.70$ p.u.

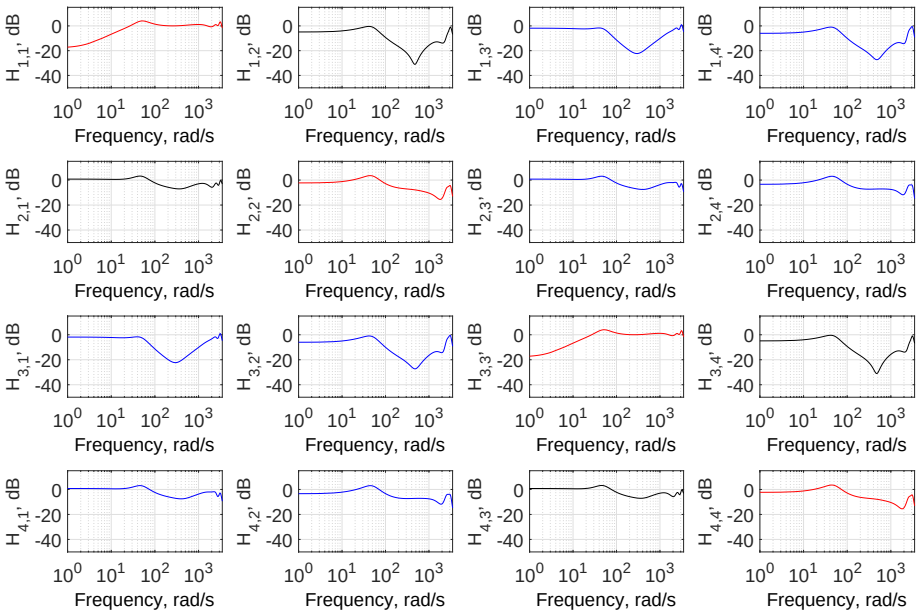

Figure 7.11: $\boldsymbol{H}^{\text{com}}$ evaluated when all converters are operating at 0.7p.u. Bode magnitude response only (with the response given in dB).

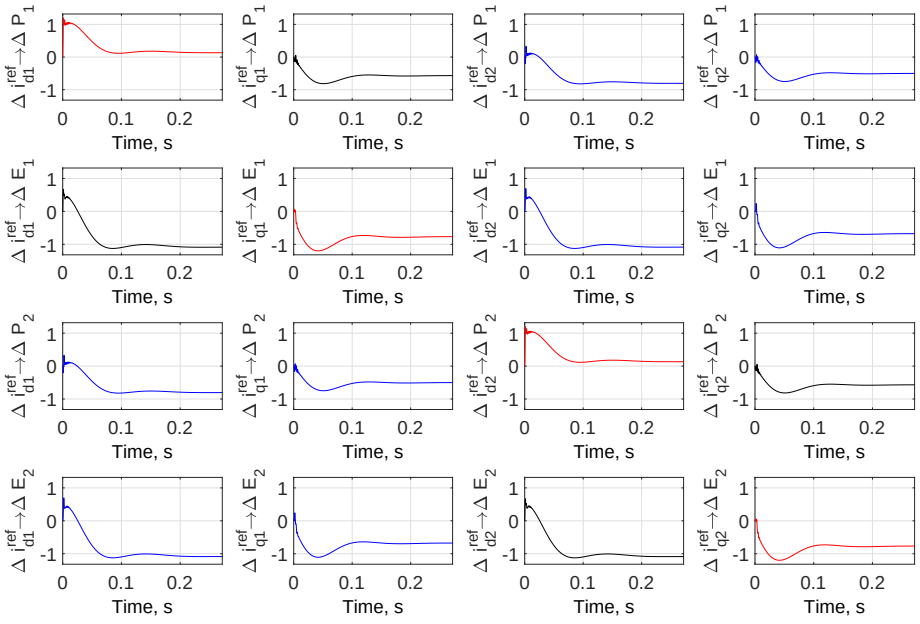

Figure 7.12: Normalised responses to small step changes in the reference values. System evaluated when $P_{1,0} = 0.70$ p.u. and $P_{2,0} = 0.70$ p.u.

Figures 7.13 and 7.14 show the poles and zeros of the combined system (plant plus controllers (with

feedback)). It can be seen that there are two pairs of symmetric transmission zeros, which move closer to the origin as the power set point of converter one is increased, imposing a restriction on the achievable bandwidth of the outer controller. Again, while the system is observably ill-conditioned (see figures 7.11), there are no poles in the right half-plane; that is, at the inner current level, the system is not unstable. That being said, in reference to figure 7.12, the ability of the converters to effectively translate set point changes in $i_{\mathrm{d}}^{\mathrm{ref}}$ to changes in the power output is highly compromised.

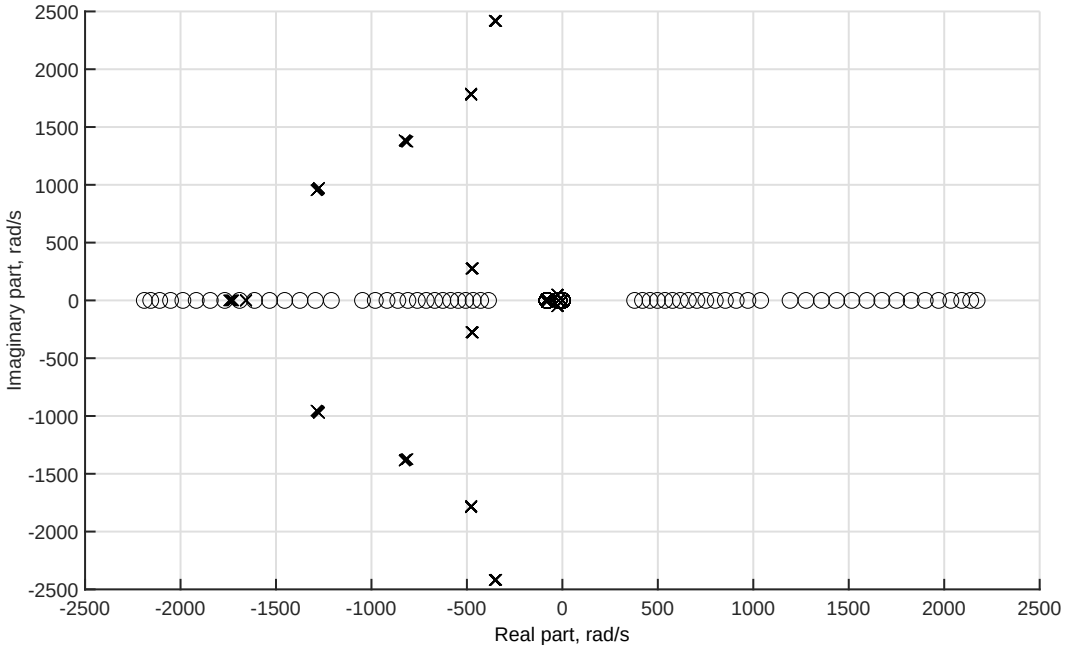

Figure 7.13: Root locus showing the poles and zeros for combined system (plant and controllers (with feedback)) for a range of operating points. For all cases considered, $P_{2,0} = 0.7$p.u. $P_{1,0}$ was varied from 0 to 0.7p.u. with steps of 0.05p.u.

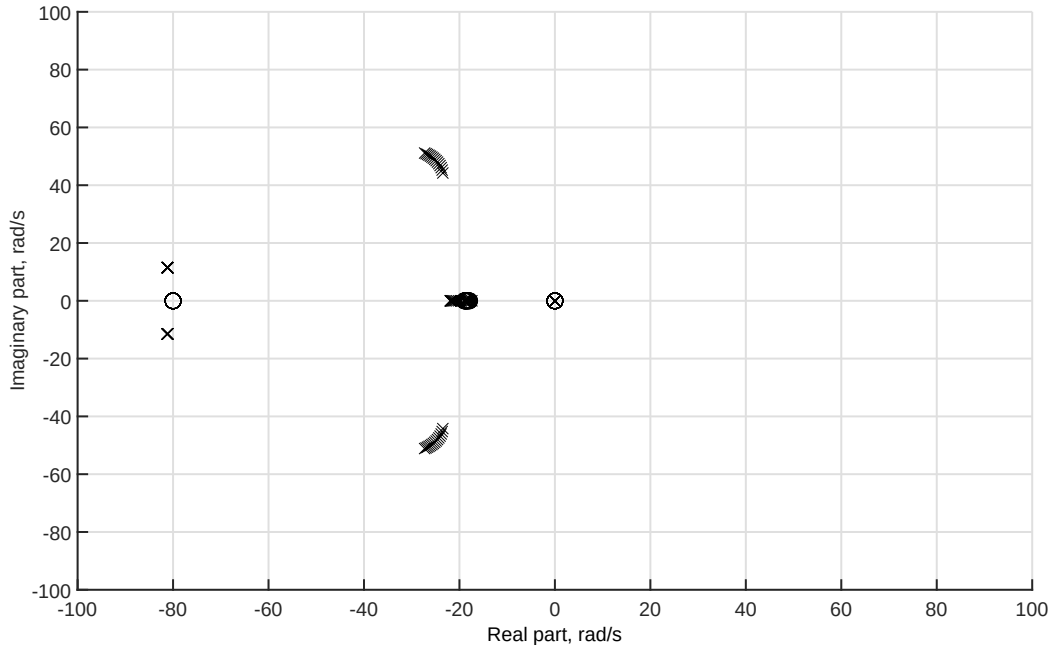

Figure 7.14: Close up of low frequency poles and zeros for combined system (plant and controllers (with feedback)) for a range of operating points. For all cases considered, $P_{2,0} = 0.7$p.u. $P_{1,0}$ was varied from 0 to 0.7p.u. with steps of 0.05p.u.

While not extensively studied, figures 7.15 and 7.16 are included to show the performance when a moderate bandwidth 2nd order PLL is employed (that found in chapter four). No local loads are present. Converter two has its power set point fixed at 0.7p.u, while the power set point of converter one is varied in the same manner as before. As the power set point of converter one rises above 0.25p.u., the system enters an unstable region.

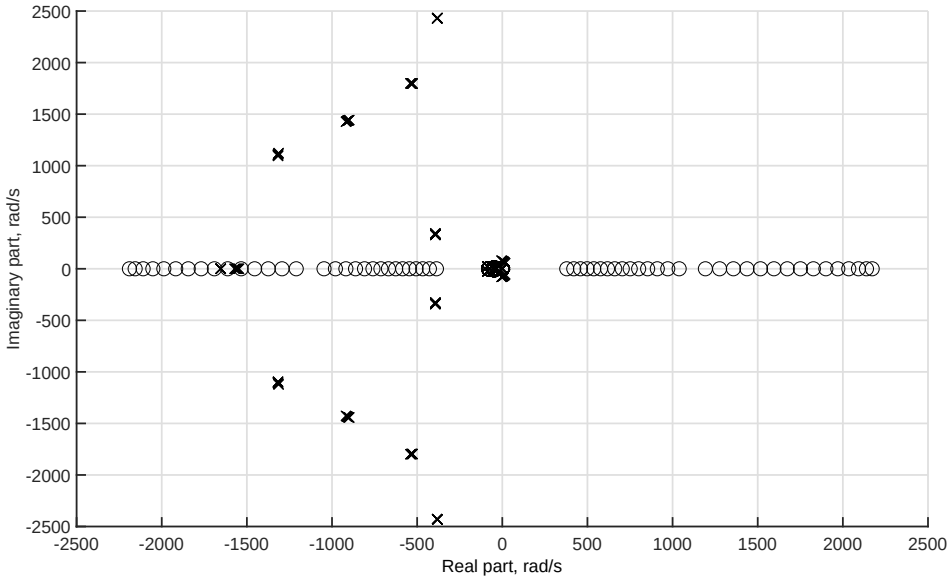

Figure 7.15: Root locus showing the poses and zeros for combined system (plant and controllers (with feedback)) for a range of operating points. For all cases considered, $P_{2,0} = 0.7$p.u. $P_{1,0}$ was varied from 0 to 0.7p.u. with steps of 0.05p.u.

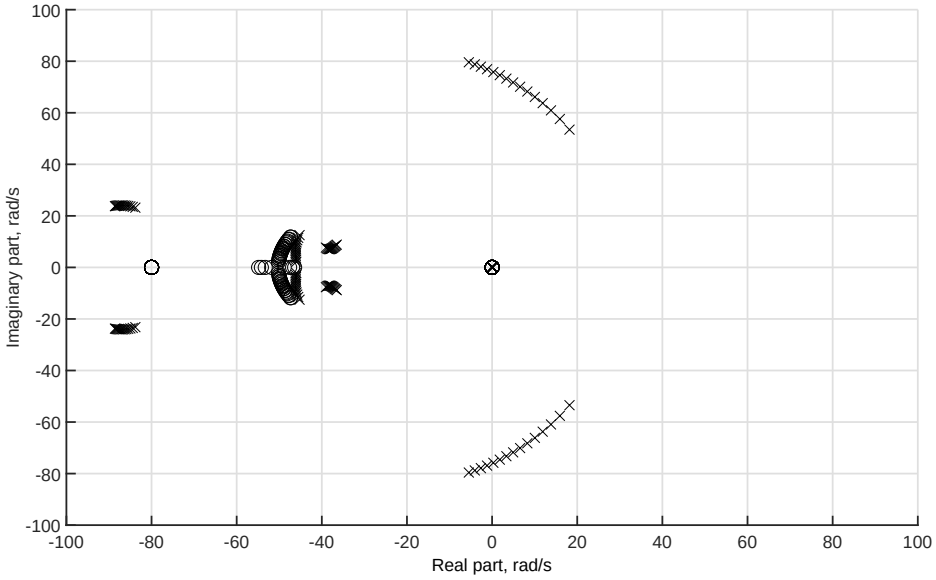

Figure 7.16: Close up of low frequency poles and zeros for combined system (plant and controllers (with feedback)) for a range of operating points. For all cases considered, $P_{2,0} = 0.7$p.u. $P_{1,0}$ was varied from 0 to 0.7p.u. with steps of 0.05p.u.

Summary of systems where all converters use dq-axis vector current control

In summary, two degrees of coupling are present: that within the converter controller, and that between converters, both of which have significant power. Both are due to a lack of a stiff voltage in proximity to the converters. In general, it can be seen that the performance of each converter depends not only on its own operating point, but also those of the other converters in the system. Ultimately, the stability of the system is dependent on numerous parameters; thus, any hard number quantifying the tipping point for a system will be confined to the system being considered, along with its global operating points.

7.3.2 Power synchronization control only

In this section, both converters employ the power synchronization controller. For this system, the small-signal system dynamics may be expressed as follows:

$$\begin{bmatrix} \Delta P_1 \\ \Delta E_1 \\ \Delta P_2 \\ \Delta E_2 \end{bmatrix} = \underbrace{\begin{bmatrix} \frac{\partial P_1}{\partial P_1^{\text{ref}}} & \frac{\partial P_1}{\partial E_1^{\text{ref}}} & \frac{\partial P_1}{\partial P_2^{\text{ref}}} & \frac{\partial P_1}{\partial E_2^{\text{ref}}} \\ \frac{\partial E_1}{\partial P_1^{\text{ref}}} & \frac{\partial E_1}{\partial E_1^{\text{ref}}} & \frac{\partial E_1}{\partial P_2^{\text{ref}}} & \frac{\partial E_1}{\partial E_2^{\text{ref}}} \\ \frac{\partial P_2}{\partial P_1^{\text{ref}}} & \frac{\partial P_2}{\partial E_1^{\text{ref}}} & \frac{\partial P_2}{\partial P_2^{\text{ref}}} & \frac{\partial P_2}{\partial E_2^{\text{ref}}} \\ \frac{\partial E_2}{\partial P_1^{\text{ref}}} & \frac{\partial E_2}{\partial E_1^{\text{ref}}} & \frac{\partial E_2}{\partial P_2^{\text{ref}}} & \frac{\partial E_2}{\partial E_2^{\text{ref}}} \end{bmatrix}}_{\boldsymbol{H}^{\text{com}}} \begin{bmatrix} \Delta P_1^{\text{ref}} \\ \Delta E_1^{\text{ref}} \\ \Delta P_2^{\text{ref}} \\ \Delta E_2^{\text{ref}} \end{bmatrix} \tag{7.63}$$

As with dq-axis vector current control, the same set of operating points are considered. Figures 7.17-7.26 show the performance of the system across a range of operating points when both converters using power synchronization control.

The system strength is again set such that the steady-state voltages at the local PCCs have high phases relative to the voltage at the slack bus when the converters operate at $P_{\zeta,0} = 0.7$ p.u..

Figure 7.26 shows that the main diagonal elements are again dominant even when $P_{1,0} = 0.7$ p.u. and $P_{2,0} = 0.7$ p.u. with the exception of a small range of frequencies as before. This, as before, is equivalent to the oscillatory behaviour seen in synchronous machines.

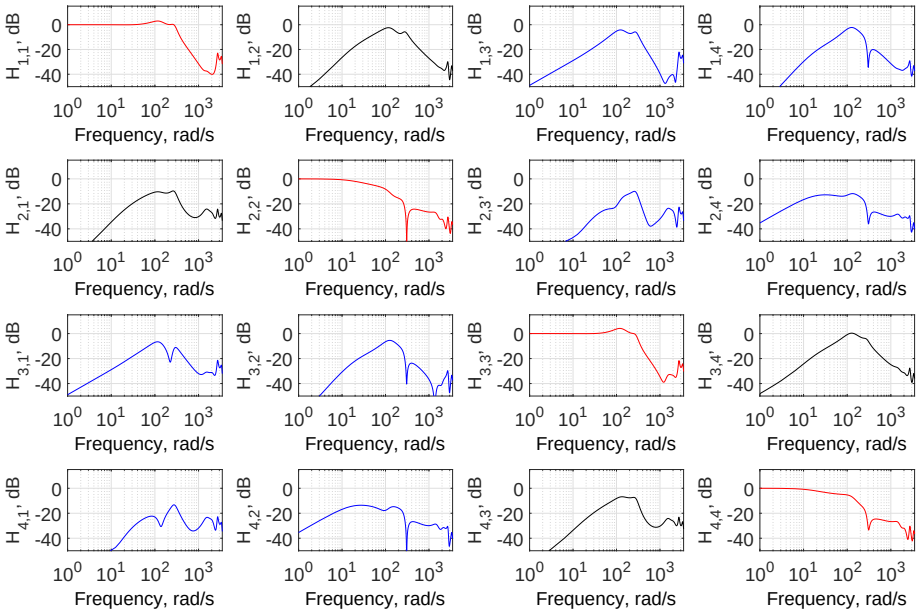

Figure 7.17: $\boldsymbol{H}^{\text{com}}$ evaluated when $P_{1,0} = 0.0$ p.u. and $P_{2,0} = 0.50$ p.u. Bode magnitude response only.

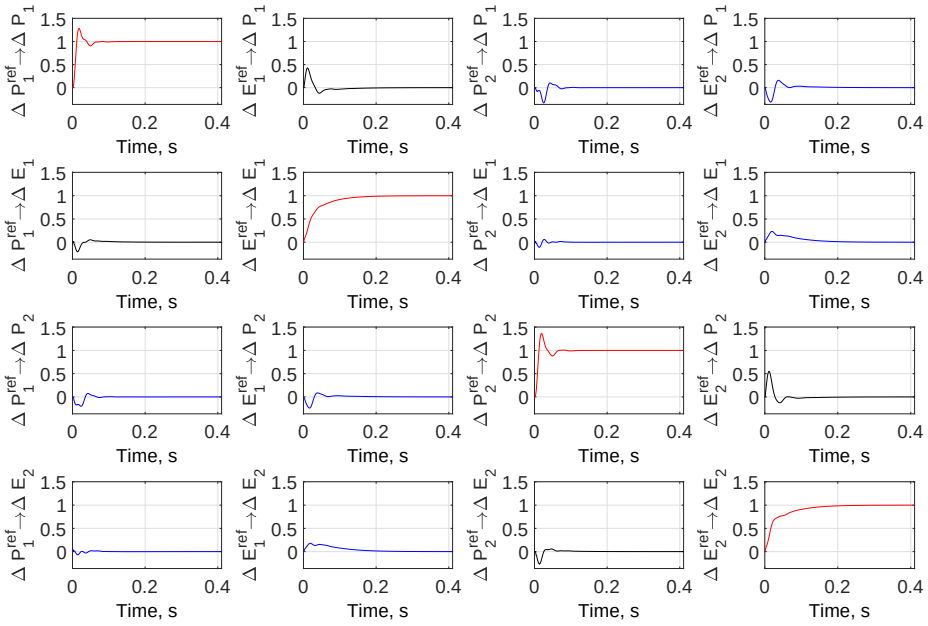

Figure 7.18: Normalised responses to small step changes in the reference values. System evaluated when $P_{1,0} = 0.0$ p.u. and $P_{2,0} = 0.50$ p.u.

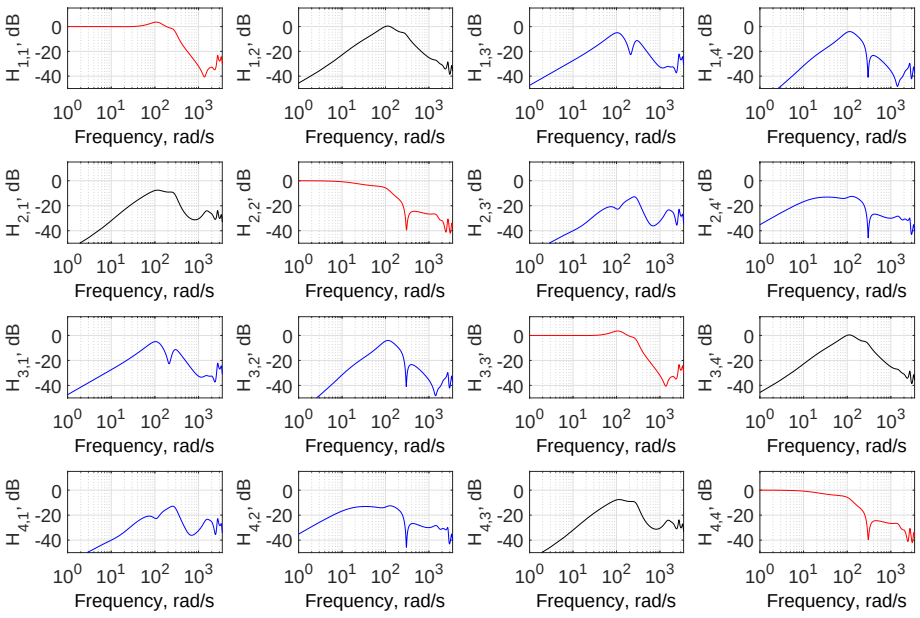

Figure 7.19: $\boldsymbol{H}^{\text{com}}$ evaluated when $P_{1,0} = 0.50$ p.u. and $P_{2,0} = 0.50$ p.u. Bode magnitude response only.

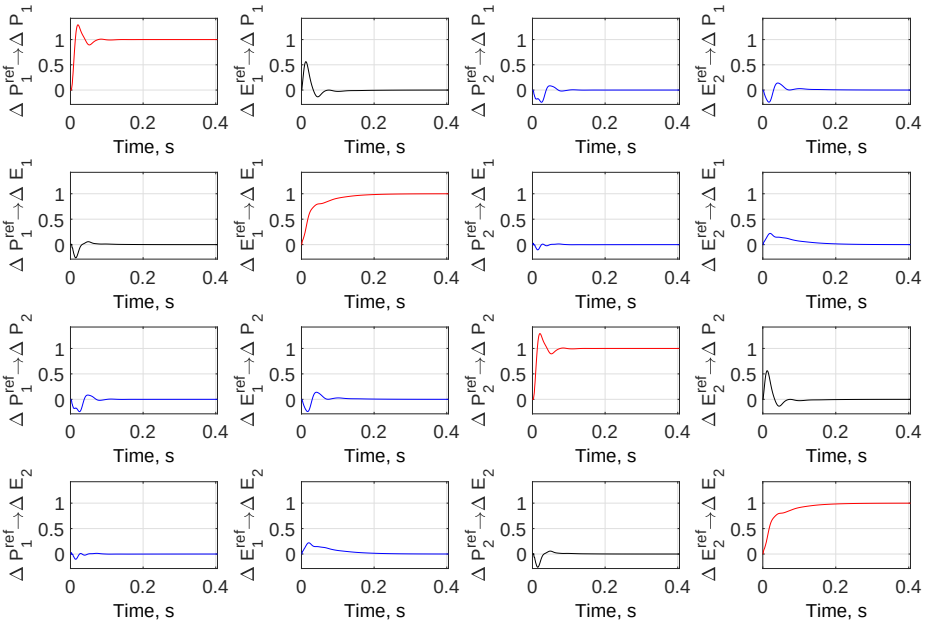

Figure 7.20: Normalised responses to small step changes in the reference values. System evaluated when $P_{1,0} = 0.50$ p.u. and $P_{2,0} = 0.50$ p.u.

In the final set of operating points considered in this section, converters two is operating at $P_{2,0}$ =0.7 p.u. active power in steady-state and the power output of converter one is varied. With the definition of the wider network transmission line, this corresponds to the voltages at the local PCCs both being 56 degrees when both converters are operating at 0.7 p.u.

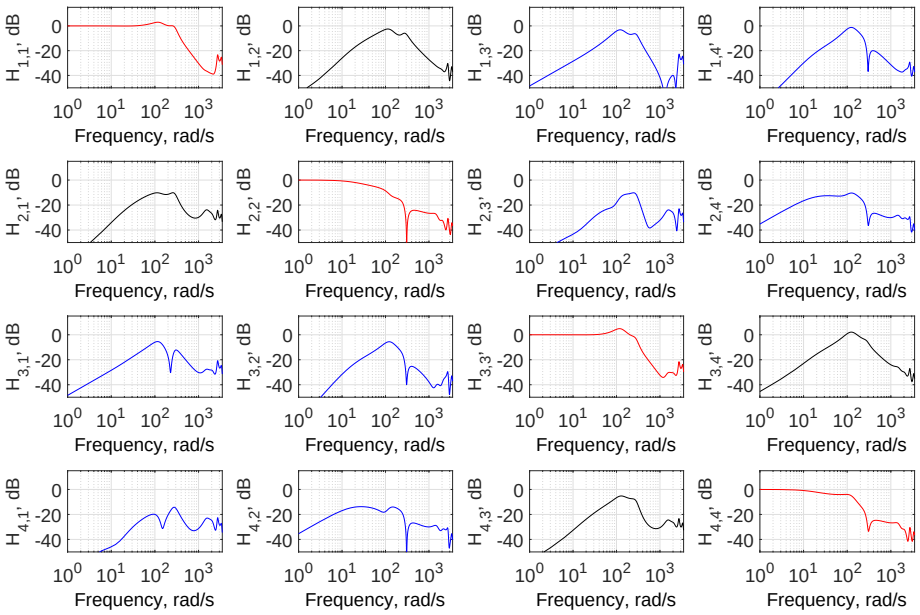

Figure 7.21: $\boldsymbol{H}^{\text{com}}$ evaluated when $P_{1,0} = 0.0$ p.u. and $P_{2,0} = 0.70$ p.u. Bode magnitude response only.

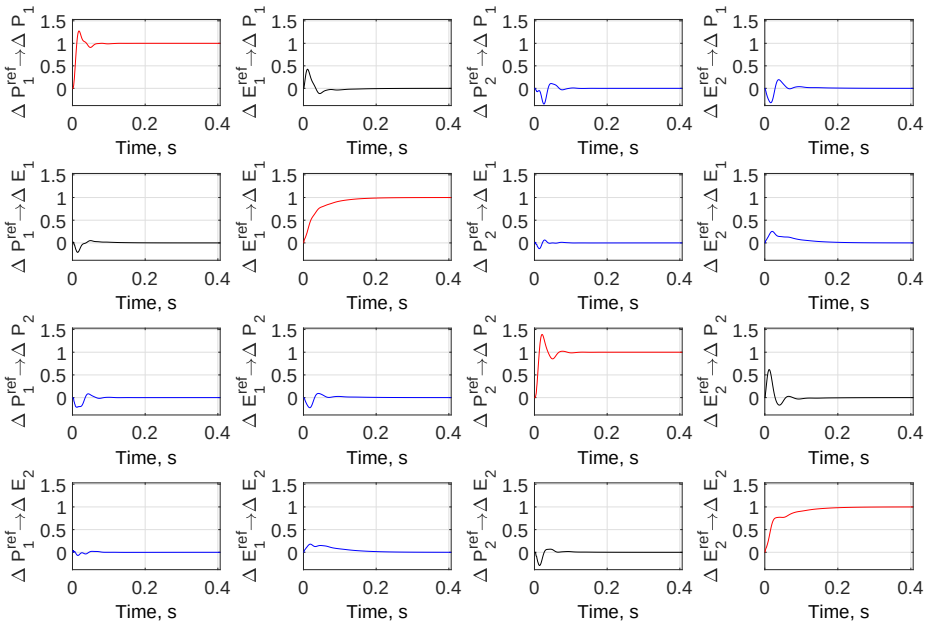

Figure 7.22: Normalised responses to small step changes in the reference values. System evaluated when $P_{1,0} = 0.00$ p.u. and $P_{2,0} = 0.70$ p.u.

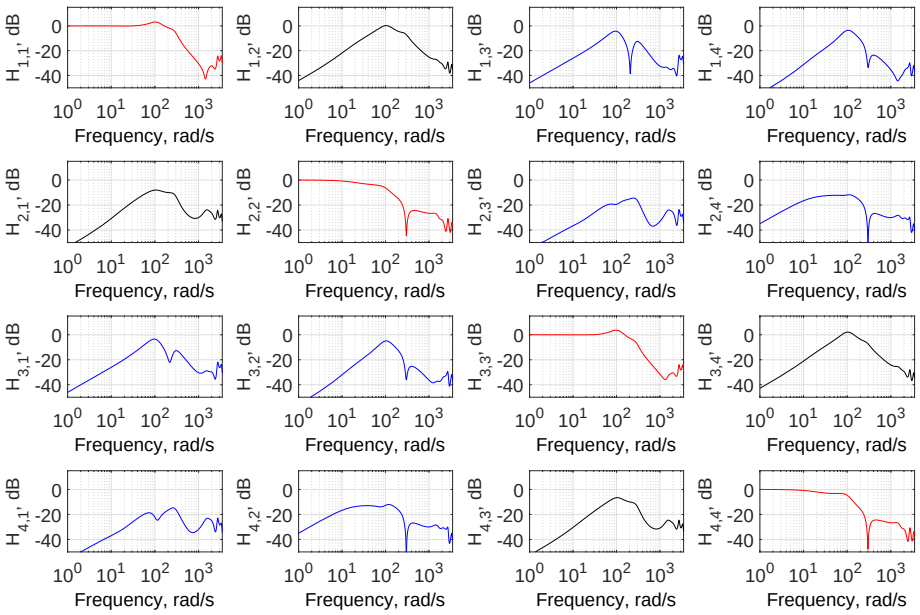

Figure 7.23: $\boldsymbol{H}^{\text{com}}$ evaluated when $P_{1,0} = 0.50$ p.u. and $P_{2,0} = 0.70$ p.u.. Bode magnitude response only.

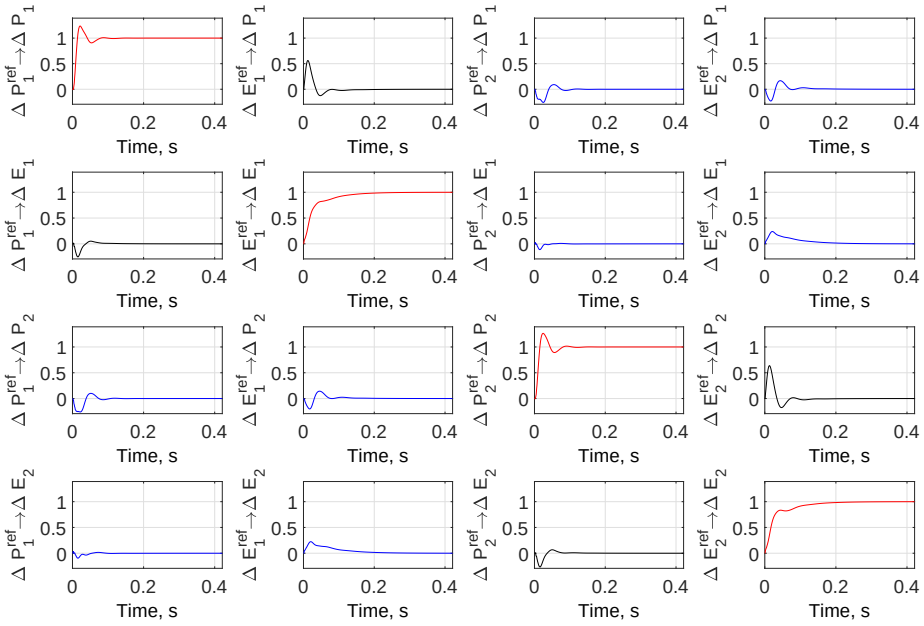

Figure 7.24: Normalised responses to small step changes in the reference values. System evaluated when $P_{1,0} = 0.50$ p.u. and $P_{2,0} = 0.70$ p.u.

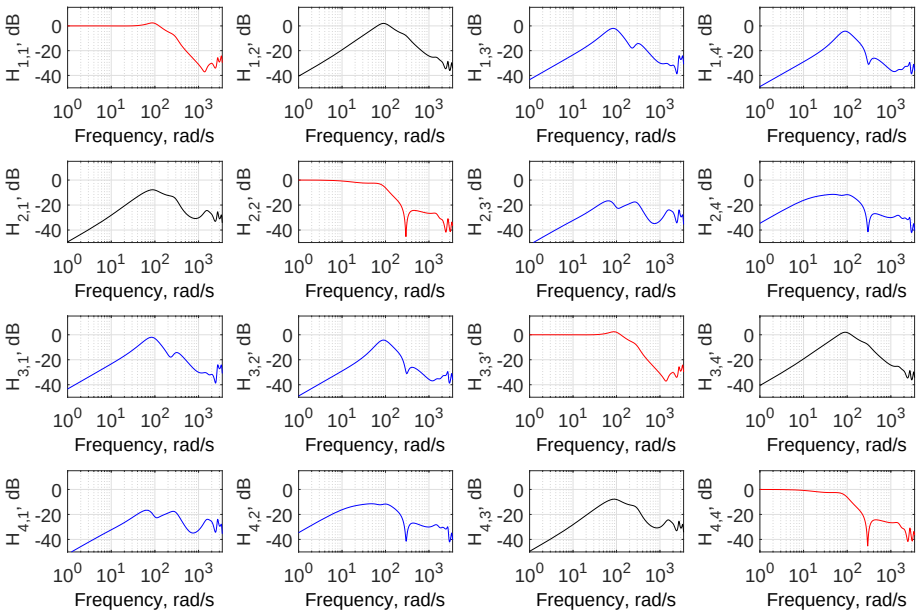

Figure 7.25: $\boldsymbol{H}^{\text{com}}$ evaluated when $P_{1,0} = 0.70$ p.u. and $P_{2,0} = 0.70$ p.u. Bode magnitude response only.

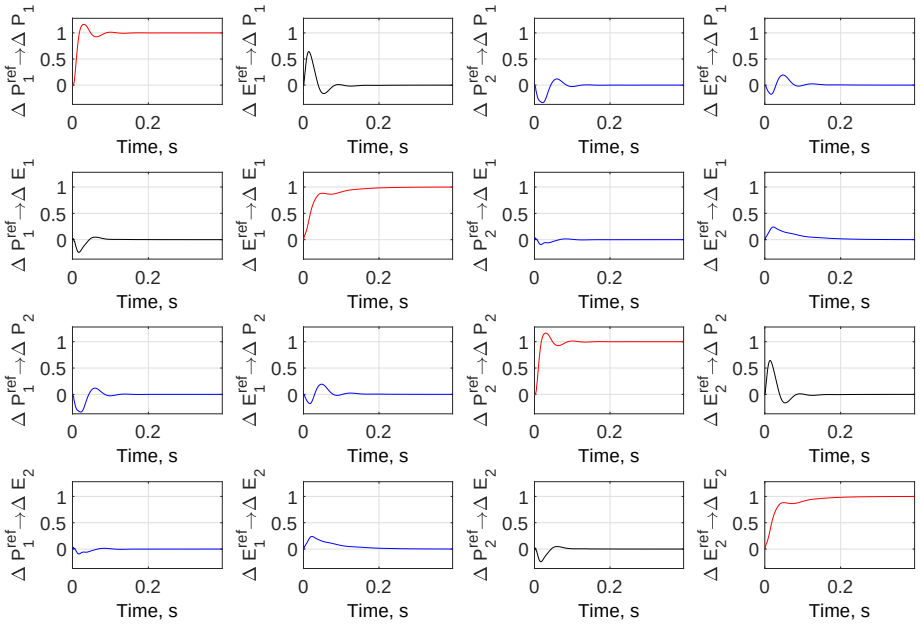

Figure 7.26: Normalised responses to small step changes in the reference values. System evaluated when $P_{1,0} = 0.70$ p.u. and $P_{2,0} = 0.70$ p.u.

Figures 7.27 and 7.28 show the poles and zeros for the combined system (controllers and plant (with feedback)). The same pair of transmission zeros observed in the dq-axis vector current control set

up can be observed.

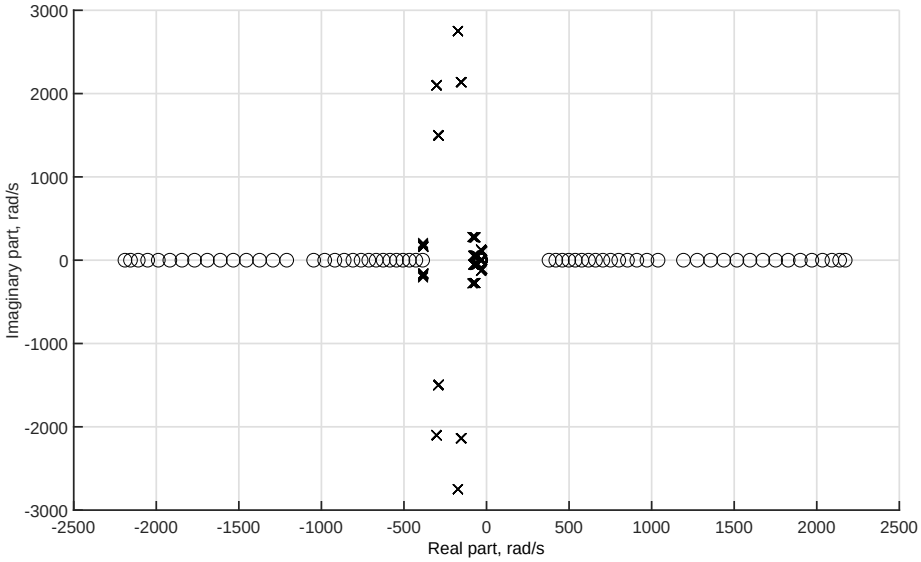

Figure 7.27: Root locus showing the poles and zeros for combined system (plant and controllers (with feedback)) for a range of operating points. For all cases considered, $P_{2,0} = 0.7$p.u. $P_{1,0}$ was varied from 0 to 0.7p.u. with steps of 0.05p.u.

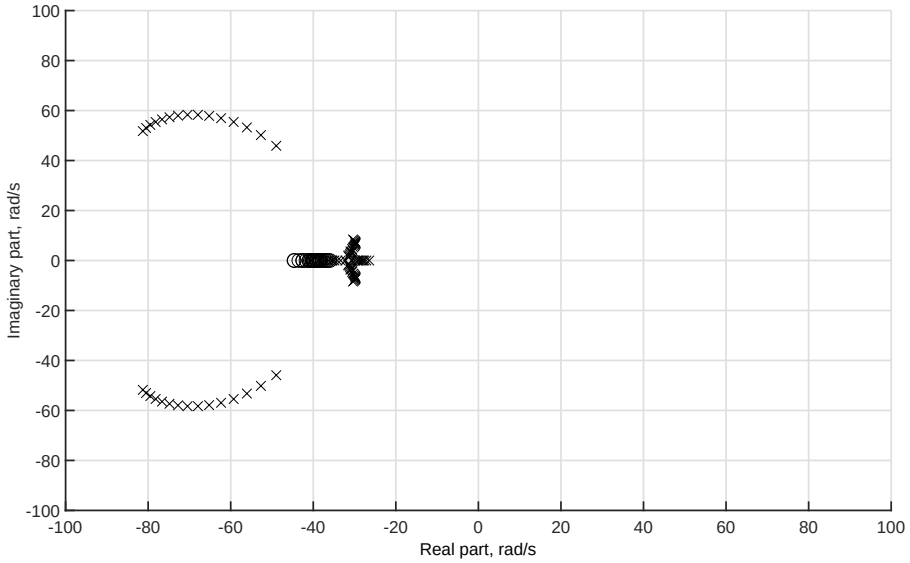

Figure 7.28: Close up of low frequency poles and zeros for combined system (plant and controllers (with feedback)) for a range of operating points. For all cases considered, $P_{2,0} = 0.7$p.u. $P_{1,0}$ was varied from 0 to 0.7p.u. with steps of 0.05p.u.

Summary of systems where all converters use power synchronization control

Unlike dq-axis vector current control, power synchronization control allows a converter to operate satisfactorily in weak AC systems with multiple converters. However, a strong off-diagonal response can be observed at around 100 rad/s. The frequency at which this occurs is consistent with that seen in chapter six. In addition, the frequency at which the strong response is observed seems to be relatively insensitive to the operating point, although its magnitude does depend on the operating point of the overall system. The fact that the location, in frequency terms, does not change from one system to another suggests that a controller modification (left as future work) could be introduced to compensate effectively for this coupling across a wide range of operating points.

7.3.3 Mixture of controllers

Two converters: one controlled using dq-axis vector current control, one controlled using power synchronization control

Let us consider the two converter case where one converter employs dq-axis vector current control and the other power synchronization control. For this system, the small-signal dynamics may be expressed as follows:

$$\begin{bmatrix} \Delta P_1 \\ \Delta E_1 \\ \Delta P_2 \\ \Delta E_2 \end{bmatrix} = \underbrace{\begin{bmatrix} \frac{\partial P_1}{\partial i_{\mathrm{d}_1}^{\mathrm{ref}}} & \frac{\partial P_1}{\partial i_{\mathrm{q}_1}^{\mathrm{ref}}} & \frac{\partial P_1}{\partial P_2^{\mathrm{ref}}} & \frac{\partial P_1}{\partial E_2^{\mathrm{ref}}} \\ \frac{\partial E_1}{\partial i_{\mathrm{d}_1}^{\mathrm{ref}}} & \frac{\partial E_1}{\partial i_{\mathrm{q}_1}^{\mathrm{ref}}} & \frac{\partial E_1}{\partial P_2^{\mathrm{ref}}} & \frac{\partial E_1}{\partial E_2^{\mathrm{ref}}} \\ \frac{\partial P_2}{\partial i_{\mathrm{d}_1}^{\mathrm{ref}}} & \frac{\partial P_2}{\partial i_{\mathrm{q}_1}^{\mathrm{ref}}} & \frac{\partial P_2}{\partial P_2^{\mathrm{ref}}} & \frac{\partial P_2}{\partial E_2^{\mathrm{ref}}} \\ \frac{\partial E_2}{\partial i_{\mathrm{d}_1}^{\mathrm{ref}}} & \frac{\partial E_2}{\partial i_{\mathrm{q}_1}^{\mathrm{ref}}} & \frac{\partial E_2}{\partial P_2^{\mathrm{ref}}} & \frac{\partial E_2}{\partial E_2^{\mathrm{ref}}} \end{bmatrix}}_{\boldsymbol{H}^{\mathrm{com}}} \begin{bmatrix} \Delta i_{\mathrm{d}_1}^{\mathrm{ref}} \\ \Delta i_{\mathrm{q}_1}^{\mathrm{ref}} \\ \Delta P_2^{\mathrm{ref}} \\ \Delta E_2^{\mathrm{ref}} \end{bmatrix} \tag{7.64}$$

The system strength is again set such that the steady-state voltages at the local PCCs have high phases relative to the voltage at the slack bus when the converters operate at $P_{\zeta,0} = 0.7$ p.u..

In the weak system case, the ability of the slack bus to aid the performance of converter one (using dq-axis vector current control) is compromised. Since converter two uses power synchronization control, it is capable of behaving as an effective voltage source. Figures 7.29 - 7.34 show the performance of the system for a variety of operating points. In all cases, the voltage at the PCC is strongly influenced by the voltage controller of converter two. In fact, the voltage loop of converter two has more impact on the voltage at the PCC of converter one than does the q-component current control loop of converter one.

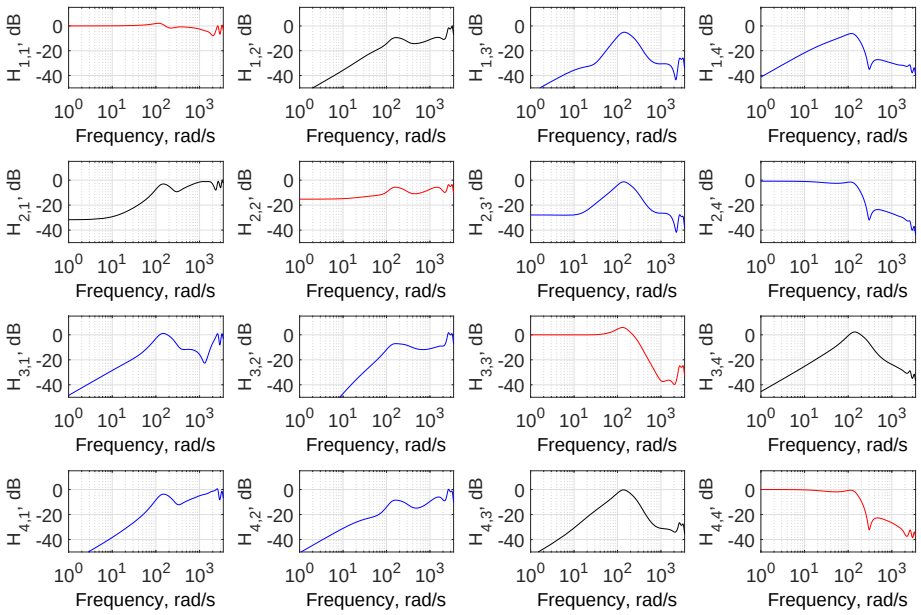

Figure 7.29: $\boldsymbol{H}^{\text{com}}$ evaluated when $P_{1,0} = 0.00$ p.u. and $P_{2,0} = 0.70$ p.u. Bode magnitude response only.

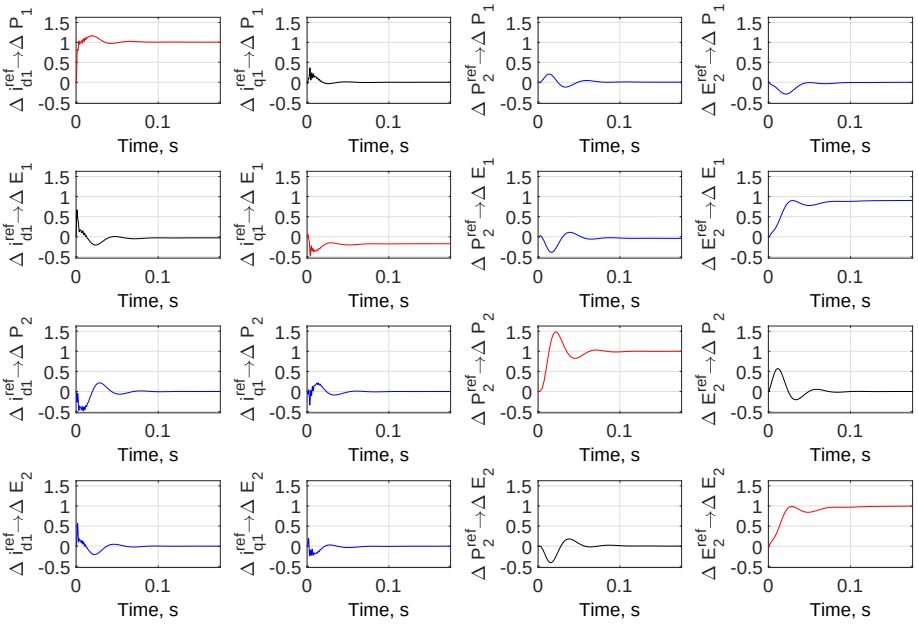

Figure 7.30: Normalised responses to small step changes in the reference values. System evaluated when $P_{1,0} = 0.00$ p.u. and $P_{2,0} = 0.70$ p.u.

When $P_{1,0} = 0.50$ p.u. and $P_{2,0} = 0.70$ p.u., the voltage at the filter bus of converter one has a phase of 43.8490 degrees relative to the slack bus, while the voltage at the filter bus of converter two has a phase of 44.9753 relative to the slack bus. For this operating point, when all converters use dq-axis vector current control, the large phase differences between the filter bus voltages and slack bus was shown to be associated with ill-conditioning and poor performance at the current level (see figures 7.9 and 7.10). However, as can be seen in figures 7.31 and 7.32, the performance of converter one, which uses dq-axis vector current control, is improved.

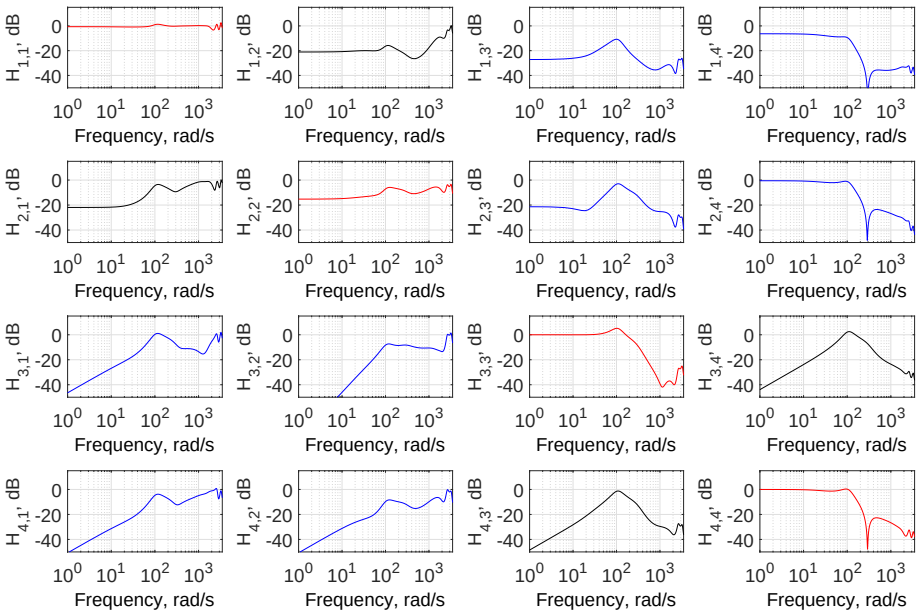

Figure 7.31: $\boldsymbol{H}^{\text{com}}$ evaluated when $P_{1,0} = 0.50$ p.u. and $P_{2,0} = 0.70$ p.u. Bode magnitude response only.

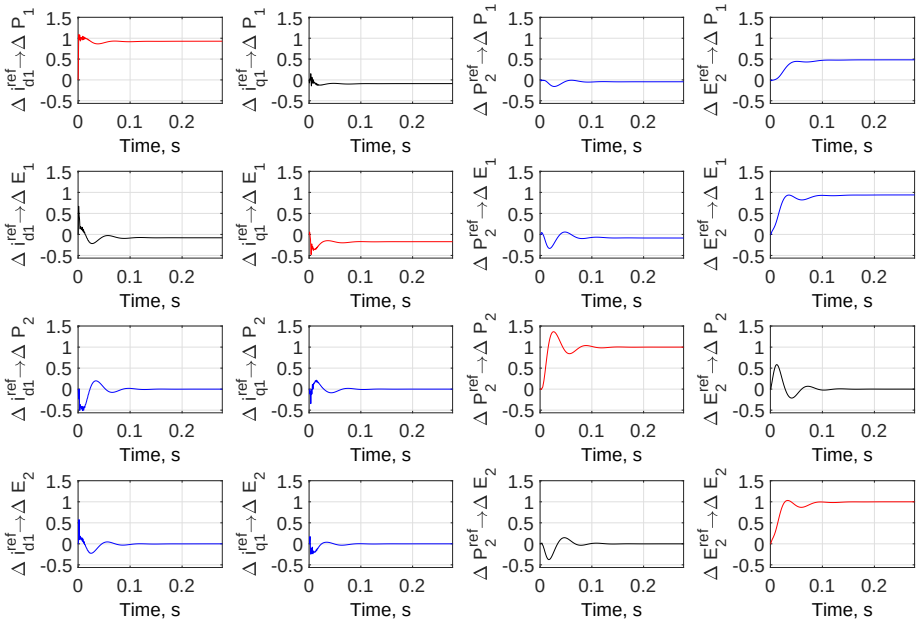

Figure 7.32: Normalised responses to small step changes in the reference values. System evaluated when $P_{1,0} = 0.50$ p.u. and $P_{2,0} = 0.70$ p.u.

In the final operating point considered in this section, the converters are both operating at 0.7p.u. active power in steady-state. With the definition of the wider network transmission line, this

corresponds to the voltages at the local PCCs both being 57.2558 degrees.

For this operating point, it can clearly be observed that converter two essentially becomes the voltage source/slack bus from the perspective of converter one. Consequently, the response of power output of converter one is positively affected by the presence of converter two (using power synchronization control). Unity response in P_1 to a unit change in $i_{\mathrm{d}_1}^{\mathrm{ref}}$ is not observed; however, P_1 is predominantly determined by $i_{\mathrm{d}_1}^{\mathrm{ref}}$, which is as desired. As will be shown, the response of P_1 to changes in $i_{\mathrm{d}_1}^{\mathrm{ref}}$ can be further boosted by introducing additional instances of power synchronization control into the system; this will also be accompanied by a reduction in $\partial P_1/\partial E_2^{\mathrm{ref}}$.

In addition, figure 7.34 shows that $\partial E_1/\partial i_{\mathrm{d}_1}^{\mathrm{ref}}$ is much weaker than observed in figure 7.12, indicative of improved system conditioning.

It is also important to stress that converter one is not able to regulate its own voltage effectively (compare $\partial E_1/\partial i_{\mathrm{q}_1}^{\mathrm{ref}}$ with $\partial E_1/\partial E_2^{\mathrm{ref}}$ in figures 7.33 and 7.34). Thus, conventional dq-axis vector current control can only really be used as a current source, with the q-component current control loop being used to regulate the reactive power output of the converter. In this sense, converter one is a slave and converter two is a master.

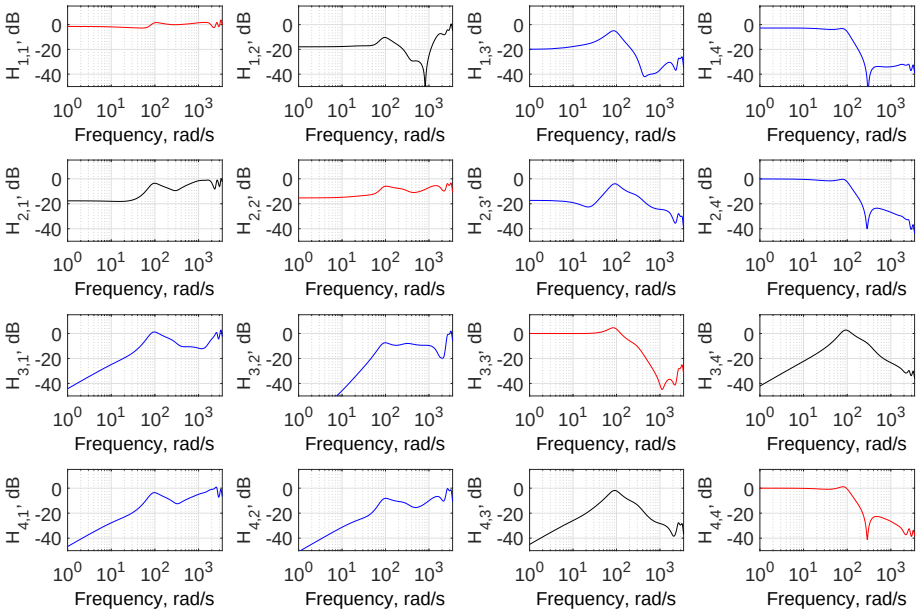

Figure 7.33: $\boldsymbol{H}^{\mathrm{com}}$ evaluated when $P_{1,0} = 0.70$ p.u. and $P_{2,0} = 0.70$ p.u. Bode magnitude response only.

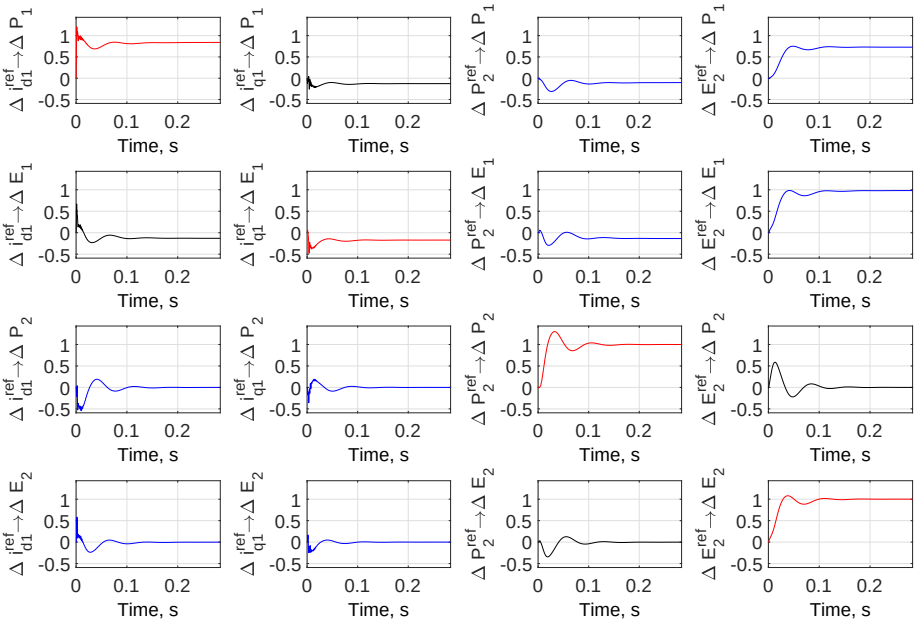

Figure 7.34: Normalised responses to small step changes in the reference values. System evaluated when $P_{1,0} = 0.70$ p.u. and $P_{2,0} = 0.70$ p.u.

Five converters: one using dq-axis vector current control, four using power synchronization control

Let us now consider the case where four converters use the power synchronization control algorithm and another uses dq-axis vector current control. In this case, the transfer function matrix is as

follows:

$$\boldsymbol{H}^{\text{com}} = \begin{bmatrix} \frac{\partial P_1}{\partial i_{\text{d}_1}^{\text{ref}}} & \frac{\partial P_1}{\partial i_{\text{q}_1}^{\text{ref}}} & \frac{\partial P_1}{\partial P_2^{\text{ref}}} & \frac{\partial P_1}{\partial E_2^{\text{ref}}} & \frac{\partial P_1}{\partial P_3^{\text{ref}}} & \frac{\partial P_1}{\partial E_3^{\text{ref}}} & \frac{\partial P_1}{\partial P_4^{\text{ref}}} & \frac{\partial P_1}{\partial E_4^{\text{ref}}} & \frac{\partial P_1}{\partial P_5^{\text{ref}}} & \frac{\partial P_1}{\partial E_5^{\text{ref}}} \\ \frac{\partial E_1}{\partial i_{\text{d}_1}^{\text{ref}}} & \frac{\partial E_1}{\partial i_{\text{q}_1}^{\text{ref}}} & \frac{\partial E_1}{\partial P_2^{\text{ref}}} & \frac{\partial E_1}{\partial E_2^{\text{ref}}} & \frac{\partial E_1}{\partial P_3^{\text{ref}}} & \frac{\partial E_1}{\partial E_3^{\text{ref}}} & \frac{\partial E_1}{\partial P_4^{\text{ref}}} & \frac{\partial E_1}{\partial E_4^{\text{ref}}} & \frac{\partial E_1}{\partial P_5^{\text{ref}}} & \frac{\partial E_1}{\partial E_5^{\text{ref}}} \\ \frac{\partial p_2}{\partial i_{\text{d}_1}^{\text{ref}}} & \frac{\partial P_2}{\partial i_{\text{q}_1}^{\text{ref}}} & \frac{\partial P_2}{\partial P_2^{\text{ref}}} & \frac{\partial P_2}{\partial E_2^{\text{ref}}} & \frac{\partial P_2}{\partial P_3^{\text{ref}}} & \frac{\partial P_2}{\partial E_3^{\text{ref}}} & \frac{\partial P_2}{\partial P_4^{\text{ref}}} & \frac{\partial P_2}{\partial E_4^{\text{ref}}} & \frac{\partial P_2}{\partial P_5^{\text{ref}}} & \frac{\partial P_2}{\partial E_5^{\text{ref}}} \\ \frac{\partial E_2}{\partial i_{\text{d}_1}^{\text{ref}}} & \frac{\partial E_2}{\partial i_{\text{q}_1}^{\text{ref}}} & \frac{\partial E_2}{\partial P_2^{\text{ref}}} & \frac{\partial E_2}{\partial E_2^{\text{ref}}} & \frac{\partial E_2}{\partial P_3^{\text{ref}}} & \frac{\partial E_2}{\partial E_3^{\text{ref}}} & \frac{\partial E_2}{\partial P_4^{\text{ref}}} & \frac{\partial E_2}{\partial E_4^{\text{ref}}} & \frac{\partial E_2}{\partial P_5^{\text{ref}}} & \frac{\partial E_2}{\partial E_5^{\text{ref}}} \\ & & & & \vdots & & & & & \\ & & & & \vdots & & & & & \\ \frac{\partial P_5}{\partial i_{\text{d}_1}^{\text{ref}}} & \frac{\partial P_5}{\partial i_{\text{q}_1}^{\text{ref}}} & \frac{\partial P_5}{\partial P_2^{\text{ref}}} & \frac{\partial P_5}{\partial E_2^{\text{ref}}} & \frac{\partial P_5}{\partial P_3^{\text{ref}}} & \frac{\partial P_5}{\partial E_3^{\text{ref}}} & \frac{\partial P_5}{\partial P_4^{\text{ref}}} & \frac{\partial P_5}{\partial E_4^{\text{ref}}} & \frac{\partial P_5}{\partial P_5^{\text{ref}}} & \frac{\partial P_5}{\partial E_5^{\text{ref}}} \\ \frac{\partial E_5}{\partial i_{\text{d}_1}^{\text{ref}}} & \frac{\partial E_5}{\partial i_{\text{q}_1}^{\text{ref}}} & \frac{\partial E_5}{\partial P_2^{\text{ref}}} & \frac{\partial E_5}{\partial E_2^{\text{ref}}} & \frac{\partial E_5}{\partial P_3^{\text{ref}}} & \frac{\partial E_5}{\partial E_3^{\text{ref}}} & \frac{\partial E_5}{\partial P_4^{\text{ref}}} & \frac{\partial E_5}{\partial E_4^{\text{ref}}} & \frac{\partial E_5}{\partial P_5^{\text{ref}}} & \frac{\partial E_5}{\partial E_5^{\text{ref}}} \end{bmatrix} \tag{7.65}$$

Only one operating point is considered for brevity reasons; this is where all converters are operating at 0.7 p.u. active power with the network line defined such that each filter bus voltage has a phase of 57.2558 degrees relative to the slack bus (to facilitate comparisons with the two-converter system results).

Due to this definition, all converters using the power synchronization controller respond to changes in reference values in the same fashion. For this reason, only the first four columns and first four rows are shown along with columns five and six from rows three and four. The latter set are included to observe the influence of one converter using power synchronization control on another using power synchronization control also. Note - in spite of the condensed results presented, the model was initialised and run with five converters to ensure no coupling was omitted.

The time domain plots also show that the steady-state error left in the power output of converter one following a unit change in $i_{\text{d}_1}^{\text{ref}}$ is smaller. The final value is 0.921 (as opposed to 0.84 in the previous subsection of section 7.3.3). Again, note how terms such as $\partial E_1/\partial i_{\text{d}_1}^{\text{ref}}$ have no power associated with them, which is an indicator of the system conditioning improving. Given results

published in literature [5], it should be possible for a conventional dq-axis vector current controller *with* standard outer controllers to accommodate for this error.

As more converters which behave like true voltage sources are added to the power system, the performance of existing converters that use dq-axis vector current control is bolstered, allowing the latter to operate closer to their rated power than they would otherwise have been able to do so. This can be observed in figures 7.35 and 7.36.

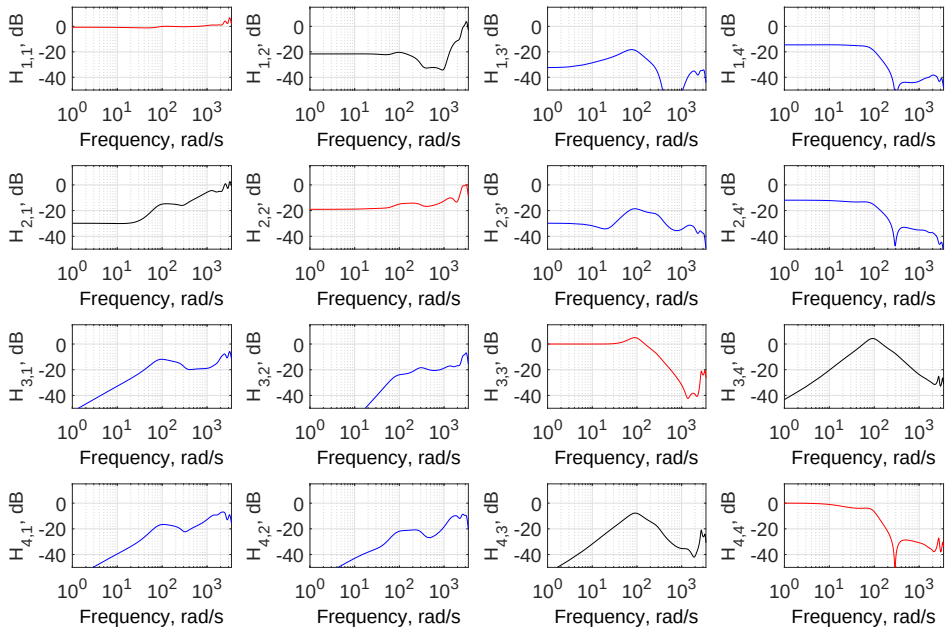

Figure 7.35: First four rows and four columns of $\boldsymbol{H}^{\text{com}}$ evaluated when all five converters are operating at 0.7p.u. Converter one uses dq-axis vector current control, while all other converters use power synchronization control. Bode magnitude response only.

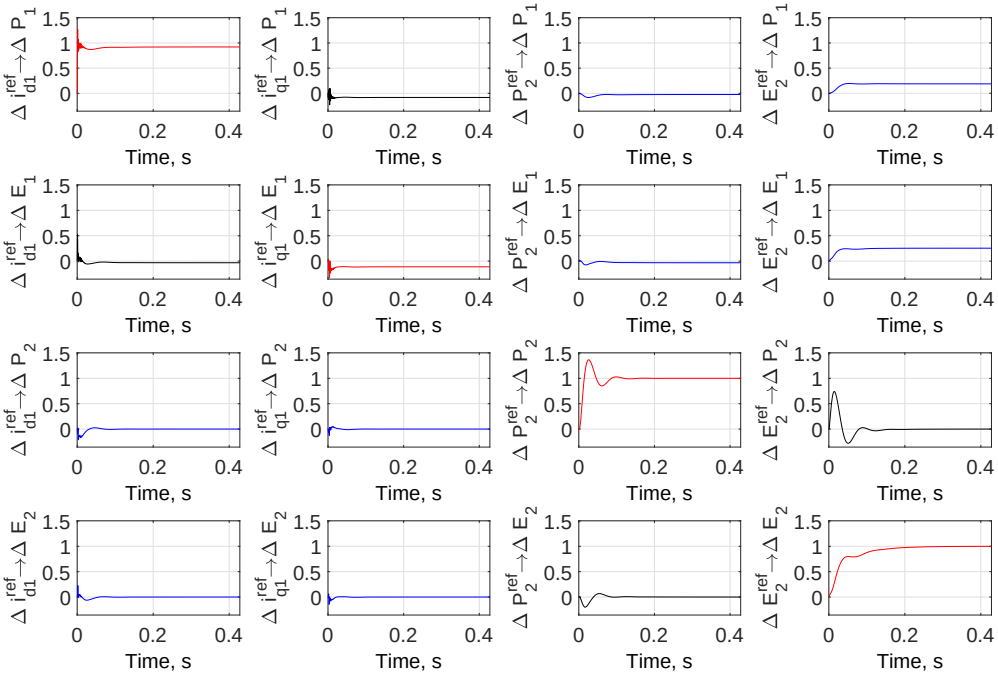

Figure 7.36: Normalised response of output variables related to converters one and two following changes in reference values in the controllers of converters one and two.

With just two converters, one using dq-axis vector current control and the other using power synchronization control, the former is exclusively a slave to one converter. However, as can be seen, in the multi-converter system, the converter which uses dq-axis vector current control is *jointly supported* by all effective voltage sources. This also means that as more and more converters which behave in a manner similar to one using power synchronization control are introduced, the stability of the dq-axis vector current controlled converter is no longer tied exclusively to the connection of a single converter which behaves as an effective voltage source. This is desirable from a fault performance perspective. This can be seen in figure 7.37.

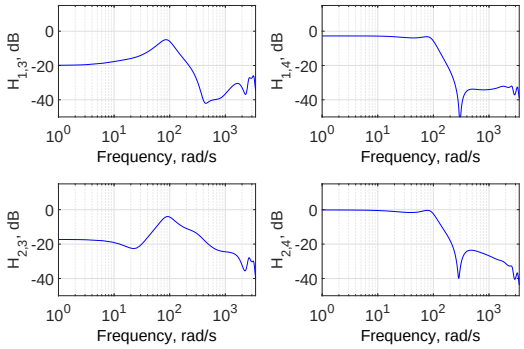

(a) Response of outputs of converter one (using dq-axis vector current control) to changes in set points on converter two (using power synchronization control) in a system comprising two converters, one of which use power synchronization control.

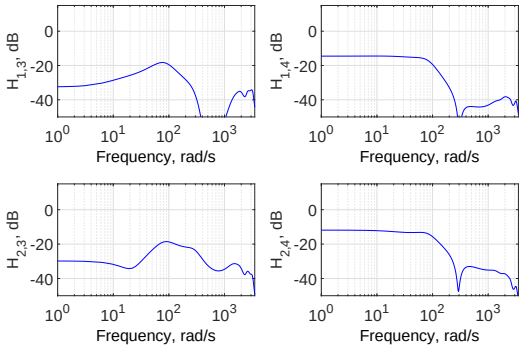

(b) Response of outputs of converter one (using dq-axis vector current control) to changes in set points on converter two (using power synchronization control) in a system comprising five converters, four of which use power synchronization control.

Figure 7.37: Sensitivity of a converter using dq-axis vector current control to power synchronization control for two- and five- converter systems. In the former, one converter uses power synchronization control, while in the latter, four use power synchronization control.

At this point, the issue which should require attention is the coupling between power and voltage control loops in the converters that use power synchronization control (or some other virtual synchronous machine controller). This can be observed in figure 7.38. To reiterate comments from the previous section (7.3.2), given the fact that the peak response in the relevant off-main diagonal elements occur at a frequency of around 100 rad/s irrespective of either the short-circuit ratio (see chapter three) or the number of power-synchronization-controlled converters, it would appear that the coupling is in some senses internalised, which would allow for a suitable controller which effectively targets this coupling to be developed.

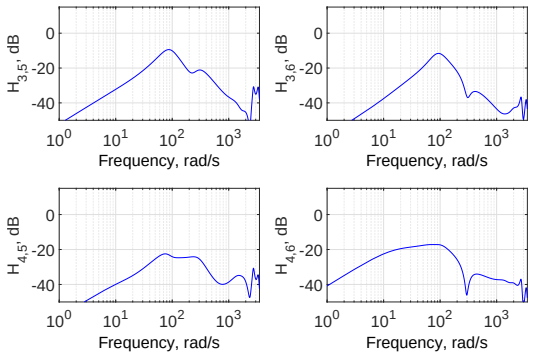

Figure 7.38: Illustration of the coupling between two instances of power synchronization control in the five converter system.

7.4 Including local loads

In this section, the effect of local loads is assessed. For brevity, only two operating points are considered: one of a five-converter system connected to a strong wider network, and one of the same five-converter system connected to a weak wider network. In both cases, all converters operate at 0.9 p.u. to focus on the problematic operating region for dq-axis vector current control. On top of this, each local line has the same local load as all other lines, set to 2.125 p.u.

7.4.1 DQ-axis vector current control only

For each operating point, Bode and time traces are presented, respectively showing the frequency and time domain results from evaluation of the linear model at this operating point. From left to right, the top row of both figures show the response (either in the frequency domain or time domain) of the active power output, P_1, of converter one to changes in the control variables, $i_{\mathrm{d}_1}^{\mathrm{ref}}$, $i_{\mathrm{q}_1}^{\mathrm{ref}}$, $i_{\mathrm{d}_2}^{\mathrm{ref}}$ and $i_{\mathrm{q}_2}^{\mathrm{ref}}$. From left to right, the second row of both figures show the response (either in the frequency domain or time domain) of the voltage magnitude at the filter bus of converter one, E_1, to changes in the control variables, $i_{\mathrm{d}_1}^{\mathrm{ref}}$, $i_{\mathrm{q}_1}^{\mathrm{ref}}$, $i_{\mathrm{d}_2}^{\mathrm{ref}}$ and $i_{\mathrm{q}_2}^{\mathrm{ref}}$. From left to right, the third row of both figures show the response (either in the frequency domain or time domain) of the active power output of converter two, P_2, to changes in the control variables, $i_{\mathrm{d}_1}^{\mathrm{ref}}$, $i_{\mathrm{q}_1}^{\mathrm{ref}}$, $i_{\mathrm{d}_2}^{\mathrm{ref}}$ and $i_{\mathrm{q}_2}^{\mathrm{ref}}$. Finally, from left to right, the fourth row of both figures show the response (either in the frequency domain or

time domain) of the voltage magnitude at the filter bus of converter two, E_2, to changes in the control variables, $i_{\mathrm{d}_1}^{\mathrm{ref}}$, $i_{\mathrm{q}_1}^{\mathrm{ref}}$, $i_{\mathrm{d}_2}^{\mathrm{ref}}$ and $i_{\mathrm{q}_2}^{\mathrm{ref}}$. The other Bode and time domain plots, covering the other converters, are not shown given the symmetry of the system.

Strong AC systems

In the first system, the definition of the system is such that the steady-state angle of the voltage at the filter bus of converter one is 12.7858 degrees relative to the slack bus. This performance of this system is shown in figures 7.39 and 7.40. Figures 7.39 and 7.40 both show the system to be well-conditioned at the current control level, implying that there will be no major issues associated with designing and tuning outer controllers. It can be seen that the active power output of converter one is almost solely affected by $i_{\mathrm{d}_1}^{\mathrm{ref}}$. Some very small influence can be seen from changing the other reference values; however, this is to be expected and should not cause any issue. By extension, the active power output of converter two behaves as desired. Weak responses to E_1 and E_2 are to be expected since the wider network is strong. To cause a converter using dq-axis vector current control to have a significant impact on the voltage, an outer AC voltage magnitude controller will need to be introduced as expected.

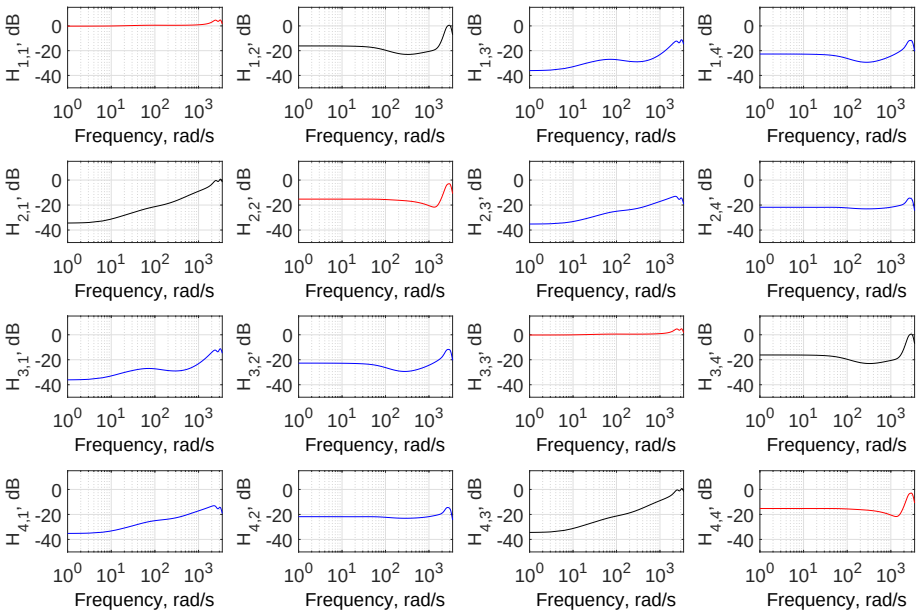

Figure 7.39: $\boldsymbol{H}^{\text{com}}$ evaluated when all converters are operating at 0.7p.u. Bode magnitude response only (with the response given in dB).

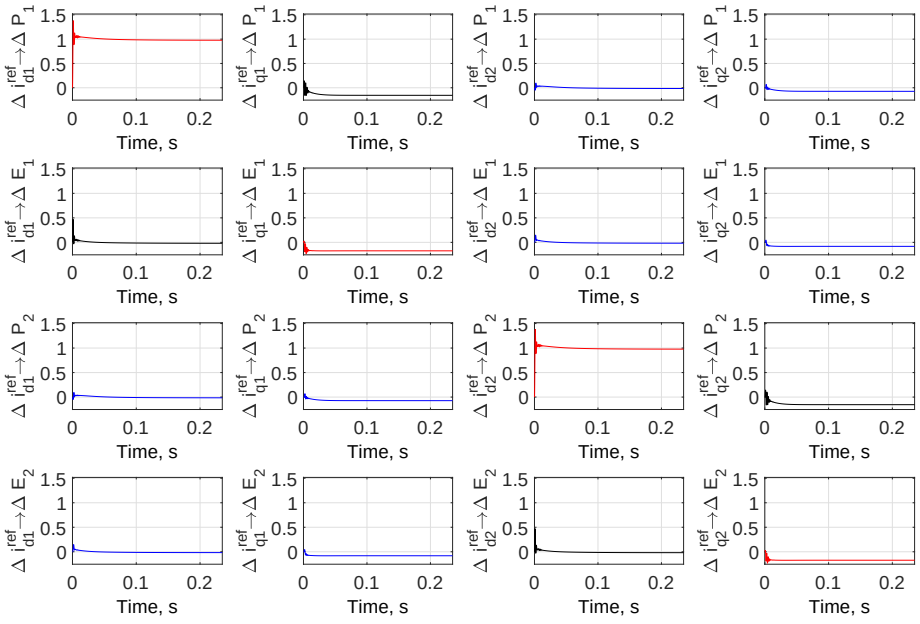

Figure 7.40: Normalised response of output variables relevant to converters one and two following changes in reference values in the controllers of converters one and two.

Weak AC systems

In the second system, the definition of the system is such that the steady-state angle of the voltage at the filter bus of converter one is 40.5909 degrees relative to the slack bus. The performance of this system is shown in figures 7.41 and 7.42. Figures 7.41 and 7.42 both show the system to be ill-conditioned at the current control level, implying that there will be major issues associated with designing and tuning outer controllers. Strong coupling can be seen between all reference variables and output variables. This is due to the voltage weakness, which was also seen in chapter 4 and section 7.3.1 of this chapter. The voltage weakness is why $i_{\mathrm{d}_2}^{\mathrm{ref}}$ is able to have a larger impact on P_1 than is $i_{\mathrm{d}_1}^{\mathrm{ref}}$. Thus, for systems including local loads, there are two sources of undesirable coupling arising from voltage weakness: that between control loops in a single converter, and that between control loops between converters. The latter introduces an additional degree of freedom that would be difficult to compensate for with outer controllers across the full operating envelope.

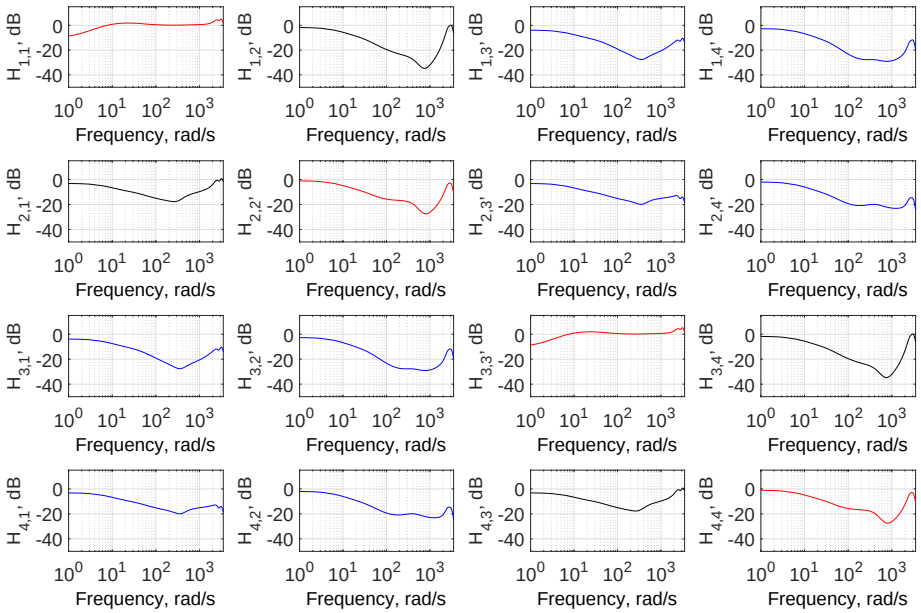

Figure 7.41: $\boldsymbol{H}^{\mathrm{com}}$ evaluated when all converters are operating at 0.7p.u. Bode magnitude response only (with the response given in dB).

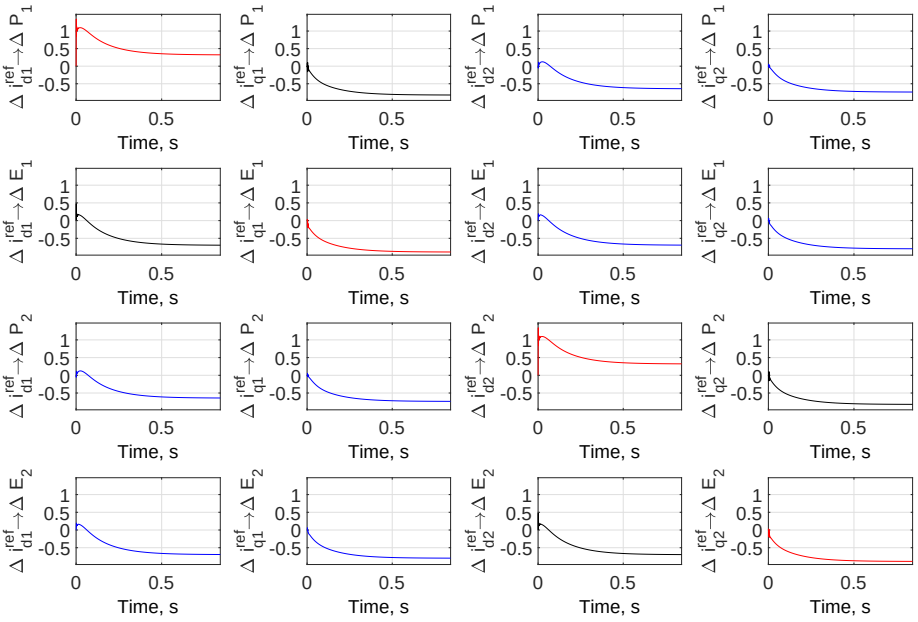

Figure 7.42: Normalised response of output variables relevant to converters one and two following changes in reference values in the controllers of converters one and two.

7.4.2 Power synchronization control only

For each operating point, Bode and time traces are presented, respectively showing the frequency and time domain results from evaluation of the linear model at this operating point. From left to right, the top row of both figures show the response (either in the frequency domain or time domain) of the active power output, P_1, of converter one to changes in the control variables, P_1^{ref}, E_1^{ref}, P_2^{ref} and E_2^{ref}. From left to right, the second row of both figures show the response (either in the frequency domain or time domain) of the voltage magnitude at the filter bus of converter one, E_1, to changes in the control variables, P_1^{ref}, E_1^{ref}, P_2^{ref} and E_2^{ref}. From left to right, the third row of both figures show the response (either in the frequency domain or time domain) of the active power output of converter two, P_2, to changes in the control variables, P_1^{ref}, E_1^{ref}, P_2^{ref} and E_2^{ref}. Finally, from left to right, the fourth row of both figures show the response (either in the frequency domain or time domain) of the voltage magnitude at the filter bus of converter two, E_2, to changes in the control variables, P_1^{ref}, E_1^{ref}, P_2^{ref} and E_2^{ref}. The other Bode and time domain plots, covering the other converters, are not shown given the symmetry of the system.

Strong AC systems

In the first system, the definition of the system is such that the steady-state angle of the voltage at the filter bus of converter one is 12.7858 degrees relative to the slack bus. This performance of this system is shown in figures 7.43 and 7.44. Figures 7.43 and 7.44 both show the system to be well-conditioned. Oscillatory behaviour can be observed, particularly from $E^{\text{ref}\zeta}$ to P_ζ. As with the multi-converter system with no local loads, this coupling is strongest around 100 rad/s. This coupling arises from the fact that multiple effective voltage regulators, including the slack bus, are in electrical proximity to each other. Moreover, considering that power flow across a reactance is proportional to both the voltage at each end of the line and the sine of the phase difference between said voltages, it is unsurprising to see a strong coupling between the voltage regulator and the power output. This phenomenon will require more attention in the future if multiple instances of virtual synchronous machines are to be installed.

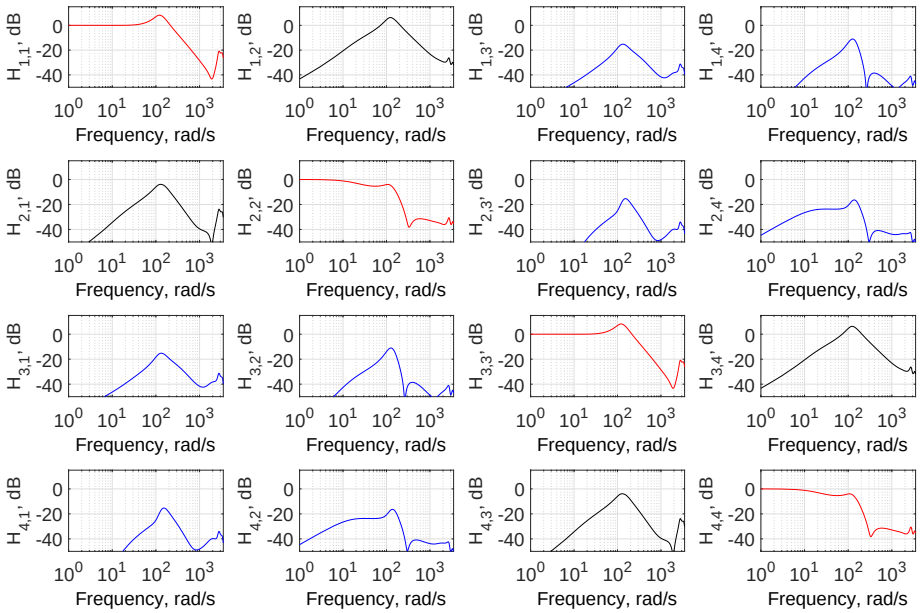

Figure 7.43: $\boldsymbol{H}^{\text{com}}$ evaluated when all converters are operating at 0.7p.u. Bode magnitude response only (with the response given in dB).

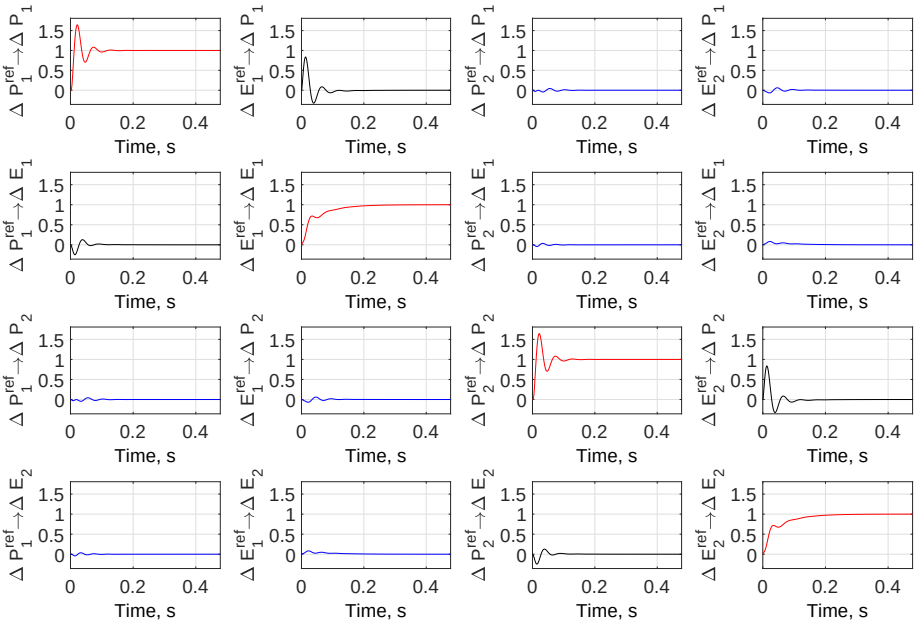

Figure 7.44: Normalised response of output variables relevant to converters one and two following changes in reference values in the controllers of converters one and two.

Weak AC systems

In the first system, the definition of the system is such that the steady-state angle of the voltage at the filter bus of converter one is 12.7858 degrees relative to the slack bus. This performance of this system is shown in figures 7.45 and 7.46. Figures 7.45 and 7.46 both show the system to be well-conditioned. Oscillatory behaviour can still be observed from E^{ref_ζ} to P_ζ. As with the multi-converter system with no local loads, this coupling is strongest around 100 rad/s. This coupling persists in the weak system because of the fact that there are still multiple effective voltage regulators in electrical proximity to each other i.e. the converters using power synchronization control.

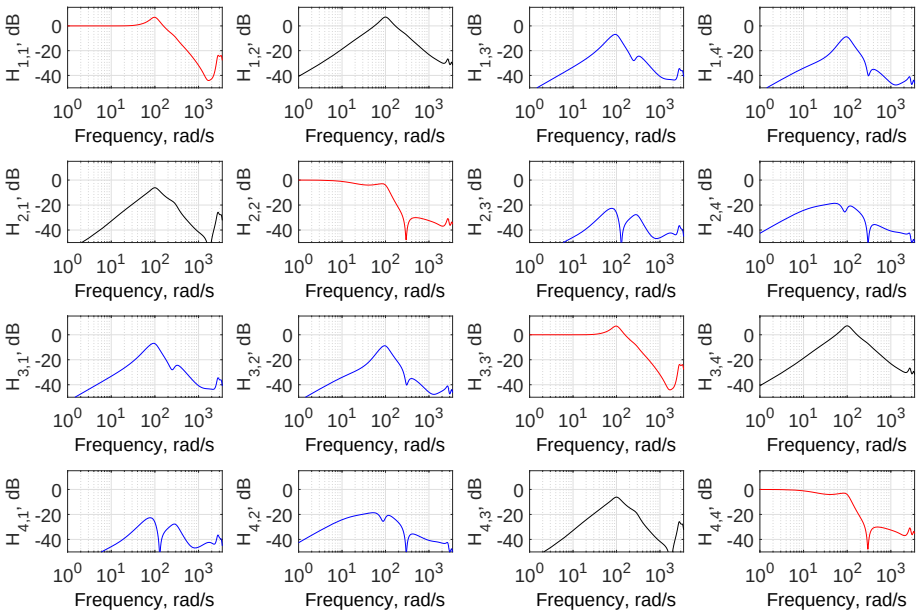

Figure 7.45: First four rows and four columns of $\boldsymbol{H}^{\text{com}}$ evaluated when all converters are operating at 0.9 p.u. Bode magnitude response only (with the response given in dB).

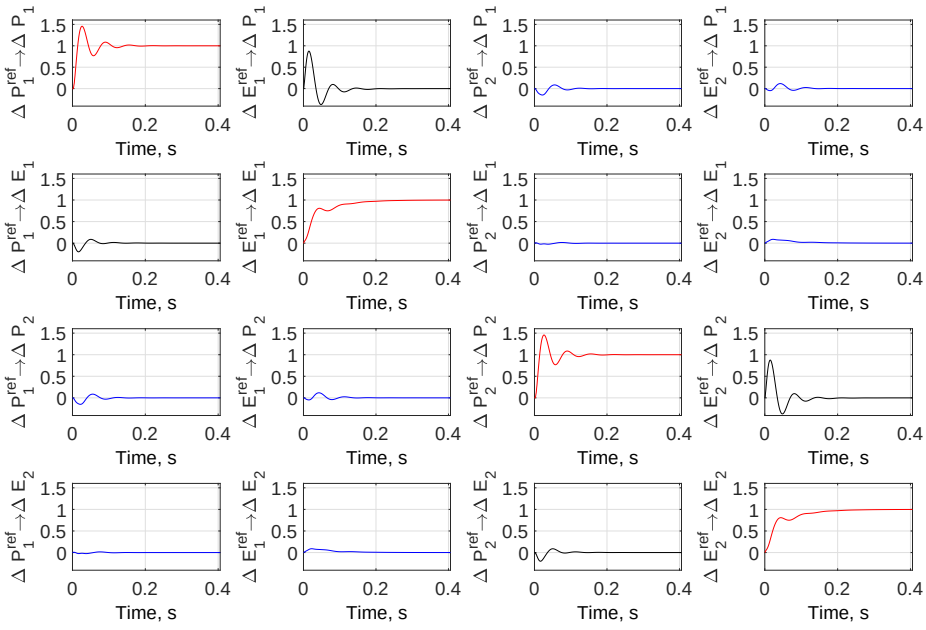

Figure 7.46: Normalised response of output variables relevant to converters one and two following changes in reference values in the controllers of converters one and two.

7.4.3 Mixture of controllers

For each operating point, Bode and time traces are presented, respectively showing the frequency and time domain results from evaluation of the linear model at this operating point. From left to right, the top row of both figures show the response (either in the frequency domain or time domain) of the active power output, P_1, of converter one to changes in the control variables, $i_{\mathrm{d}_1}^{\mathrm{ref}}$, $i_{\mathrm{q}_1}^{\mathrm{ref}}$, $i_{\mathrm{d}_2}^{\mathrm{ref}}$ and $i_{\mathrm{q}_2}^{\mathrm{ref}}$. From left to right, the second row of both figures show the response (either in the frequency domain or time domain) of the voltage magnitude at the filter bus of converter one, E_1, to changes in the control variables, $i_{\mathrm{d}_1}^{\mathrm{ref}}$, $i_{\mathrm{q}_1}^{\mathrm{ref}}$, P_2^{ref} and E_2^{ref}. From left to right, the third row of both figures show the response (either in the frequency domain or time domain) of the active power output of converter two, P_2, to changes in the control variables, $i_{\mathrm{d}_1}^{\mathrm{ref}}$, $i_{\mathrm{q}_1}^{\mathrm{ref}}$, P_2^{ref} and E_2^{ref}. Finally, from left to right, the fourth row of both figures show the response (either in the frequency domain or time domain) of the voltage magnitude at the filter bus of converter two, E_2, to changes in the control variables, $i_{\mathrm{d}_1}^{\mathrm{ref}}$, $i_{\mathrm{q}_1}^{\mathrm{ref}}$, P_2^{ref} and E_2^{ref}. The other Bode and time domain plots, covering the other converters, are not shown given the symmetry of the system.

Strong AC systems

In the strong system case, converter one, using dq-axis vector current control, can rely on both the converters using power synchronization control (converters two, three, four and five) along with the slack bus to provide a stiff voltage at the filter bus of converter one, yielding good performance in the dq-axis vector current controller. Some oscillatory behaviour can be observed in the power synchronization control scheme, primarily due to $\partial P/\partial E^{\mathrm{ref}}$. Again, the strongest response occurs around 100 rad/s.

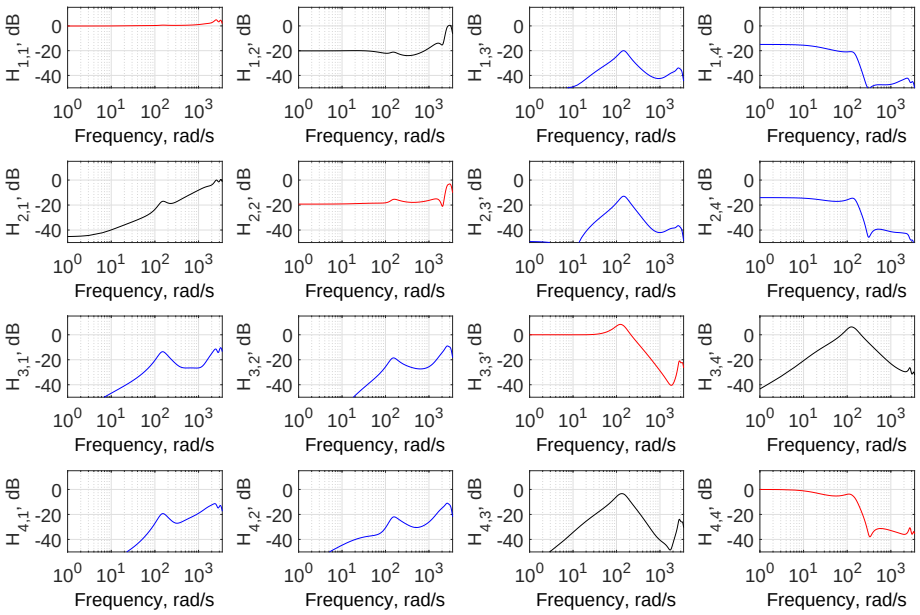

Figure 7.47: $\boldsymbol{H}^{\text{com}}$ evaluated when all converters are operating at 0.7p.u. Bode magnitude response only (with the response given in dB).

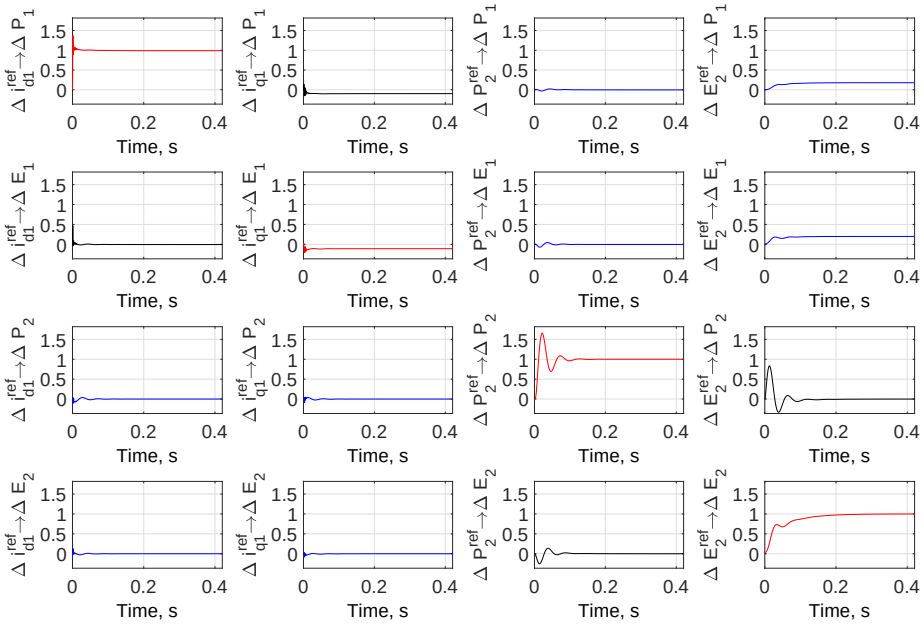

Figure 7.48: Normalised response of output variables relevant to converters one and two following changes in reference values in the controllers of converters one and two.

Weak AC systems

As observed when there were no local loads, the converters using power synchronization control are able to provide voltage support, which allows the PLL in the dq-axis current controller on converter one to perform satisfactorily, which leads to good overall performance. Again, note how a single instance of power synchronization control does not, on its own, impact heavily on the output of converter one (which uses dq-axis vector current control).

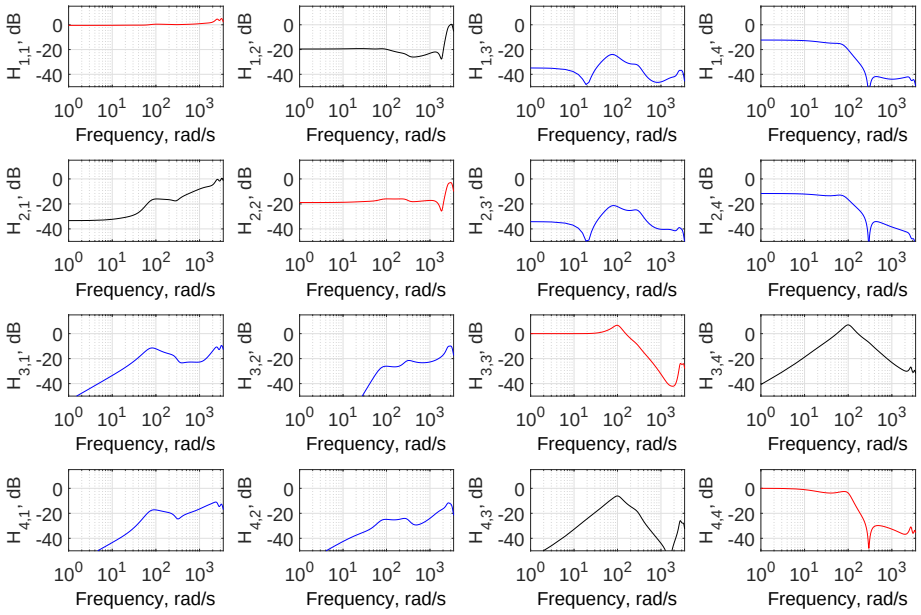

Figure 7.49: $\boldsymbol{H}^{\text{com}}$ evaluated when all converters are operating at 0.7p.u. Bode magnitude response only (with the response given in dB).

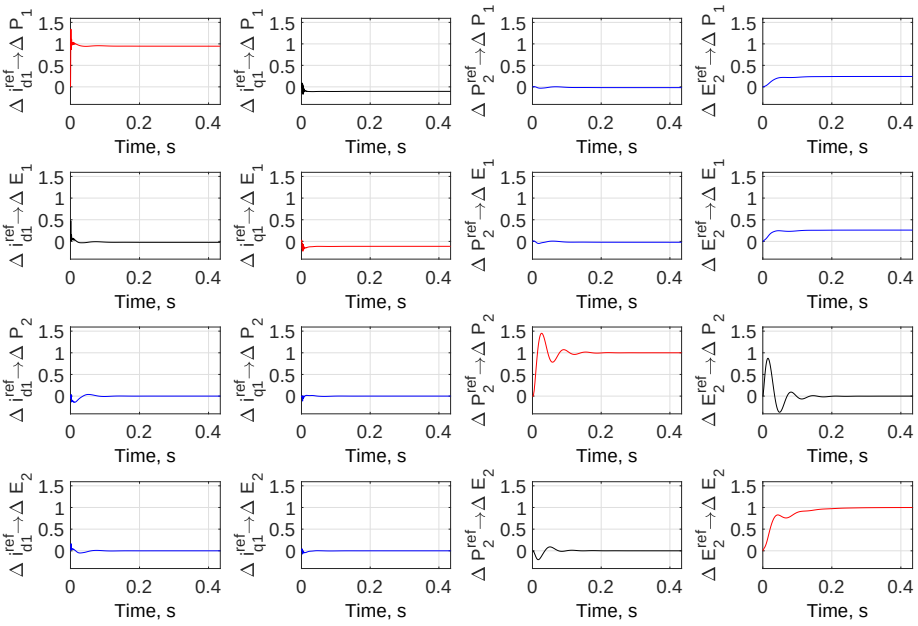

Figure 7.50: Normalised response of output variables relevant to converters one and two following changes in reference values in the controllers of converters one and two.

As with multi-converter systems without local loads, there are simply too many operating points to consider. In other words, some topologies will feature local loads of a certain nature that permits desirable behaviour of the inner current controllers. A thorough evaluation of such operating points is left as future work. The linear model herein described, however, should significantly aid the evaluation of said operating points.

7.5 Summary

In this chapter, linearised models developed in the previous chapters have been extended to analyse multi-converter systems. The models presented in this chapter have the following properties:

1. Modular and scalable - By adopting a modular approach to the modelling, the model can easily be implemented in a way that is not system specific i.e. the number of converters in the system does not need to be set at the start of the analysis.

2. Automatic - Often, researchers create non-unified linear models of a plant and controller, be-

fore using software such as Simulink to evaluate the closed-loop performance. By unifying the controller(s) and plant, there is no need to use external software; all feedback is automatically self-contained in the state-space matrices.

3. Fast - While not novel, speed is important for engineers. Even when using MATLAB, a global operating point (an ensemble of the local points of all converters) for an eight-converter system could be evaluated in seven seconds; in C++, the equivalent process took less than one second if BLAS is fully utilised. If an algorithm scales (speed-wise) better than another, it allows researchers, manufacturers and transmission system operators to study more complex systems more quickly and easily.

4. Flexible - Given controllers will vary from manufacturer to manufacturer, real systems will have mixtures of controllers; thus, the models presented in this chapter were developed specifically to allow for such system realisations. In addition, the models have the ability to assess the impact of local loads on small signal stability.

It was shown that the performance of a converter using the dq-axis vector current control algorithm is heavily dependent on external influences. This could be system short-circuit ratio or the presence of another converter in relative electrical proximity. For the two-converter system where both converters employed dq-axis vector current control, when one converter operated at a low power set point, said converter was able to provide some voltage stability that allows the other converter to operate in a more desirable manner than it would have been able to do when isolated. However, as both converters operate closer to their rated powers, this effect disappears.

Power synchronization control showed good performance in the multi-converter system when the converters were electrically isolated from a slack bus. However, converters which use power synchronization control and are in electrical proximity to one another may begin to experience virtual rotor oscillations.

Due to the present popularity of the dq-axis vector current control algorithm, systems containing a mixture of controllers were analysed. It was shown that including converters using the power synchronization control algorithm does improve the performance of the active power control of a converter using dq-axis vector current control, essentially by bringing voltage stability to otherwise

weak AC systems. The ability of the dq-axis vector current control scheme to regulate the local voltage was poor, being dominated by the influence of other converter controllers. In this sense, dq-axis vector current control behaves as a slave, with converters using power synchronization control behaving as masters.

Chapter 8

Conclusions & Future work

8.1 Conclusions

This work has shown the various challenges that are to be expected in coming years when converters represent larger parts of the network. Although wind turbine control engineers and even network operators believe frequency support to be the primary concern for networks, the service that will be demanded the most in the future is voltage support. Attempting to provide frequency support without first taking into account the issues surrounding voltage support can result in reduced overall stability. This could be inferred from the impact of adding outer loop controllers as was done in chapter 4.

In chapter 4, the limitations of the dq-axis vector current control algorithm in high impedance systems were explored. It was shown that the small-signal stability was strongly governed by the stiffness of the voltage at the measurement point. In addition, it was revealed that the dq-axis vector current control scheme may experience additional coupling issues when applied to MMC-HVDC systems; specifically, coupling may arise between the control loops and the PWM process. A linearised model suitable for integration to more complex systems was developed.

Chapter 5 featured an analysis of proportional resonant control in weak (high impedance) systems. It was found that proportional resonant control was particularly sensitive to low frequency system resonances.

A third algorithm, power synchronization control, was reviewed in chapter 6. Power synchronization control was found to be substantially less sensitive to the system impedance. Linearised models for studying both controllers were derived and properly validated using a frequency scanning technique.

In chapter 7, a unified linear state-space model was developed which has the following attributes:

1. High degree of modularity, which makes it readily scalable, which is desirable from a programming perspective
2. Unified dynamics of the plant and controllers active in the system, which makes it easy to determine the poles and zeros of the system without using any other software/codes.
3. Sufficiently flexible to handle different combinations of controllers, which will be of use to transmission system operators who have to consider system in which a mixture of controllers may be active at any one time.
4. Easily identifiable entry points, which makes it suitable for coupling with other codes that represent other parts of the system (DC bus(es) and, potentially, aerodynamic systems).

Using the unified linear state-space model, it was shown that by applying the power synchronisation control algorithm to a small number of appropriately placed converters in a power system, it was shown that the remaining converters, assumed to be controlled using the dq-axis vector current algorithm, could be stable at operating points that they would otherwise not have been.

8.2 Future work

Since it was shown that stability depends quite strongly on the capacity factors, a statistical model which represents the combined probabilities of wind profiles across GB and the British Isles could be developed. Integration of such a model would make it possible to identify which unstable operating points are likely, unlikely or have negligible chances of occurrence. If electric vehicles also become more prevalent, the statistical model could include user patterns for electric vehicles also.

In addition, an in-depth study of the dynamics of future power systems during a range of faults would be desirable. Future work could involve addressing frequency stability issues that are associated

with low inertia systems.

The development of more linearised state-space models of existing controllers would be desirable since this would add to the library, permitting more varied studies.

Bibliography

[1] M. P. Kazmierkowski and L. Malesani, "Current control techniques for three-phase voltage-source PWM converters: A survey," *IEEE Transactions on industrial electronics*, vol. 45, no. 5, pp. 691–703, 1998.

[2] M. Durrant, H. Werner, and K. Abbott, "Model of a VSC HVDC terminal attached to a weak AC system," in *Control Applications, 2003. CCA 2003. Proceedings of 2003 IEEE Conference on*, vol. 1, pp. 178–182, IEEE, 2003.

[3] L. Zhang, *Modeling and control of VSC-HVDC links connected to weak AC systems.* PhD thesis, KTH, 2010.

[4] L. Zhang, L. Harnefors, and H.-P. Nee, "Power-synchronization control of grid-connected voltage-source converters," *IEEE Transactions on Power systems*, vol. 25, no. 2, pp. 809–820, 2010.

[5] A. Egea-Alvarez, S. Fekriasl, F. Hassan, and O. Gomis-Bellmunt, "Advanced vector control for voltage source converters connected to weak grids," *IEEE Transactions on Power Systems*, vol. 30, no. 6, pp. 3072–3081, 2015.

[6] M. Ashabani and Y. A.-R. I. Mohamed, "Integrating VSCs to weak grids by nonlinear power damping controller with self-synchronization capability," *IEEE Transactions on Power Systems*, vol. 29, no. 2, pp. 805–814, 2014.

[7] K. Givaki and L. Xu, "Stability analysis of large wind farms connected to weak AC networks incorporating PLL dynamics," 2015.

[8] Q.-C. Zhong and G. Weiss, "Synchronverters: Inverters that mimic synchronous generators," *IEEE Transactions on Industrial Electronics*, vol. 58, no. 4, pp. 1259–1267, 2011.

[9] L. Zhang, L. Harnefors, and H.-P. Nee, "Modeling and control of VSC-HVDC links connected to island systems," *IEEE Transactions on Power Systems*, vol. 26, no. 2, pp. 783–793, 2011.

[10] N. Pogaku, M. Prodanovic, and T. C. Green, "Modeling, analysis and testing of autonomous operation of an inverter-based microgrid," *IEEE Transactions on power electronics*, vol. 22, no. 2, pp. 613–625, 2007.

[11] A. D. Banadaki, F. D. Mohammadi, and A. Feliachi, "State space modeling of inverter based microgrids considering distributed secondary voltage control," in *Power Symposium (NAPS), 2017 North American*, pp. 1–6, IEEE, 2017.

[12] R. Ierna, J. Zhu, A. J. Roscoe, M. Yu, A. Dysko, C. D. Booth, and H. Urdal, "Effects of VSM convertor control on penetration limits of non-synchronous generation in the GB power system," in *15th Wind Integration Workshop*, 2016.

[13] N. Mohan and T. M. Undeland, *Power electronics: converters, applications, and design*. John Wiley & Sons, 2007.

[14] P. Kundur, N. J. Balu, and M. G. Lauby, *Power system stability and control*, vol. 7. McGraw-hill New York, 1994.

[15] A. Lesnicar and R. Marquardt, "An innovative modular multilevel converter topology suitable for a wide power range," in *Power Tech Conference Proceedings, 2003 IEEE Bologna*, vol. 3, pp. 6—-pp, IEEE, 2003.

[16] R. Marquardt, "Modular Multilevel Converter: An universal concept for HVDC-Networks and extended DC-Bus-applications," in *Power Electronics Conference (IPEC), 2010 International*, pp. 502–507, IEEE, 2010.

[17] P. Rodriguez, R. Teodorescu, I. Candela, A. V. Timbus, M. Liserre, and F. Blaabjerg, "New positive-sequence voltage detector for grid synchronization of power converters under faulty grid conditions," in *Power Electronics Specialists Conference, 2006. PESC'06. 37th IEEE*, pp. 1–7, IEEE, 2006.

[18] J. Zhu, C. D. Booth, G. P. Adam, A. J. Roscoe, and C. G. Bright, "Inertia emulation control strategy for VSC-HVDC transmission systems," *IEEE Transactions on Power Systems*, vol. 28, no. 2, pp. 1277–1287, 2013.

[19] G. P. Adam, K. H. Ahmed, S. J. Finney, K. Bell, and B. W. Williams, "New breed of network fault-tolerant voltage-source-converter HVDC transmission system," *IEEE Transactions on Power Systems*, vol. 28, no. 1, pp. 335–346, 2013.

[20] S. Ademi and M. Jovanovic, "Vector control strategies for brushless doubly-fed reluctance wind generators," in *Environment Friendly Energies and Applications (EFEA), 2012 2nd International Symposium on*, pp. 44–49, IEEE, 2012.

[21] A. D. Giles, L. Reguera, and A. J. Roscoe, "Optimal controller gains for inner current controllers in VSC inverters," 2015.

[22] L. Harnefors and H.-P. Nee, "Model-based current control of AC machines using the internal model control method," *IEEE Transactions on Industry Applications*, vol. 34, no. 1, pp. 133–141, 1998.

[23] D. N. Zmood and D. G. Holmes, "Stationary frame current regulation of PWM inverters with zero steady-state error," *IEEE Transactions on power electronics*, vol. 18, no. 3, pp. 814–822, 2003.

[24] D. N. Zmood, D. G. Holmes, and G. H. Bode, "Frequency-domain analysis of three-phase linear current regulators," *IEEE Transactions on Industry Applications*, vol. 37, no. 2, pp. 601–610, 2001.

[25] W. Chen, C. Chen, Z.-f. SONG, and C.-l. XIA, "Proportional-resonant Control for Dual PWM Converter in Doubly Fed Wind Generation System [J]," *Proceedings of the CSEE*, vol. 15, p. 2, 2009.

[26] J. Hu, Y. He, L. Xu, and B. W. Williams, "Improved control of DFIG systems during network unbalance using PI–R current regulators," *IEEE Transactions on Industrial Electronics*, vol. 56, no. 2, pp. 439–451, 2009.

[27] S. Li, X. Wang, Z. Yao, T. Li, and Z. Peng, "Circulating current suppressing strategy for MMC-HVDC based on nonideal proportional resonant controllers under unbalanced grid conditions," *IEEE Transactions on Power Electronics*, vol. 30, no. 1, pp. 387–397, 2015.

[28] P. Mitra, L. Zhang, and L. Harnefors, "Offshore wind integration to a weak grid by VSC-HVDC links using power-synchronization control: A case study," *IEEE Transactions on Power Delivery*, vol. 29, no. 1, pp. 453–461, 2014.

[29] S. M. Ashabani and Y. A.-R. I. Mohamed, "A flexible control strategy for grid-connected and islanded microgrids with enhanced stability using nonlinear microgrid stabilizer," *IEEE Transactions on Smart Grid*, vol. 3, no. 3, pp. 1291–1301, 2012.

[30] Q.-C. Zhong, P.-L. Nguyen, Z. Ma, and W. Sheng, "Self-synchronized synchronverters: Inverters without a dedicated synchronization unit," *IEEE Transactions on Power Electronics*, vol. 29, no. 2, pp. 617–630, 2014.

[31] T. C. Y. Wang, Z. Ye, G. Sinha, and X. Yuan, "Output filter design for a grid-interconnected three-phase inverter," in *Power Electronics Specialist Conference, 2003. PESC'03. 2003 IEEE 34th Annual*, vol. 2, pp. 779–784, IEEE, 2003.

[32] S. V. Araújo, A. Engler, B. Sahan, and F. L. M. Antunes, "LCL filter design for grid-connected NPC inverters in offshore wind turbines," in *Power Electronics, 2007. ICPE'07. 7th Internatonal Conference on*, pp. 1133–1138, IEEE, 2007.

[33] G. Shen, X. Zhu, J. Zhang, and D. Xu, "A new feedback method for PR current control of LCL-filter-based grid-connected inverter," *IEEE Transactions on Industrial Electronics*, vol. 57, no. 6, pp. 2033–2041, 2010.

[34] R. Teodorescu, F. Blaabjerg, M. Liserre, and P. C. Loh, "Proportional-resonant controllers and filters for grid-connected voltage-source converters," *IEE Proceedings-Electric Power Applications*, vol. 153, no. 5, pp. 750–762, 2006.

[35] X. Wang, F. Blaabjerg, and P. C. Loh, "Virtual RC damping of LCL-filtered voltage source converters with extended selective harmonic compensation," *IEEE Trans. Power Electron*, vol. 30, no. 9, pp. 4726–4737, 2015.

Appendix A

Cross coupling terms in a dq frame

Cross-coupling terms arise because of the presence of derivative terms in the equations in an abc frame. Consider a generic vector of a three-phase voltage or current. Let this be $\boldsymbol{a}^{\mathrm{abc}}$. To express this in a dq frame, it must be operated on by a Park transformation, $\boldsymbol{P}$:

$$\boldsymbol{a}^{\mathrm{g}} = \boldsymbol{P}\{\boldsymbol{a}^{\mathrm{abc}}\} \tag{A.1}$$

When an equation in the abc frame contains a derivative, operating on the equation with a Park transformation means that the vector $\boldsymbol{a}^{\mathrm{abc}}$ and the operator $\boldsymbol{P}$ are separated by a differentiator: $\boldsymbol{P}\{\mathrm{d}\boldsymbol{a}^{\mathrm{abc}}/\mathrm{d}t\}$.

By the product rule,

$$\frac{\mathrm{d}\boldsymbol{P}\boldsymbol{a}^{\mathrm{abc}}}{\mathrm{d}t} = \frac{\mathrm{d}\boldsymbol{P}}{\mathrm{d}t}\boldsymbol{a}^{\mathrm{abc}} + \boldsymbol{P}\frac{\mathrm{d}\boldsymbol{a}^{\mathrm{abc}}}{\mathrm{d}t} \tag{A.2}$$

Hence,

$$\boldsymbol{P}\frac{\mathrm{d}\boldsymbol{a}^{\mathrm{abc}}}{\mathrm{d}t} = \frac{\mathrm{d}\boldsymbol{P}\boldsymbol{a}^{\mathrm{abc}}}{\mathrm{d}t} - \frac{\mathrm{d}\boldsymbol{P}}{\mathrm{d}t}\boldsymbol{a}^{\mathrm{abc}} \tag{A.3}$$

The first term on the right hand side can be identified as $\mathrm{d}\boldsymbol{a}^{\mathrm{g}}/\mathrm{d}t$. The second term is evaluated by

considering the definition of the Park transformation matrix:

$$\begin{aligned}
\frac{\mathrm{d}\boldsymbol{P}}{\mathrm{d}t} &= \frac{\mathrm{d}\theta}{\mathrm{d}t}\frac{\mathrm{d}\boldsymbol{P}}{\mathrm{d}\theta} \\
&= \omega\frac{\mathrm{d}}{\mathrm{d}\theta}\begin{bmatrix}\cos\theta & \cos(\theta-2\pi/3) & \cos(\theta+2\pi/3)\\ \sin\theta & \sin(\theta-2\pi/3) & \sin(\theta+2\pi/3)\end{bmatrix} \\
&= \omega\begin{bmatrix}-\sin\theta & -\sin(\theta-2\pi/3) & -\sin(\theta+2\pi/3)\\ \cos\theta & \cos(\theta-2\pi/3) & \cos(\theta+2\pi/3)\end{bmatrix} \\
&= -\omega\begin{bmatrix}0 & 1\\ -1 & 0\end{bmatrix}\begin{bmatrix}\cos\theta & \cos(\theta-2\pi/3) & \cos(\theta+2\pi/3)\\ \sin\theta & \sin(\theta-2\pi/3) & \sin(\theta+2\pi/3)\end{bmatrix} \\
&= -\omega\begin{bmatrix}0 & 1\\ -1 & 0\end{bmatrix}\boldsymbol{P}
\end{aligned} \tag{A.4}$$

Thus,

$$\boldsymbol{P}\frac{\mathrm{d}\boldsymbol{a}^{\mathrm{abc}}}{\mathrm{d}t} = \frac{\mathrm{d}\boldsymbol{a}^{\mathrm{g}}}{\mathrm{d}t} + \omega\begin{bmatrix}0 & 1\\ -1 & 0\end{bmatrix}\boldsymbol{a}^{\mathrm{g}} \tag{A.5}$$

Hence, a cross-coupling term is an unavoidable feature of the dq transformation when derivative terms are involved. This is why the inner current controller has de-coupling terms.

Appendix B

Sample code for linearised models

The following sections contain MATLAB codes that can be used for analysing single-converter systems.

B.1 Common codes

B.1.1 Steady state solver

The following code determines all relevant steady-state values for a given operating point around which a linearised model is evaluated.

```
function F = root8d(x)

global Power;
global Voltages;
global Components;

%Grid frequency in per unit:
w1 = 1;
%Power:
```

```
10 if Components.Cf == 0
11     %Voltage components at the PCC:
12     u_fd0 = x(1) - x(3)*Components.Rc + w1*Components.Lc*x(4);
13     u_fq0 = x(2) - x(4)*Components.Rc - w1*Components.Lc*x(3);
14
15     F(1) = x(3)*u_fd0 + x(4)*u_fq0 - Power.P0;
16 else
17     F(1) = x(5)*x(7) + x(6)*x(8) - Power.P0;
18 end
19 %Voltage magnitude:
20 F(2) = sqrt(x(1)^2 + x(2)^2) - Voltages.V0;
21 %Circuit equations:
22 if Components.Cf == 0
23     F(3) = x(1) - Voltages.E0 - (Components.Rc + Components.Rn)*x(3) +
           ...
24          w1*(Components.Lc + Components.Ln)*x(4);
25     F(4) = x(2) - (Components.Rc + Components.Rn)*x(4) - ...
26          w1*(Components.Lc + Components.Ln)*x(3);
27 else
28     F(3) = x(1) - x(5) - Components.Rc*x(3) + w1*Components.Lc*x(4);
29     F(4) = x(2) - x(6) - Components.Rc*x(4) - w1*Components.Lc*x(3);
30     F(5) = x(3) - x(7) + w1*Components.Cf*x(6);
31     F(6) = x(4) - x(8) - w1*Components.Cf*x(5);
32     F(7) = x(5) - Voltages.E0 - x(7)*Components.Rn + w1*Components.Ln*x
           (8);
33     F(8) = x(6) - x(8)*Components.Rn - w1*Components.Ln*x(7);
34 end
```

```
1 function [steady_state] = get_steady_state_values(components,x)
2
```

```
w1 = 1;
%Extract all the values:
steady_state.v_d0 = x(1);
steady_state.v_q0 = x(2);
steady_state.i_cd0 = x(3);
steady_state.i_cq0 = x(4);
%Handle L and LC filter cases:
if components.Cf == 0
    steady_state.u_fd0 = steady_state.v_d0 - ...
        steady_state.i_cd0*components.Rc + ...
        w1*components.Lc*steady_state.i_cq0;
    steady_state.u_fq0 = steady_state.v_q0 - ...
        steady_state.i_cq0*components.Rc - ...
        w1*components.Lc*steady_state.i_cd0;
    steady_state.i_nd0 = steady_state.i_cd0;
    steady_state.i_nq0 = steady_state.i_cq0;
else
    steady_state.u_fd0 = x(5);
    steady_state.u_fq0 = x(6);
    steady_state.i_nd0 = x(7);
    steady_state.i_nq0 = x(8);
end
%Work out all the steady-state angles:
steady_state.theta_v0 = atan2(steady_state.v_q0,steady_state.v_d0);
steady_state.theta_u0 = atan2(steady_state.u_fq0,steady_state.u_fd0);
%Work out the steady-state magnitude of the filter bus voltage:
steady_state.U_f0 = sqrt(steady_state.u_fd0^2 + steady_state.u_fq0^2);
```

B.1.2 linearised models of plant

The following code contains an implementation of the state-space models found in chapter 3.

L filter

```
function [ss_lin] = lin_state_space_l_filter(components,steady_state
    ,...
     AC_control,simulink)
%
w1 = 1;
%Get the relevant information:
Rc = components.Rc;
Lc = components.Lc;
Rn = components.Rn;
Ln = components.Ln;
%Get the steady-state values:
if simulink == 1
     u_fd0 = steady_state.simulation.u_g0(1);
     u_fq0 = steady_state.simulation.u_g0(2);
     i_nd0 = steady_state.simulation.i_ng0(1);
     i_nq0 = steady_state.simulation.i_ng0(2);
    %Voltage magnitude:
     U_f0 = sqrt(u_fd0^2 + u_fq0^2);
else
     u_fd0 = steady_state.u_fd0;
     u_fq0 = steady_state.u_fq0;
     i_nd0 = steady_state.i_nd0;
     i_nq0 = steady_state.i_nq0;
    %Voltage magnitude:
     U_f0 = sqrt(u_fd0^2 + u_fq0^2);
```

```
25 end
26 %Calculate the A-matrix:
27 ss_lin.A = [-(Rc+Rn)/(Lc+Ln),w1;-w1,-(Rc+Rn)/(Lc+Ln)];
28 %B matrix:
29 ss_lin.B = [1/(Lc+Ln),0;0,1/(Lc+Ln)];
30 %Generic C matrix:
31 if AC_control == 1
32     C = [1,0,0,0;...
33          0,1,0,0;...
34          0,0,1,0;...
35          0,0,0,1;...
36          u_fd0,u_fq0,i_nd0,i_nq0;...
37          0,0,u_fd0/U_f0,u_fq0/U_f0];
38 else
39     C = [1,0,0,0;...
40          0,1,0,0;...
41          0,0,1,0;...
42          0,0,0,1;...
43          u_fd0,u_fq0,i_nd0,i_nq0;...
44          u_fq0,-u_fd0,-i_nq0,i_nd0];
45 end
46 %D matrix:
47 ss_lin.D = C*[0,0;...
48      0,0;...
49      Ln/(Lc+Ln),0;...
50      0,Ln/(Lc+Ln)];
51 %Actual C matrix:
52 ss_lin.C = C*[1,0;...
53      0,1;...
54      Lc*Ln/(Lc+Ln)*(Rn/Ln-Rc/Lc),0;...
```

```
55      0,Lc*Ln/(Lc+Ln)*(Rn/Ln-Rc/Lc)];
```

LC filter

```
1  function [ss_lin] = lin_state_space_lc_filter(components,steady_state
       ,...
2       AC_control,simulink)
3  %
4  w1 = 1;
5  %Get the relevant information:
6  Rc = components.Rc;
7  Lc = components.Lc;
8  Cf = components.Cf;
9  Rn = components.Rn;
10 Ln = components.Ln;
11 %Get the steady-state values:
12 if simulink == 1
13      u_fd0 = steady_state.simulation.u_g0(1);
14      u_fq0 = steady_state.simulation.u_g0(2);
15      i_nd0 = steady_state.simulation.i_ng0(1);
16      i_nq0 = steady_state.simulation.i_ng0(2);
17     %Voltage magnitude:
18      U_f0 = sqrt(u_fd0^2 + u_fq0^2);
19 else
20      u_fd0 = steady_state.u_fd0;
21      u_fq0 = steady_state.u_fq0;
22      i_nd0 = steady_state.i_nd0;
23      i_nq0 = steady_state.i_nq0;
24     %Voltage magnitude:
25      U_f0 = sqrt(u_fd0^2 + u_fq0^2);
26 end
```

```
%Calculate the A-matrix:
ss_lin.A = [-Rc/Lc,w1,-1/Lc,0,0,0;...
    -w1,-Rc/Lc,0,-1/Lc,0,0;...
    1/Cf,0,0,w1,-1/Cf,0;...
    0,1/Cf,-w1,0,0,-1/Cf;...
    0,0,1/Ln,0,-Rn/Ln,w1;...
    0,0,0,1/Ln,-w1,-Rn/Ln];
%B matrix:
ss_lin.B = [1/Lc,0;0,1/Lc;0,0;0,0;0,0;0,0];
%Generic C matrix:
if AC_control == 1
    ss_lin.C = [1,0,0,0,0,0;...
        0,1,0,0,0,0;...
        0,0,1,0,0,0;...
        0,0,0,1,0,0;...
        0,0,i_nd0,i_nq0,u_fd0,u_fq0;...
        0,0,u_fd0/U_f0,u_fq0/U_f0,0,0];
else
    ss_lin.C = [1,0,0,0,0,0;...
        0,1,0,0,0,0;...
        0,0,1,0,0,0;...
        0,0,0,1,0,0;...
        0,0,i_nd0,i_nq0,u_fd0,u_fq0;...
        0,0,-i_nq0,i_nd0,u_fq0,-u_fd0];
end
%D matrix:
ss_lin.D = zeros(6,2);
```

B.1.3 Bode plots

```
function [] = bode_plotting(compare,save,order,sys_settings,phase,P0
```

```
    ,...
2       omega,H,omega_fs,response_fs,varagin)
3
4 %Get current directory:
5 current_directory = cd;
6
7 %% Magnitude plotting:
8
9 %fontsize = 20;
10 fontsize = 20;
11
12 figure('units','normalized','outerposition',[0 0 1 1])
13 hold on
14 grid on
15 %fontsize = 16;
16
17 mag_H = abs(H);
18
19 if compare == 0
20       xlim_vec = [1 5000];
21       ylim_vec = [10^-2 20];
22 else
23       xlim_vec = [1/sys_settings.w_base 5000/sys_settings.w_base];
24       ylim_vec = [-30 10];
25 end
26
27 subplot(2,2,1);
28 hold on
29 if compare == 1
30       semilogx(omega,20*log10(squeeze(mag_H(1,1,:))),'b')
```

```
31      set(gca,'xscale','log','Fontsize',fontsize)
32  else
33      loglog(omega*sys_settings.w_base,(squeeze(mag_H(1,1,:))),'b')  %20*
            log10(...)
34      %If frequency scanning is done:
35      if nargin == 10
36          loglog(omega_fs*sys_settings.w_base,response_fs(:,1),'.r','
                MarkerSize',20)
37      end
38      set(gca,'xscale','log','yscale','log','Fontsize',fontsize)
39  end
40  grid on
41  xlabel('Frequency, rad/s','FontSize',fontsize,'Color','k');
42  ylabel('|H_{1,1}|','Fontsize',fontsize);
43  xlim(xlim_vec)
44  ylim(ylim_vec)
45
46  subplot(2,2,2);
47  hold on
48  if compare == 1
49      semilogx(omega,20*log10(squeeze(mag_H(1,2,:))),'b')
50      set(gca,'xscale','log','Fontsize',fontsize)
51  else
52      loglog(omega*sys_settings.w_base,(squeeze(mag_H(1,2,:))),'b')
53      %If frequency scanning is done:
54      if nargin == 10
55          loglog(omega_fs*sys_settings.w_base,response_fs(:,2),'.r','
                MarkerSize',20)
56      end
57      set(gca,'xscale','log','yscale','log','Fontsize',fontsize)
```

```
58 end
59 grid on
60 xlabel('Frequency, rad/s','FontSize',fontsize,'Color','k');
61 ylabel('|H_{1,2}|','Fontsize',fontsize);
62 xlim(xlim_vec)
63 ylim(ylim_vec)
64
65 subplot(2,2,3);
66 hold on
67 if compare == 1
68     semilogx(omega,20*log10(squeeze(mag_H(2,1,:))),'b')
69     set(gca,'xscale','log','Fontsize',fontsize)
70 else
71     loglog(omega*sys_settings.w_base,(squeeze(mag_H(2,1,:))),'b')
72     %If frequency scanning is done:
73     if nargin == 10
74         loglog(omega_fs*sys_settings.w_base,response_fs(:,3),'.r','
              MarkerSize',20)
75     end
76     set(gca,'xscale','log','yscale','log','Fontsize',fontsize)
77 end
78 grid on
79 xlabel('Frequency, rad/s','FontSize',fontsize,'Color','k');
80 ylabel('|H_{2,1}|','Fontsize',fontsize);
81 xlim(xlim_vec)
82 ylim(ylim_vec)
83
84 subplot(2,2,4);
85 hold on
86 if compare == 1
```

```
87      semilogx(omega,20*log10(squeeze(mag_H(2,2,:))),'b')
88      set(gca,'xscale','log','Fontsize',fontsize)
89  else
90      loglog(omega*sys_settings.w_base,(squeeze(mag_H(2,2,:))),'b')  %20*
            log10
91      if nargin == 10
92          loglog(omega_fs*sys_settings.w_base,(response_fs(:,4)),'.r','
                MarkerSize',20)
93      end
94      set(gca,'xscale','log','yscale','log','Fontsize',fontsize)
95  end
96  grid on
97  xlabel('Frequency, rad/s','FontSize',fontsize,'Color','k');
98  ylabel('|H_{2,2}|','Fontsize',fontsize);
99  xlim(xlim_vec)
100 ylim(ylim_vec)
101
102 %Change directory and save:
103 str_0 = 'd:\Users\pkb12186\Desktop\Models\Thesis\Images\one_converter\
        vcc\';
104 %L or LC filter:
105 if sys_settings.Cf == 0
106     str_1 = 'L\';
107 else
108     str_1 = 'LC\';
109 end
110 %SCR:
111 if (1/sys_settings.Ln) == 1
112     str_2 = 'V\';
113     str_scr = '1';
```

```
114 else
115     str_2 = 'Q\';
116     str_scr = num2str(1/sys_settings.Ln);
117 end
118 %PLL order:
119 if order == 1
120     str_3 = '1st_order\';
121 elseif order == 2
122     str_3 = '2nd_order\';
123 end
124
125 cd(strcat(str_0,str_1,str_2,str_3))
126
127 P0_str = num2str(P0*100);
128
129 if save == 1
130     if nargin == 10
131         saveas(gcf,strcat('vcc_scr_',str_scr,'_p_0',P0_str,'
            _bode_validation'),'epsc')
132     else
133         saveas(gcf,strcat('vcc_scr_',str_scr,'_p_0',P0_str,'_bode'),'
            epsc')
134     end
135 end
136
137 %% Phase plotting:
138
139 if phase == 1
140     fontsize = 20;
141
```

```
142     figure('units','normalized','outerposition',[0 0 1 1])
143     hold on
144     grid on
145
146     subplot(2,2,1);
147     hold on
148     semilogx(omega*sys_settings.w_base,180/pi*...
149         unwrap(atan2(squeeze(imag(H(1,1,:))),squeeze(real(H(1,1,:))))),
            'b')
150     %set(gca,'xscale','log','Fontsize',fontsize)
151     grid on
152     %Add the axis labels:
153     xlabel('Frequency, rad/s','FontSize',fontsize,'Color','k');
154     ylabel('Argument, degrees','Fontsize',fontsize);
155     xlim(xlim_vec)
156
157     subplot(2,2,2);
158     hold on
159     semilogx(omega*sys_settings.w_base,180/pi*...
160         unwrap(atan2(squeeze(imag(H(1,2,:))),squeeze(real(H(1,2,:))))),
            'b')
161     %set(gca,'xscale','log','Fontsize',fontsize)
162     grid on
163     %Add the axis labels:
164     xlabel('Frequency, rad/s','FontSize',fontsize,'Color','k');
165     ylabel('Argument, degrees','Fontsize',fontsize);
166     xlim(xlim_vec)
167
168     subplot(2,2,3);
169     hold on
```

```
170     semilogx(omega*sys_settings.w_base,180/pi*...
171         unwrap(atan2(squeeze(imag(H(2,1,:))),squeeze(real(H(2,1,:))))),
            'b')
172     %set(gca,'xscale','log','Fontsize',fontsize)
173     grid on
174     %Add the axis labels:
175     xlabel('Frequency, rad/s','FontSize',fontsize,'Color','k');
176     ylabel('Argument, degrees','Fontsize',fontsize);
177     xlim(xlim_vec)
178
179     subplot(2,2,4);
180     hold on
181     semilogx(omega*sys_settings.w_base,180/pi*...
182         unwrap(atan2(squeeze(imag(H(2,2,:))),squeeze(real(H(2,2,:))))),
            'b')
183     %set(gca,'xscale','log','Fontsize',fontsize)
184     grid on
185     %Add the axis labels:
186     xlabel('Frequency, rad/s','FontSize',fontsize,'Color','k');
187     ylabel('Argument, degrees','Fontsize',fontsize);
188     xlim(xlim_vec)
189
190     %saveas(gcf,strcat('vcc_scr_',str_scr,'_p_0',P0_str,'_phase'),'epsc
        ')
191
192 end
193 %Restore directory:
194 cd(current_directory)
```

B.2 Vector current control

B.2.1 main function

Note - the following code contains function calls for non-linear models, the codes for which have not been provided. These can be commented out where appropriate; this will make no difference to the functioning of the linear model.

```
%% Analysis of a converter controlled by VCC feeding Xn,Rn:

clear
clc
close all

%Yes I know - I really hate using global variables, but MATLAB is
    MATLAB...
global Voltages;
global Power;
global Components;
global AC_control;

str_base_1 = 'D:\Users\pkb12186\Desktop\Models\High impedance systems';
str_base_2 = '\Single converter systems\Vector current control\';
str_base = strcat(str_base_1,str_base_2);
str_matlab = 'Matlab scripts (for initialisation and Bode plotting)';
str_simulink = 'Simulink state-space models\abc models';

lin_analysis = 1;
frequency_scanning = 0;
show_phase = 0;
step_change = 0;
```

```
23 pz_mapping = 1;
24 outer_control = 1;
25 compare = 0;
26 save = 0;
27 %Per-unit nominal angular frequency:
28 w1 = 1;
29 %Range of angular frequencies (in per unit):
30 omega = horzcat((0.00002:0.00002:0.01),(0.02:0.01:10));
31 %Associated range of s:
32 s = 1i*omega;
33 %Get system settings:
34 [sys_settings] = get_system_settings();
35 %Get controller settings:
36 [controller] = get_vcc_settings(sys_settings);
37 %Define the SCR:
38 for i = 1
39     %Which P0 values should be simulated for the given value of SCR:
40     if i == 1
41         AC_control = 1;
42         if controller.pll.order == 1
43             P0_vec = 0:0.05:0.85;
44         else
45             P0_vec = 0:0.05:0.85;
46         end
47     else
48         AC_control = 0;
49         P0_vec = [0,0.5,0.9];
50     end
51
52     if pz_mapping == 1
```

```
53          figure('units','normalized','outerposition',[0 0 1 1])
54      end
55
56      for j = 1:length(P0_vec)
57
58          cd(strcat(str_base,str_matlab))
59
60          P0 = P0_vec(j);
61          %Define the grid parameters in terms of the per unit system
                being
62          %used in this work:
63          sys_settings.Xn = 1/i;
64          sys_settings.Ln = sys_settings.Xn;
65
66          %% Steady-state values at all relevant points:
67
68          %Steady-state voltage magnitudes:
69          E0 = 1;
70          V0 = 1;
71
72          Power.P0 = P0;
73          Voltages.V0 = V0;
74          Voltages.E0 = E0;
75          Components.Rc = sys_settings.Rc;
76          Components.Lc = sys_settings.Lc;
77          Components.Cf = sys_settings.Cf;
78          Components.Rn = sys_settings.Rn;
79          Components.Ln = sys_settings.Ln;
80          %Non-linear steady-state solver:
81          fun = @root8d;
```

```
82          if sys_settings.Cf == 0
83              x0 = [0,0,0,0];
84          else
85              x0 = [0,0,0,0,0,0,0,0];
86          end
87          x = fsolve(fun,x0);
88
89          [steady_state] = get_steady_state_values(sys_settings,x);
90
91          %% Linear model:
92
93          if lin_analysis == 1
94              if sys_settings.Cf == 0
95                  [ss_lin] = lin_state_space_l_filter(sys_settings,...
96                      steady_state,AC_control);
97              else
98                  [ss_lin] = lin_state_space_lc_filter(sys_settings,...
99                      steady_state,AC_control);
100             end
101             %Run the s-domain model:
102             [H] = lin_model(ss_lin,sys_settings,steady_state,controller
                    ,s);
103             %Show the results:
104             if frequency_scanning == 0 && pz_mapping == 0
105                 bode_plotting(compare,save,controller.pll.order,...
106                     sys_settings,show_phase,P0,omega,H);
107             end
108             %Unified state-space models:
109             if outer_control == 0
110                 [ss_model] = create_state_space_lin_model_vcc_inner(...
```

```
111                     ss_lin,controller,steady_state,sys_settings);
112
113                 if compare == 1
114                     figure('units','normalized','outerposition',[0 0 1
                            1])
115                     bode(ss_model,omega)
116                     grid on
117                 end
118             elseif outer_control == 1
119                 [ss_model] = create_state_space_lin_model_vcc_outer(...
120                     ss_lin,controller,steady_state,sys_settings);
121             end
122             %Plot poles and zeros:
123             if pz_mapping == 1
124                 if j == length(P0_vec)
125                     complete = 1;
126                 else
127                     complete = 0;
128                 end
129
130                 pz_plots(ss_model,sys_settings,controller,complete,
                        outer_control);
131             end
132         end
133
134         %% Some steady-state values for the non-linear model (initial):
135
136         cos_theta_u0 = cos(steady_state.theta_u0);
137         sin_theta_u0 = sin(steady_state.theta_u0);
```

```
138         i_cd0_c =  steady_state.i_cd0*cos_theta_u0 + steady_state.i_cq0
                *sin_theta_u0;
139         i_cq0_c = -steady_state.i_cd0*sin_theta_u0 + steady_state.i_cq0
                *cos_theta_u0;
140
141         %% Non-linear model (abc frame based):
142
143         %Phase of the grid dq frame at t = 0:
144         phase = 0;
145         %Convert bridge voltage to abc frame:
146         [v_abc] = dq_to_abc(steady_state.v_d0,steady_state.v_q0,phase);
147         %Convert phase reactor current to abc frame:
148         [ic_abc] = dq_to_abc(steady_state.i_cd0,steady_state.i_cq0,
                phase);
149         %Convert phase reactor current to abc frame:
150         [e_abc] = dq_to_abc(steady_state.u_fd0,steady_state.u_fq0,phase
                );
151         %Convert phase reactor current to abc frame:
152         [in_abc] = dq_to_abc(steady_state.i_nd0,steady_state.i_nq0,
                phase);
153         %Create initial values:
154         if sys_settings.Cf == 0
155             X0 = ic_abc;
156         else
157             X0 = [ic_abc,e_abc,in_abc];
158         end
159
160         if sys_settings.Cf == 0
161             [A_abc,B_abc,C_abc,D_abc] = non_lin_state_space_l_filter
                    (...
```

```
162                 sys_settings);
163         else
164             [A_abc,B_abc,C_abc,D_abc] = non_lin_state_space_lc_filter
                    (...
165                 sys_settings);
166         end
167         %Remaining C matrices:
168         C1_abc = [eye(3),zeros(3,6)];
169         C2_abc = [zeros(3),eye(3),zeros(3)];
170         C3_abc = [zeros(6,3),eye(6)];
171
172         %% Run Simulink model (frequency scanning):
173
174         if lin_analysis == 1 && frequency_scanning == 1 && pz_mapping
                == 0
175             global switch_on;
176             global omega_sim;
177             %Initial settings:
178             switch_on = 0;
179             %Call the model to be excited:
180             [omega_fs,response_fs] = run_frequency_scanning(
                    sys_settings,...
181                 str_base,str_simulink,controller);
182             %Show the results:
183             bode_plotting(compare,save,controller.pll.order,
                    sys_settings,show_phase,...
184                 P0,omega,H,omega_fs,response_fs);
185         end
186
187         %% Run Simulink model (step changes in reference values):
```

```
188
189         if step_change == 1
190
191 %Get current directory:
192 current_directory = cd;
193 %Change directory to allow Simulink models to run:
194 cd(strcat(str_base,str_simulink))
195
196 init = 1;
197 tsim = 1400;
198 t_step = 200*sys_settings.w_base;
199 step_i = 0.1;
200 switch_d = 1;  %#ok<NASGU>
201 switch_q = 0;          %#ok<NASGU>
202
203 if controller.pll.order == 1
204
205     set_param('vector_current_control_1st_order_pll','LoadInitialState'
        ,'off');
206     set_param('vector_current_control_1st_order_pll','SaveFinalState','
        on','FinalStateName',...
207         'myOperPoint','SaveCompleteFinalSimState','on');
208
209 elseif controller.pll.order == 2
210
211     set_param('vector_current_control_2nd_order_pll','LoadInitialState'
        ,'off');
212     set_param('vector_current_control_2nd_order_pll','SaveFinalState','
        on','FinalStateName',...
213         'myOperPoint','SaveCompleteFinalSimState','on');
```

```
214
215 end
216 %Run the model:
217 if controller.pll.order == 1
218     sim('vector_current_control_1st_order_pll')
219 elseif controller.pll.order == 2
220     sim('vector_current_control_2nd_order_pll')
221 end
222
223 i_cd0_c = initial_state.data(end,1);
224 i_cq0_c = initial_state.data(end,2);
225 init = 0;
226
227 if controller.pll.order == 1
228
229     set_param('vector_current_control_1st_order_pll','LoadInitialState'
        ,'on',...
230         'InitialState','myOperPoint');
231     set_param('vector_current_control_1st_order_pll','SaveFinalState','
        off');
232
233 elseif controller.pll.order == 2
234
235     set_param('vector_current_control_2nd_order_pll','LoadInitialState'
        ,'on',...
236         'InitialState','myOperPoint');
237     set_param('vector_current_control_2nd_order_pll','SaveFinalState','
        off');
238
239 end
```

```
240
241 tsim = 2600;
242 t_step = 6*sys_settings.w_base;
243 step_i = 0.1;
244 %Change id ref and analyse response:
245 switch_d = 1;  %#ok<NASGU>
246 switch_q = 0;          %#ok<NASGU>
247 %Call the model:
248 if controller.pll.order == 1
249     sim('vector_current_control_1st_order_pll')
250 elseif controller.pll.order == 2
251     sim('vector_current_control_2nd_order_pll')
252 end
253
254 y1 = y1_abc;
255
256 %Change iq ref and analyse response:
257 switch_d = 0;
258 switch_q = 1;
259 %Call the model:
260 if controller.pll.order == 1
261     sim('vector_current_control_1st_order_pll')
262 elseif controller.pll.order == 2
263     sim('vector_current_control_2nd_order_pll')
264 end
265 %
266 y2 = y1_abc;
267 %Bring back to the original folder:
268 cd(current_directory)
269
```

```
270                 %Plot the results:
271                 power_plotting(sys_settings,controller,P0,y1,y2);
272             end
273         end
274     end
```

B.2.2 Combined linear model of controller and plant

Frequency response data

```
1  function [H] = lin_model(ss_lin,components,steady_state,controller,s)
2  %Create space for the transfer function matrix:
3  H = zeros(2,2,length(s));
4  %Grid frequency (per unit):
5  w1 = 1;
6  %Get the relevant information for the system:
7  Lc = components.Lc;
8  Cf = components.Cf;
9  %Get the controller information:
10 kp_pll = controller.pll.kp;
11 ki_pll = controller.pll.ki;
12 alpha_f = controller.icc.alpha_f;
13 kp_icc = controller.icc.kp;
14 ki_icc = controller.icc.ki;
15 %Get the outer loop controller information:
16 kp_apc = controller.apc.kp;
17 ki_apc = controller.apc.ki;
18 kp_vp = controller.dec.kp_vp;
19 ki_vp = controller.dec.ki_vp;
20 kp_pv = controller.dec.kp_pv;
```

```
21 ki_pv = controller.dec.ki_pv;
22 kp_avc = controller.avc.kp;
23 ki_avc = controller.avc.ki;
24 %Get the steady-state values:
25 v_d0 = steady_state.v_d0;
26 v_q0 = steady_state.v_q0;
27 i_cd0 = steady_state.i_cd0;
28 i_cq0 = steady_state.i_cq0;
29 u_fd0 = steady_state.u_fd0;
30 u_fq0 = steady_state.u_fq0;
31 %Get the steady-state angles:
32 theta_v0 = atan2(v_q0,v_d0);
33 theta_u0 = atan2(u_fq0,u_fd0);
34 %Voltage magnitude at the bridge:
35 V0 = sqrt(v_d0^2 + v_q0^2);
36 %Run through all frequencies, calculating the network response:
37 for k=1:length(s)
38     %Network transfer matrix:
39     if Cf == 0
40         G = ss_lin.C*((s(k)*eye(2) - ss_lin.A)\ss_lin.B) + ss_lin.D;
41     else
42         G = ss_lin.C*((s(k)*eye(6) - ss_lin.A)\ss_lin.B) + ss_lin.D;
43     end
44     %Split the network transfer matrix into three parts:
45     G1 = G(1:2,1:2);
46     G2 = G(3:4,1:2);
47     G3 = G(5:6,1:2);
48     %Low-pass filter:
49     H_LP = alpha_f/(s(k)+alpha_f);
50     %PLL controller gain:
```

```
51      CPLL = kp_pll + ki_pll/s(k);
52      %Inner current controller gain:
53      Ci = kp_icc + ki_icc/s(k);
54      %Ci matrices:
55      if controller.pll.order == 1
56          C1 = 1/(1+CPLL*(u_fq0*sin(theta_u0)+u_fd0*cos(theta_u0)))*...
57              [-CPLL*sin(theta_u0),CPLL*cos(theta_u0)];
58      elseif controller.pll.order == 2
59          C1 = 1/(s(k)+CPLL*(u_fq0*sin(theta_u0)+u_fd0*cos(theta_u0)))
                *...
60              [-CPLL*sin(theta_u0),CPLL*cos(theta_u0)];
61      end
62      C2 = [cos(theta_u0),sin(theta_u0);-sin(theta_u0),cos(theta_u0)];
63      C2_inv = [cos(theta_u0),-sin(theta_u0);sin(theta_u0),cos(theta_u0)
            ];
64      C3 = [u_fq0*cos(theta_u0)-u_fd0*sin(theta_u0);...
65          -u_fq0*sin(theta_u0)-u_fd0*cos(theta_u0)];
66      C4 = [i_cq0*cos(theta_u0)-i_cd0*sin(theta_u0);...
67          -i_cq0*sin(theta_u0)-i_cd0*cos(theta_u0)];
68      C5 = [-Ci,-w1*Lc;w1*Lc,-Ci];
69      C6 = [Ci,0;0,Ci];
70      C7 = [H_LP,0;0,H_LP];
71      C8 = [-V0*sin(theta_v0);V0*cos(theta_v0)];
72      C9 = 1;%/(s(k)*pi/33 + 1);
73      %Calculate kappa:
74      kappa = C9*C2_inv*(C5*(C2*G1+C4*C1*G2)+...
75          C7*(C2*G2+C3*C1*G2))+C8*C1*G2;
76      %Calculate I - kappa:
77      eye_kappa = eye(2) - kappa;
78      %Calculate H (closed loop transfer function of the power system,
```

```
79      %including the controllers):
80      H_inner = G3*(eye_kappa\(C9*C2_inv*C6));
81      %Outer loop controllers:
82      C21 = [(kp_apc+ki_apc/s(k)),(kp_vp+ki_vp/s(k));...
83          -(kp_pv+ki_pv/s(k)),-(kp_avc+ki_avc/s(k))];
84      %Overall transfer function:
85      H(:,:,k) = H_inner;
86      %(eye(2) + H_inner*C21)\(H_inner*C21);
87      %s(k)*vertcat(C1,C1);%
88  end
```

Unified linear state-space model

```
1   function [ss_model] = create_state_space_lin_model_vcc_inner(ss_lin,...
2       controller,steady_state,components)
3   %State-equation matrices:
4   Ae = ss_lin.A;
5   Be = ss_lin.B;
6   %Re-order rows to make consistent with thesis equations:
7   Ce = vertcat(ss_lin.C(5:6,:),ss_lin.C(1:4,:));
8   De = vertcat(ss_lin.D(5:6,:),ss_lin.D(1:4,:));
9   %Number of electrical states:
10  Ne = length(Ae(1,:));
11  %Grid frequency (per unit):
12  w1 = 1;
13  Lc = components.Lc;
14  %Get the controller information:
15  order = controller.pll.order;
16  kp_pll = controller.pll.kp;
17  ki_pll = controller.pll.ki;
18  af = controller.icc.alpha_f;
```

```
kp_cc = controller.icc.kp;
ki_cc = controller.icc.ki;
%Number of controller states:
if order == 1
    Nc = 5;
elseif order == 2
    Nc = 6;
end
%Get the steady-state values:
v_d0 = steady_state.v_d0;
v_q0 = steady_state.v_q0;
i_cd0 = steady_state.i_cd0;
i_cq0 = steady_state.i_cq0;
u_fd0 = steady_state.u_fd0;
u_fq0 = steady_state.u_fq0;
U0 = sqrt(u_fd0^2 + u_fq0^2);
%Get the steady-state angles:
theta_v0 = atan2(v_q0,v_d0);
theta_u0 = atan2(u_fq0,u_fd0);
%Voltage magnitude at the bridge:
V0 = sqrt(v_d0^2 + v_q0^2);

%% Current controller state-space model:

%Define the first linking matrix:
T1 = [0,0,0,0,1,0;0,0,0,0,0,1];
%Define the PLL state-space matrices:
if order == 1
    Apll = -ki_pll*U0/(1 + kp_pll*U0);
    Bpll = ki_pll/(1 + U0*kp_pll)*(1 - U0*kp_pll/(1 + U0*kp_pll))*...
```

```
49          [0,0,0,0,-sin(theta_u0),cos(theta_u0)];
50      Cpll = 1;
51      Dpll = kp_pll/(1 + kp_pll*U0)*[0,0,0,0,-sin(theta_u0),cos(theta_u0)
            ];
52  elseif order == 2
53      Apll = [-U0*kp_pll,-U0*ki_pll;1,0];
54      Bpll = [0,0,0,0,-sin(theta_u0),cos(theta_u0);0,0,0,0,0,0];
55      Cpll = [kp_pll, ki_pll];
56  end
57  %Define the second linking matrix:
58  T2 = [0,0,1,0,0,0;0,0,0,1,0,0];
59  %Define the abc -> dq frame transformation state-space matrices:
60  C2a = [cos(theta_u0),sin(theta_u0);-sin(theta_u0),cos(theta_u0)]*T2;
61  C2b = [cos(theta_u0),sin(theta_u0);-sin(theta_u0),cos(theta_u0)]*T1;
62  C3 = [i_cq0*cos(theta_u0)-i_cd0*sin(theta_u0);...
63      -i_cq0*sin(theta_u0)-i_cd0*cos(theta_u0)];
64  C4 = [u_fq0*cos(theta_u0)-u_fd0*sin(theta_u0);...
65      -u_fq0*sin(theta_u0)-u_fd0*cos(theta_u0)];
66  if order == 1
67      Cabc1 = [C2a;C2b] + [C3;C4]*Dpll;
68  elseif order == 2
69      Cabc1 = [C2a;C2b];
70  end
71  Cabc2 = [C3;C4]*Cpll;
72  %Define the low-pass state-space matrices:
73  Alp = -af*eye(2);
74  Blp1 = [0,0,af,0;0,0,0,af]*Cabc1;
75  Blp2 = [0,0,af,0;0,0,0,af]*Cabc2;
76  Clp = [0,0;0,0;1,0;0,1];
77  %Define the modifier:
```

```
78 M = [1,0,0,0;0,1,0,0;0,0,0,0;0,0,0,0];
79 %Define the M matrices:
80 Mcc1 = M*Cabc1;
81 Mcc2 = M*Cabc2;
82 %Define the current controller state-space matrices:
83 Bccz = eye(2);
84 Bcc = [-1,0,0,0;0,-1,0,0];
85 Ccc = [ki_cc,0;0,ki_cc];
86 Dccz = [kp_cc,0;0,kp_cc];
87 Dcc = [-kp_cc,-w1*Lc,1,0;w1*Lc,-kp_cc,0,1];
88 %Define the dq -> abc frame transformation state-space matrices:
89 C8 = [cos(theta_u0),-sin(theta_u0);sin(theta_u0),cos(theta_u0)];
90 C9 = [-V0*sin(theta_v0);V0*cos(theta_v0)];
91 %Define Cdq, Ddq and Edq:
92 Cdq = [zeros(2,6),[C8*Dcc*Mcc2+C9*Cpll,C8*Dcc*Clp,C8*Ccc]];
93 Ddq = C8*Dccz;
94 if order == 1
95     Edq = C8*Dcc*Mcc1 + C9*Dpll;
96 elseif order == 2
97     Edq = C8*Dcc*Mcc1;
98 end
99 %Calculate lambda:
100 lambda = eye(2) - Edq*De;
101 %Lambda terms:
102 lambda_cdq = lambda\Cdq;
103 lambda_ddq = lambda\Ddq;
104 lambda_edq = lambda\Edq;
105 %Define stage one unified state-space model:
106 Avcc = [Apll,zeros(order,4);Blp2,Alp,zeros(2);Bcc*Mcc2,Bcc*Clp,zeros(2)
    ];
```

```
A1 = [Ae, zeros(Ne,Nc); zeros(Nc,Ne), Avcc];
Bvcca = [Bpll; Blp1; Bcc*Mcc1];
B1 = [zeros(Ne,6); Bvcca];
B2 = [Be; zeros(Nc,2)];
Bvccb = [zeros(order+2,2); Bccz];
B3 = [zeros(Ne,2); Bvccb];
%Unify:
A_lin = A1 + B1*([Ce, zeros(Ne,Nc)] + De*(lambda_cdq + ...
    lambda_edq*[Ce, zeros(Ne,Nc)])) + B2*(lambda_cdq + ...
    lambda_edq*[Ce, zeros(Ne,Nc)]);
B_lin = B3 + B1*De*lambda_ddq + B2*lambda_ddq;
%Refine the output equation:
C_lin = [Ce, zeros(Ne,Nc)]+[De*lambda_edq*Ce, zeros(Ne,Nc)]+De*lambda_cdq
    ;
D_lin = De*lambda_ddq;
%Define the third linking matrix:
T3 = [1,0,0,0,0,0;0,1,0,0,0,0];
%Define the final unified output equation so it only focuses on dP and
    dE:
C_lin = T3*C_lin;
D_lin = T3*D_lin;
%Put into a ss model:
ss_model = ss(A_lin, B_lin, C_lin, D_lin);


%% Old material:

% A_lin = [Be; Bpll*De; Blp1*De; Bcc*Mcc1*De]*lambda_cdq + ...
%     [Ae+Be*lambda_edq*Ce, zeros(6);...
%     Bpll*(Ce + De*lambda_edq*Ce), Apll, zeros(2,4);...
```

```
135 %       Blp1*(Ce + De*lambda_edq*Ce),Blp2,Alp,zeros(2);...
136 %       Bcc*Mcc1*(Ce + De*lambda_edq*Ce),Bcc*Mcc2,zeros(2,4)];
137 % B_lin = [Be;Bpll*De;Blp1*De;Bcc*Mcc1*De]*lambda_ddq + [zeros(10,2);
      Bccz];
```

B.3 Power synchronization control

B.3.1 main function

Note - the following code contains function calls for non-linear models, the codes for which have not been provided. These can be commented out where appropriate; this will make no difference to the functioning of the linear model.

```
1  %% Analysis of a converter controlled by PSL feeding Xn,Rn:
2
3  clear
4  clc
5  close all
6
7  global Voltages;
8  global Power;
9  global Components;
10 %Range of angular frequencies (in per unit):
11 omega = horzcat((0.00002:0.00002:0.01),(0.02:0.01:15));
12 %Associated range of s:
13 s = 1i*omega;
14 %Modulation index of the converter (f_s/freq_nom):
15 Mod_Ind = 33;
16 %Define grid frequency:
17 freq_nom = 50;
18 %Associated angular frequency:
```

```
19 w_base = 2*pi*freq_nom;
20 %Express this in per unit terms:
21 w1 = 1;
22 %Define the base power:
23 P_base = 350e6;
24 %Define the base voltage:
25 V_base = 195e3;
26 %Define the parameters of filter and for the converter:
27 Xc = 0.2;
28 Lc = Xc;
29 Rc = 0.01;
30 Xf = 1/0.17;
31 Cf = 1/Xf;
32 %High pass current control parameters:
33 controller.psl.kv = 0.45;
34 controller.psl.alpha_v = 40/w_base;
35 %Gains of the power synchronization controller:
36 controller.psl.ki = 50/w_base;
37 %Gains of the voltage controller:
38 controller.vol.ki = 60/w_base;
39 %Define the short-circuit ratio:
40 for i = 1:5
41     %Which P0 values should be simulated for the given value of SCR:
42     if i == 1
43         AC_control = 1;
44         P0_vec = [0,0.1,0.2,0.3,0.4,0.5,0.6,0.7,0.75,0.85];
45     else
46         AC_control = 0;
47         P0_vec = [0,0.5,0.9];
48     end
```

```
49      for j = 1:length(P0_vec)
50
51          cd(strcat(str_base,str_matlab))
52
53          P0 = P0_vec(j);
54          %Define the grid parameters in terms of the per unit system
                being
55          %used in this work:
56          Xn = 1/i;
57          Ln = Xn;
58          Rn = 0.01;
59
60          %% Steady-state values at all relevant points:
61
62          E0 = 1;
63          V0 = 1;
64
65          Power.P0 = P0;
66          Voltages.V0 = V0;
67          Voltages.E0 = E0;
68          Components.Rc = Rc;
69          Components.Lc = Lc;
70          Components.Cf = Cf;
71          Components.Rn = Rn;
72          Components.Ln = Ln;
73          %
74          fun = @root8d;
75          x0 = [0,0,0,0,0,0,0,0];
76          x = fsolve(fun,x0);
77
```

```
78          [steady_state] = get_steady_state_values(Components,x);
79
80          %% Linear model:
81
82          if Components.Cf == 0
83              [ss_lin] = lin_state_space_l_filter(Components,steady_state
                );
84          else
85              [ss_lin] = lin_state_space_lc_filter(Components,
                steady_state);
86          end
87
88          [H] = lin_model(ss_lin,Components,controller,s,steady_state);
89
90          bode_plotting(Components.Cf,i,show_phase,P0,omega,...
91              w_base,H);
92
93          %% Poles and zeros:
94
95          %Bring back to the original folder:
96          cd(strcat(str_base,str_matlab))
97
98          if lin_analysis == 1
99              %pz_analysis(H,omega,w_base);
100         end
101
102     end
103 end
```

B.3.2 Combined linear model of controller and plant

Frequency response data

```
function [H] = lin_model(ss_lin,components,controller,s,steady_state)
%Create space for the transfer function matrix:
H = zeros(length(s),2,2);
%Get the steady-state values:
v_d0 = steady_state.v_d0;
v_q0 = steady_state.v_q0;
i_cd0 = steady_state.i_cd0;
i_cq0 = steady_state.i_cq0;
%Angles:
theta_v0 = steady_state.theta_v0;
%Run through all frequencies, calculating the frequency response:
for k=1:length(s)
    %Network response:
    if components.Cf == 0
        G = ss_lin.C*((s(k)*eye(2) - ss_lin.A)\ss_lin.B) + ss_lin.D;
    else
        G = ss_lin.C*((s(k)*eye(6) - ss_lin.A)\ss_lin.B) + ss_lin.D;
    end
    %Split the network transfer function matrix:
    G1 = G(1:2,:);
    G2 = G(3:4,:);
    %High pass filter:
    H_HP = controller.psl.kv*s(k)/(s(k)+controller.psl.alpha_v);
    %C matrices:
    C10 = [controller.psl.ki/s(k),0;0,controller.vol.ki/s(k)];
    C11 = -C10;
    C12 = [cos(theta_v0),sin(theta_v0);-sin(theta_v0),cos(theta_v0)];
```

```
28      C13 = [i_cq0*cos(theta_v0)-i_cd0*sin(theta_v0) ,0;...
29          i_cq0*sin(theta_v0)-i_cd0*cos(theta_v0) ,0];
30      C14 = -H_HP*eye(2);
31      C15 = [0 ,1;0 ,0];
32      C16 = [cos(theta_v0),-sin(theta_v0);sin(theta_v0),cos(theta_v0)];
33      C17 = [-v_q0 ,0;v_d0 ,0];
34      %Calculate I - kappa:
35      eye_kappa = (eye(2)-((C17+C16*(C15+C14*C13))*C11*G1 + ...
36          C16*C14*C12*G2));
37      H(k,:,:) = G1*(eye_kappa\((C17+C16*(C14*C13+C15))*C10));
38  end
```

Unified linear state-space model

```
1  function [ss_model] = create_state_space_lin_model(ss_lin ,controller
       ,...
2       steady_state ,components)
3  %State-equation matrices:
4  Ae = ss_lin.A;
5  Be = ss_lin.B;
6  %Re-order rows to make consistent with thesis equations:
7  Ce = vertcat(ss_lin.C(5:6,:),ss_lin.C(1:4,:));
8  De = vertcat(ss_lin.D(5:6,:),ss_lin.D(1:4,:));
9  %Grid frequency (per unit):
10 w1 = 1;
11 Lc = components.Lc;
12 Rc = components.Rc;
13 %Get the controller information:
14 kp_apc = controller.psl.kp;
15 ki_apc = controller.psl.ki;
16 kp_avc = controller.vol.kp;
```

```
17 ki_avc = controller.vol.ki;
18 %Filtering terms:
19 av = controller.psl.alpha_v;
20 kv = controller.psl.kv;
21 kc = controller.vol.kc;
22 %Get the steady-state values:
23 v_d0 = steady_state.v_d0;
24 v_q0 = steady_state.v_q0;
25 i_cd0 = steady_state.i_cd0;
26 i_cq0 = steady_state.i_cq0;
27 u_fd0 = steady_state.u_fd0;
28 u_fq0 = steady_state.u_fq0;
29 %Get the steady-state angles:
30 theta_v0 = atan2(v_q0,v_d0);
31 %Define w (equation 6.6):
32 w_d0 = u_fd0 + kc*(Rc*i_cd0 - w1*Lc*i_cq0);
33 w_q0 = u_fq0 + kc*(Rc*i_cq0 + w1*Lc*i_cd0);
34 %Associated magnitude:
35 W0 = sqrt(w_d0^2 + w_q0^2);
36 %Define the outer controller state-space matrices (equations 6.9 and
      6.10):
37 Bolz = eye(2);
38 Bol = -[1,0,0,0,0,0;...
39       0,0,kc*(Rc*w_d0+w1*Lc*w_q0)/W0,kc*(Rc*w_q0-w1*Lc*w_d0)/W0,w_d0/W0,
           w_q0/W0];
40 Col = [ki_apc,0;0,ki_avc];
41 Dolz = [kp_apc,0;0,kp_avc];
42 Dol = -Dolz*[1,0,0,0,0,0;...
43       0,0,kc*(Rc*w_d0+w1*Lc*w_q0)/W0,kc*(Rc*w_q0-w1*Lc*w_d0)/W0,w_d0/W0,
           w_q0/W0];
```

```
%Define the first linking matrix (equation 6.13):
T1 = [0,0,1,0,0,0;0,0,0,1,0,0];
%Define the abc -> dq frame transformation state-space matrices:
C3 = [cos(theta_v0),sin(theta_v0);-sin(theta_v0),cos(theta_v0)]*T1;
C4 = [i_cq0*cos(theta_v0)-i_cd0*sin(theta_v0),0;...
    i_cq0*sin(theta_v0)-i_cd0*cos(theta_v0),0];
C6 = [0,1;0,0];
%Define the effect of the high-pass filter state-space matrices (-ve
    sign):
Ahp = [-av,0;0,-av];
Bhp = [kv,0;0,kv];
Chp = [av,0;0,av];
Dhp = [-kv,0;0,-kv];
%Define the C7 and C8 matrices (equations 6.23 and 6.24 respectively):
C7 = [cos(theta_v0),-sin(theta_v0);sin(theta_v0),cos(theta_v0)];
C8 = [-v_q0,0;v_d0,0];
%Define Cdq, Ddq and Edq (equation 6.26):
Cdq = [zeros(2,6),[(C7*(Dhp*C4+C6) + C8)*Col,C7*Chp]];
Ddq = (C7*(Dhp*C4+C6)+C8)*Dolz;
Edq = (C7*(Dhp*C4+C6)+C8)*Dol + C7*Dhp*C3;
%Calculate lambda (global coefficient for equation 6.37):
lambda = eye(2) - Edq*De;
%Lambda terms (coefficients for equation 6.37):
lambda_cdq = lambda\Cdq;
lambda_ddq = lambda\Ddq;
lambda_edq = lambda\Edq;
%Define stage one unified state-space model (equation 6.36):
A1 = [Ae,zeros(6,4);zeros(4,6),[zeros(2,4);Bhp*C4*Col,Ahp]];
B1 = [zeros(6,2);[Bolz;Bhp*C4*Dolz]];
B2 = [Be;zeros(4,2)];
```

```
73 B3 = [zeros(6);[Bol;Bhp*(C3 + C4*Dol)]];
74 %Define unified state-space model (integrating equation 6.37 into 6.36)
       :
75 A_lin = A1 + B2*(lambda_cdq + [lambda_edq*Ce,zeros(2,4)]) + ...
76     B3*([Ce,zeros(6,4)] + De*(lambda_cdq + [lambda_edq*Ce,zeros(2,4)]))
           ;
77 B_lin = B1 + B2*(lambda_ddq) + B3*De*lambda_ddq;
78 %Refine the output equation (reformulation of equation 6.37):
79 C_lin = [Ce,zeros(6,4)];% + [De*lambda_edq*Ce,zeros(6)] + De*lambda_cdq
       ;
80 D_lin = De*lambda_ddq;
81 %Define the second linking matrix (equation 6.35 moved to state-space):
82 T = [1,0,0,0,0,0;0,1,0,0,0,0];
83 %Define the final unified output equation so it only focuses on dP and
       dE:
84 C_lin = T*C_lin;
85 D_lin = T*D_lin;
86 %Put into a ss model:
87 ss_model = ss(A_lin,B_lin,C_lin,D_lin);
```

B.4 Proportional resonant control

B.4.1 main function

Note - the following code contains function calls for non-linear models, the codes for which have not been provided. These can be commented out where appropriate; this will make no difference to the functioning of the linear model.

```
1 %% Analysis of a converter controlled by VCC feeding Xn,Rn:
2
3 %MMC will not require capacitor bank, whereas the 2-level system will.
```

```
%Want to design a controller which has the same gains with and without
%capacitor bank.

clear
clc
close all

global Voltages;
global Power;
global Components;
%Define grid frequency:
freq_nom = 50;
%Associated angular frequency:
w_base = 2*pi*freq_nom;
%Express this in per unit terms:
w0 = 1;
%Range of angular frequencies (in per unit):
omega = horzcat((0.00002:0.00002:0.01),(0.02:0.01:15));
%Associated range of s:
s = 1i*omega;
%Modulation index of the converter (f_s/freq_nom):
Mod_Ind = 33;
%Define the base power:
P_base = 350e6;
%Define the base voltage:
V_base = 195e3;
%Define the parameters of filter and for the converter:
Xc = 0.2;
Lc = Xc;
Rc = 0.01;
```

```
34 Xf = 1/(0.17);
35 Cf = 1/Xf;
36 %Low-pass filter:
37 controller.lpf.af = 80/w_base;
38 %PLL gains: these are set according to Lidong's thesis
39 controller.pll.kp = 20/w_base;
40 controller.pll.ki = 20/w_base;
41 %Bandwidth of the inner current controller:
42 alpha_c = 2500/w_base;
43 %Gains of the resonant controllers (this can be set according to ICC kp
       ):
44 controller.rc.kp = alpha_c*Lc;
45 %Gain for the integral part of the resonant controller:
46 controller.rc.ki = 15*controller.rc.kp;
47 %Resonant frequency and damping (provides a bit of leeway for freq. var
       ):
48 controller.rc.w_res = w0;
49 controller.rc.w_cut = 15/w_base;
50 %Gains of the outer loop controllers (same for 2- and multi-level conv)
       :
51 controller.apc.kp = 000/w_base;
52 controller.apc.ki = 060/w_base;
53 controller.avc.kp = 000/w_base;
54 controller.avc.ki = 060/w_base;
55 %Decoupling terms:
56 controller.dec.kp_pv = -50/w_base;
57 controller.dec.ki_pv = 0/w_base;
58 %Decoupling terms (affects P wobble):
59 controller.dec.kp_vp = 0/w_base;
60 controller.dec.ki_vp = -30/w_base;
```

```
%Define the SCR:
SCR_val = [1,3,5];
%Run through SCR values:
for i = 1:length(SCR_val)
    %Which P0 values should be simulated for the given value of SCR:
    if i == 1
        AC_control = 1;
        P0_vec = [0,0.1,0.2,0.3,0.4,0.5,0.6,0.7,0.75,0.8];
    else
        AC_control = 1;
        P0_vec = [0,0.5,0.9];
    end

    for j = 1:length(P0_vec)

        P0 = P0_vec(j);
        %Define the grid parameters in terms of the per unit system
            being
        %used in this work:
        Xn = 1/i;
        Ln = Xn;

        if Cf == 0
            Rn = 0.01;
        else
            Rn = 0.03;%0.01 for MMC, 0.03 for 2-level.
        end

        %% Steady-state values at all relevant points:

```

```
90          %Steady-state voltage magnitudes:
91          E0 = 1;
92          V0 = 1;
93
94          Power.P0 = P0;
95          Voltages.V0 = V0;
96          Voltages.E0 = E0;
97          Components.Rc = Rc;
98          Components.Lc = Lc;
99          Components.Cf = Cf;
100         Components.Rn = Rn;
101         Components.Ln = Ln;
102         %Non-linear steady-state solver:
103         fun = @root8d;
104         if Components.Cf == 0
105             x0 = [0,0,0,0];
106         else
107             x0 = [0,0,0,0,0,0,0,0];
108         end
109         x = fsolve(fun,x0);
110
111         [steady_state] = get_steady_state_values(Components,x);
112
113         %% Linear model:
114
115         if Components.Cf == 0
116             [ss_lin] = lin_state_space_l_filter(Components,...
117                 steady_state,AC_control,0);
118         else
119             [ss_lin] = lin_state_space_lc_filter(Components,...
```

```
120                     steady_state,AC_control,0);
121             end
122             %Run the linearised model:
123             [H] = lin_model(ss_lin,Components,steady_state,controller,s,0);
124             %Poles and zeros:
125             %pz_analysis(s,H,omega,w_base,controller);
126
127             bode_plotting(Components.Cf,controller.dec,i,show_phase,...
128                 P0,omega,w_base,H);
129         end
130 end
```

B.4.2 Combined linear model of controller and plant

```
1  function [H] = lin_model(ss_lin,components,steady,cont,s,...
2      simulink)
3  %Create space for the transfer function matrix:
4  H = zeros(length(s),2,2);
5  %
6  w0 = 1;
7  %See if a capacitor bank is included:
8  Cf = components.Cf;
9  %Get the controller information:
10 kp_pll = cont.pll.kp;
11 ki_pll = cont.pll.ki;
12 kp_res = cont.rc.kp;
13 ki_res = cont.rc.ki;
14 w_cut = cont.rc.w_cut;
15 w_res = cont.rc.w_res;
16 %Get the outer loop controller information:
```

```
17 kp_apc = cont.apc.kp;
18 ki_apc = cont.apc.ki;
19 kp_vp = cont.dec.kp_vp;
20 ki_vp = cont.dec.ki_vp;
21 kp_pv = cont.dec.kp_pv;
22 ki_pv = cont.dec.ki_pv;
23 kp_avc = cont.avc.kp;
24 ki_avc = cont.avc.ki;
25 %Get steady-state values:
26 if simulink == 1
27     u_fd0 = steady.simulation.u_c0(1);
28     u_fq0 = steady.simulation.u_c0(2);
29     %Get the steady-state angles:
30     theta_u0 = atan2(u_fq0,u_fd0);
31
32     i_ref_d0 = +steady.simulation.i_cg0(1);
33     i_ref_q0 = +steady.simulation.i_cg0(2);
34 else
35     u_fd0 = steady.u_fd0;
36     u_fq0 = steady.u_fq0;
37     %Get the steady-state angles:
38     theta_u0 = atan2(u_fq0,u_fd0);
39     %
40     i_ref_d0 = steady.i_cd0*cos(theta_u0) + steady.i_cq0*sin(theta_u0);
41     i_ref_q0 = steady.i_cq0*cos(theta_u0) - steady.i_cd0*sin(theta_u0);
42 end
43 %Low-pass filter:
44 H_LP = cont.lpf.af./(s + cont.lpf.af);
45 %Run through all frequencies, calculating the network response:
46 for k=1:length(s)
```

```
47      %Network transfer matrix:
48      if Cf == 0
49          G = ss_lin.C*((s(k)*eye(2)-ss_lin.A)\ss_lin.B)+ss_lin.D;
50      else
51          G = ss_lin.C*((s(k)*eye(6)-ss_lin.A)\ss_lin.B)+ss_lin.D;
52      end
53      %Split the network transfer matrix into three parts:
54      G1 = G(1:2,1:2);
55      G2 = G(3:4,1:2);
56      G3 = G(5:6,1:2);
57      %PLL controller gain:
58      CPLL = kp_pll + ki_pll/s(k);
59      %Modify accordingly:
60      CPLL = CPLL*H_LP(k);
61      %Resonant controller gain (see Zmood frequency domain analysis
            paper):
62      Hs_up = kp_res + ki_res*w_res*(s(k)+1i*w0)/...
63          ((s(k)+1i*w0)^2+2*w_cut*(s(k)+1i*w0)+w_res^2);
64      Hs_down = kp_res + ki_res*w_res*(s(k)-1i*w0)/...
65          ((s(k)-1i*w0)^2+2*w_cut*(s(k)-1i*w0)+w_res^2);
66      %Ci matrices:
67      C1 = 1/(1 + CPLL*(u_fq0*sin(theta_u0) + u_fd0*cos(theta_u0)))*...
68          [-CPLL*sin(theta_u0),CPLL*cos(theta_u0)];
69      C2 = [cos(theta_u0),-sin(theta_u0);sin(theta_u0),cos(theta_u0)];
70      C3 = 1/2*[Hs_up+Hs_down,-1i*(Hs_up-Hs_down);...
71          1i*(Hs_up-Hs_down),Hs_up+Hs_down];
72      C4 = C3*[-i_ref_q0;i_ref_d0];
73      C5 = -C3;
74
75      kappa = C2*C4*C1*G2 + C5*G1;
```

```
76      %Calculate I - kappa:
77      eye_kappa = eye(2) - kappa;
78      %Calculate H (closed loop transfer function of the power system,
79      %including the controllers) plus the low pass filtering:
80      H_inner = H_LP(k)*G3*(eye_kappa\(C2*C3));
81      %Outer loop controllers:
82      C21 = [(kp_apc+ki_apc/s(k)),(kp_vp+ki_vp/s(k));...
83          -(kp_pv+ki_pv/s(k)),-(kp_avc+ki_avc/s(k))];
84      %Overall transfer function:
85      H(k,:,:) = (eye(2) + H_inner*C21)\(H_inner*C21);
86  end
```